Investigations into the roles of Histamine Receptor H1 and extracellular vesicles in ovarian cancer cell behaviour

Emanuela Carollo

This thesis is submitted in partial fulfilment of the requirements of the award of Doctor of Philosophy at

Oxford Brookes University

Department of Biological and Medical Science

July 2021

Author's Declaration

I, Emanuela Carollo, declare that this thesis titled 'Investigations into the roles of Histamine Receptor H1 and extracellular vesicles in ovarian cancer cell behaviour" and submitted for assessment is an original work of my own. Any works of other authors used within this thesis, or the work presented in it are properly acknowledged. A list of the references employed is included.

Acknowledgments

Finally, this PhD journey has come to an end. I would like to thank my supervisors Prof Dave Carter and Prof Susan Brooks for trusting me as a scientist and as a person and for stimulate my curiosity towards science and its world. I would also like to thank Dr Ryan Pink who has contributed with scientific advice to this project and whom has also been a good friend and listener.

This time would have not been the same without the presence of my lab/office mates. Therefore, a big thank you goes to: Genevieve, Lia, Vicente, Lizzie, Lorena, Bianca, Fabrizio, Elise, Aditi, Jenny, Ellie, Priya, Soozanna, Jamie, Joanna, Helena, Elena, Jordi and Isabel. Working with you has been a very good fun. You all have thought me so much about science, life and English! You have celebrated with me every small achievement and lent me your shoulder in the hardest time, showing me how behind the word “work-mate” lays the word “friend”.

To my housemates and melocotoño friends thank you for being a constant presence and support throughout these four years: Jacopo, Sofia, Dan, Eirini, Alberto, Teresa, Patri, Antonio, Dani, Carlota, Ismael, Tom, Matt, Mei Yee and Romain. You all have been the best adventure buddies I could ask for, pillars of this wonderful journey, keeper of my laughs and tears; you have been a warm and sunny home in this distant and gloomy country. Another big thank you goes to all the other Oxford friends: Catherine, Roland, Mark, Fernando, Rose and the Mexican crew for all the beers, food and face masks shared together!

My profound gratitude goes to Martina, Carla and Navid. Countless are the hours spent talking with you about life, dreams, and the thousands of trips yet to come. Thank you for always been by my side; no matter where in the world we will be you are always close to me…and if not Zoom will provide for us!

Valeria, Magda, Francesca (Cur), Rosanna, Fabiana, Francesca (Kekkona), Attilio, Francesca (Giaki) e Francesco: neanche un milione di grazie sarebbero abbastanza per ripagare il mio debito con voi. Durante questi anni siete state una costante risorsa di forza e di gioia, mi avete capita lì dove nessun’altro poteva. Grazie per ascoltare sempre i miei lamenti e per aiutarmi a vedere il lato positivo di ogni cosa. Per tutti gli altri amici italiani, grazie per farmi sentire a casa ogni volta che torno.

Grazie ai miei zii Dario, Riccardo, Costantino, Lucio e Luigi, le mie zie Paola, Lilia e Rita ed i miei cugini Alessia, Guido, Fabio, Davide e Leonardo. Avete sempre creduto in me (anche quando io non ci riuscivo), non mi avete mai fatto dubitare di me stessa o del vostro amore. Voi tutti siete stati figure essenziali nella mia crescita. Anche se le vicissitudini della vita non ci permettono di essere tutti insieme fisicamente, voi siete sempre nella parte più profonda del mio cuore. Sono felice ed orgogliosa di potervi definire “la mia famiglia”. Vi voglio bene.

Ultime, ma non per importanza, mia madre Clara e nonna Titti. A voi va un super cosmico ringraziamento. Grazie per combattere insieme a me ogni giorno, per spingermi sempre a superare i miei limiti rimanendo li, salde, pronte ad aiutarmi in ogni circostanza. Senza il vostro amore, le vostre parole di conforto e la vostra energia non sarei qui oggi a dire: anche questa e fatta!

Abstract

Ovarian cancer (OC) diagnosis usually occurs very late, when metastatic spread has already started and patient's survival is very low. One of the many soluble factors that can promote cancer metastasis is histamine, a compound involved in a plethora of physiological and pathological processes, including cancer. Indeed, activation of histamine receptor H1 (HRH1) by histamine stimulates growth of OC cells *in vitro* and promotes the release of extracellular vesicles (EVs) in different cell lines. EVs are heterogeneous small vesicles involved in intracellular communication, which also modulate various steps of the metastatic process.

The main hypothesis of this thesis is that HRH1 mediates several cancerous behaviours associated with OC metastatic spread, by regulating EV release. The specific aims were 1) to analyse the correlation of histamine receptors gene expression with invasion and migration rates of OC cell lines *in vitro* and with tumour stage of OC clinical samples; 2) to study the involvement of HRH1 in different cellular behaviours associated with cancer metastasis; 3) to investigate the involvement of HRH1 in EV release and how they affect OC cell invasion *in vitro*.

The results show that the level of HRH1 mRNA positively correlates with *in vitro* migration and invasion rate of OC cells lines and higher expression was found in stage IV of OC clinical samples compared to stage II/III. Low HRH1 correlates with increased disease free survival, although no correlation was found with overall survival. HRH1 expression was modulated in three OC cell lines (SKOV3, OVCAR3 and OVCAR5), via siRNA transfection, chemical activation (via histamine) or inhibition (via chlorpheniramine) and its effect on cellular behaviour was evaluated through different *in vitro* assays. Results showed that HRH1: 1) does not modulate gene expression of EMT-related genes; 2) does not influence adhesion of OC cells to endothelial cells; 3) reduces cell invasion through a Matrigel® layer and 4) reduces their movement from the edge of a simulated 'wound'. Histamine increases the number of EVs released from SKOV3 cells and their ability to degrade a collagen substrate but did not modify EV protein contents compared to control EVs. EVs were able to rescue the reduction of invasion caused by HRH1 knockdown, while histamine failed to rescue the invasion of cells knocked down for Rab27a (a major regulator of EV production), suggesting a potential interplay between HRH1 and Rab27a in modulating EV release and cell invasion.

Overall, these results suggest that HRH1, via modulation of EV biogenesis, can impair OC cells invasion and migration *in vitro*.

For Guido

A Guido

Table of contents

Table of figures

Table of tables

Abbreviation

(c)DNA	(complementary) Deoxyribonucleic acid
(E)GFP	(Enhanced) green fluorescent protein
(m/r/t)RNA	(messenger/ribosomal/transfer) Ribonucleic acid
(q)PCR	(quantitative)Polymesase chain reaction
AC	adenylyl cyclase
ACTB	Actin beta
ADAM	Disintegrin and metalloproteinase
AKT	Protein kinase B
ALIX	Apoptosis-linked gene 2–interacting protein X/programmed cell death 6 interacting protein
APC	Allophycocyanin
ATP	Adenosine triphosphate
BRCA1/2	Breast cancer type 1/2 susceptibility gene
BRAF	B-Rapidly Accelerated Fibrosarcoma
BRIP1	BRCA1-interacting protein 1
BSA	Bovine serum albumin
CA125	Cancer antigen 125
cAMP	3',5'-cyclic adenosine monophosphate
CD9	Cluster of differentiation 9
CD44	Cluster of differentiation 44
CD63	Cluster of differentiation 63
CD81	Cluster of differentiation 81
CDH1	Cadherin-1
CFSE	Carboxyfluorescein succinimidyl ester
CRUK	Cancer research UK
Cq	Quantification cycle
CTCF	Corrected total cell fluorescence
DAO	Diamine oxidase
DAPI	4',6-diamidin-2-fenilindolo
DTT	Dithiothreitol
EC	Endothelial cells
ECL	Enhanced chemiluminescent
ECM	Extracellular matrix
EDTA	Ethylenediaminetetraacetic acid

EGF(R)	Epidermal growth factor (receptor)
EMT	Epithelial to mesenchymal transition
EOC	Epithelial ovarian cancer
EpCAM	Epithelial cell adhesive molecule
ERK	Extracellular signal-regulated kinases
ESCRT	Endosomal sorting complex responsible for transport
EV	Extracellular vesicle
FBS	Foetal bovine serum
FDR	False discovery rate
FITC	Fluorescein isothiocyanate
GFP	Green fluorescent protein
GOI	Gene of interest
GPCR	G protein-coupled receptors
GTP	Guanosine-5'-triphosphate
HDC	L-histidine decarboxylase enzyme
HGF	Hepatocyte growth factor
HGS(OC)	high-grade serous (ovarian cancer)
HMT	Histamine N-methyltransferase
HR	Hazard ratio
HRH1/2/3/4	Histamine receptor H1/2/3/4
IC50	Half maximal inhibitory concentration
ILV	Intraluminal vesicle
LGS(OC)	Low grade serous (ovarian cancer)
LFQ	Label free quantification
MAPK	Mitogen activated protein kinase
MEK	Mitogen activates protein kinase kinase
MET	Mesenchymal to epithelial transition
MHC-I/II	Major histocompatibility complex I/II
MMP	Matrix metalloproteinase
MTT	3-(4,5-Dimethylthiazol-2-yl)-2,5-diphenyltetrazolium bromide
MVB	Multivesicular body
nSMase	Neutral sphingomyelinase
NTA	Nanoparticle tracking analysis
OC	Ovarian Cancer
PBS	Phosphate buffered saline

PDAC	Pancreatic ductal adenocarcinoma
PFA	Paraformaldehyde
PIK3CA	Phosphatidylinositol-4,5-bisphosphate 3-kinase catalytic subunit alpha
PKA/C	Protein kinase A/C
PLC	Phospholipase C
PM	Plasma membrane
PTEN	Phosphatase and tensin homolog
RAB	Ras-associated binding protein
RIPA	Radioimmunoprecipitation assay buffer
RPMI	Roswell park memorial institute medium
RT	Room temperature
SD	Standard deviation
SEC	Size exclusion chromatography
SFM	Serum free media
SNAP23	Synaptosomal-associated protein 23
SNARE	Soluble N-ethylmaleimide sensitive fusion protein attachment receptor protein
STAT1/4	signal transducer and activator of transcription 1/4
STR	Short tandem repeat
TCGA	The cancer genomic atlas
TEM	Transmission electron microscopy
TfR	Transferrin receptor
TGFα/β	Transforming growth factor α/β
TIRF	Total internal reflection fluorescence microscopy
TNFα	Tumour necrosis factor α
TP53	Tumour protein p53
TSG1	Tumor suppressor TSG1
uPA	Urokinase-type plasminogen activator
VEGF(R)	Vascular endothelial growth factor (receptor)
VPS4	Vacuolar protein associated sorting 4
ZEB1/2	Zinc finger E-box-binding homeobox 1/2

Measurement units

v/v	volume per volume
w/v	weight per volume
bp	basepair(s)

^{o}C	Degrees Celcius
Da	Dalton(s)
G	Gravitational constant
h	hour(s)
l	litre(s)
m	meter(s)
M	Molar

Metric prefixes

k	kilo; 10^{3}
c	centi; 10^{-2}
m	milli; 10^{-3}
µ	micro; 10^{-6}
n	nano; 10^{-9}

Chapter 1

Introduction

1. Introduction

1.1. Ovarian cancer

1.1.1. Incidence and mortality

Ovarian cancer (OC) is the 7th most common type of cancer among women (Bray et al. 2018), and the deadliest gynaecological malignancy (Torre et al. 2018). Almost 320,000 new cases of OC are diagnosed in the world (Sung et al. 2021) and around 6,000 in the UK, each year (CRUK). Even though OC prevalence is one-tenth lower than breast, colorectal, lung and pancreatic cancer, its lethality is much higher; indeed, more than 60% of patients will succumb OC, with 207,252 women dying each year in the world (Torre et al. 2018) and 4,182 in the UK (Table 1.1) (CRUK).

Table 1.1: Number of cases, deaths, and percentage of survival of breast, colorectal, lung, ovarian and prostate cancer registered annually in the UK (data obtained from CRUK, accessed June 2021).

Cancer type	Cases	Deaths	10 year survival (%)
Breast	55,176	11,547	76
Colorectal	42,137	16,571	53
Lung	47,838	35,137	10
Ovarian	7,433	4,182	35
Prostate	48,487	11,855	78

The high mortality rate associated to OC is a consequence of the asymptomatic growth of the cancer and the lack of early biomarkers (Yoneda et al. 2012). Indeed, 75-80% of OC cases present at stages III or IV, when the disease has already spread to the peritoneal cavity or upper abdominal organs, with a 5 years survival rate lower than 29%; only 15-20% of OC cases are diagnosed at localised stage (stage I) when the 5 years survival rate is still high (>90%) (Table 1.2) (Cho and Shih 2009; Matulonis et al. 2016; Reid et al. 2017; Lheureux et al. 2019).

Table 1.2: One- and five-year percentage of survival of OC patients in stage I, II, III and IV (data obtained from CRUK, accessed June 2021).

OC stage	1 year survival (%)	5 year survival (%)
I	98	93.3
II	89.9	67.7
III	73.2	23.9
IV	53.8	13.4

Many risk factors are associated with OC incidence. Firstly, OC is an age-related disease, and it is considered a postmenopausal disease. Median age at diagnosis is 50-79 years (Chan et al. 2006); older age is associated with more advanced disease and a lower survival rate (Momenimovahed et al. 2019) (Table 1.3).

Table 1.3: One- and five-year percentage of survival of OC patients in stage I, II, III and IV classified by age at the time of diagnosis (data obtained from UK statistic authority, accessed January 2021).

	Stage I		Stage II		Stage III		Stage IV	
Age	1 year survival (%)	5 year survival (%)	1 year survival (%)	5 year survival (%)	1 year survival (%)	5 year survival (%)	1 year survival (%)	5 year survival (%)
15-44	99.5	96.9	93.7	77.9	92.4	46.9	67.6	27.5
45-54	98.9	93.4	95.5	81.9	89.6	33.9	79.1	20.4
55-64	98.9	94.1	96.5	68.8	83.5	28.6	70.6	15.4
65-74	97.3	92.8	93.3	52.2	77.7	13.5	57.8	5.3
75-99	98.3	92.2	79.2	70.9	53.9	29.6	32.5	14.5

Reproductive factors like early menarche, high number of lifetime ovulatory cycles and late menopause are at the base of the OC "incessant ovulation" theory and are related with a higher incidence of OC (Tung *et al.*, 2003; Kim *et al.*, 2017). The "incessant ovulation" theory proposes that the continuous rupture of the ovulating follicle damages the ovarian epithelium and traumatises the ovarian surface (Fathalla 1971). This induces invagination of the ovarian epithelium and formation of clefts and inclusion cysts that potentially will undergo malignant transformation (Fleming et al. 2006). Therefore, factors that induce production of sex hormones such as oestrogen, follicle-stimulating hormone and luteinizing hormone and consequent proliferation of the ovarian epithelium during ovulation, are thought to be associated with OC incidence (Lukanova and Kaaks 2005). On the contrary, any factor that contributes to the reduction of ovulation (pregnancy, use of oral contraception and others) has a protective effect against OC (Tung et al. 2003; Momenimovahed et al. 2019). The presence of previous benign gynaecological conditions such as endometriosis, ovarian cysts or pelvic inflammatory disease, can increase the incidence of particular subtypes of OC (Melin et al. 2006; Kim et al. 2014b). For example, endometriosis is thought to be associated with OC as the two disease might share risk factors such as genetic susceptibility, and/or pathogenesis rather than a causal association (Sayasneh et al. 2011; Lu et al. 2015; Kori et al. 2016). Genetic variations of the breast cancer gene 1 and 2 (*BRCA1* and *BRCA2*) genes are associated with 50% risk of developing OC by the age of 70 (Easton et al. 1995; Walsh et al. 2011) and account for the majority of hereditary cases. Mutations in other genes such as BRCA1-interacting protein 1 (*BRIP1*) and *RAD51* can moderately increase the risk of OC (Ramus et al. 2015; Song et al. 2015). Finally, other factors such as cigarette smoking, alcohol

consumption, diet, low physical activity, and obesity are all associated with increased incidence of OC. For example, several studies have shown an association between body mass and OC. Indeed, presence of low-grade chronic inflammation and inflammatory cytokines produced by fat cells (normally associated with obesity) can deregulate sex hormone levels and increase OC risk (Tworoger and Huang 2016). All of these factors have been associated with a 5-29% increase of specific OC subtypes (Beral et al. 2012; Olsen et al. 2013; Webb and Jordan 2016).

1.1.2. Classification

OC is a nonspecific term for a variety of tumours that involve the ovary. Indeed, OC is a heterogeneous disease characterised by different morphological, histological and genetic traits (Kroeger Jr and Drapkin 2017). Depending on the anatomic structures from which the tumour presumably originates, OC can be classified into three major categories: A) sex-cord stromal tumours, B) germ cell tumours and C) epithelial ovarian cancer (EOC), (Chen et al. 2003). Each type then contains a number of different tumour subtypes depending on the cell morphology and genetic traits. When a tumour combines one or more subtypes is defined as "mixed" (Chen et al. 2003).

A) Sex cord stromal tumours are infrequent and represent around 7% of OC cases. They are of mesenchymal or mesonephric origin and are thought to arise from the primitive sex cords cells (granulosa and Sertoli cells) or stromal cells of the ovary (Shim et al. 2013; Al Harbi et al. 2021).

B) Germ cell tumours account for around 20% of all ovarian neoplasms, although only 5% of them are malignant and the rest (95%) are benign mature cystic teratomas. They are thought to originate from primordial germ cells and mostly appear in adolescence and early adulthood (Zalel et al. 1996; Parkinson et al. 2011; Shaaban et al. 2014).

C) Epithelial ovarian cancers (EOCs) arise from the epithelial layer covering the surface of the ovaries (Cho & Shih, 2009; Koulouris & Penson, 2009) and account for around 90% of all malignant OC cases. (Chen et al. 2003). Depending on the morphological and histological characteristics of the epithelial cells, EOC can be further subdivided into five main categories that are: 1) serous, 2) endometrioid, 3) clear cell, 4) mucinous and 5) malignant Brenner EOC (Table 1.4).

1) Serous carcinomas, accounts for the majority of EOC cases (90%) and is further divided in high-grade serous (HGSC) and low-grade serous (LGSC) OC. HGSOC accounts for 70-80% of all EOC deaths (Bowtell et al. 2016). Although serous EOCs were thought for a long time to originate from cysts on the surface of the epithelium or from alteration of the epithelial layer of the ovary, in the past 20 years more evidence has accumulated showing that as many as 60% of serous EOCs cases might arise from the Fallopian tube (Piek et al. 2001; Kroeger Jr

and Drapkin 2017). In fact, it has been postulated that the shed tubal epithelium can implant on the ovary and originate inclusion cysts that give rise to serous neoplasm (Piek et al. 2001; Li et al. 2011). Indeed many early serous OCs have been identified in the distal end of the Fallopian tube, and as the tumour grows it eventually obliterates the ovarian tissue and appears to have arisen from the latter (Kurman and Shih 2011).

2) Endometrioid and 3) clear cell carcinomas originate from endometriotic lesion (endometriomas) and are associated with implants of endometriosis elsewhere in the pelvis (Veras et al. 2009).

4) Mucinous and 5) malignant Brenner tumours are the least common types of EOC, comprising around 8% of all cases. Their origin is still unclear; and although their epithelium closely resembles gastrointestinal mucosa, they are considered to come from transitional cells at or close the junction of fallopian tube (Prat 2012).

EOCs can also be classified according to their morphological and molecular characteristics in type I and type II tumours (Shih and Kurman 2004) (Table 1.4).

Type I tumours are mostly low-grade, generally indolent tumours and appear as a unilateral, large cystic neoplasms, usually associated with an elevated survival time (82 months average) compared with type II tumours (30 months) (Gershenson et al. 2006). Type I OCs progress in a stepwise manner from well-recognised benign precursor lesions to malignant tumours (Singer et al. 2002). They normally account for only 10% of OCs deaths. Type I EOCs include endometrioid carcinoma, clear cell carcinoma, LGSC and mucinous carcinoma. They are typically genetically stable (less susceptible to mutation) and mostly present with driving mutations in Ki-ras2 Kirsten rat sarcoma viral oncogene homolog (*KRAS*), B-Rapidly Accelerated Fibrosarcoma (*BRAF*), phosphatase and tensin homolog (*PTEN*) and phosphatidylinositol-4,5-bisphosphate 3-kinase catalytic subunit alpha (*PI3KCA*) genes (Kuo et al. 2009a).

Type II tumours include more aggressive tumours like HGSC, high grade endometrioid and undifferentiated carcinomas. They represent ≈75% of all OC cases, are normally high grade, poorly differentiated, show a high propensity to metastasise and are normally diagnosed at advanced stage leading to poor survival (average 30 months) (Lengyel 2010). This group shows greater morphologic and molecular homogeneity, is genetically unstable and is characterised by tumour protein p53 (*TP53*) and cyclin E1 (*CCNE1*) mutations (Kurman and Shih 2016).

Table 1.4: Classification of epithelial ovarian cancer based on the site of origin, histopathological characteristics, their molecular classification, key mutation and association with disease progression.

<table>
<tr><th>Molecular classification</th><th colspan="2">Histopathological classification</th><th>Mutations</th><th>Precursor site of origin</th><th>Disease progression</th></tr>
<tr><td rowspan="6">Type I (≈25%) (Kurman and Shih 2011)</td><td colspan="2">Endometrioid carcinoma (10%)</td><td>BRAF, CTNNB1, PTEN, PIK3CA (Sato et al. 2000; Willner et al. 2007; Wu et al. 2007)</td><td rowspan="2">Endometriotic tissue</td><td rowspan="5">Normally low grade,
present at low stage,
non invasive,
normally associated with better prognosis than Type II tumours.
Average survival time: 82 months (Gershenson et al. 2006)</td></tr>
<tr><td colspan="2">Clear cell carcinoma (10%)</td><td>ARID1A, PIK3CA (Kuo et al. 2009b; Jones et al. 2011)</td></tr>
<tr><td colspan="2">Mucinous carcinoma (5%)</td><td>KRAS (Mucinous and Tumors 1994)</td><td rowspan="2">Cell situated at or near the junction of the ovary with the fallopian tube</td></tr>
<tr><td colspan="2">Malignant Brenner tumour (3%)*</td><td>PI3K/AKT (Kurman and Shih 2011)</td></tr>
<tr><td rowspan="3">Serous (70%)</td><td>Low grade serous carcinoma (30%)</td><td>BRAF, ERBB2, KRAS, PIK3CA (Afify et al. 1999; Singer et al. 2003; Willner et al. 2007)</td><td rowspan="3">Fallopian tube pre malignant lesion</td></tr>
<tr><td rowspan="3">Type II (≈75%) (Kurman and Shih 2011)</td><td>High grade serous carcinoma (70%)</td><td rowspan="3">BRAC1, BRAC2 (Senturk et al. 2010), TP53 (Ahmed et al. 2010)</td><td rowspan="4">High-grade, malignant tumours, normally with a tendency to invade
usually diagnosed at late stage of the disease (III-IV),
associated with poor survival (average 30 months) (Lengyel 2010)</td></tr>
<tr><td colspan="2">High grade endometrioid (<2%)</td><td>Endometriotic tissue</td></tr>
<tr><td colspan="2">Mixed Mulleran tumours (carcinosarcoma, undifferentiated) (<1%)</td><td>Not identified</td></tr>
</table>

1.1.3. Treatment

Although it is recognised that OC comprises several distinct subtypes, a one-size fits approach has been used in the management of OC for a long time. The identification of specific molecular markers associated with different OC subtypes has resulted in a better understanding of this disease allowing a shift of OC management from a one-size fits approach to a more tailored approach (Lee et al. 2019; Lheureux et al. 2019). When OC is low grade and confined to one ovary (generally Type I OC, stage I/II), treatment consists of removal of the affected ovary or debulking surgery (removal of as much cancerous tissue as possible from the ovaries and the peritoneal cavity) that may or may not be followed by chemotherapy. In the case of advanced stage cancers (stage III/IV), complete removal of cancerous tissue is almost impossible; therefore, patients are firstly treated with chemotherapy (neoadjuvant-chemotherapy) and undergo surgery only if they successfully respond to treatment (reduction of the tumour size) (Cortez et al. 2018).

The first drug to be approved for OC treatment, and still the most commonly used one, is cisplatin. By binding to the N-7 atoms of purines, cisplatin forms DNA adducts that distort the DNA conformation inhibiting replication and transcription (Peng et al. 2010). This induces a DNA damage response and consequently activates multiple signalling pathways that induce cell-cycle arrest and apoptosis (Wiltshaw et al. 1979; Galluzzi et al. 2012). However, the high rate of cisplatin resistance in OC is a major obstacle to treatment and clinical management of the disease (Ozols 1991; Giaccone 2000; Cannistra 2004; Köberle et al. 2010). Indeed, OC cells can activate several different mechanisms to acquire resistance to cisplatin. For example, cancer cells can reduce drug uptake and reduce accumulation of cisplatin internally (Loh et al. 1992; Mellish et al. 1993); they can present impaired DNA repair mechanisms that either do not recognise cisplatin DNA adducts or become tolerant towards unrepaired DNA lesions, ultimately generating impaired apoptotic signals (Galluzzi et al. 2012). In addition, defects in signalling pathways associated with apoptosis following DNA damage can confer post-target resistance in cells (Vousden and Lane 2007). The specific molecular mechanisms underpinning cisplatin resistance will not be further discussed as they lie beyond the scope of this thesis, but further information can be found in the extensive review of Galluzzi et al (2012).

Due to the high rate of cisplatin resistance other platinum-derived drugs (oxaliplatin and carboplatin) were introduced into the clinical management of OC with the aim to reduce the cytotoxic effects of cisplatin and overcome resistance. Unfortunately, as the active molecule in these compounds is still cisplatin, tumours resistant to cisplatin have been shown to also be resistant to the other platinum drugs (Kidani et al. 1978; Harrap 1985).

Nowadays, other therapeutics have been introduced in OC treatment, including taxane-based drugs (paclitaxel) (Mcguire et al. 1996), poly ADP (Adenosine diphosphate) ribose polymerase (PARP) inhibitors and monoclonal antibodies (bevacizumab, an anti-vascular endothelial growth factor (VEGF)-A) (Jayson et al. 2014; Matulonis et al. 2016; Lheureux et al. 2019). Even though most patients show a high response to first line treatment, almost 45% ultimately relapse, gaining a chemo-resistant phenotype. For these patients, palliative care is the only viable management option. The combination of cisplatin resistance together with the appearance of the disease at more advanced stages are the causes the high mortality rate associated to OC.

1.2. Metastasis

Metastasis is the result of a multistage process that leads to the development of a secondary tumour in a part of the body distant from the primary one (Brooks et al. 2010; Valastyan and Weinberg 2011; Lambert et al. 2017; Fares et al. 2020). Metastasis is the primary cause of cancer mortality, in fact almost 90% of cancer deaths are related to a metastatic stage of the disease (Reid et al. 2017). The metastatic spread can take place through different routes: cancer cells can reach blood or lymphatic vessels, enter them and disseminate through them to distant organs or lymph nodes; these processes are known as hematogenous or lymphatic dissemination, respectively (Alitalo and Detmar 2012). Alternatively, cancer cells remain confined to the region where they originate and disseminate by "direct extension" to the neighbouring organs (Kaiser 1989; Thomakos et al. 2019). The latter is the favoured mechanisms of metastatic dissemination of OC, together with lymphatic dissemination (Thomakos et al. 2019). In order to disseminate via one or the other routes, cancer cells often undergo epithelial to mesenchymal transition (EMT), a process that is driven by a phenotypic "plasticity" of tumour cells and enables them to acquire an invasive phenotype, resist to genotoxic stress and apoptosis and to disseminate (further discussed in section 1.2.1) (Lengyel 2010; Chaffer et al. 2016; Gupta et al. 2019).

1.2.1. Epithelial to mesenchymal transition and tumour plasticity

EMT is a reversible process during which, epithelial cells, usually immotile and tightly bound to each other and to the extracellular matrix (ECM) (Fouad and Aanei 2017) (Figure 1.1 A), undergo molecular and biochemical alterations resulting in acquisition of a mesenchymal phenotype. This phenotype allows cells to disaggregate from the tumour mass and to move to surrounding organs (Kalluri and Neilson 2003). One of the first changes during EMT consists of epithelial cells losing their apical-basal polarity due to the loss of tight junctions, adherens junctions and desmosomes (Figure 1.1 B). This is the result of the loss of cellular adhesion molecules, including cadherins and integrins, and to the

reorganization of the cytoskeleton following downregulation of cytokeratins (Ribatti et al. 2020). Cadherins are adhesive molecules that maintain intracellular adhesion by interacting with the cytoskeleton via the cytosolic proteins catenins (α,β,γ) (Cavallaro and Christofori 2004). Integrins are a family of glycoproteins that form heterodimeric receptors with ECM molecules enabling cell-ECM interactions (Hood and Cheresh 2002). Down-regulation of cadherins, (in particular E-cadherin), integrins, (in particular $\alpha_6\beta_4$ integrin), claudins and epithelial cell adhesion molecule (EpCAM) diminishes intracellular adhesiveness and allows cells to detach from the primary tumour (Hay 1995). Many mechanisms have been identified as responsible for controlling loss of adhesive molecules, including inactivating mutations, transcriptional control, non-coding RNAs and others, extensively reviewed by Craene and Berx (2013).

The best characterised regulatory network during EMT involves a series of transcription factors. Initially, the snail family transcriptional repressor 1 (SNAI1) was identified to directly bind to the *CDH1* promoters (which encodes E-cadherin) and repress its transcription (Batlle et al. 2000; Cano et al. 2000). Since then many other transcription factors including SNAI2 (Hajra et al. 2002), zinc finger E-box-binding homeobox 1 and 2 (ZEB1, ZEB2) (Comijn et al. 2001; Vandewalle et al. 2005), E47 (Pérez-Moreno et al. 2001), twist-related protein 1 and 2 (TWIST1 and TWIST2) (Yang et al. 2004; Mani et al. 2007) were identified for their ability of not only repress E-cadherin transcription (directly or indirectly) but also to regulate expression of other junctional proteins like claudins and desmosomes, facilitating the initiation of the "dedifferentiation programme" (De Craene et al. 2005; Moreno-Bueno et al. 2006) (Figure 1.1 B).

Simultaneously with the loss of adhesive molecules, cells undergoing EMT upregulate other proteins such as vimentin, fibronectin, neural cadherin (N-cadherin), β_1 and β_3 integrins and matrix metalloproteinases (MMPs). The overexpression of these molecules results in cells acquiring a mesenchymal phenotype, showing elongated morphology with front end-to-back end polarity and forming only transient contacts with their neighbouring cells (Dongre and Weinberg 2019) (Figure 1.1 C). At this point cancer cells have all the required characteristics to degrade the underlying ECM and invade the adjacent stroma (Dongre and Weinberg 2019).

What is interesting about the EMT is that it is a reversible process and cancer cells exhibiting a mesenchymal phenotype can revert back to an epithelial phenotype by undergoing mesenchymal to epithelial transition (MET). Therefore, EMT does not operate as a binary switch that shunts cells from fully epithelial to fully mesenchymal extremes, but cancer cells may actually be in a spectrum of states between epithelial and mesenchymal phenotypes, and distinct and definable markers of one or the other may not be identifiable (Yang et al. 2020).

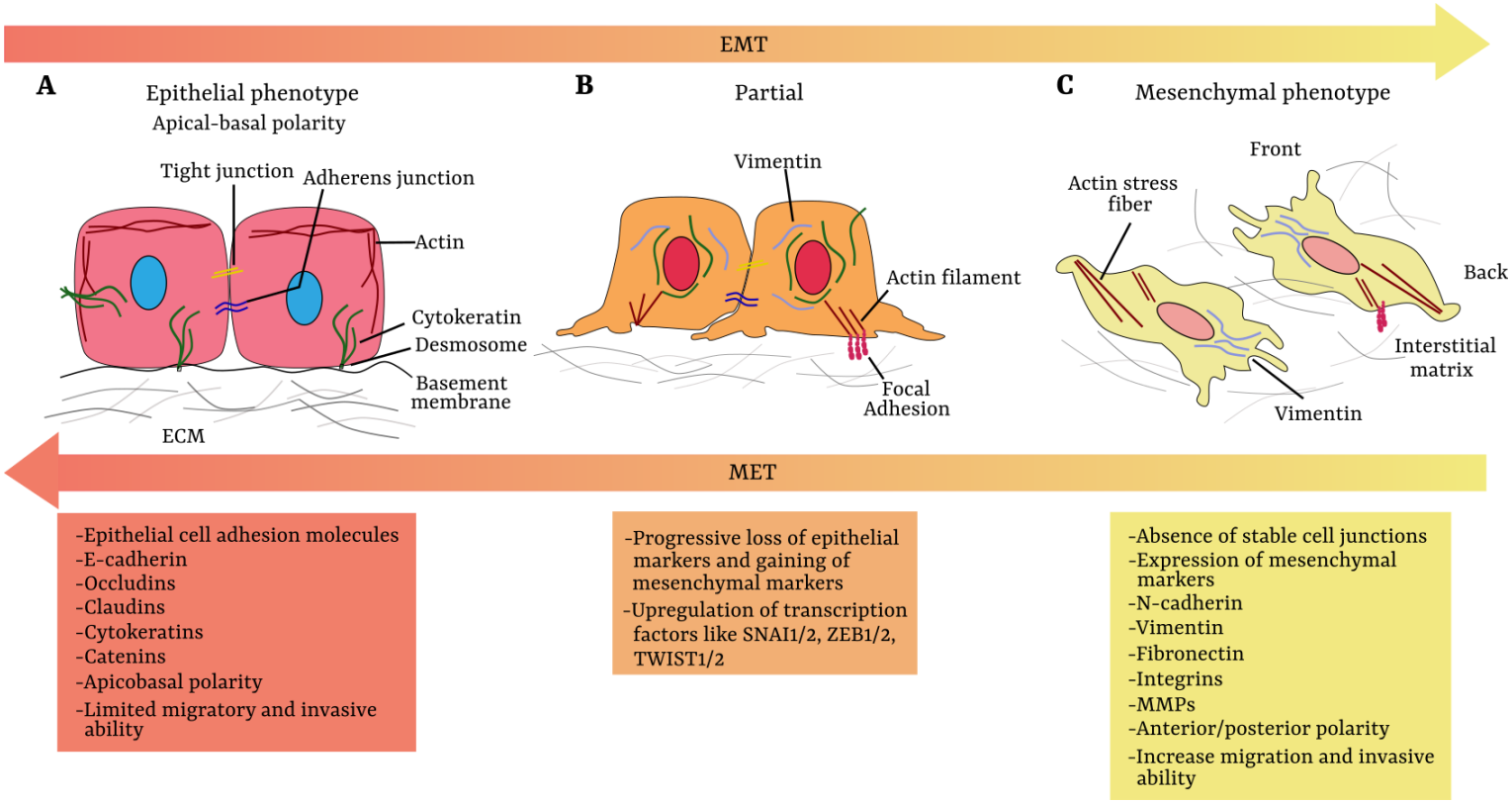

Figure 1.1: Schematic representation of EMT/MET progression.

A) Epithelial cells show apical-basal polarity through tight junctions, adherens junctions and are tethered to the basement membrane by hemidesmosomes. These cells express classical epithelial markers (listed in the red box) that enable them to be tightly bound to each other maintaining cell polarity. B) Initiation of EMT results in a transition of polarised epithelial cells toward mesenchymal cells through activation of several transcription factors described in the orange box. C) The progressive loss of epithelial features is accompanied by acquisition of mesenchymal features; cell display front end-to-back end polarity, extensively reorganise their cytoskeleton and express a distinct set of molecules (listed in the yellow box) that maintain their mesenchymal state and promote their invasion and migration to surrounding tissues. Mesenchymal cells can revert back to epithelial cells by undergoing the MET process.

1.2.2. Haematogenous and lymphatic dissemination

Neoplastic cells must successfully complete a cascade of events in order to leave the primary tumour and establish a secondary tumour site (Brooks et al. 2010). The metastatic cascade originates in the primary tumour where the shortage of oxygen and nutrients stimulates the formation of new blood vessels. Tumour cells release "angiogenic activators" like VEGF, basic fibroblast growth factor (bFGF), angiogenin, transforming growth factor (TGF)-α, TGF-β, tumour necrosis factor (TNF)-α and activate surrounding endothelial cells (Nishida et al. 2006). Thus, the endothelial cells migrate and proliferate inducing the formation of new blood vessels, a process known as angiogenesis (Figure 1.2 A). The newly formed vessels are irregular, show an uneven diameter and abnormal branching pattern, and often reveal an incomplete basement membrane and lack of intact endothelial junctions, that enhance their permeability (Dvorak et al. 1988; Steinberg et al. 1990; Vermeulen et al. 1995; Hewitt et al. 1997). The unusual leakiness of the blood vessels will help them not only to provide the tumour with nutrients but will also serve as a way to escape the primary tumour (Bergers and Benjamin 2003).

In order to become motile, cancer cells undergo EMT (described in section 1.2.1), gain a more mesenchymal phenotype, dissociate from the epithelial cell sheets and advance in the malignant transformation (Thiery et al. 2009) (Figure 1.2 B). Cells begin to invade the surrounding tissues (Figure 1.2 C). During invasion, cells detach from the main tumour, adhere to the ECM and degrade it through release of extracellular matrix proteases (Sahai 2005). The ECM-cell and cell-cell interactions enables the transmission of information between cells and the surrounding environment, altering their ability to proliferate, migrate and survive in both physiological and pathological conditions (Fares et al. 2020). Numerous proteolytic enzymes are release by either tumour cells or by the tumour microenvironment, including the urokinase-type plasminogen activator (uPA) (Mahmood et al. 2018), MMPs (Cathcart et al. 2015; Gonzalez-Avila et al. 2019), and cathepsins (Tan et al. 2013). Degradation of ECM allows cancer cells to bypass physical barriers like the basement membrane to access more distant locations (Sahai 2005). This process is a fundamental step of the metastatic cascade and is a trigger for further cancer progression and metastasis (Krakhmal et al. 2015).

Through dynamic cytoskeletal changes, localised proteolysis and cell-matrix interactions, cancer cells migrate towards blood vessels (Figure 1.2 C), adhere to endothelial cells, which retract allowing the tumour cells to bass between them and intravasate (Figure 1.2 D) (Brooks et al. 2010). Once in the blood vessel, cancer cells need to survive physical challenges, such as shear forces generated by the blood flow and immune response attack (Molloy and van 't Veer 2008). Cancer cells interact with the endothelium, platelets and leukocytes and disseminate via the haematogenous circulation (Figure 1.2 E). The interaction between cancer cell and endothelium partially resembles the leukocyte-endothelial interaction; although, the mechanism of tumour cell adhesion differs from leukocyte recruitment to

inflammatory sites, both process share the same molecules to form contact with the endothelium (Witz 2008; Desgrosellier and Cheresh 2010; Läubli and Borsig 2010). Initially, weak interactions are formed between cancer cells and selectins expressed on endothelial cells, allowing the cancer cell to roll on the endothelium (Bendas and Borsig 2012). While early tethering and rolling of cancer cells on the endothelium is a reversible process, upregulation of integrins and members of the Ig superfamily stabilise the interaction and allows cancer cells to migrate outside the blood vessel and extravasate to the target organ (Smith 2000) (Figure 1.2 F). Here cancer cells exit the blood vessel, colonise the tissue (Reymond et al. 2013) and undergo MET, acquiring the epithelial phenotype back (Yao et al. 2011). Cancer cells remain dormant for some time before starting proliferating again, generating a secondary tumour (Chambers et al. 2002).

Cancer cell can also infiltrate into lymphatic vessels and, through a mechanism similar to the one just described, can colonise close and distant lymph nodes and reach circulation, contributing to metastatic dissemination (Brown et al. 2018; Farnsworth et al. 2018; Pereira et al. 2018). Indeed, it has been proposed that OC cells favour lymphatic disseminate to hematogenous metastasis. By accumulating into the peritoneal lymphatic vessels, cancer cells can block them impeding lymphatic clearance of the peritoneum, with consequent ascites formation and further OC dissemination (Feki et al. 2009). Lymph node metastasis is seen in more than 60% of OC cases, particularly in pelvic and para-aortic lymph nodes (Goff et al. 2004; Ferrandina et al. 2007; Nakao et al. 2009; Jayson et al. 2014). For this reason, since 1985, the International Federation of Gynaecology and Obstetrics (FIGO) included lymph node metastasis for identification of stage III or IV OC (Thomakos et al. 2019).

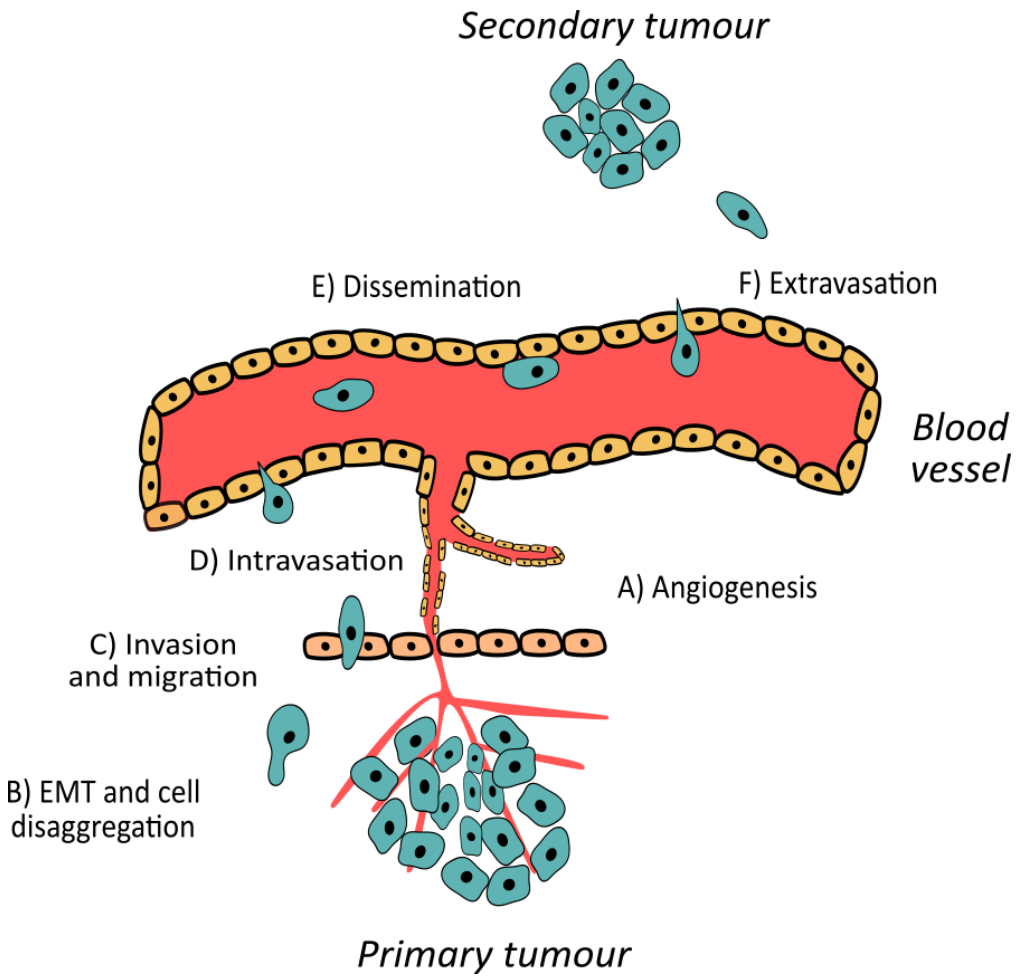

Figure 1.2: Schematic representation of the metastatic cascade.
Formation of new blood vessels occurs in the primary tumour (A) due to a hypoxic environment. Cancer cells undergo EMT and detach from the primary tumour (B), invade the surrounding membrane and move towards the blood vessel (C). Once cells reached the blood vessel, they intravasate into it (D) and move into the circulation (E). When reached the target organ, cells adhere to the vessel, extravasate (F) and penetrate in the new organ generating a secondary tumour.

1.2.3. Ovarian cancer metastasis

As described previously, OC metastasis does not follow the classical hematogenous dissemination pathway, instead it directly extends to the peritoneal cavity, where the lack of an anatomic barrier makes OC dissemination a passive process (Motohara et al. 2019). The "soil" for OC metastasis is either the omentum, a fatty layer covering the abdomen and pelvis, or the peritoneum, a serous membrane consisting of a single layer of mesothelial cells supported by a thin layer of ECM. These two layers cover most of the ovaries proximal organs such as the uterus and Fallopian tubes, bladder, rectum, stomach and the small bowel (Yeung et al. 2015; Motohara et al. 2019) (Figure 1.3). OC dissemination demonstrates the "seed and soil" hypothesis proposed by Paget (1889), as demonstrated by Tarin and colleagues (1984) in their study. The authors studied the clinical effect of a peritoneovenus shunt in cancer dissemination in 29 patients living with ascites caused by inoperable cancers. The patients were subjected to the peritoneovenous shunt, that drained the excess of ascitic fluid from the peritoneum

to the systemic circulation, via the jugular vein. Despite patients experienced a massive infusion of malignant cells for up to 27 months, they either did not develop aggressive metastases in the lung or the metastases were of no clinical importance (Tarin et al. 1984).

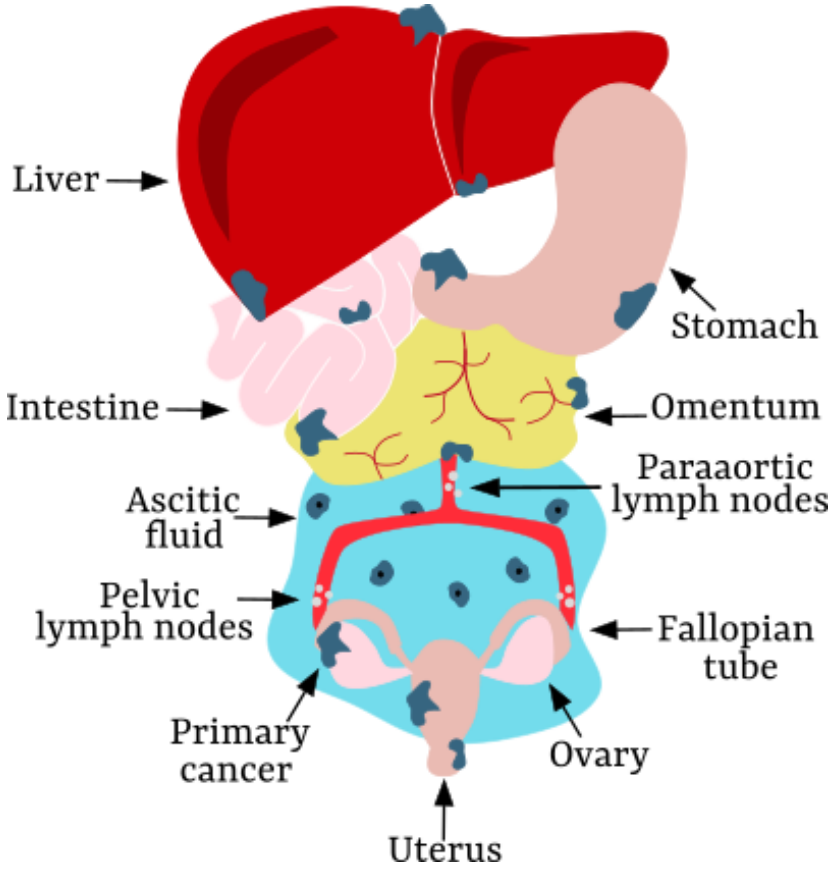

Figure 1.3: Schematic representation of OC spread.
At early stage, the tumour (dark blue mass in the figure) is localised to the ovary. Once the capsule is disrupted, the tumour spreads to the surrounding organs. Ovarian cancer directly extends to the uterus and Fallopian tubes and colonise them. Some OC cells are exfoliated from the ovarian surface and are transported by the ascitic fluid to the peritoneal cavity were OC cells implant to the omentum, and to the mesothelial layer covering the stomach, intestine, liver and other peritoneal organs. Tumour cells can also spread through the lymphatics vessels that drain the ovaries to the pelvic and paraaortic lymph nodes.

Before OC cells detach from the primary tumour, they often undergo EMT (described in section 1.2.1) that allows them to acquire an invasive phenotype, resist stress and apoptosis, and to disseminate (Lengyel 2010). During EMT, OC cells lose E-cadherin expression due to both its transcription regulation and also to the abundance of growth factors like TGF-β, epidermal growth factor (EGF), and hepatocyte growth factor (HGF) (Thiery et al. 2009). These soluble molecules, normally present in the follicular fluid during ovulation (Dean et al. 2017), regulate the function of transcription factors like SNAI1/2 through activation of non-canonical PI3K/Protein kinase B (also known as AKT) and mitogen activated protein kinase kinase (MEK)/extracellular signal-regulated kinases (ERK) pathways, favouring EMT

(Grotegut et al. 2006; Peinado et al. 2007). E-cadherin levels are lower in detached OCs or metastatic sites than in the primary tumour (Veatch et al. 1994). Cells start to express N- and P-cadherins and $\alpha_2\beta_1$ and $\alpha_3\beta_1$ integrins that cluster with the collagen of the ECM and activate MMP-1 and -9 that further cleave α-integrin and E-cadherin, facilitating cell detachment from the epithelial layer, a process referred to as "exfoliation" (Al-Alem and Jr 2015). The exfoliation process is promoted by the mechanical forces produced by the rubbing of internal organs on the epithelial layer during respiration.

OC cells detach as single cells or more often as spheroids (clusters of cells) and then passively disseminate in the peritoneal cavity through the physiological movement of the peritoneal fluid. The increased leakiness of the vasculature induced by release of VEGF and the obstruction of lymphatic vessels by cancer cells impedes the full absorption of the peritoneal fluid, promoting ascites formation in the peritoneal cavity (Order et al. 1972). Ascites represents a reservoir of ECM components, chemokines, cytokines and proteins that support OC cells survival and growth and facilitates their spread to distant sites of the abdomen. Detached cancer cells usually "float" in the ascites as spheroids and need to survive anoikis (induction of apoptosis caused by detachment from the ECM) and the immune system surveillance in order to disseminate. Interestingly, cancer cells in these spheroids show high levels of E-cadherin and EpCAM and reduced expression of N-cadherin, MMPs and other mesenchymal markers (Latifi et al. 2012; Wintzell et al. 2012). In this context, expression of cadherins might be necessary to avoid detachment-induced apoptosis and also help cells to resist chemotherapy (Bates et al. 2000; Frankel et al. 2001)

Cells attach preferably to the mesothelium, by expressing several integrins (particularly $\alpha_5\beta_1$-integrin that favours the binding to fibronectin) (Wagner et al. 2011), CD44 (surface receptor for hyaluronic acid) (Strobel et al. 1997) and cancer antigen 125 (CA125) (Rump et al. 2004). Upregulation of MMP-2 enables degradation of fibronectin and vitronectin into smaller fragments, and expression of $\alpha_5\beta_1$ and $\alpha_v\beta_3$ integrins allows cell adhesion to them. Once attached to the mesothelium, OC cells starts to adapt to the new microenvironment and recruit tumour stroma cells, generating a favourable microenvironment that will benefit the formation of a secondary tumour (Lengyel 2010; Mitra 2016; Weidle et al. 2016).

An interesting discovery by Pradeep and colleagues shed light on the ability of OCs to spread via hematogenous dissemination. By using a parabiosis mouse model, where two mice are surgically united to share the blood circulation, the authors demonstrated that SKOV3 ovarian cancer cells are able to spread from the host-mouse (directly injected with SKOV3 cells) to the guest-mouse, by first colonizing the omentum and subsequently reaching the peritoneum and abdominal organs (Pradeed et al. 2014). The process of metastasis in ovarian cancer is incompletely understood and requires

further investigation, and in particular the role of soluble cell signalling factors has been under-explored.

1.3. Extracellular vesicles

1.3.1. Definition and classification

Extracellular vesicles (EVs), are a heterogeneous group of small cell-derived vesicles involved in cell-to-cell signalling, ranging from 30 nm to 5 µm in diameter, surrounded by a lipid bilayer. The EV secretion pathway was described for the first time in 1980's by two different groups studying transferrin receptor (TfR) recycling during reticulocyte maturation (Harding and Stahl 1983; Pan and Johnstone 1983). Though once considered exclusively a way to dispose of cellular waste, EVs are now considered a novel mechanism of cellular communication. EVs can be classified in three major categories: microvesicles, apoptotic bodies and exosomes (Figure 1.4) (van der Pol et al. 2012; Akers et al. 2013). EVs are produced by all cell types and can be found in biofluids such as blood, urine, saliva and even tears (El Andaloussi et al. 2013; Colombo et al. 2014; Doyle and Wang 2019).

Microvesicles are release in the extracellular space by outward budding and scission of the plasma membrane (PM). Their release is the result of a finely regulated and dynamic mechanism involving phospholipid redistribution and cytoskeletal protein contraction. They are heterogeneous in diameter, with a size ranging between 200 nm and 1 µm, and they carry a range of biological molecules including proteins, RNAs and lipids, sharing some similarity with the exosomal cargo, described below (e.g. endosomal sorting complex required for transport (ESCRT) associated proteins and tetraspanins) (Muralidharan-chari et al. 2010; Tricarico et al. 2017).

Apoptotic bodies are large vesicles, with size between 100 nm and 5 µm, released by the blebbing of the PM of cells undergoing apoptosis. Dissociated cytoplasmic, nuclear and organelle fragments are trapped in the forming bleb and are expelled in the extracellular environment. Therefore, apoptotic bodies are characterised by a cytoplasmic component and express tetraspanin surface markers also found in microvesicles and exosomes (Kakarla et al. 2020).

Exosomes are small vesicles, surrounded by a lipid-bilayer, with a diameter between 40 and 150 nm. Exosomes are derived from the endosomal pathway, involved in the internalization of extracellular ligands, their recycling to the PM or their degradation (Gould and Lippincott-Schwartz 2009; El Andaloussi et al. 2013). During maturation into late endosomes, the limiting membrane of the multivesicular body (MVB) undergoes an inward budding, generating intraluminal vesicles (ILVs). Generally, the main fate of MVBs is to fuse with the lysosome and degrade the unwanted biological

material (Mullock et al. 1998); however, years of research highlight a new mechanism by which MVBs can fuse with the PM and release their ILVs into the extracellular milieu. From the moment of release, ILVs are referred to as exosomes (Johnstone et al. 1987). During ILV formation several proteins, lipids, cytosolic component, RNAs and DNAs are actively sorted into them and can be transferred to recipient cells or be released in the extracellular space, facilitating cellular communication (Colombo et al. 2013; Kowal et al. 2014).

Overlap in the size, density and markers between EV subtypes means that these characteristics are not enough to discriminate them. In addition, these overlapping features impede the isolation of homogeneous subpopulations of EVs, as most of the extraction methods are based on size (size exclusion chromatography, ultracentrifugation), density (ultracentrifugation) and affinity to surface biomarkers (immunoaffinity extraction). This project will focus mostly on the functional role of small (50-200 nm) EVs that will be defined as "EVs" throughout this thesis.

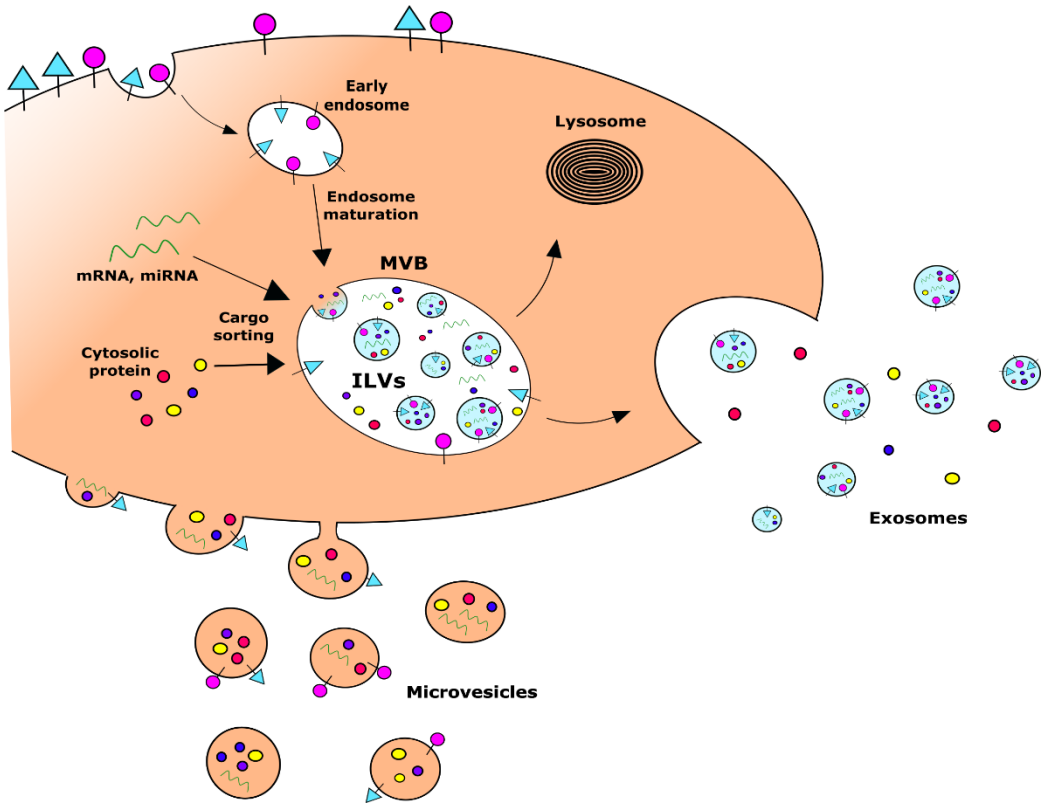

Figure 1.4: Schematic representation of exosome formation.
PM invaginates incorporating cell surface-associated proteins (e.g. receptors, membrane proteins, glycoproteins) forming the early endosome (EE)). Active mechanisms sort RNAs, cytosolic proteins and other biological components into the EE, and intraluminal vesicles (ILVs) began to form. EE matures and forms multivesicular bodies (MVBs); MVBs escape the canonical pathway of fusion with the lysosome and moves to the PM, fuse with it and release the ILVs to the extracellular environment: exosomes are released.

1.3.2. Biogenesis

Exosome biogenesis is the result of the release of the ILVs contained in the MVBs into the extracellular space. MVB biogenesis is driven by at least two different mechanisms: an ESCRT-dependent mechanism and an ESCRT–independent mechanism (Akers et al. 2013). The latter can be triggered by proteins such as tetraspanins (Perez-Hernandez et al. 2013), lipid structures such as ceramide (Trajkovic 2008) or sphingomyelin metabolites (Kajimoto et al. 2013) and other molecules.

The ESCRT machinery is composed by four main protein complexes named ESCRT-0, -I, -II and -III that cooperate with accessory proteins like vacuolar protein associated sorting 4 (VPS4) and Apoptosis-linked gene 2–interacting protein X (ALIX) to generate MVBs (Babst et al. 2002; Henne et al. 2013). ESCRT-0 is responsible for recognition of ubiquitinylated cargo, ESCRT I and II are directly involved in membrane budding, while ESCRT III is responsible for membrane scission (Hurley 2008; Wollert et al. 2009; Hanson and Cashikar 2012). ESCRT-0, through hepatocyte growth factor-regulated tyrosine kinase substrate (HRS), recognises mono-ubiquitylated proteins in the endosomal membrane and sequesters them; then it recruits ESCRT-I complex through TSG101 (tumour susceptibility gene 101 protein). ESCRT I and II interact generating a supercomplex that induces membrane budding. The supercomplex localises mostly at the neck of the bud and stabilises it. The ESCRT-I complex, either via ESCRT-II or by interaction with ALIX, recruits the ESCRT-III that catalyses the scission of the membrane neck (Hurley and Hansin 2010). In order to disassemble the ESCRT machinery, the Adenosine triphosphate(ATP)ase Vps4 is recruited to the membrane. This protein through hydrolysis of ATP provides the energy necessary for membrane budding and scission. Indeed, it has been shown *in vitro* that absence of Vps4 activity induces accumulations of ESCRT machinery to the membrane and blocks cargo processing (Babst et al. 1998).

Several ESCRT-independent mechanisms involved in exosome biogenesis have been identified. When MVBs are formed they need to move towards the PM in order to fuse with it. Their movement towards the PM depends on interaction with actin and microtubules of the cytoskeleton and is regulated by a variety of proteins, of which the Rab Guanosine-5'-triphosphate(GTP)ase family are key components (Hutagalung and Novick 2011). The Rab GTPase are proteins belonging to the Ras GTPases protein family. By switching between GTP- (active) and guanosine diphosphate (GDP)-bound (inactive) states, they regulate various steps of membrane trafficking and associate with membrane transport and fusion in the endocytic pathway (Zerial and Mcbride 2001; Wandinger-Ness and Zerial 2014).

Indeed, the Rab27a and Rab27b proteins have been identified as key regulators of different tasks in the EV release pathway (Ostrowski et al. 2010). Transient transfection of both Rab27a and Rab27b in HeLa (cervical cancer) cells were linked with a reduction in the number of secreted EVs, although their

silencing did not affect their protein content, suggesting that both Rab27a and Rab27b are involved in EV release but do not control cargo sorting (Ostrowski et al. 2010). Specifically, Rab27a silencing in HeLa cells produced bigger MVBs, without altering their localization and reduced their docking to the PM. Therefore, it was suggested that Rab27a is required for docking of MVB at the PM and that in its absence vesicles fuse with each other instead of with the PM, leading to formation of enlarged compartments. In contrast, Rab27b knockdown induced production of smaller, clustered, MVBs mostly localised at the cell periphery, suggesting its involvement in mediating MVB transfer from microtubules to actin-rich cortex (Ostrowski et al. 2010). The role of Rab27a in EV secretion was further confirmed in other research, further highlighting its involvement in EV release (Blanc and Vidal 2018).

Lipids can also mediate EV biogenesis. In fact, lipids are essential players in vesicular transport and collaborate closely with several proteins to control processes like membrane deformation, fission and fusion (Brügger and Bankaitis 2012; McMahon and Boucrot 2015). Lipidomic analyses of EV content have identified high amounts of cholesterol, sphingolipids and ceramides, and low amounts of phosphatidylcholine. Several studies have shown the involvement of lipids in EV biogenesis. Neutral sphingomyelinases (nSMase) are a family of enzymes that hydrolase sphingomyelin (the most abundant lipid in the PM) into phosphorylcholine and ceramide; the latter provides structural rigidity to the PM as well as to the EV membrane (Shamseddine et al. 2015). GW4869, a cell-permeable compound, acts as a potent and specific non-competitive inhibitor of nSMase. Trajkovic and colleagues demonstrated that inhibition of nSMase with GW4869 blocks EV release by decreasing the formation of ceramide. It has been stipulated the cone-shaped structure of ceramide forms a spontaneous negative curvature of the membrane by creating large lipid raft domains that are important for EV biogenesis (Trajkovic et al. 2008). Particularly, GW4869 administration to MCF7 (breast cancer) cells inhibits exosome release, yet inversely increases MV biogenesis (Menck et al. 2017). This is a clear indication that ceramide serves a unique function in the biogenesis of different EV subpopulations (Kosaka et al. 2013).

1.3.3. Cargo and functions

EVs serve as “messengers” between their cell of origin and both neighbouring and distant cells, playing an important role in cell-to-cell communication. EVs carry a variety of biological products like proteins, lipids and nucleic acids (DNA and RNAs) (Villarroya-Beltri et al. 2015) that are taken up by recipient cells and can modify their behaviour.

Lipids

The EV membrane consists of a lipid bilayer with a composition very similar to that of the cell of origin (Llorente et al. 2013). Indeed, different lipids, including sphingomyelin, cholesterol, ceramide and

phosphatidylserine are enriched in EVs and provide them with rigidity and support (Llorente et al. 2013). In contrast, phosphatidylcholine and diacylglycerol are decreased in the EV membrane compared to the membrane of parental cells (Laulagnier et al. 2004). The enrichment of sphingomyelin at the expense of phosphatidylcholine suggests an active phospholipid sorting during EV biogenesis from the MVB limiting membrane. Moreover, the presence of sphingomyelin and unsaturated lipids confers a higher rigidity to the membrane of EVs (Laulagnier et al. 2004). Another major difference between EVs and parental cell PM composition is that phosphatidylserine is redistributed between the two membrane leaflets in the EV membrane, while it is retained on the inner leaflet of the PM (Record 2013; Record et al. 2014). This has been postulated to facilitate EV uptake from recipient cells (Fitzner et al. 2011).

RNAs

The presence of functional RNAs inside EVs and their ability to be transferred to recipient cells was first shown in two different publications (Ratajczak et al. 2006; Valadi et al. 2007). Since then, thousands of publications have demonstrated the presence of messenger RNA (mRNA), microRNA (miRNA), long non-coding RNA and ribosomal RNA (rRNA) inside EVs (Kim et al., 2017; Yáñez-Mó et al., 2015). RNA transferred through EVs can modulate several cellular functions like promotion or suppression of cell survival and proliferation (Bruno et al. 2012), modulation of immune response (Fabbri et al. 2012), increase metastatic burden in mice (Yokoi et al. 2017) or transfer of chemotherapy resistance (Au Yeung et al. 2016).

DNAs

Double stranded DNA, single stranded DNA and mitochondrial DNA have been identified as part of the EV cargo (Cai et al. 2016). The DNA is taken up by target cells where it localises to the cytoplasm or to the nuclei (Waldenström et al. 2012). The function of EV DNA has not been widely explored, but it has been postulated that it could serve as a cancer biomarker (Thakur et al. 2014).

Proteins

Extensive research has focused on the protein content of EVs. EVs are normally highly enriched in cytoskeletal, cytosolic, heat shock and PM proteins, and proteins associated with EV biogenesis and vesicle trafficking machinery (Yáñez-Mó et al. 2015). ESCRT-associated proteins such as ALIX, TSG101, tetraspanins such as CD9, CD63 and CD81 (Escola et al. 1998) are very abundant in EV samples and are often used as “markers” for their characterization. Moreover, proteins involved in signal transduction such as EGF receptor (EGFR), major histocompatibility complex (MHC) I and II and other transmembrane proteins can be found in EVs, while endoplasmic reticulum, mitochondrial, nuclear

and lysosomal markers (such as calnexin, cytochrome C, histones, GM130) are normally absent in EVs and can be used as negative markers during vesicles characterization (Théry et al. 2001; Doyle and Wang 2019).

1.3.4. Roles of EVs in cancer and metastasis

Tumour-derived EVs can induce recipient cells to acquire a tumour-promoting phenotype and are involved in cancer formation, development and progression (Becker et al. 2016; Xu et al. 2018). Additionally, EVs can also affect the tumour microenvironment, inducing angiogenesis, tumour cell invasion and migration, initiate resistance to cell death, evade immune response, reprogram cellular energy metabolism and drug resistance (Peinado et al. 2013; Fang et al. 2018; Fontana et al. 2021).

Angiogenesis

The hypoxic status of a tumour in combination with a lack of nutrients induces endothelial cells (ECs) to form new blood vessels, process described in section 1.2.2. EVs can positively or negatively modulate angiogenesis (Todorova et al. 2017). Tumour derived-EVs can induce angiogenesis by transfer of pro-angiogenic factors including TGF-β1 (Webber et al., 2015), EGFR (Al-Nedawi et al. 2009), miRNA-210 (King et al. 2012; Kosaka et al. 2013) or miRNA-23a (Hu *et al.*, 2017), or by directly stimulating EC proliferation, migration and maturation (Nazarenko et al. 2010). Moreover, EVs can carry a mutant form of VEGF that can activate VEGF receptor, enhancing angiogenesis and inhibiting the therapeutic effect of bevacizumab by binding to it (Feng et al. 2017).

EMT

It has been shown that EVs can play a role in EMT (described in section 1.2.1) by either transport of mesenchymal proteins to recipient cells, or by inducing EMT in recipient cells through release of oncogenic signalling (Greening et al. 2015). Tauro and colleagues have shown that EVs released from cancer cells are highly enriched in metastatic markers (vimentin, MMP-1, MMP-19 and MMP-14) and present low abundance of proteins involved in cell-cell/cell-matrix contact (e.g. E-cadherin, EpCAM) (Tauro et al. 2013). Several studies reported that EVs released from metastatic cell lines can induce mesenchymal features in endothelial cancer cells through delivery of EGFR (Garnier et al. 2012), miRNA-105 (Zhou et al. 2014), or miRNA-200 (Le et al. 2014). Interestingly, EVs derived from more mesenchymal-like cells are able to activate endothelial cells and promote vascular niche formation to a greater extent than EVs released from more epithelial-like cells (Pasquier et al. 2014). In addition, functional experiments have shown that treatment of non-metastatic/normal cells with EVs derived from tumour cells undergoing EMT can induce the EMT phenotype in recipient cells (Galindo-Hernandez et al. 2014).

Invasion and migration

EVs mediate intercommunication between cancer cells and the surrounding tumour microenvironment mediating their invasion and migration (described in section 1.2.2). Tumour-derived EVs can alter the tumour microenvironment and stimulate it to support tumour growth and dissemination (Cho et al. 2011; Webber et al. 2015; Wei et al. 2017). For example, CD44 was found in OC cells-secreted exosomes that were transferred and internalised by human peritoneal mesothelial cells (HPMC). CD44 led to an increase of MMP-9 secretion and down regulation of E-cadherin by HPMC, favouring OC progression (Nakamura et al., 2017). miRNA-21 is shuttled into EVs produced by cancer associated fibroblast (CAF) cells and transferred to OC cell lines. When taken up, miRNA-21 inhibits apoptosis and confers chemoresistance to OCs cells by repressing the translation of the apoptosis protease-activating factor-1 (Au Yeung et al. 2016). In contrast, non-tumour cells can produce EVs that reduce tumour cell migration and invasion (Chen et al., 2017; Luga et al., 2012). In a xenograft mouse model, miRNA-7 has been identified in macrophage-derived EVs. These EVs are taken up by OC cells, decreases the activation of EGFR/AKT/ERK1/2 pathway and inhibits OC metastasis (Hu et al. 2017). EVs have been demonstrated to carry several enzymes that break down the ECM, such as members of the MMP family (Clancy et al., 2015; Hoshino et al., 2013; Runz et al., 2007; Yokoi et al., 2017), a disintegrin and metalloproteinase (ADAM) (Shimoda et al. 2014) and extracellular matrix metalloproteinase inducer (EMMPRIN) (Menck et al. 2015; Colangelo and Azzam 2020). Graves and colleagues identified MMP-2, MMP-9 and uPA in ascites-derived EVs from women affected by OC. Treatment of OC cells with these EVs induced their invasion (Graves et al. 2004).

Several studies have shown that EVs are able to control direction and speed of migrating cells *in vivo* (Sung et al. 2015), stabilise the leading edge protrusion (Sung et al. 2011) and that migrating cells leave an EV trail that might serve as chemotactic signal for other migrating cells (Sung et al. 2020).

Intravasation, circulation and extravasation

In order to migrate to other organs, cancer cells need to enter the blood vessels, circulate in the blood stream and exit at the target site (section 1.2.2). EVs can impair tight junctions, altering the endothelial structure, allowing cancer cells to enter the circulation (Zhou et al. 2014).

Once in circulation, cancer cells need to survive mechanical damage and immunological signalling. Tumour-derived EVs can modulate the immune system in numerous ways, contributing to cancer cell survival (Whiteside 2016). For example, EVs can directly release factors causing apoptosis of T cells (Kim *et al.*, 2005) or, through TGF-β signalling, can stimulate differentiation of myeloid cells thus suppressing the T cell response (Valenti *et al.*, 2006).

Once they reach the target organ, cancer cells need to adhere to the endothelium and enter the tissue. Platelets can support adhesion of cancer cells to the endothelium by inducing E-, L- or P- selectin expression (Natoni et al. 2016). Platelet-derived EVs contain P-selectin and aid extravasation (Heijnen et al. 2014).

Secondary tumour formation

Prior to the formation of hematogenous metastasis, cancer cells can prime target organs by forming "pre-metastatic niches", favourable microenvironments that support their survival and outgrowth. Numerous cells, chemokines, cytokines and other soluble factors are needed for pre-metastatic niche formation (Peinado et al. 2017). EVs actively contribute to this process by increasing vascular leakiness (Zhou et al. 2014), stimulating resident stromal cells (Hoshino et al. 2015) and modulating the immune response (Costa-Silva et al. 2015).

Hoshino and colleagues (2015) showed that EVs from breast (MDA-MB-231 and MDA-MB-468) and pancreatic (BxPC-3 and HPAF-II) cancer cell lines could 'colonise' specific metastatic sites and could 'direct' circulating tumour cells to the secondary site. This suggests that organotropic tumour EVs prime pre- metastatic niches to facilitate metastasis. Moreover, the authors show that EV organostropism was related to expression of specific integrins, such as ITG-β4 (Hoshino et al. 2015). The role of EVs in organotropic metastasis was further confirmed by Costa-Silva et al (2015); the authors demonstrated that EVs derived from pancreatic cancer cells are able to "educate" the liver of wild-type mice for metastatic colonization. EVs are taken up by Kupffer cells (stellate liver macrophages) where they induce TGF-β release. TGF-β stimulates production of fibronectin from hepatic stellate cell and recruits bone marrow-derived macrophages and neutrophilis, 'priming' the site for further liver metastasis (Costa-Silva et al. 2015).

Although the role of EVs in different aspects of cancer has been extensively studied, several questions remain concerning the mechanisms of EV release from cancer cells and how this may influence EV content and function.

1.4. Histamine

1.4.1. Histamine biogenesis and functions

Histamine (2-[4-imidazolyl]-ethylamine) is an endogenous biogenic amine that lately has been proposed to be involved in cancer progression and EV biogenesis. Histamine was first identified in the human body in 1927 (Best et al. 1927). It is synthesised from the amino acid L-histidine through

oxidative decarboxylation by the L-histidine decarboxylase enzyme (HDC) (Schayer 1952) and it is rapidly metabolised by the histamine N-methyltransferase (HMT) or diamine oxidase (DAO) (Maslinski and Fogel 1991) (Figure 1.5).

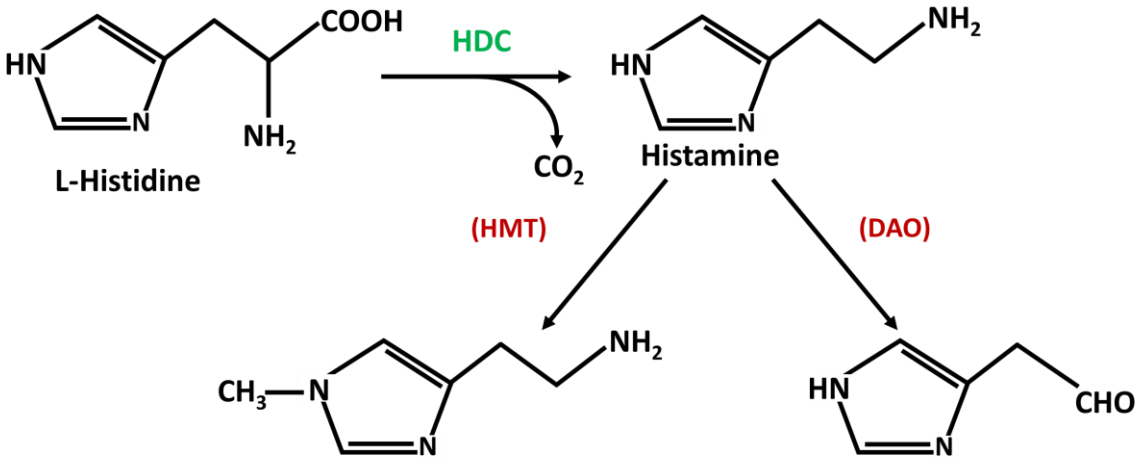

Figure 1.5: Schematic representation of histamine biogenesis and metabolism.
Histidine decarboxylase (HDC) removes a carboxylic group from the amino acid L-histidine inducing synthesis of histamine. Histamine is degraded by two different enzymes: 1) histamine N-methyltransferase (HMT) is a cytosolic enzyme and inactivates histamine by methylating the imidazole ring. 2) Diamine oxidase (DAO) is located extracellularly and inactivates histamine by removing its amino group.

Histamine is produced by many cell types that can be classified in two categories: 1) *de novo* producers, such as enterochromaffin-like cells (endocrine cell found in the digestive tract, responsible for the production of gastric acid) and neurones, that produce and directly release histamine without storing it and 2) *storing cells* like mast cells, platelets and basophils, where histamine is produced and then stored in secretory granules and released upon certain stimuli. There are several factors that induce histamine release, including allergens crosslinking with the receptor FcεRI, neuropeptides, cytokines, chemokines, complement factors, lipoprotein, hyperosmolarity, hypoxia, superoxidases, physical factors like extreme temperature, certain foods, and alcohol (Jutel et al. 2009). By activation of its four receptors, histamine regulates a plethora of physiological processes including vasodilation and vasoconstriction, increase/reduction of vascular permeability, smooth muscle contraction/relaxation (in particular in the bronchi and intestine), and increased mucosal and gastric secretion (Patel and Mohiuddin 2020). Histamine has also been shown to play various roles in neurotransmission, immune modulation (by increasing immune cell chemotaxis towards sites of inflammation), modulation of allergic reactions, haematopoiesis, and regulation of cell differentiation, proliferation and regeneration, in both health and in pathological conditions (Ichikawa et al. 2012). Indeed, recent studies on histamine receptors have demonstrated that the histamine pathways extend well beyond its established role (Medina et al. 2011)

1.4.2. Histamine receptors

Histamine receptors are a family of G protein-coupled receptors (GPCRs) named histamine receptor 1 (HRH1), histamine receptor 2 (HRH2), histamine receptor 3 (HRH3) and histamine receptor 4 (HRH4). Histamine receptors share the GPCR common structures: they contain seven transmembrane segments, an extracellular amino terminus domain and an intracellular carboxyl terminus domain. While the extracellular domain forms a ligand-binding pocket, the cytoplasmic region interacts with the soluble signal (G protein) and with an "effector component" that leads to the biological response (Kobilka 2007). Histamine receptors are widely distributed, they are activated by different stimuli, bind to different Gα protein subunits ($G\alpha_s$, $G\alpha_{i/o}$, $G\alpha_{q/11}$, and $G\alpha_{12/13}$) and exert a variety of effects (Figure 1.6).

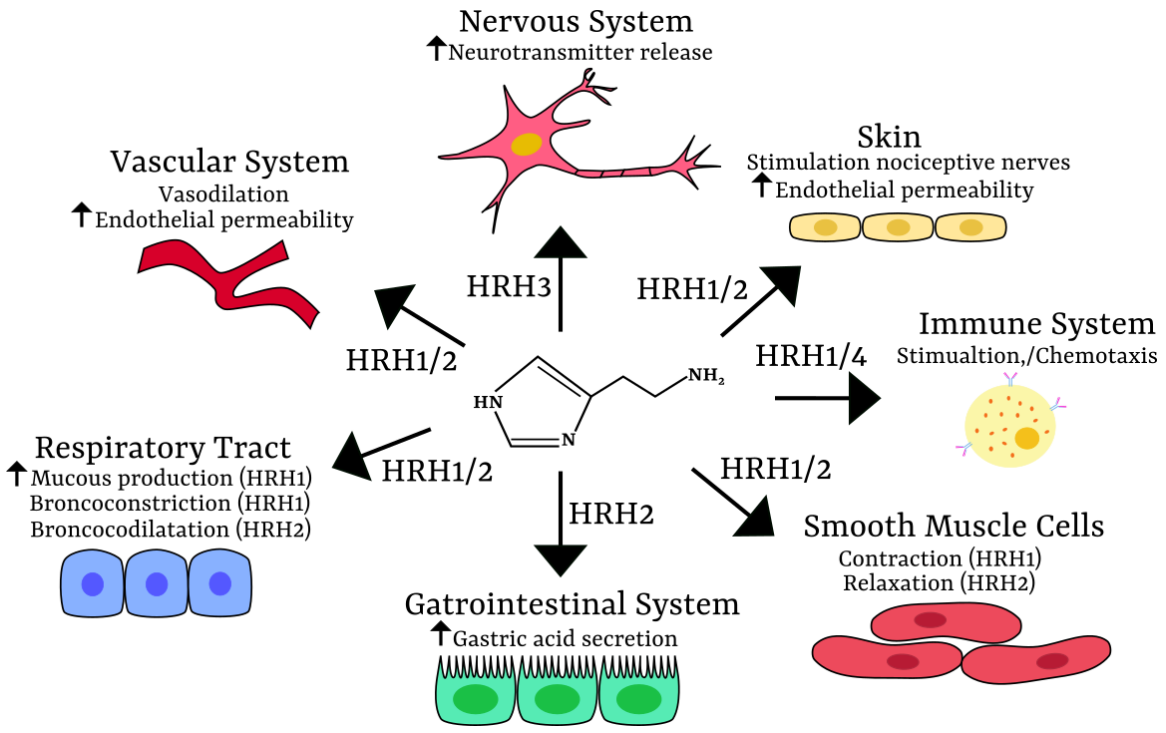

Figure 1.6: Schematic representation of the effect exerted by histamine through the activation of its four receptors.

Histamine is implicated in several pathophysiological effects in the body. Via activation of HRH1, histamine induces vasodilatation and increases endothelial permeability, stimulates nociceptive nerves in the skin, activates the immune system and mediates inflammation, induces contraction of smooth muscle cells in the bronchi and urinary tract and induces mucus deposition in the airways. HRH2 mediates vasodilatation, induces relaxation of muscle cells in the respiratory tract and in the bladder and stimulates gastric acid secretion. HRH3 is mostly located in the brain and serves autoreceptor and heteroreceptor functions, it decreases release of histamine, acetylcholine and serotonin, modulates nociception and food intake. HRH4 activates the immune system, controls cytokine production and regulates chemotaxis in mast cells and eosinophils.

Histamine receptor 1 (HRH1)

HRH1 is encoded by a gene located on chromosome 3p25 (Fukui et al. 1994). The encoded receptor is a 487 amino acids long $G\alpha_{q/11}$ coupled protein, characterised by a large III intracellular loop and a short C-terminal domain. HRH1 is mostly expressed on the surface of blood vessels and sensory nerves, but it has also been identified in the gastrointestinal tract, hepatocytes, chondrocytes, monocytes, neutrophils, dendritic cells, T and B lymphocytes (Shahid et al. 2010). When phosphorylated, HRH1 activates its downstream effector phospholipase C (PLC), which breaks down phosphatidylinositol 4,5-biphosphate into inositol 1,4,5-triphosphate and 1,2-diacylglycerol (Gutowski et al. 1991); the two products induce an increment of intracellular Ca^{2+} level that results in smooth muscle contraction, blood vessel dilatation and rise in vascular permeability. HRH1 is responsible for regulating the allergic response and inflammation (Shahid et al. 2010; Monczor and Fernandez 2016). However, an increasing amount of evidence suggests that HRH1 can be activated regardless of its binding with a ligand. Its constitutive activation can control gene expression by interaction of the $G_{\beta\gamma}$ subunits with the nuclear

factor-κB (Bakker et al. 2001). In addition, HRH1 can also signal outside its canonical pathway, and activates several factors such as adenylyl cyclase (AC) with consequent accumulation of 3',5'-cyclic adenosine monophosphate (cAMP) and activation of the mitogen activated protein kinases (MAPKs) (Robinson and Dickenson 2001; Buschauer et al. 2015), signal transducer and activator of transcription (STAT) 1 (Sakhalkar et al. 2005), STAT4 (Liu et al. 2006), production of nitric oxide (Leurs et al. 1991) and arachidonic acid release from phospholipids (Murayama et al. 1990). Several studies have highlighted the involvement of HRH1 in pathological processes like cancer cell growth, proliferation and survival (Rivera et al. 2000; Medina and Rivera 2010).

Histamine receptor 2 (HRH2)

HRH2 is encoded by an intron-less gene located on chromosome 5q35 and was first discovered in 1972 by Sir James Black (Black et al. 1972). Like HRH1, HRH2 is expressed by a variety of cells including gastric mucosal, parietal, smooth muscle, heart, endothelial, epithelial, neuronal and immune cells. HRH2 is coupled with a $G\alpha_s$ and therefore when activated it binds to the downstream effector adenylyl cyclase (AC), generating cAMP that activates several effectors including protein kinase A (PKA) (Traiffort et al. 1992). HRH2 stimulation induces gastric secretion (Black and Shankley 1985) and heart contraction (Hescheler et al. 1987). In several processes, HRH2 activation antagonises HRH1 effects; for example, in the respiratory system, HRH1 induces smooth muscle cell contraction and consequent bronchoconstriction, whereas HRH2 activation leads to dilation of smooth muscle cells and bronchodilation (Nathan et al. 1981). Interestingly, some of the effects exerted through HRH2 are a consequence of the activation of alternative pathways, such as the activation of tyrosine kinase receptors such as ERK1/2 or PI3K (Luo et al. 2013; Alonso et al. 2016).

Histamine receptor 3 (HRH3)

The *HRH3* gene is located on chromosome 20q13 and, in contrast to HRH1 and HRH2, many of its splice variants have been identified (Drutel et al. 2001). HRH3 is mostly expressed in different areas of the brain and in nociceptive fibres, and it mediates several neurological functions like memory and feeding processes and the sleep-wake cycle (Pillot et al. 2002). An interesting function of HRH3 is its ability to inhibit the release of several neurotransmitters including dopamine, GABA, acetylcholine, noradrenaline, glutamate and histamine itself (Nieto-alamilla and Márquez-gómez 2016). HRH3 is coupled with a $G\alpha_{i/o}$ protein and negatively regulates the activity of AC and its downstream pathway (Clark and Hill 1996; Lovenberg et al. 1999). Its activation can also result in the stimulation of non-

canonical pathways, such as MAPK, PI3K and phospholipase A_2, and it can also impair the function of ion channels.

Histamine receptor 4 (HRH4)

HRH4 is encoded by a gene located on chromosome 18q11 and it is mostly expressed in the bone marrow, spleen, thymus, liver, intestinal cells and peripheral cells like neutrophils, eosinophil, mast cells and T cells (Nakamura et al. 2000; Zhu et al. 2001). HRH4 is functionally coupled to a $G_{i/o}$ protein, that inhibits AC and its downstream signalling pathway; in addition HRH4 activation can stimulate MAPK and PLC (Oda et al. 2000). HRH4 seems to cause chemotaxis of mast cells and eosinophils, control of cytokine secretion, and activation of immune cells (Gantner et al. 2002; Hofstra et al. 2003; Ling et al. 2004).

1.4.3. HRH1 and cancer

The involvement of histamine in cancer progression and metastasis has been studied since the 1960s (eg Kahlson and Rosengren 1968), but its role still remains controversial. Immunohistochemistry has shown that histamine content increases in some human cancer tissues like ovarian, endometrial and cervical carcinoma when compared with adjacent healthy tissue (Chanda and Ganguly 1995; Predescu et al. 2019). In particular, bioinformatic analysis discovered HRH1 expression in several cancer tissues including brain, bladder, colorectal, breast, lung, head and neck, skin and ovarian cancers, and its association with prognosis was different in different cancer types (Wang et al. 2014). For instance, high levels of expression of HRH1 were correlated with poor prognosis in lung cancer, soft tissue cancer, brain cancer, colorectal cancer and B-cell lymphoma, while low levels of HRH1 expression were related with poor survival in multiple myeloma, bladder, ovarian and eye cancers. It is important to note that the relationship between HRH1 expression and prognosis varied between different cancer types, and even between different cases of the same cancer type; indeed, out of six breast cancer samples, low expression of HRH1 was associated with poor survival in three cases, while high levels of HRH1 were related to poor survival in the other three cases. The authors proposed that HRH1 does not function only as a tumour suppressor or oncogene, but its function is multidimensional (Wang et al. 2014).

The molecular function of HRH1 in OC has mostly been studied using cell lines. Histamine activation of HRH1 stimulates Ca^{2+}accumulation that triggered OVCAR3 (an OC cell line) proliferation; this response is abrogated by administration of pyrilamine, an HRH1 antagonist (Popper and Batra 1994). Similar findings were also confirmed in SKOV3 cells (another OC cell line), where HRH1 activation upon histamine treatment stimulates their proliferation (Batra and Fadeel 1994).

Moreover, the involvement of HRH1 in cell growth and in cell behaviours associated with different steps of the metastatic cascade has been demonstrated. Administration of histamine or HRH1 specific agonist decreases PANC-1 (pancreatic cancer cell line) cell adhesion to plastic, augmentes their motility in a wound healing assay and increases the gelatinolytic activity of MMP-2 in a zymography assay (Cricco et al. 2006). These effects led the authors to propose that histamine may play a crucial role in tumoral progression towards metastasis in pancreatic carcinoma cells (Cricco et al. 2006). In breast cancer cell lines, HRH1 pharmacological inhibition leads to the suppression of cell proliferation, through sub-G0 accumulation, and promotion of cell motility and apoptosis via activation of ERK signalling pathway (Fernández-Nogueira et al. 2018). Similarly, Stoyanov and colleagues (2012), through cell proliferation and BrdU uptake analysis, demonstrated that histamine administration to lung cancer (A549) cells induces their proliferation and increases DNA synthesis; indeed, co-incubation of A549 cells with both histamine, pyrilamine (HRH1 antagonist) and cimetidine (HRH2 antagonist) significantly decreases cell proliferation, further supporting the involvement of histamine in cell growth. The authors also demonstrated that this effect was due to activation of ERK signalling (Stoyanov et al. 2012). Genotoxic effects and inhibition of cell migration and invasion attributed to HRH1 pharmacological inhibition have also been shown in melanoma and bladder cancer cell lines (Jangi et al. 2006; Ma et al. 2020). Histamine signalling is therefore associated with proliferation and different aspects of metastatic cell behaviour, including cell migration, adhesion and expression of proteolytic enzymes, but its precise role in OC progression remains to be clearly defined.

1.4.4. HRH1 and EVs

Very little is known regarding the involvement of histamine in EV biogenesis and release. Verweij and colleagues (2018), used Total Internal Reflection Fluorescence (TIRF) microscopy to show that constant administration of histamine to HeLa (cervical cancer cell line) and HUVEC (primary endothelial cells) cells immediately increases the number of CD63 positive MVB fusing with the PM. By monitoring intracellular Ca^{2+} level through TIRF microscopy, they observed a 10 second delay between EV release and calcium entry in the cell, suggesting that histamine- induced EV release is a calcium independent event that does not require Ca^{2+} influx. Phospho-proteomic analysis revealed that the rise in the release of EVs is due to the activation of a protein network starting with HRH1 and ending with activation of synaptosomal-associated protein 23 (SNAP23), a N-ethylmale-imide-sensitive factor-attachment protein receptors (SNARE) protein involved in membrane fusion events (Verweij et al. 2018). This was the first publication linking HRH1 activation with EV release. The same year, another paper showed that the use of the antihistamine ketotifen, a HRH1 selective antagonist, reduced EV biogenesis in cervix and breast cancer cells (Khan et al. 2018). Although initial evidence shows an active

involvement of HRH1 in EV release, further work is needed to decipher the role of histamine and HRH1 in EV release and the molecular mechanisms involved.

1.5. Aims and objectives

EVs are mediators of intercellular communication and have been reported to play key roles in all stages of the metastatic cascade. Recent findings highlight an involvement of histamine in EV production. This discovery, together with the emerging role of histamine in cancer development and progression points to the possibility that histamine, by modulating EV release, can regulate cancer progression and dissemination. In this project, it was hypothesised that histamine, via activation of HRH1, could induce EV release and modify metastasis-related properties of OC cell lines.

The aims of this project were to 1) investigate the expression of HRH1 in different models of OC and its role in different steps of the metastatic cascade and 2) to study if HRH1 could regulate EV release and how this affects OC invasion *in vitro*. The specific objectives were:

- To investigate HRH1 expression in OC cell lines and in clinical samples of OC and validate HRH1 expression in in three different OC cell lines

- To study whether HRH1 inhibition or activation can modify metastasis-associated cellular behaviours of OC cells *in vitro*

- To understand how HRH1 affects EV biogenesis and content, with particular focus on the role of EVs in modulating cell invasion and matrix degradation *in vitro*

Chapter 2

Materials and methods

2. Materials and methods

2.1. Cell culture

2.1.1. Cell lines

All the different cell lines used in this project are listed in Table 2.1. Three different OC cell lines were used: SKOV3, OVCAR3 and OVCAR5 and were purchased from the National Cancer Institute, Frederick Cancer Division of Cancer Treatment and Diagnosis Tumour/Cell Line Repository (Bethesda, USA). These cell lines were chosen to have a selection of cells characterised by a different invasion potential *in vitro* (Hallas-potts et al. 2019). SKOV3 are one of the most invasive OC cell line available and they are highly tumorigenic *in vivo* (Elias et al. 2015). OVCAR3 are described as a poorly invasive and migrating cell line *in vitro* and *in vivo* (Lokman et al. 2012). Previously unpublished data from our lab show that OVCAR5 are more invasive than OVCAR3 cells but less than SKOV3. HME (immortalised epithelial breast cells) were obtained from ATCC (American Type Culture Collection) and were used as calibrator to normalise for HRH1 expression analysis. HUVEC cells were used to study the adhesive behaviour of OC cells and were purchased from Lonza.

Table 2.1: Cell name, place of origin and growth conditions for all cells used in this project.
Percentages of concentration are given as v/v. Roswell park memorial institute medium (RPMI); endothelial cell growth basal media (EBM), Dulbecco's Modified Eagle Medium/Nutrient Mixture F-12 (DMEM/F12); foetal bovine serum (FBS); human fibroblast-derived growth factor- β (hFGF-β); vascular endothelial growth factor (VEGF); recombinant analogue of insulin growth factor (R3-IGF-1); epidermal growth factor (EGF).

Cell line	Type	Origin	Medium	Supplements	Purchased from
SKOV3	Epithelial, serous carcinoma	Ovary, ascites (Fogh J., 1975)	RPMI-1640 (Gibco™)	10% FBS (Gibco™)	National Cancer Institute
OVCAR3	Epithelial, HGSC	Ovary, ascites (Hamilton T.C et al., 1982)	RPMI-1640 (Gibco™)	10% FBS (Gibco™)	National Cancer Institute
OVCAR5	Epithelial, HGSC	Ovary, ascites (Hamilton T.C. et al., 1984)	RPMI-1640 (Gibco™)	10% FBS (Gibco™)	National Cancer Institute
HUVEC	Human umbilical vein/vascular endothelial cells (primary cell)	Umbilical vein/vascular endothelium (Hoshi and McKeehan, 1984)	EBM-2 (Lonza)	• 2% FBS • 0.4% hydrocortisone • 0.1% hFGF-B • 0.1% VEGF • 0.1% R3-IGF-1 • 0.1% EGF • 0.1% Gentamycin and amphotericin	Lonza
hTERT-HME1	Human epithelial breast non-cancer cell line	Mammary epithelium of patient undergoing reduction mammoplasty surgery (no cancer history) (Van der Haegen and Shay, 1993)	DMEM/F12 (Sigma-Aldrich®)	• 10% FBS (Gibco™) • 20 ng/mL EGF (PeproTech®) • 10 g/ml insulin (Sigma-Aldrich®) • 100 g/ml hydrocortisone (Sigma-Aldrich®)	American Type Culture Collection

2.1.2. Cell revival from frozen stock

A 25cm^2 (OVCAR3, HUVEC) or a 75cm^2 (SKOV3, OVCAR5, HME) cell culture flask was filled with 3 ml or 10 ml of pre-warmed complete media, respectively, and placed into a 37°C cell culture incubator with 5% CO_2 v/v atmosphere in order to equilibrate the medium. All cell lines were thawed from liquid nitrogen in a 37°C warm water bath until ice was completely melted. Once fully thawed, the cell suspension was transferred to a 15 ml Falcon tube containing 10 ml of pre-warmed complete media and spun down at 300 x rcf for 5 minutes. The supernatant was discarded, cells were re-suspended in 5 ml of complete media and then transferred to the pre-equilibrated cell culture flask, that was then placed back in a cell culture incubator.

2.1.3. Cell sub-culturing

Cell confluence was assessed every day by using a Nixon TMS inverted microscope. Media was removed and replaced with fresh pre-warmed complete media every two days when cultures were

less than 75% confluent. When cultures were more than 75% confluent, they were passaged to maintain cell growth. Media was removed and cells washed with phosphate-buffered saline (PBS) (GIBCO™). Tryspin/ethylenediamine tetra acetic acid (EDTA) (Gibco™) 0.5% w/v in PBS was added in sufficient amount to cover the entire surface of the flask (e.g., 1 ml for 25cm^2 flask, 3 ml for 75cm^2 flask, 5 ml 175 cm^2 flask). Flasks were placed back in the incubator until cells were fully detached (usually 5 minutes). Once cells were fully detached, pre-warmed complete media was added to the flask to inactivate the trypsin. The minimum amount of media added was at least 2X the amount of trypsin/EDTA used. Cell suspension was transferred to a 50 ml Falcon tube and spun down at 300 x rcf for 5 minutes. Media was then discarded, and the cell pellet re-suspended in 10 ml of media. One ml of the re-suspended cells was added to a new 75cm^2 flask and the remaining 9 ml were discarded; flask was returned to the cell culture incubator.

2.1.4. Freezing and stock

Cell stocks were made to ensure availability of cells at early passage for subsequent experiments. Cells were detached and spun down following the method described previously (section 2.1.3); once spun down, 1,000,000 cells were re-suspended in 1 ml freezing media (50% complete medium + 40% foetal bovine serum (FBS) + 10% dimethyl sulfoxide (DMSO) (Corning ™)) and placed in cryogenic vials (Thermo Fisher Scientific). The vials were placed in a Mr Frosty™ freezing container (Nalgene™) and placed at -80°C. The use of a Mr Frosty freezing container allows temperature to decrease gradually (one degree per minute). After one day, vials were transferred to liquid nitrogen for long-term storage.

2.1.5. Cell count

Cell were brought into suspension following the protocol previously described in section 2.1.3. Once spun down, the cell pellet was re-suspended in 1 ml of pre-warmed media. Ten µl of cell suspension was mixed with 10 µl of trypan blue (BioRad), and then the mix was placed into cell counting slides (BioRad) in duplicate and counted using a TC10™/TC20™ Cell Counter (BioRad).

2.2. Mycoplasma contamination testing

Mycoplasmas are small bacteria not visible when imaging cells with light microscopy. Mycoplasmas can modify cell characteristics upon infection (e.g. cell growth, metabolism and morphology) (Drexler and Uphoff 2002). Therefore, it is important to regularly test cell lines and adopt good laboratory practice. In order to test cell lines for mycoplasma contamination, DNA was isolated from cultured cells. Briefly, cells were cultured for 2 - 3 days in a 25 cm^2 flask (no medium change) until approximately 60-80% confluent. The cells were detached from the flask using cell scrapers. Approximately 4 ml of cell suspension were transferred in centrifuge tubes and spun at 10,000 x rcf for 15 minutes to pellet

the cells and any floating microorganisms, including mycoplasma. The supernatant was discarded, and the pellet was re-suspended in 200 µl PBS. The DNA was extracted using a PureLink® Genomic DNA Kit (Invitrogen™), following the manufacturers' instructions. The DNA was eluted in 50 µl PureLink™ genomic elution buffer. DNA concentration and purity were quantified using the NanoDrop™ One Microvolume UV-Vis spectrophotometer (Thermo Fisher Scientific). All DNA samples were diluted to 50 ng/µl and the e-Myco™ mycoplasma polymerase chain reaction (PCR) detection kit (iNtRON) was used following the manufacturer's instructions. PCR products with positive and negative controls were run on a 2% agarose gel with SafeView nucleic acid stain (nbs biologicals) and examined for mycoplasma presence (Figure 2.1).

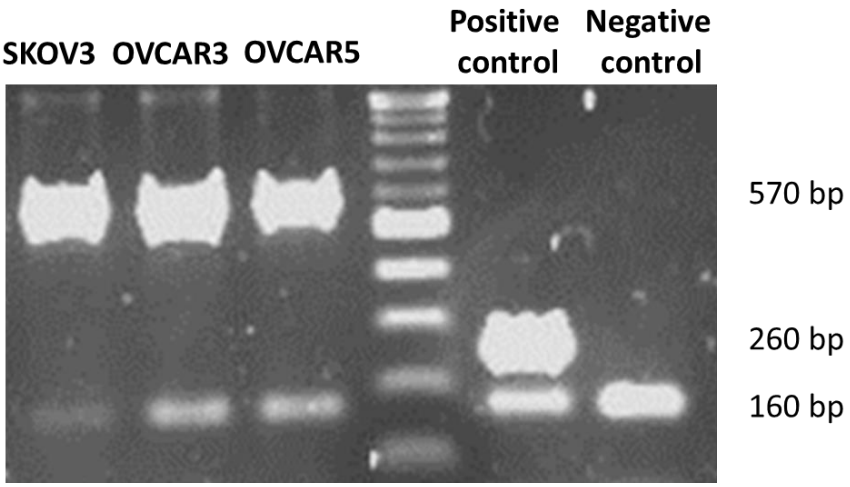

Figure 2.1: Mycoplasma testing of SKOV3, OVCAR and OVCAR5.
PCR product analysis of the mycoplasma test in the three ovarian cancer cell lines. From left to right: SKOV3, OVCAR3, OVCAR5, 100 bp DNA ladder, positive control, negative control. The 160 pb band indicates the amplification of TNFα and it is used as internal control. The 260 bp band in the positive control indicates mycoplasma contamination. The 570 bp band serves as a sample control and is the amplification product of a human/ mammalian-specific gene. The absence of the 260 bp bands in experimental samples indicates the absence of mycoplasma infection.

2.3. Short tandem repeat profiling

Short tandem repeat (STR) profiling is the analysis of short tandem repetitive sequences in the human genome; these sequences are highly variable among individuals and can be used for identification purposes. As it has been reported that cell lines can be cross-contaminated with other cell lines (Drexler et al. 1999), it is important to frequently authenticate them. SKOV3, OVCAR3 and OVCAR5 were cultured for 2 - 3 days in a 25 cm^2 flask (no medium change) until approximately 60-80% confluent and then DNA was isolated as described in section 2.2. A sample of the same DNA that was used for mycoplasma testing (section 2.2) was sent to the University of Liverpool, Institute of Translational Medicine, for STR profiling. The GenePrint® 10 System (Promega) was used, following the manufacturers' protocol. A PCR reaction was run on 5 ng of DNA to amplify 9 genetic loci (D5S818,

D13S317, D7S820, D16S539, VWA, TH01, AM, TPOX, CSF1PO). The products and the allelic ladder were then mixed with a size standard and fragment analysis was performed using the 3130 Genetic Analyser (Applied Biosystems). The results obtained from the genetic analyser were compared against the ATCC STR profile information of each cell line (Table 2.2)

Table 2.2: Authentication of SKOV3, OVCAR3 and OVCAR5.

Cell line	D5S818	D13S317	D7S820	D16S539	vWA	TH01	AM	TPOX	CSF1PO
SKOV3 ATCC	11	8,11	13,14	12	17,18	9,9.3	X	8,11	11
SKOV3 experiment	11	8,11	13,14	12	17,18	9,9.3	X	8,11	11
OVCAR3 ATCC	11,12	12	10	11	17	9,9.3	X	8,	11,12
OVACR3 experiment	11,12	12	10	12	17	9	X	8	11,12
OVCAR5 ATCC	11,13	10,13	10	11	16	7,9.3	X	8,11	10
OVCAR5 experiment	11,13	10,13	10	11	16	7,9.3	X	8,11	10

2.4. Transfection

In this project HRH1 and Rab27a were knocked down by using transient transfection with siRNA. Briefly, SKOV3, OVCAR3 and OVCAR5 were plated in 6 well plates (Table 2.3) and grown until they reached 70% confluency. Cells were next transfected by using DharmaFECT 3 (Thermo Fisher Scientific), following manufacturers' protocol. The following siRNA were used for transfection: 50 nM of MISSION® siRNA universal negative controls (Sigma®, construct without homology for any known sequence, 5 μM stock), 50 nM of a siRNA silencer specific for HRH1 (Thermo Fisher Scientific, 5 μM stock), 50 nM of Rab27a siRNA (siGENOME, SMARTPool, 5 μM stock). Equal volumes of siRNA control (tube A) and siRNA targeting a specific gene (tube B) mixes and double the volume of DharmaFECT (tube C) mix (Table 2.4) were prepared. Mixes were equilibrated at room temperature (RT) for 5 minutes. Tube C content was divided in 2 equal volumes and added to tube A and tube B, mixed to ensure the formation of a homogeneous solution and let stand for 20 minutes at RT. One point six ml of fresh serum free media (SFM) was added to each well, and then 400 μl of mix A or mix B were added to the well. Cells were then placed back in a cell culture incubator for 24 h, and then used for downstream application.

For TIRF microscopy (see section 2.18), SKOV3 were transfected by using a tetraspanin (TSPAN)-based optical reporters with a pH sensitive green fluorescent protein (GFP) (pHluorin) reporter. In this specific case a CD81-pHluorin was used for transfection and was kindly provided by Professor Aled Clayton, Cardiff University. Briefly, SKOV3 were plated in an 8 well glass bottom μ-slide (Thistle Scientific) and cultured until they reached 60% confluency. Cells were then transfected with 500 ng of CD81-pHluorin

DNA by using the FuGENE HD transfection reagent (Promega). A ratio of 3:1 FuGENE to DNA was used for transfection following manufacturer's instruction.

Table 2.3: Number of cell/well used for experiment.

Cell type	Number of cell/well
SKOV3	1×10^5
OVCAR3	1.5×10^5
OVCAR5	1.5×10^5

Table 2.4: Quantities used to make transfection mixes A, B and C.

Component	Tube A (50 nm)	Tube B (50 nm)	Tube C
siRNA Control	20 µl of 5 uM stock	--	--
siRNA HRH1 or Rab27a	--	20 µl of 5 uM stock	--
DharmaFECT	--	--	4 µl
SFM	180 µl	180 µl	396 µl
Final volume	200 µl	200 µl	400 µl

2.5. Gene expression

2.5.1. RNA extraction

For RNA extraction the Direct-zol RNA MiniPrep Kit (ZymoResearch) was used following the manufacturers' instructions. Briefly, cells were lysed in TRIzol and either processed or stored at -80°C up to one week. An equal volume of 96% ethanol was added to the mix. The mix was moved to a Zymo-spin IIC column and spun at 14,500 x rcf for 1 minute. The column was washed with 400 µl of RNA wash buffer. A first DNAse treatment was done by adding 5 µl of DNase I and 75 µl of DNA digestion buffer on the top of the membrane and incubating for 15 minutes at RT. The column was washed two times with 400 µl of Direct-zol RNA prewash liquid and then with 700 µl of RNA wash buffer followed by a dry-spin at 14,500 x rcf for 1 minute. RNA was eluted in 30 µl nuclease-free water. Concentration and purity of RNA were measured using the NanoDrop™ One Microvolume UV-Vis Spectrophotometer (Thermo Fisher Scientific).

2.5.2. DNAse I treatment

Before performing a RT-qPCR it is good practice to perform a DNAse I treatment to eliminate all the genomic DNA (gDNA) that can be carried over in the RNA preparation. DNase I is an endonuclease able to digest single stranded and double-stranded DNA into mono and oligonucleotides. Although most of the primers used to amplify the complementary DNA (cDNA) were designed only to bind at the exon-exon junction, this was not achieved for HRH1 primers making it difficult to discern between gDNA and cDNA. For this reason, two DNase I treatments were performed on all RNA samples. The first treatment was made during RNA extraction (section 2.5.1). The second treatment was done using the AMPD1-1KT DNase I kit (Sigma-Aldrich®) with modification to the manufacturers' instructions. Samples were prepared in 8-well strip as described in the optimization section of Table 2.5. The mix was incubated for 30 minutes at RT (instead than 10 minutes as suggested by the manufacturer); 1 µl of Stop solution was added and DNase I was inactivated by placing samples at 70°C for 10 minutes. High temperature is also able to denature RNA hairpins so that it can be directly reverse transcribed. Samples were then placed on ice for 2 minutes before proceeding with the reverse transcription protocol (section 2.5.3).

Table 2.5: Components and quantities used to prepare DNAs I mix.

Component	Quantity per sample (manufacture's instruction)	Optimization
RNA ng	DNase I digests up to 1 mg of plasmid DNA in 10 minutes	300 ng
10 x Reaction Buffer	1 µl	2 µl
DNase I amplification grade, 1 unit/ µl	1 µl	2 µl
Nuclease- free water	Up to 10 µl	Up to 10 µl
Final volume	10 µl	10 µl

2.5.3. Reverse transcription (RT)

Reverse transcription (RT) is a technique used to generate cDNA starting from a single stranded RNA. This technique allows to analyse RNA through PCR techniques. In this project a 2 steps RT-qPCR was used. The High Capacity cDNA Reverse Transcription Kit (Thermo Fisher Scientific) was used following the manufacturer's instructions (Table 2.6). Ten µl of the mix were added to each RNA tube and the thermal profile was performed (Table 2.6). When the reaction ended, 60 µl of nuclease-free water were added to each sample before processing them.

Table 2.6: Reverse transcription components, quantity, and thermal profiler.

Component	Quantity per sample
10X RT Buffer	2 µl
10X Rt Random Primers	2 µl
25X dNTP Mix (100 mM)	0.8 µl
MultiScribe™ reverse Transcriptase, 50 U/ µl	1 µl
Nuclease-free water	4.2 µl
Final volume	10 µl

	Step 1	Step 2	Step 3	Step 4
Temperature (°C)	25	37	85	4
Time	10 min	2 h	5 min	∞

2.5.4. Real time PCR

Real time PCR or quantitative PCR (qPCR) is a technique that allows the amplification of a targeted DNA molecule to be monitored in real time, enabling quantitative comparisons to be made between samples. In this project two different methods were used to quantify gene expression: 1) a DNA-binding dye, SYBR Green, was used to detect amplified DNA of HRH1, Rab27a and β-Actin (ACTB) while 2) TaqMan assay was used to identify EMT markers and ACTB. ACTB was used as house-keeping gene in both experiments. Before selecting this gene, four different house keeping genes including ACTB, Glyceraldehyde 3-phosphate dehydrogenase (GAPDH), Pumilio RNA Binding Family Member 1 (PUM)1 and Glucuronidase β (GUSβ) were tested as suggested by (Li et al. 2009). Genes stability was analysed through geNorm and ACTB was selected for further experiments.

2.5.4.1. SYBR Green

SYBR Green binds to the double strand DNA that is generated during the PCR, increasing the fluorescence yield of the dye. The more DNA that is produced during the PCR, the more fluorescence is detected at each cycle. This fluorescence is captured with a detector. iTaq Universal SYBR Green Supermix (2X) was purchased from BioRad. Primers for HRH1 and ACTB were designed using OLIGO 7 software (Molecular Biology Insights) and purchased from Sigma-Aldrich® (Table 2.7). Primers for Rab27a were obtained from the following publications (Dong et al. 2012; Nanbo et al. 2018) and purchased from Sigma-Aldrich® (Table 2.7). For each gene of interest, a master mix containing specific primers and the required reagents was prepared (Table 2.8, left); the mix was produced for the required number of reactions with a 10% extra for pipetting errors. Seventeen µl of the mix were added to each well of a 96-well plate and then 3 µl of the cDNA template were added to each well. The reaction was run in triplicate for each gene of interest. The plate was then placed in CFX96 Touch™ thermal-cycler (Bio-Rad) and the thermal profile (Table 2.8) was performed.

Table 2.7: Primers used for expression analysis through qPCR.

Primer/Probe	Sequence 5'→3'	Dye	Annealing temperature
HRH1 – Forward primer	TGGTGGTGGATCTGTCTTGA	None	58°C
HRH1 – Reverse primer	CCGGTTGACGGCTACATAGT	None	60°C
Rab27a – Forward primer	GAAGCCATAGCACTCGCAGAG	None	58°C
Rab27a – Reverse primer	ATGACCATTTGATCGCACCA	None	54.8°C
ACTB - Forward primer	GGCACCCAGCACAATGAAG	None	58.7°C
ACTB - Reverse primer	CATACTCCTGCTTGCTGATCCA	None	58.9°C
ACTB – Probe	CTCCTCCTGAGCGCAAGTACTCCGTG	5' HEX-3' NFQ	68.8°C
Assay 20x	**Catalogue number**	**Dye**	**Annealing temperature**
CDH1	Hs01023895_m1	5' FAM-3' MBG	60°C
Vimentin	Hs00958111_m1	5' FAM-3' MBG	60°C

Table 2.8: Components and quantities used for SYBR green qPCR mix. (left). Thermal profiler used in qPCR (right).

Component	Quantity per sample
iTaq Universal SYBR® Green supermix	10 µl
Fwd and Rv primer mix (4 µM)	2 µl
cDNA	3 µl
Nuclease-free water	5 µl
Final volume	20 µl

	Polymerase activation and DNA denaturation	Denaturation	Annealing/extension + plate read at 60°C	Melt curve analysis
Temperature (°C)	95	95	60	65-95
Time	30 sec	5 sec	30 sec	5 sec/step
Cycles		35 cycles		

2.5.4.2. TaqMan

TaqMan assay (or 5' nuclease assay) uses a set of primers, a probe and a polymerase with exonuclease activity. The probe contains two types of fluorophores: when the probe is intact, the quencher is close to the reporter fluorophore, thus reducing its fluorescence (Figure 2.2 A). While the reaction happens (Figure 2.2 B), the polymerase amplifies the product and degrades the TaqMan probe; this separates the quencher from the reporter allows activation of the reporter and increase in the fluorescent signal (Figure 2.2 C, D). The more denaturing-annealing cycles are repeated, the more chance there are for the TaqMan probe to bind and therefore the more emitted light is detected. The convenience of the TaqMan assay is that different fluorescent dyes with different emission spectra can be attached to the probes thus allowing multiplex PCR (multiple genes are measured at the same time in the same well).

In this way experimental samples can be co-amplified with an internal control, reducing pipetting errors (Arya et al. 2005).

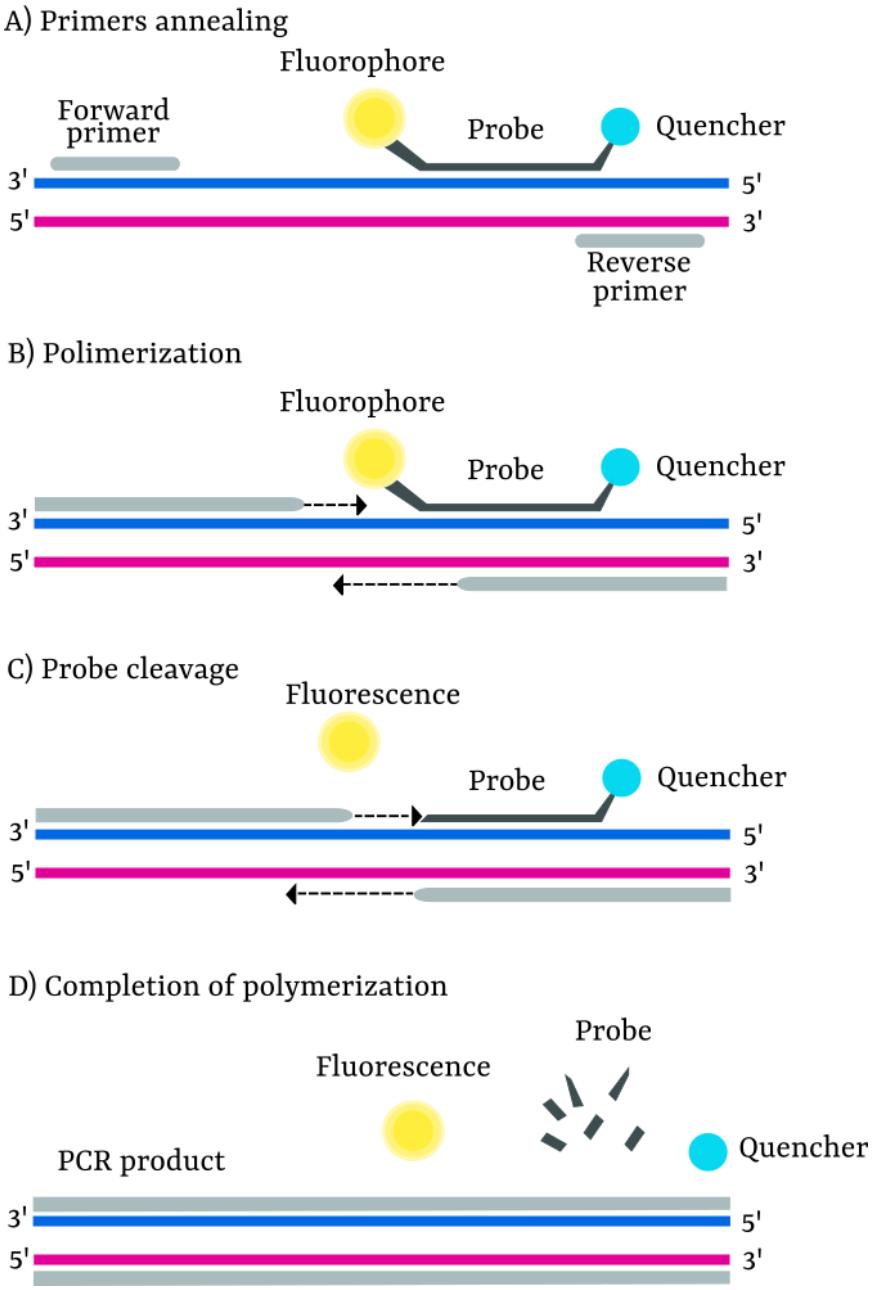

Figure 2.2: TaqMan probe-based real-time PCR.
A) Primers and probes anneal to the complementary target sequence. The probe contains a fluorophore (yellow circle on the left) and a fluorescence quencher (blue circle on the right). B) Polymerization takes place during the extensions step of every PCR cycle. C) As the DNA polymerase copies the template it excises the fluorophore from the probe, thus displacing it form the quencher with consequent release of fluorescence. D) Fluorescence accumulates in the reaction mix at every PCR cycle and is detected in real time.

Primers for ACTB and ACTB probes were designed using OLIGO 7 software (Molecular Biology Insights) and purchased from Sigma-Aldrich® (Table 2.7). Detection assays for E-cadherin (CDH) and vimentin

were purchased from Thermo Fischer Scientific. Ssoadvanced™ Universal Probes Supermix was purchased from BioRad.

The ACTB assay was assembled by mixing 15 µl of forward primer with 15 µl of reverse primer and 5 µl of ACTB probs; the mix was topped up to 100 µl final volume by adding 65 µl RNase-free water. The ACTB assay was then mixed with either the CDH1 or vimentin assay and with the required reagents following table 2.9 and master mixes for each assay was obtained. The mix was produced for the required number of reactions with a 10% extra for pipetting errors. Fifteen µl of reaction were added to each well of a 96-well plate and then 3 µl of the cDNA template were added to each well. The reaction was run in duplicates for each gene of interest. The plate was then placed in CFX96 Touch™ thermal-cycler (Bio-Rad) and the thermal profile (Table 2.9, right) was performed.

Table 2.9: Components and quantities used for TaqMan mix (left). Thermal profiler used in qPCR analysis (right).

Component	Quantity per sample
SsoAdvanced™ Universal Probes Supermix (2x)	7.5 µl
20x CDH1 or vimentin assay	0.75 µl
20x ACTB assay*	0.75 µl
Nuclease-free water	3 µl
cDNA	3 µl
Final volume	15 µl

	Polymerase activation and DNA denaturation	Denaturation	Annealing/extension + plate read at 60°C
Temperature (°C)	95	95	60
Time	30 sec	15 sec	30 sec
Cycles		35 cycles	

2.5.5. qPCR data analysis

qPCR data were analysed using the ΔΔCq method. This method enables calculation of how much the gene of interest varies compared to a reference gene, after a treatment, assuming reaction efficiency to be the same across both samples. With this method, quantification cycle (Cq) of the gene of interest (GOI) is adjusted against the Cq of a reference gene (normaliser) measured in the same samples. This calculation is done on both the test sample and on the calibrator sample. The ΔΔCq (Δ represents the difference) value is incorporated to determine the fold difference in expression. In this project, the genes of interest were HRH1, Rab27a, CDH1 and vimentin; the gene used to normalise was β-Actin and the calibrator was the RNA extracted from HME; the same RNA was used across all qPCR experiments to allow comparison.

$\Delta Cq\ calibrator = Cq\ GOI^{calibrator} - Cq\ normaliser^{calibrator}$

$\Delta Cq\ sample = Cq\ GOI^{sample} - Cq\ normaliser^{sample}$

$\Delta\Delta Cq = \Delta Cq$ sample $- \Delta Cq$ calibrator

Fold change $= 2^{-\Delta\Delta Cq}$

2.6. Chemical treatments

Histamine

Histamine (Sigma-Aldrich®) was prepared fresh before every experiment. Histamine was diluted in media at 5 mM concentration, and then added to cells at 100 µM concentration for times ranging between 4 h and 48 h.

Chlorpheniramine

Chlorpheniramine (Sigma-Aldrich®) was prepared fresh before every experiment. It was diluted in media at 10 mM concentration, and then added to cell at 250 µM concentration for times ranging between 4 h and 48 h.

GW4869

GW4869 (Sigma-Aldrich®) was dissolved in DMSO to generate a stock with a concentration of 2 mg/ml. Each time before performing the experiment, the stock was diluted in media at 10 µM concentrations and added to cells for 48 h.

2.7. Gene expression correlation analysis

A gene expression dataset of six OC cells lines of the NCI-60 cell line panel was obtained from the Cell Miner database (Cell Miner GSE32474), generated by Reinhold et al. (2012). Invasion rates through a Matrigel® layer and migration rates in a wound healing assay for six OC cell lines (IGROV-1, OVCAR3, OVCAR4, OVCAR5, OVCAR8 and SKOV3) were obtained from the thesis of Dr Laura Mulchay (2016). Pearson correlation analysis was used to evaluate a potential correlation between histamine receptors mRNA expression and invasion and migration rates of the six OC cell lines. Coefficients of determination (R squared) and p-values were obtained from Pearson correlation and used to estimate correlation significance.

A microarray dataset containing gene expression levels of 403 OC clinical samples was obtained from the TCGA database (The Cancer Genome Atlas Research Network 2011). The dataset comprised clinical information of 21 patients in stage II, 319 stage III patients and 61 stage IV patients. Gene expression values, tumour stage, overall survival and progression free survival information were used for the analysis. Patients were grouped by stage, median expression of the histamine receptors was calculated and used to calculate fold changes of expression between tumour stages. Two tailed t-test was used to calculate significance across samples. Patients were then divided in two groups based on the expression of HRH1 mRNA: low expressing patients (patients in which HRH1 mRNA levels were lower

than the median values of HRH1 expression) and high expressing patients (patients in which HRH1 mRNA levels were higher than the median value of HRH1 expression). Kaplan-Meier curves were generated for patient's overall survival and progression free survival, without considering patient's stage, by using GraphPad Prism version 8. Hazard ratio (HR), 95% confidence intervals, and log-rank p values were determined and presented on the main plots. Different online tools were used to retrieve information regarding HRH1 gene expression in OC samples (UALCAN). Additional Kaplan-Meier overall survival and progression free survival curves for OC patients were obtained from "The Kaplan-Meier plotter" database (http://kmplot.com/analysis/) (Győrffy et al. 2010). The Kaplan-Meier plotter generates survival analysis using data from Gene Expression Omnibus (GEO-www.ncbi.nlm.nih.gov/geo/) database and The Cancer Genome Atlas (Affymetrix HG-U133A, HG-U133A 2.0, and HG-U133 Plus 2.0 microarrays, http://cancergenome.nih.gov). This database includes gene expression data and survival information from a total of 1287 OC patients (Gyorffy et al. 2012). So far, a number of genes have been identified and validated by using this online tool in ovarian cancer (Ortega et al. 2014; Gayarre et al. 2016), lung cancer (Dötsch et al. 2015; You et al. 2015a) and breast cancer (Tilghman et al. 2013; Hong et al. 2015). The Kaplan-Meier plotter database was accessed in May 2021; patients in stage II, III and IV were automatically split by the software into two groups (expressing high or low level of HRH1) according to various quantile expressions of the proposed biomarker.

2.8. Immunofluorescence

In a cell culture hood, coverslips were first sterilised by dipping them in 70% and 100% ethanol and then they were air dried in 12-well plates. Coverslips were coated with 0.1 mg/ml poly-d-lysine (Sigma Aldrich®) for 1 h at RT to assist homogenous monolayer formation and prevent cell detachment. After 1 h, the coverslips were washed three times with PBS. Cells were plated following table 2.10. Culture media was added to wells and cells were allowed to grow for one day in a cell culture incubator. Growth media was then removed from the wells and cells were gently washed with pre-warmed PBS twice. Cells were fixed using 4% paraformaldehyde (PFA) in PBS for 30 minutes at 4°C and then they were gently washed with cold PBS three times to ensure full removal of the fixing agent. They were then permeabilised using 0.1% Triton X-100 (Sigma Aldrich®) in PBS for 10 minutes at RT. To ensure complete removal of the permeabilising agent, cells were washed three times with PBS. Cells were incubated in 1% bovine serum albumin (BSA) (blocking agent) in PBS for 1 h at RT on a rocking platform to prevent non-specific labelling. A dilution of 1:50 mouse monoclonal anti HRH1 primary antibody (Santa Cruz Biotechnology, catalogue number sc-374621) in blocking agent was prepared and cells were incubated at 4°C on a rocking platform overnight. Cells were washed three times for 5 minutes with PBS on the rocking platform. A dilution of 1:1000 of goat anti-Mouse IgG H&L (heavy & light

chains) (Alexa Fluor® 594) (Thermo Fisher Scientific, catalogue number A-11005) secondary antibody cocktail in the same blocking agent was prepared in dark to avoid photobleaching. Cells were labelled with secondary antibody for 30 minutes at RT in the dark on the rocking platform. To ensure full removal of the secondary antibody, cells were washed thoroughly with PBS three times for 5 minutes each in the dark. Coverslips were then mounted on glass slides using Prolong Gold Antifade 4',6-diamidin-2-fenilindolo (DAPI) mounting media (Thermo Fisher Scientific). Slides were stored in the dark at 4°C until imaged.

Table 2.10: Number of cell/well used in the experiment.

Cell type	Number of cells/well
SKOV3	5.0×10^4
OVCAR3	8.0×10^4
OVCAR5	7.0×10^4
HME	8.0×10^4

Cells were imaged using a Zeiss Axio Imager 72 upright microscope fitted with an ORCA-Flash 4.0 Digital CMOS camera (Hamamatsu). HRH1 and DAPI were visualised by using a 590 and 405 nm laser, respectively. The images were then analysed using the open-source software Fiji (Schindelin et al. 2012) and parameters such as area, integrated density and mean grey value were measured. Corrected total cell fluorescence (CTCF) was calculated for each cell lines on excel. The CTCF is a method that allows to calculate the fluorescence of a signal in relation to the area of the analysed object. CTCF was calculated as follows:

CTCF = integrated density – (area of selected cell × mean fluorescence of background)

Integrated density = area x mean fluorescence

The ratio between CTCF of OC cells and HME CTCF was calculated for each independent experiment. The average of the three independent experiments were combined for statistical analysis.

2.9. Western Blot

A western blot was used to visualise HRH1 and GAPDH proteins. SKOV3, OVCAR3 and OVCAR5 were seeded in 10 mm Petri dishes at a concentration of 1 x 10^6 and allowed to grow for one day. Growth media was then removed, and cells were washed with cold PBS on ice. 100 µl of 1X radioimmunoprecipitation assay buffer (RIPA) (Sigma-Aldrich) in PBS supplemented with Halt™ protease inhibitor cocktail (Thermo Fisher Scientific) (1:100 dilution) were added to each plate and

cells were scraped. Cells were collected by pipetting and moved to an Eppendorf® tube and they were allowed to lyse for 30 minutes at 4°C on a tube rotator. Cells were then centrifuged at 14,000 x rcf for 15 minutes at 4°C. Protein concentration was measured by using a Pierce™ BCA protein assay kit (Thermo Fisher Scientific). Twenty µg of proteins were used for cells analysis; protein samples were combined with 4X LDS NuPage loading buffer (Invitrogen) and 5X Dithiothreitol (DTT, stock solution 1M). Samples were brought to a final volume of 20 µl by adding 1X RIPA buffer. Samples were heated at 95°C for 5 minutes and spun down to ensure full collection of the sample, which was either processed immediately (as described below) or stored at -20°C overnight.

Protein samples were loaded onto precast NuPAGE™ 4 to 12%, Bis-Tris, 1.0 mm, Mini Protein Gels, 12 well (Thermo Fisher Scientific) and run at 125 V for 100 minutes using NuPAGE™ running buffer (Thermo Fisher Scientific) according to the manufacturer's instructions. Proteins were then transferred to a nitrocellulose membrane by wet transfer for 2 h at 150 V in a cold room at the temperature of 4ºC using NuPAGE™ transfer buffer (Thermo Fisher Scientific) (20X stock solution was diluted in water and 15% methanol was added to the final solution). Nonspecific binding sites were blocked with a blocking solution made of 5% w/v skimmed milk powder in PBST (PBS/ 0.10% Tween (Sigma Aldrich®)) for 1 h at RT. Membranes were cut to size if needed and incubated with a polyclonal rabbit anti HRH1 (Proteintech®, catalogue number 13413-1-AP) primary antibody diluted in blocking solution overnight at 4°C. The day after, membranes were washed in PBST three times for 5 minutes on a shaking rack and then incubated 1 h at RT with a solution of HRP-conjugated polyclonal goat anti rabbit IgG secondary antibody (Abcam, catalogue number ab6721) diluted in blocking buffer. Membranes were washed in PBST three times for 5 minutes, incubated with 1 mL of clarity western enhanced chemiluminescence (ECL) (BioRad) substrate for 1 minute and visualised using a ChemiDoc imaging system (BioRad). Membranes were thoroughly washed with PBST for 2 h on a rocking platform to fully remove ECL and they were incubated 1 h at RT with a monoclonal mouse anti GAPDH primary antibody (Abcam, catalogue number ab8245) in blocking solution. Membranes were then washed three times in PBS and incubated for 1 h at RT with a polyclonal goat anti mouse IgG secondary antibody (BioRad, catalogue number 1706516). Membranes were washed again and processed as just described. A full list of the antibodies used can be found in table 2.11.

Table 2.11: Antibodies used for HRH1 quantification by WB.

Target	Host Species	Dilution	Supplier, Cat no
HRH1	Rabbit, polyclonal	1:200	Proteintech, 13413-1-AP
GAPDH	Mouse, monoclonal	1:1,000	Abcam, ab8245
Rabbit IgG	Goat	1:10,000	Abcam, ab6721
Mouse IgG	Goat	1:10,000	BioRad, 1706516

2.10. IC50 determination

Half-maximal inhibitory concentration (IC50) indicates how much of a pharmacologic agent is required to inhibit a given biological activity by half for a given cell line (Aykul and Martinez-Hackert 2016). To calculate the IC50 of histamine (HRH1 agonist) and chlorpheniramine (HRH1 antagonist) the 3-(4,5-Dimethylthiazol-2-yl)-2,5-diphenyltetrazolium bromide (MTT) assay was used. MTT is a yellow compound that turns to its non-soluble purple derivate, formazan, when reduced by cells. The higher the metabolic activity of cells the more purple precipitate will be produced. A solubilization solution is added to the formazan creating a purple-coloured solution, the absorbance of which is read at 570 nm with a spectrophotometer.

Ten thousand SKOV3 or 15,000 OVCAR3 or OVCAR5 cells per well were seeded into 48-well plates and when 70% confluent, increasing concentrations of chlorpheniramine (Sigma-Aldrich®) (ranging from 10 nM to 1 mM) or histamine (Sigma-Aldrich®) (ranging from 10 nM to 1 mM) were added to them. After 48 hours, cells were washed with PBS and the MTT assay was performed. MTT (Sigma-Aldrich®) was dissolved in complete media with a concentration of 2 mg/ml and 200 µl were added to each well and incubated for 3 h into a cell culture incubator. After this time, the MTT was removed and 200 µl of solubilisation solvent (4 mM HCl, 0.1% IGEPAL® (Sigma-Aldrich) in isopropanol) were added to each well and absorbance was measured straight away at 570 nm using a SpectraMax i3x plate reader (Molecular Devices).

MTT absorbance of blank wells (wells containing only media but not cells) was subtracted from the absorbance of experimental wells in order to remove the background. The ratio of experimental well and control well was calculated, and the percentage of viable cells extrapolated. Cell viability data was analysed by using an in-built Nonlinear Regression model with variable slope (four parameters) through GraphPad Prism 8t, hat produced inhibitory dose-response curves and IC50 values.

2.11. Cell proliferation

To assess the effect of histamine and chlorpheniramine on cell proliferation rates, 100,000 SKOV3, OVCAR3 and OVCAR5 were plated in 6 well plates and grown for one day. Two ml of media (control), 100 µM histamine or 250 µM chlorpheniramine were added to corresponding well and plates were placed back into a humidified cell culture incubator. Cell number was measured at time points 0, 6, 24 and 48 h by manual counting using a hemocytometer; viable cells were differentiated from dead cells by using a 1:1 dilution of cells and trypan blue (BioRad) (described in section 2.1.5). The number of viable cells were normalised to their control, and the mean of three biological replicates were used for further statistical analysis.

2.12. Static adhesion assay

A static adhesion assay (Wilhelmsen et al. 2013) was used to assess the ability of OC cells upon activation or inhibition of HRH1 to adhere to an endothelial cell monolayer (Figure 2.3).

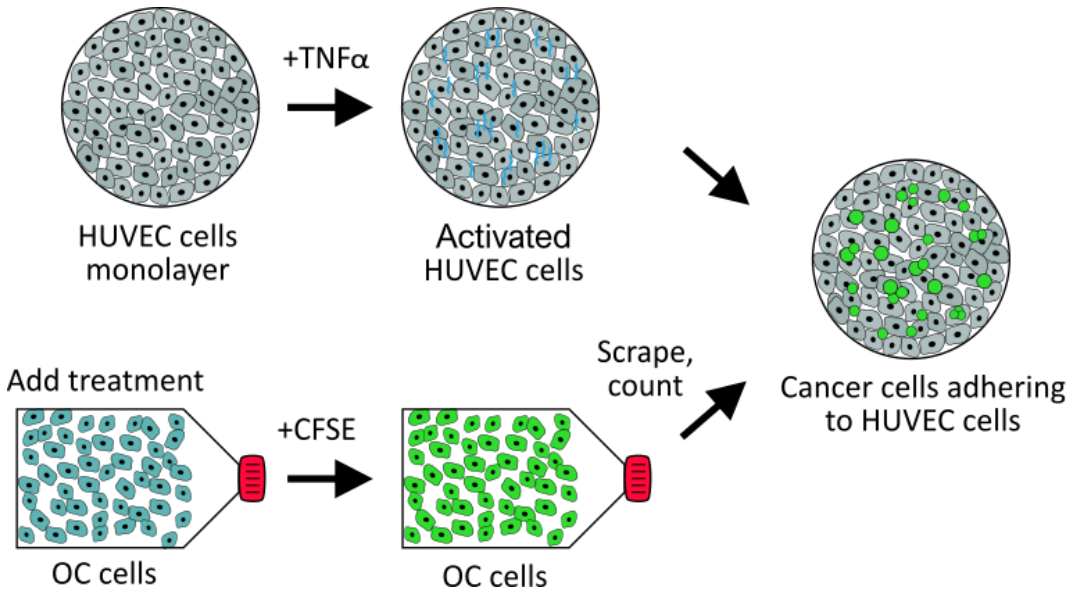

Figure 2.3: Adhesion assay schematic representation.
HUVEC cells were plated onto sterile coverslips in 24 well plates and grown until 100% confluent. TNFα was added to them, and cells were incubated for 24 h. Meanwhile, cancer cells were seeded in t25 cm^2 flasks and allow to grow. Cells were treated with siRNAs, or histamine or antihistamine, and 24 h later they were stained with CFSE. Next, cells were scraped, counted, and introduced onto the activated HUVEC cells. Non adherent cells were removed, and the coverslip was fixed and mounted. Area of adherent cells was calculated.

2.12.1. Endothelial cell preparation

Thirteen mm coverslips (thickness #1, Marinefeld) were sterilised by dipping in 70% ethanol and 100% ethanol. Coverslips were coated with 0.2% w/v bovine gelatine (Sigma-Aldrich®) in PBS, pH 7.4, in 24-well plates. One hundred thousand HUVEC cells were plated on top of the gelatine of each coverslip and cultured to 100% confluency. On the day prior to the experiment, cells were "activated" by

treatment with 10 ng/ml of tumour necrosis factor (TNF)-α (Sigma-Aldrich®, stock of 10 µg/ml in PBS) for 24 h in a cell culture incubator.

2.12.2. Cancer cell preparation

The adhesion assay was performed on either cells transfected with siRNAs or with cells treated with histamine and chlorpheniramine.

For the transfection experiments, OC cells were cultured in 6-well plates up to 70% confluency. Cells were then transiently transfected with siRNA control, siRNA specific for HRH1, or with media containing only transfection reagent (non-transfected cells), as previously described in section 2.4. After 24 h, cells were washed with PBS and stained with 10 µM carboxyfluorescein succinimidyl ester (CFSE) in PBS (Sigma-Aldrich®) for 10 minutes in a cell culture incubator. Cell were next thoroughly washed with PBS to remove excess dye, detached from wells using a cell scraper, centrifuged at 300 x rcf for 5 minutes to form a cell pellet, and resuspended in SFM. For cells treated with histamine and antihistamine, OC cells were cultured in three t25 cm^2 culture flasks up to 70% confluency. Cells were then treated with control media, 100 µM histamine, or 250 µM chlorpheniramine for 24 h and treated as described above.

2.12.3. Static adhesion assay

One hundred thousand CFSE-stained OC cells were introduced onto the HUVEC monolayer in SFM (400 µl per well) and allowed to interact for 15 or 30 minutes in a cell culture incubator. Non-adherent cells were gently eluted with PBS. Coverslips where fixed with 4% PFA (pH 6.9, Sigma-Aldrich®) for 15 minutes at RT, mounted with ProLong™ Diamond Antifade (Thermo Fisher Scientific) mounting medium and imaged using a Zeiss Axio Imager Z2 upright microscope with an ORCA-Flash 4.0 digital CMSO camera. To visualise stained cells a 488 nm laser was used; each coverslip was fully imaged using the tile settings and the Plan-Apochromat 10x/0.45 lens (Zeiss) (10X eyepiece).

2.12.4. Image analysis

Tiles were opened in Fiji and 20 random images were selected for further analysis. The area occupied by stained cells was measured with the “Analyse Particle” plug in; a macro was written to speed up the analysis, particles size value was kept constant across the different independent replicates while threshold values were the same across technical replicates but not across biological replicates, due to staining intensity variability.

For transfected cells, the ratio between “non-transfected cells” and siRNA control cells or siRNA HRH1 cells was calculated for each independent experiments; mean values were then combined and used for statistical analysis.

For histamine and chlorpheniramine treated cells, each technical replicate was normalised against control cells (treated with SFM) and their average was used for statistical analysis.

2.13. Wound healing assay

A wound healing assay (Liang et al. 2007) was used to analyse the motility rate of OC cells after pharmacological or chemical inhibition of HRH1.

2.13.1. Cell preparation, wound healing assay and gap closure imaging

Prior to starting the experiment, the bottom part of a 12-well plate was marked with two parallel lines and one line perpendicular to the future 'wound line' to allow imagining of exactly the same 'wounded' area over time (Figure 2.4). One x 10^5 SKOV3 and 1.5 x 10^5 OVCAR3 or OVCAR5 cells were then seeded into 12 well plates. Cells were then either treated with siRNAs or pharmacologically. For the transfection experiment, a siRNA control, siRNA HRH1 or media containing only transfection reagent were added to the cells once they reached 70% confluency (see section 2.4 for further details). On the following day, the cell monolayer was 'wounded' (Figure 2.4 A). For cells to be treated pharmacologically, they were cultured until 90% confluence, serum starved for one day and then a 'wound' was made, and control media, 100 µM histamine or 250 µM chlorpheniramine were added (Figure 2.4 B). In all cases, the 'wound' was made using a p200 pipette tip. Cells were then washed twice with PBS to ensure full removal of floating cells and either SFM alone or SFM supplemented with the appropriate pharmacological treatment was added (1 ml per well). Cells were placed in a cell culture incubator and were imaged at different time points (0, 4, 8, 12, 24 h) using a Pimovert microscope with an LD5xPh1 objective (Zeiss). For transfected cells, transfection efficiency was checked by RT-qPCR as described in method section 2.5.4.

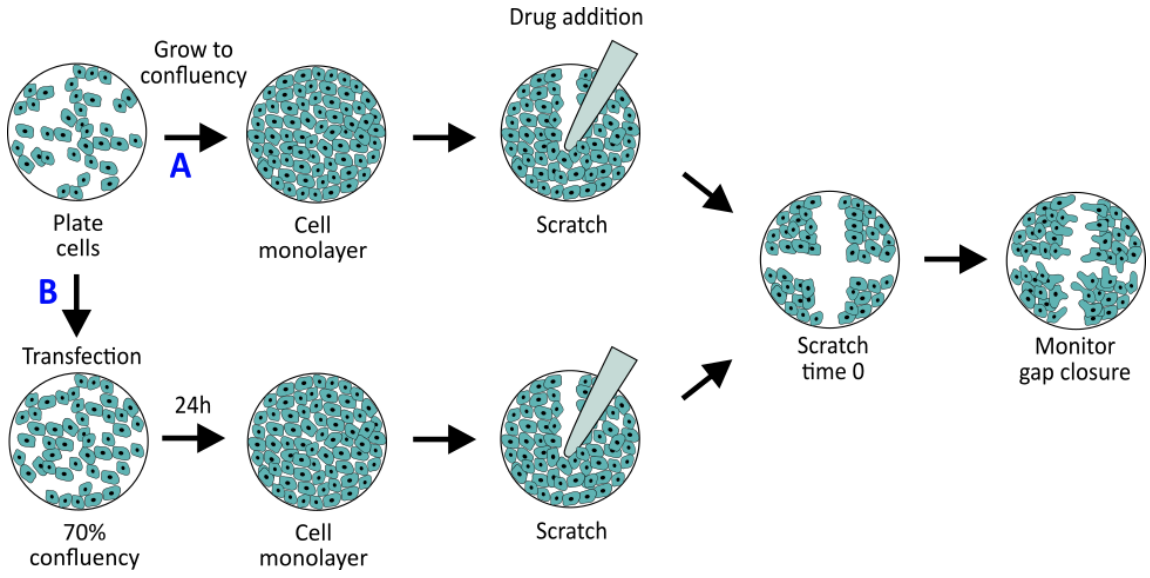

Figure 2.4: Schematic representation of the wound healing assay.
Cells were plated in a 12 well plate and then treated either via route A or B. A) Cells were grown to confluency, they were 'wounded' and fresh media containing different pharmacological treatments was added to each well of the plate. B) Cell were grown up to 70% confluency, then they were transfected, and the 'wound' performed on the following day. In both cases, 'wound' closure was imaged at intervals for up to 24 h, and 'wound' opening percentage was calculated.

2.13.2. Image analysis

'Wound' opening percentage was analysed using the Fiji plug in "MRI Wound Healing Tool". This plug-in measures the cell-free area for each image. The parameters were adjusted for each image, maximizing the accuracy of the analysis. The final 'wound' size at time points 4, 8 ,12, 24 h was subtracted to the 'wound' size at time 0 h to obtain the migration area. The four technical replicates were averaged; for transfected cells, the average was used to calculate the ratio of transfected cells to the 'non-transfected cells'. The average of three biological replicates were combined and used for statistical analysis.

2.14. Matrigel® invasion assay

To analyse the capacity of cells to invade, a Matrigel® invasion assay was used. This assay is based on the transwell invasion assay (Boyden 1962) with the addition of a layer of ECM, in this case Matrigel® (Figure 2.5) (Hall and Brooks 2014). Matrigel® is a gelatinous mixture of proteins obtained from the Engelbreth-Holm-Swarm mouse sarcoma. It contains a mixture of collagen, laminin and heparan sulphate proteoglycans together with growth factors (TGF-β and EGF) and other proteins. These components provide adhesive peptide sequences, prevent differentiation, and promote proliferation of many cell types.

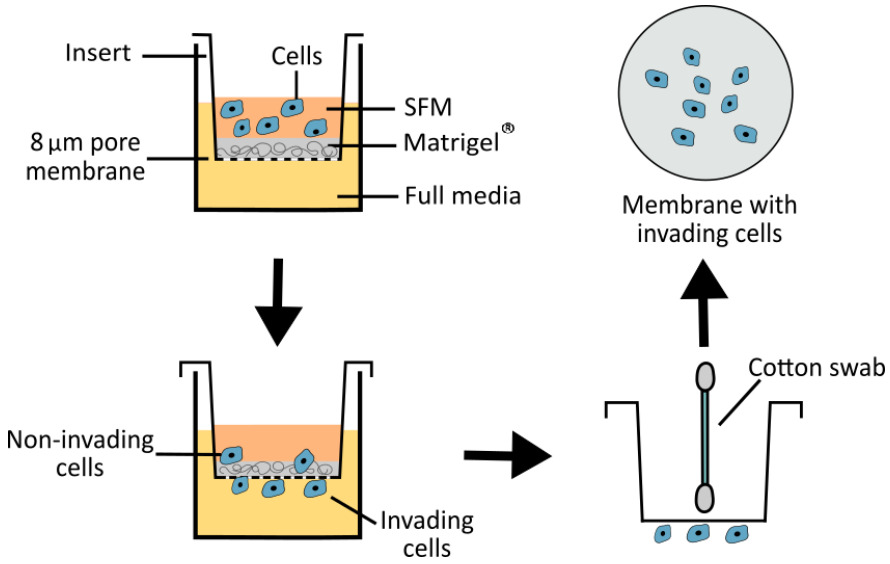

Figure 2.5: Schematic representation of Matrigel® invasion assay.
Cell were plated on a transwell insert on top of a Matrigel® layer and incubated for 48 h (top left); invading cells moved through the Matrigel® layer and attached to the bottom part of the porous membrane (bottom left). Inserts

were removed from the well and non-invading cells, located at the top of the membrane, were removed by using a cotton-swab (bottom right). Membranes were cut from the inserts, cell were stained and imaged (top right).

BioCoat™ Matrigel® (Corning®) plates were thawed for 1 h at RT. To rehydrate the matrix, 500 µl and 700 µl of pre-warmed SFM were added to the inserts and the wells, respectively, and the plates were placed in a cell culture incubator for 2 h. After this time, SFM was removed; 650 µl of pre warmed complete media was added to each experimental well of the plate. Empty wells were filled with 650 µl of PBS to avoid experimental wells drying out.

2.14.1. Cell preparation

SKOV3, OVCAR3 and OVCAR5 were cultured under standard conditions. The day before the experiment, media was replaced with SFM and cells were serum starved for 24 h. Different experimental conditions were used, and cells were treated in different ways, as described below.

2.14.1.1. Standard Matrigel® assay

SKOV3 and OVCAR3 were plated following quantities listed in table 2.12 in 250 µl of SFM, and were allowed to invade for 48 h.

2.14.1.2. Matrigel® assay on transfected cells

One x 10^5 SKOV3, 1.5 x 10^5 OVCAR3 and OVCAR5 were plated in a 6 well plate and after 24 h cells were transfected either with siRNA control or with a siRNA specific for HRH1 as described in section 2.4. Twenty-four h after transfection, cells were detached and plated on top of the Matrigel® inserts (following quantities in table 2.12) in 250 µl of SFM and were allowed to invade for 24 and 48 h.

2.14.1.3. Matrigel ® assay on SKOV3 treated with chemical compounds

SKOV3 were seeded in a 75 cm^2 flask and 24 hours later cells were detached and plated onto the Matrigel® inserts following table 2.12; 250 µl of either control media, 100 µM histamine or 250 µM chlorpheniramine were added to each insert and cells were allowed to invade for 48 h. All treatments were done in pre-warmed SFM. For the GW4869 treatment, 250 µl of control media (supplemented with DMSO), 100 µM histamine ,10 µM GW4869 (Sigma-Aldrich, dissolved in DMSO) or a combination of both compounds were added to the respective wells and cells were allowed to invade for 48 h.

2.14.1.4. Matrigel® assay on SKOV3 treated with siRNAs and EVs

On day 1 of the experiment (Figure 2.6), 1 x 10^6 SKOV3 were seeded in two t175 cm^2 cell culture flasks and allowed to grow for one day. Media was then replaced with SFM and incubated for 48 h. EVs were then extracted following the method described in section 2.15. On day 2 of the experiment, 1 x 10^5 SKOV3 were seeded in a 6 well plate, and the following day (day 3) cells were transfected with siRNAs as described in section 2.4. On day 4, 1.5 x 10^4 SKOV3 siRNA control or SKOV3 knocked down for HRH1 were plated onto each insert, then either PBS or EVs were added, and cells were allowed to invade for 48 h. The total number of EVs released by SKOV3 cells was assessed by NTA (as described in section

2.16.1). The total number of released EVs was divided by the number of SKOV3 used for extraction obtaining the number of "EVs per cell". The same amount of EVs was added to recipient cells.

<table>
<tr><th>Day 1</th><th>Day 2</th><th>Day 3</th><th>Day 4</th><th>Day 6</th></tr>
<tr><td rowspan="2">Seed SKOV3 for EV extraction</td><td>Replace media with FBS-depleted media</td><td rowspan="2">Incubate</td><td rowspan="2">EV extraction
+
Plate cells On Matrigel®</td><td rowspan="2">Process Matrigel®</td></tr>
<tr><td>Seed SKOV3 for transfection</td><td>SiRNAs transfection</td></tr>
</table>

Figure 2.6: Experimental layout for the Matrigel® assay on SKOV3.
On day 1, SKOV3 cells were seeded for EV extraction, and on day 2 media was changed to FBS-depleted media and conditioned for 48 h. On day 2, SKOV3 were seeded in a six well plate and 24 h later were transfected with siRNAs (day 3). On day 4, EVs were extracted, siRNAs treated cells were counted and plated on the Matrigel® membranes and either PBS or EVs were added to them. Cells were allowed to invade for 48 h and on day 6 Matrigel® membranes were processed.

2.14.1.5. SKOV3 KD for Rab27a

As described in section 2.4, 1.5 x 10^4 SKOV3 were plated in a six well plate and allowed to grow for one day. The next day cells were transfected with siRNA control or siRNA for Rab27a (as described in section 2.4) and were allowed to grow for 24 h. The following day, cells were plated onto the Matrigel® inserts, and either control media or 100 μM histamine were added to them. Cells were allowed to invade for 48 h and then membranes were processed for image analysis, as described below in section 2.14.2.

Table 2.12: Number of cells plated per well in the Matrigel® assay in relation with the time they were allowed to invade.

Cell type	Number of cells per well	Time of invasion
SKOV3	3.5 x 10^4	24h
	1.5 x 10^4	48h
OVCAR3	5.0 x 10^4	24h
	2.0 x 10^4	48h
OVCAR5	5.0 x 10^4	24h
	2.0 x 10^4	48h

2.14.2. Cell fixation and staining

Inserts were washed once in pre-warmed SFM and again with PBS. Invaded cells were fixed with 4% PFA (Sigma-Aldrich®), pH 6.9 for 15 minutes at RT, washed twice with PBS for 5 minutes and then permeabilised with 0.1% Triton X-100 (Sigma-Aldrich®) for 15 minutes at RT. Cells were stained either with 1% crystal violet (Sigma-Aldrich®) in water for 10 minutes at RT, or with 10 µM CFSE (Sigma-Aldrich®) for 10 minutes at RT. Non invading cells were removed by wiping the top of the membranes with a cotton swab. Membranes were cut using a scalpel (Swann-Morton™) and mounted on a glass slide. Crystal violet-stained cells were mounted using ProLong™ Diamond antifade mounting media (Thermo Fisher Scientific), while CFSE stained cells were mounted using ProLong™ Gold Antifade Mountant with DAPI (Thermo Fisher Scientific).

2.14.3. Cell imaging and image analysis

Invaded cells were imaged using a Zeiss Axio Imager 72 upright microscope fitted with an ORCA-Flash 4.0 Digital CMOS camera (Hamamatsu). At least ten images were taken for each membrane by using either the Plan-Apochromat 10x/0.45 or the 20x/0.8 objectives (Zeiss) (10X eyepiece) depending on the staining used. For imaging crystal violet-stained cells transmitted light was used, while DAPI+CFSE stained cells were visualise by using a 405 nm laser and 488 nm laser, respectively. Invaded cells were counted by using the cell counter plugin in Fiji. The percentage of cell that had invaded through the membrane was calculated for each condition, and the ratio of the treatment groups on the control cells was calculated for each independent experiment. Mean values of independent experiments were combined for statistical analysis.

2.15. EV extraction

Cell were plated in either five t175 cm^2 (for collagen degradation assay) or fifteen t175 cm^2 (for western blot and proteomic assays) cell culture flasks and cultured until they reached 60% confluence. At this point, media was removed and replaced with SFM supplemented with appropriate treatments and cell were placed back in the incubator. After 4 or 48 h (depending on the downstream application), conditioned media was collected and processed for EV extraction. Media was centrifuged at 300 x rcf for 5 minutes (Megafuge 16 benchtop Centrifuge, Thermo/Hereaus) to remove dead cells, and then at 16,500 x rcf for 20 minutes at 4°C (Avanti JXN-26, High Speed Centrifuge, JA14.50 Tapered Rotor, Beckman Coulter) to remove debris and large EVs. Conditioned media was then concentrated to 500 µl by using Vivaspin 20 (100 kDa, Ge Healthcare) concentrator column at 3,000 x rcf (Megafuge 16 benchtop Centrifuge, Thermo/Hereaus). Samples were then processed through size exclusion chromatography (SEC). Before processing the sample, SEC columns were prepared. Econo-Pac® chromatography columns (14 cm, BioRad) were filled with 14 mL of Sepharose agarose gel filtration media (GE Healthcare, particle size 45 µm-165 µm) and topped up with PBS. Columns were allowed to

settle for 2 h at RT. After this time, a column bed support was placed on top of the Sepharose to avoid the latter being disturbed during washing. Columns were washed three times with 10 mL of PBS. During the last wash, 1 mL of PBS was left on top of the column bed support to avoid drying out, and samples were processed. The sample was pipetted onto the column and columns were topped up with 10 mL of PBS; flow-through was immediately collected in 500 µl fractions (fraction 1 to 15). Fraction 7-10 were identified as "EV containing fractions" (see section 5.3.1) and were used for further experiments. Samples were either used the same day, stored at 4°C for up to three days, or at -80°C for long-term storage.

2.16. EV characterization

EV characterization requires a variety of techniques to visualise their morphology, surface markers and size. In this project, nanoparticle tracking analysis (NTA) was used to quantify EV concentration and size, transmission electron microscopy (TEM) to visualise their morphology, and western blot and MACSPlex were employed to study their protein markers.

2.16.1. Nanoparticle Tracking Analysis

NTA is a technique used to study particle size and distribution. NTA can visualise and analyse particles ranging between 10 nm to 1 µm in solution, based on their Brownian motion (random motion of particles suspended in a fluid). A laser light scattering microscope illuminates particles; the light scattered by each particle is captured using a camera; the motion is then analysed through a software and is related to particle size and concentration. In this project, EV size and concentration was calculated using the ZetaView PMX 110 instrument (Particle Metrix, GmbH), supplied with the analysis software. Briefly, the machine was calibrated with 100 nm polystyrene beads (Applied Microspheres) at a concentration of 1:25,000. SEC fractions were diluted 1:100 or 1:1,000 (depending on the original concentration of particles in the sample) in 1 mL final volume of PBS and run through the machine. Data was acquired at RT, with the following settings: sensitivity 80, frame rate 30 frames per second (fps), shutter speed 100, brightness minimum 25, minimum pixel size 5 and maximum size pixel 1,000. Half-second videos were recorded, analysed at 11 positions, and size and concertation of EVs was automatically calculated by the ZetaView software version 8.04.12.

2.16.2. Transmission Electron Microscopy

To analyse EV morphology, TEM was used in this project. Carbon 300 mesh copper grids (TAAB, C267) were glow discharged for 20 second at 15 mA; 10 µl of EV samples were pipetted onto them and incubated for 2 minutes at RT. Excess liquid was removed by dabbing grids with filter paper. Grids were then allocated on top of a 20 µl drop of 2% uranyl acetate (Agar Scientific) for 10 seconds, left to air

dry and stored in a dust proof box at RT. Grids were imaged by Dr Flavia Moreira-Leite at 100 kV by using a Jeol JEM-1400 Flash transmission electron microscope with Gatan OneView 16 Megapixel camera.

2.16.3. Western Blot

In order to confirm the enrichment of EV markers, a western blot was performed on EVs extracted from SKOV3 cells. Briefly, SKOV3 cells were plated in forty-five t175 cm^2 cell culture flasks and on the following day the media was replaced as following: fifteen flasks were treated with SFM, fifteen flasks with 100 µM histamine in SFM and fifteen flasks with 250 µM chlorpheniramine in SFM. Non-conditioned media (media added to fifteen empty flasks) was used as control. Media was conditioned for 48 h and EVs extracted as described previously in section 2.15. Both cells and EVs were processed as described in section 2.9.; 10 µg of proteins was used for both cell and EV analysis. Protein samples were prepared by adding 4X LDS NuPage loading dye (Invitrogen) to the protein mix. Samples were brough to a final volume of 40 µl with 1X RIPA buffer and then were heated at 95°C for 5 minutes. Gels were run as described in section 2.9. A list with full details of the antibodies used for EVs characterization is reported in table 2.13.

Table 2.13: Specification of the antibodies used for EV characterization.

Target	Host	Dilution	Manufacturer
CD81	Mouse, monoclonal	1:1,000	Abcam, ab79559
HSP70	Rabbit, polyclonal	1:1,000	Abcam, ab79852
CD63	Mouse, monoclonal	1:1,000	Novus Biologicals, NBP2-42225
TSG101	Rabbit, polyclonal	1:1,000	Abcam, ab30871
ALIX	Mouse, monoclonal	1:1,000	Abcam, ab117600
Cytochrome c	Rabbit, monoclonal	1:1,000	Abcam, ab150422
GM130	Rabbit, monoclonal	1:1,000	Abcam, ab52649
Rabbit IgG	Goat	1:10,000	Abcam, ab6721
Mouse IgG	Goat	1:10,000	BioRad, 1706516

2.16.4. MACSPlex

The MACSPlex assay is a qualitative assay able to visualise up to 37 potential EV surface antigens using a cytofluorimeter. The assay comprises a cocktail of 39 beads fluorescently labelled: 37 are coated with antibodies for EV surface antigens and 2 are coated with internal isotype negative controls. Each bead can be identified based on their respective fluorescent intensity. Briefly, before processing conditioned media for EV extraction, 150 µl of conditioned media was obtained from SKOV3 treated with SFM, 100

µM histamine or 250 µm chlorpheniramine. Non-conditioned media was used as a control. Media samples were incubated with 15 µl of antibody-coated MACSPlex exosomes capture beads (Miltenyi Biotec) overnight on a tube rotator in the dark. The next day, 500 µl of MACSPlex buffer (Miltenyi Biotec) was added to each tube and they were spun down at 3,000 x rcf for 5 minutes. Supernatant was discarded and 135 µl of solution (buffer + EVs) was left in the tube to avoid accidental removal of the beads. To ensure full removal of unbound material, 500 µl MACSPlex buffer was added to the samples and incubated for 15 min in the dark on a tube rotator. Samples were centrifuged again at 3,000 x rcf for 5 minutes; supernatant was discarded leaving 135 µl of sample. A cocktail of allophycocyanin (APC)-labelled detection antibodies against CD9, CD63 and CD81 (Miltenyi Biotec) was added to the bead-captured EVs; the addition of the detection reagents enables the formation of sandwich complexes between the capture beads, the EVs and the detection reagent allowing EV visualization. Samples were incubated for 1 h on a tube rotator disk in the dark to ensure complete binding of detection reagent to biological material. Samples were washed twice with 500 µl of MACSPlex buffer as previously described. Samples were finally re-suspended in MACSPlex buffer and analysed by using a Cytoflex S flow cytometer instrument (Beckman Coulter). APC mean fluorescent intensity of beads incubated with non-conditioned media was subtracted from all samples. Percentage of antigen expression was calculated in relation to CD9 expression for each experiment.

2.17. Collagen degradation assay

To study the ability of EVs to break down the ECM, a collagen assay was used. EVs were extracted from cells treated either with control media or with 100 µM histamine or with 250 µM chlorpheniramine for 48 h following the protocol in section 2.15; all treatments were made in SFM. To be able to distinguish potential effects related to soluble media factors, fresh media was added to an empty flask, incubated for 48 h and used as a control.

2.17.1. Calculation of EV number

The number of "EVs per surface" was calculated. This method allows to calculate how many EVs are produced in a specific surface and plate an equivalent amount in the recipient surface. In this case, five t175 cm^2 cell culture flasks were used to extract the EV samples. The surface area of one t175 cm^2 flask is 175 cm^2 thus the surface area of five t175 is 875 cm^2. The collagenase experiment was performed in a 96-well plate; the surface area of one well of a 96-wells plate is 0.32 cm^2. The dilution factor to use for preparing the EV samples was calculated as the surface area of the 5 t175 cm^2 flasks divided by the surface area of one well of a 96-well plate. EV samples were prepared using the dilution factor and a final concentration of 100x "EVs per surface" was used for the assay. Samples were brought to a final volume of 100 µl by adding the working reagent (WR) solution.

2.17.2. Collagen and sample preparation

The DQ™ collagen, type I from bovine skin, fluorescein isothiocyanate (FITC) conjugated (D12060, Thermo Fisher Scientific) was used for this assay. DQ collagen is a solution of intact collagen quenched to a fluorescent dye (FITC) so that the fluorescence is almost non-existent. When the collagen molecules are hydrolysed by appropriate enzymes, the FITC dye detaches from it, releasing the fluorescence; fluorescence can be read at a specific wavelength using a spectrophotometer. 1 mg/ml DQ™ collagen stock was diluted to a 25 µg/ml solution with 1X WR, pH 7.6 (sodium chloride 1.5 M, Trish HCl 0.5 M, Calcium chloride 50 mM). A 96 well plate was used for the assay; 80 µl of WR, 20 µl of DQ™ collagen and 100 µl of EV samples were added to each well. 1, 0.05, 0.01, 0.005, 0.0001 and 0.00005 U/mL of collagenase (Sigma Aldrich®) were used as positive controls. Collagen degradation was measured at time 0, 2, 6, 12, 18 and 24 h and by reading the FITC absorbance at 530 nm using a spectrophotometer. Four different wells were use as technical replicates for each condition. The absorbance of blank wells (containing only WR) was subtracted from the absorbance of experimental wells to remove the background signal. The mean value was calculated for each independent experiment, and they were combined for statistical analysis.

2.18. TIRF microscopy

Total internal reflection fluorescence (TIRF) microscopy is a technique that uses an evanescent wave to only excite fluorophore molecules that are in a small area immediately adjacent to the glass surface used. This technique has recently become the method of choice to detect single molecules and to investigate biological process at the interface or on the surface of a cell, as it only detects surface-bound fluorophores (and not the non-bound molecules presented in the media), selectively reducing the background fluorescence, improving the signal-to-noise ration and overall, the quality of the image acquired (Tonzani 2009; Mattheyses et al. 2010).

2.18.1. Cell preparation and image acquisition

In this project, TIRF microscopy was used to image multivesicular body-plasma membrane (MVB-PM) fusion events enabling the visualization of EV release. Initially, SKOV3 were transiently transfected with a CD81-pHluorin reporters (as described in section 2.4). The CD81-pHluorin reporter consists of a TSPAN (CD81) based optical reporter cloned with a pH sensitive GFP (pHluorin) molecule; normally, the pHluorin is located to the outer membrane of ILVs and because it is exposed to an acidic pH (5.5) it does not emit fluorescence. Upon fusion of MVBs with the PM, ILVs are released in the extracellular space and the sudden change of pH from acidic to neutral pH (7.4) activates the pHluorin, generating fluorescent flashes. Thus, each flash observed represent an MVB-PM fusion event. Twenty four h post transfection, cells were washed in Tyrode's solution, pH 5.5 (2 mM $CaCl_2$, 2.5 mM KCl, 119 mM NaCl, 2

mM $MgCl_2$, 30 mM glucose, 25 mM 2-(N-morpholino) ethanesulfonic acid) to remove the presence of unwanted structures (such as exocytosed exosomes or focal adhesions) from the coverslip. Cells were than imaged in Tyrode's solution, pH 7.4 (2 mM $CaCl_2$, 2.5 mM KCl, 119 mM NaCl, 2 mM $MgCl_2$, 30 mM glucose, 25 mM HEPES) in a 37°C humidified imaging chamber. Images were kindly acquired by Dr Stefan Balint, Kennedy Institute of Rheumatology, Oxford University. For histamine imaging, the Tyrode's solution was supplemented with 100 μM histamine and cells were imaged immediately after media addition, for a time frame of 0-5 minutes. Twelve cells were imaged in total (the same number of cells was imaged for the control). For chlorpheniramine treated cells, Tyrode's solution was supplemented with either 10 or 250 μM chlorpheniramine and cells were imaged in time-interval of 5 minutes for 35 minutes. Two cells were imaged for each time point for both treatments (a total of cells 14 per condition). Only cells expressing moderate levels of CD81-pHluorin were chosen for imaging, with field of view containing only one cell per acquisition. An Olympus IX83 inverted microscope, fitted with a Photometrics Evolve 512 Delta camera was used for acquiring images with a UAPON OTIRF 150x/1.45 objective. Images were acquired at 0.40 frames per second (fps).

2.18.2. Image analysis

All images were analysed through Fiji by using the AMvBE macro, developed by Bebelman et al. (2020). The images were opened through the AMvBE macro and the following parameters were used for analysis:

- Time window per event correction (in no. of frames): 4
- Condition for fluorescence decrease after exocytosis (minimum no. of frames): 2
- Condition for fluorescence increase before exocytosis (minimum no. of frame). 2
- Minimum event size to be considered (in micrometres): 0.3
- If the decay condition is not fulfilled, the threshold value (N) for exocytosis event rescue such that mean + N*STD: 3
- Manual threshold for vesicle movement (unit in no. of vesicle diameter, which represents the amount of vesicle diameters the vesicle is allowed to move): 2

All the sudden increases in fluorescence intensity that could potentially represent a fusion event were manually selected; and then each selected event was analysed by the software. Events that fulfilled all the selected parameters were reported as positive fusion events and were identified by a green circle on the corresponding image frame. Events that did not fulfil one or more parameters were indicated by the software as yellow or red circles and were not included in the analysis. Information regarding the number of CD81 MVB-PM fusion events, their fluorescence level and their size were collected for all events and used for statistical analysis.

2.19. Liquid chromatography-mass spectrometry for proteomics

Liquid chromatography-mass spectrometry (LC-MS) is a technique that allows identification of molecules in a sample; proteins are first separated by size by using liquid chromatography and then the content is quantified via mass spectrometry. During mass spectrometry analysis, molecules are ionised (converted to gas-phase ions) and positive and negative charged ions are generated; the newly generated ions are sorted and separated according to their mass-to-charge (m/z) ratios. The m/z ratios and their relative abundance are sent to a data system that generates a mass spectrum. In this case, label-free quantification (LFQ) was used; this method is less accurate than stable isotope-based labelling (SILAC) however is less time consuming and less costly (Asara et al. 2008; Cox et al. 2014). One of the methods used for LFQ proteomics is MaxLFQ; with this method, LC-MS is used together with a peptide sequence database that allows the identification of the proteins found within the sample. Proteins are first digested into peptide fragments that are then separated and quantified using LC-MS (Cox et al. 2014). The fingerprints of these fragments are then used to identify their parent proteins using the MaxQuant software (Tyanova et al. 2016).

2.19.1. Sample preparation

SKOV3 were plated in thirty t175 cm^2 cell culture flasks and cultured for two days. On day three, media was removed, and cells were washed twice with sterile PBS (Gibco™). Fifteen t175 cm^2 cell culture flasks were treated with SFM and 100 µM histamine was added to the other fifteen t175 cm^2 cell culture flasks. Cells were incubated for 4 h and then EVs were extracted as previously explained in section 2.15. EV samples were concentrated to a final volume of 20 µl by centrifuging them at 3,000 x rcf in a 5 kDa Vivaspin (GE Healthcare), as described in section 2.15. Samples were stored at -80 °C (for up to one month) prior to downstream application. Four different biological replicates were collected, and samples were sent to the Discovery Proteomics Facility at the Target Discovery Institute (TDI), Oxford University, for further analysis. Protein extraction and LC-MS was undertaken by Dr Svenja Hester, following their protein extraction method.

All samples were analysed using a shotgun deep read sequencing by liquid chromatography coupled with mass spectrometry analysis using an Orbitrap Fusion Lumos Tribrid (Thermo Fisher Scientific) tandem mass spectrometer. The raw data generated were processed by the facility using the MaxQuant software.

2.19.2. Data analysis

LFQ intensity were used for data processing through the Perseus (MaxQuant) software. Data were filtered and potential contaminants were eliminated from the protein list. LFQ values were transformed to Log_2 values, and all samples were grouped together based on the treatment (n=4 for

both control and histamine). Additionally, data were filtered and only protein expressed in at least three replicates of at least one condition were further analysed. Missing data were imputed by using the software function "Replace missing values from normal distribution"; with this function the software itself looks at the distribution of data, assuming they are normally distributed, and it calculates centre and width of the distribution. The software will then shrink the distribution by a factor of "0.3" and shift it down by a factor of "1.8 standard deviation" and it will simulate random values to fill up the missing values. In this way, the missing values will fall on the right side of the distribution, as this is where protein with low abundance are expressed. Data were then processed for statistical analysis. A t-test analysis was used to compare the protein content of control and histamine- induced EVs. P-values were calculated either applying a Benjamini-Hoechberg false discovery rate (FDR) correction of 0.01 or 0.05 or by just running a t-test without further corrections. Venn diagrams and upset plots were generated by using the online tool https://intervene.shinyapps.io/intervene/. Volcano plots were generated through Perseus. Go terms analysis were carried out by using the online database DAVID (Huang et al. 2009b; Huang et al. 2009a)

2.20. Statistics and reproducibility

For statistical analysis, GraphPad Prism version 8 statistical software was used, unless otherwise specified. Throughout the thesis, the statistic test used for analysis is specified for each figure, as appropriate. Sample sizes for each experiment were chosen without using any statistical methods but were planned with adequate power based on previous studies. No samples or data points were arbitrarily excluded, except for the Matrigel® invasion assay in section 5.3.5. For this experiment, one value for the siRNA HRH1 + PBS and siRNA HRH1 + EVs conditions was excluded for statistical analysis, as it was identified as an outlier by using the Grubbs test.

Chapter 3

Histamine receptor in ovarian cancer models

3 Histamine receptors in ovarian cancer models

3.1 Introduction

Wide attention has been paid to histamine and histamine receptors and their ability to regulate cell growth and proliferation in the past years. Several studies have focused on understanding how histamine is functional in cancer development, growth and metastatic behaviour (Cianchi et al. 2008; Medina and Rivera 2010). Indeed, histamine can regulate various biological processes associated with tumour growth including cell proliferation, migration, differentiation, and apoptosis, and it exerts different responses based on its local concentration and the type of receptor subtype activated (Faustino-Rocha et al., 2017). Histamine and the enzymes necessary for its biogenesis and degradation have been identified in a variety of cancers. Several studies have found histamine concentration to be higher in the plasma of women with breast cancer compared with healthy individuals (Chanda and Ganguly 1987; Sieja et al. 2005; von Mach-Szczypiński et al. 2009); moreover, histamine concentration has been shown to be higher in breast, colorectal and skin cancer tissues compared with both healthy surrounding tissues of the same patients and with healthy tissues obtained from healthy individuals (Chanda and Ganguly 1995; Sieja et al. 2005; von Mach-Szczypiński et al. 2009).

Deregulation of all four histamine receptors has been identified in several human cancers as reviewed by Medina *et al*. (2011). Preliminary bioinformatic studies using gene expression values of human pancreatic ductal adenocarcinoma (PDAC) tissues (obtained from the TCGA database) showed a 32 fold increase of HRH1 mRNA in PDAC compared to normal pancreatic tissues and this increase was seen in 100% of the PDAC samples (Rodriguez et al. 2018). *In vivo* analysis of PDAC tumours isolated from KPC mice (model of PDAC) confirmed this bioinformatic data, with PDAC tissue showing high HRH1 expression compared to normal mouse pancreatic tissue (Salmerón et al. 2020). Similarly, a recent meta-analysis from Wang and colleagues (2014) investigating prognostic values of human HRH1 in different cancers demonstrated that while high level of expression of HRH1 is associated with poor survival in patients with cancers of the breast, lung, soft tissue, brain, colorectum, and in B-cell lymphoma, low level of HRH1 expression is related to poor survival of people affected from myeloma, bladder or ovarian cancers (Wang et al. 2014). These findings show how clinical studies analysing the association between HRH1 and cancer prognosis produced different results in different cancer types and highlight the need for further research.

The beneficial use of antihistamine in combination with first line therapies for cancer patients has been reported by several clinical studies. For example, Fritz *et al*. (2020) showed that amongst 61,000 women diagnosed with breast cancer, loratadine or desloratadine (both inverse agonist of HRH1) users showed improved survival relative to nonusers (Fritz et al. 2020). Similarly, a cohort study on the effect

of cationic amphiphilic antihistamines on patients diagnosed with non-localised cancers (e.g cancer at the breast, digestive organs, respiratory system and thoracic organs, male or female genital organs, lymphatic and hematopoietic tissue, urinary tract and more) showed that loratadine, astemizole and ebastine (selective HRH1 antagonists) were associated with reduced mortality, particularly in patients simultaneously undergoing chemotherapy (Ellegaard et al. 2016). A retrospective study by Verdoodt and colleagues (2019) on EOC patients did not show a correlation of antihistamine users with overall survival; however, antihistamine use shows an inverse association with serous ovarian cancer risk in pre-menopausal women, and an inverse association independently of menopausal status with mucinous ovarian cancer risk (Verdoodt et al. 2019).

Even though there is evidence implicating a role for histamine and its receptors in cancer progression and outcome, their role in ovarian cancer pathogenesis and progression has not been entirely elucidated, and further investigation is needed to establish the mechanisms by which they affect ovarian cancer cells.

A previous correlation analysis between gene expression and invasion, migration, motility, and cell proliferation rates of six ovarian cancer cell lines belonging to the NCI60 cells panel were carried out in our laboratory by a former master research student, Mohammad A. Miah. Genes showing a significant correlation were run through an Ingenuity Pathway Analysis (IPA) to determine which cellular pathways these genes were involved in. This analysis identified 112 genes, including HRH1, that were associated with OC migration and invasion. This preliminary work identified a potential role for HRH1, but further investigation is needed to explore the expression of HRH1 with respect to ovarian cancer progression.

3.2 Aim and objectives

The aim of the work described in this chapter was to confirm and further analyse the correlation between histamine receptor's expression and OC invasion, migration and metastatic potential. The specific objectives were:

- To investigate a potential relationship between histamine's receptors expression in OC cells lines and their invasive and migratory rates
- To study the expression of histamine's receptors in a microarray dataset of OC specimens, and investigate if there was a correlation with patient's overall survival or progression free survival
- To explore HRH1 mRNA and protein levels in a panel of OC cell lines
- To determine the invasion rate of two of the cell lines used in this project, SKOV3 and OVCAR3, through a Matrigel ® layer

3.3 Results

3.3.1. HRH1 positively correlates with the invasion and migration rates of OC cells, while no correlation is found for the other histamine receptors.

In order to investigate the correlation of histamine receptors expression with OC cell behaviour, existing publicly available datasets were first made use of. In the 1980s, the NCI60 panel of 60 cell lines, covering a wide variety of cancer types, was created as a tool to screen compounds for their anticancer activity. Of these 60 cell lines, six of them (IGROV1, OVCAR3, OVCAR4, OVCAR5, OVCAR8 and SKOV3) are representative of OC and were used in this project. The Cell Miner database produced by Reinhold et al. (2012), is an online tool which integrates gene transcripts, microRNAs and chemical compound activity data across different platforms using the NCI60 database.

From the Cell Miner database, RNA microarray data were obtained from a microarray dataset (RNA Affy HG-U133 Plus 2.0, GSE32474) and histamine receptors expression level in the six different OC cell lines plotted in a heatmap (Figure 3.1 A). Heatmaps are a tool to visually represent gene expression data. Among the four different histamine receptors, HRH1 appeared to be expressed differently in the six OC cell lines, with SKOV3 bearing its highest expression and IGROV1 its lowest expression (Figure 3.1 A). HRH2 and HRH3 were expressed at very similar levels by the six cell lines, while HRH4 expression was lower than the detection limit of the assay and was therefore not further analysed. To evaluate if the expression levels of HRH1, HRH2 and HRH3 were related to the *in vitro* invasion and migration behaviour of the six OC cell lines belonging to the NCI60 panel, data previously generated by Mulcahy (2016) (former PhD student in the lab) were used. By using a Matrigel® invasion assay and a transwell migration assay, Mulcahy assessed the *in vitro* invasion and migration ability of IGROV1, OVCAR3, OVCAR4, OVCAR5, OVCAR8 and SKOV3, respectively (Mulcahy 2016) (Figure 3.1 B). As these data were normally distributed, Pearson correlation analysis was chosen to evaluate the presence of a potential linear relationship between gene expression levels and *in vitro* characteristics. From correlation analysis, HRH1 expression showed a Pearson's correlation coefficient (R) of 0.811 ($p=0.05$) with invasion rates of the cell lines (Figure 3.1 C) and a Pearson's R of 0.0816 ($p=0.048$) when correlated with the migration rate of OC cells through a transwell membrane (Figure 3.1 D). HRH2 and HRH3 expression levels showed no correlation with either migration or invasion behaviour of the six cell lines (Figure 3.1 E). Taken together, these results reveal that six OC cell lines, IGROV1, OVCAR3, OVCAR4, OVCAR5, OVCAR8 and SKOV3, express three of the four histamine receptors. In particular, HRH1 expression has a linear positive correlation with OC cells invasion and migration *in vitro*, meaning that cells expressing a higher HRH1 level migrate and invade faster than cells expressing a low level of HRH1.

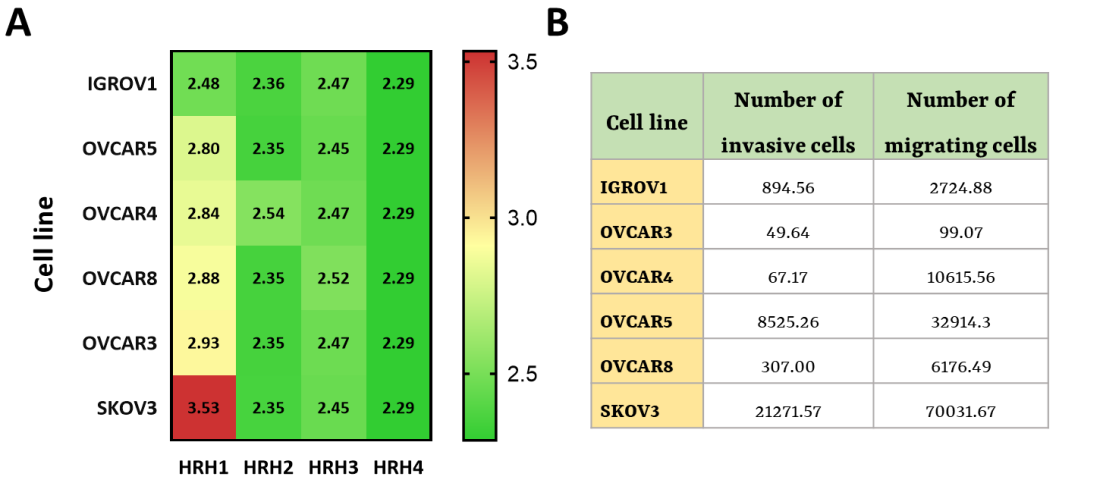

Cell line	Number of invasive cells	Number of migrating cells
IGROV1	894.56	2724.88
OVCAR3	49.64	99.07
OVCAR4	67.17	10615.56
OVCAR5	8525.26	32914.3
OVCAR8	307.00	6176.49
SKOV3	21271.57	70031.67

E

Gene	Biological process	Pearson	
		R	P value
HRH1	invasion	**0.811**	**0.05**
	migration	**0.816**	**0.048**
HRH2	invasion	- 0.300	0.563
	migration	-0.189	0.720
HRH3	invasion	-0.539	0.270
	migration	-0.519	0.291

Figure 3.1: Histamine receptors expression in six OC cell lines and their correlation with invasion and migration in vitro.

A) Heat-map showing mRNA expression level of the four histamine receptors in the six OC cell lines belonging to the NCI-60 panel. Data were obtained from the Cell Miner (GSE32474) dataset. The individual rectangles in the heatmap are coloured with a range of colours proportionated to gene expression values (green for lower expression, yellow for medium expression, red for higher expression). Each rectangle contains the expression levels of a specific histamine receptor (columns) in a specific cell line (row). B) In vitro cell invasion (through a Matrigel® layer) and migration (through a transwell) rates of IGROV1, OVCAR3, OVCAR4, OVCAR5, OVCAR8 and SKOV3 were obtained from Mulcahy (2016). Pearson correlation analysis showing HRH1 expression in relation to C) OC invasion and D) OC migration *in vitro*. E) Pearson correlation coefficient (R) and p-value of HRH1, HRH2 and HRH3 gene expression and *in vitro* invasion and migration rates of six OC cell lines.

3.3.2. HRH1 is expressed in OC clinical samples and its expression correlates with OC stage

In order to explore whether HRH1 expression correlates with OC stage, a dataset containing mRNA expression data from 403 clinical samples of HGSOC was obtained from the TCGA database (The Cancer Genome Atlas Research Network 2011). Patients' age ranged between 30- to 90-years, and among these 21 patients presented the disease at stage II, 319 at stage III and 61 at stage IV (Figure 3.2 A). Stage information were missing from ten patients, and these were therefore excluded from the analysis (Figure 3.2 A). The remaining 393 patients were grouped by stage (II, III, IV) and the mRNA expression of HRH1, HRH2, HRH3 and HRH4 was reported using a heatmap (Figure 3.2 B). As seen in figure 3.2 B, among the four histamine receptors, HRH1 mRNA was expressed in clinical samples from patients in all stages, with late-stage OC samples (III and IV) showing a higher degree of expression compared to stage II samples (Figure 3.2 B). No difference in HRH2 expression levels was found between samples from patients at different cancer stages, while HRH3 and HRH4 detection levels were as low as the technique detection limits. Moreover, median expression values for each histamine receptor were calculated for each patient stage group, and fold change of expression were calculated between stage IV and III, or stage IV and II (Figure 3.2 C). Clinical samples obtained from patients in stage IV expressed significantly higher level of HRH1 mRNA compared to stage II patients ($p=0.003$) and showed a trend to be increased when compared to patients in stage III, although this did not reach statistical significance ($p=0.054$) (Figure 3.2 C). On the other hand, even though HRH2 mRNA was detectable across different stages (Figure 3.2 B), its expression was very low and no association with disease progression was found (stage II v IV $p=0.56$, stage III v IV $p=0.72$) (Figure 3.2 C). HRH3 and HRH4 mRNA levels were very low and were therefore not further analysed (Fig 3.2 B, C).

As HRH1 mRNA was highly expressed in late-stage patients, its correlation with patient's overall survival and progression free survival was explored by using Kaplan-Meier curves. Kaplan-Meier curve is a visual representation used to estimate the survival of two groups of patients in a specific time frame, and to show what the probability of an event (for example, survival) is at a certain time interval (Rich et al. 2010; Barakat et al. 2019). The time intervals are not defined by a fixed length of time but depend on the occurrence of an event. The events of interest are death of a patient or when a patient is censored (either did not experience the death event or its follow-up was lost). The data are collected from the day the patients entered a study until the day they died or their follow-up was lost (Tolley et al. 2016). Kaplan-Meier plotter can be utilised for the analysis of individual genes or groups of genes (Rich et al. 2010). In this project, overall survival and progression free survival data were used for survival analysis. Overall survival of a cancer patients is the length of time from the date of the diagnosis or the start of the treatment to the date the patient is still alive. Progression free survival is

the length of time during and after the treatment of cancer, during which the patient lives with the disease without it growing or spreading around the body. Overall survival of 389 OC patients and progression free survival of 315 OC patients was related with HRH1 mRNA level of expression. Without considering the disease stage, patients were grouped into two categories depending on the level of expression of HRH1: high expressing patients (patients in which HRH1 expression was higher than the median value) and low expressing patients (patients in which HRH1 expression was lower than the median value). Kaplan-Meier overall survival curve showed no correlation between HRH1 and overall survival in OCs patients (p= 0.98), with both groups showing the same probability of death (hazard ratio (HR) =0.9947) (Figure 3.2 D), and a very similar median survival time (41.31 months for low expressing patients compared to 44.36 of high expressing patients). Similar results were obtained with patients' progression free survival (p=0.90, HR=0.98) (Figure 3.2 E), with low expressing patients showing a similar median progression free survival time (16.07 months) than high expressing patients (17.48 months). Kaplan-Meier plots obtained from an online database (Gyorffy et al. 2012) showed similar results for overall survival of patients, where patients with high HRH1 (median survival time 46.1 months) presented the same probability of death (HR=0.9, p=0.19) as patients with low HRH1 (median survival time 41.9 months) (Figure 3.2 F). However, the progression free survival curve showed patients presenting low level of HRH1 (median survival time 18.1 months) to have significantly better survival then patient presenting high HRH1 (median survival time 16 months) (HR=1.18, p=0.024), the opposite result to the TCGA data (Figure 3.2 G). Taken together, these findings show that HRH1 and HRH2 mRNA are expressed in ovarian biopsies obtained from OC patients, and in particular, HRH1 is significantly higher in patients with stage IV of the disease. Moreover, HRH1 expression does not correlate with patients' overall survival while its correlation with progression free survival is controversial and depends on the dataset analysed.

A

Stage	Number of patients	Age				
		Missing	<50	50-59	60-69	>69
II	21	0	3	8	5	5
III	319	8	63	95	78	76
IV	61	2	15	22	13	9
Total	392	10	81	125	96	90

B

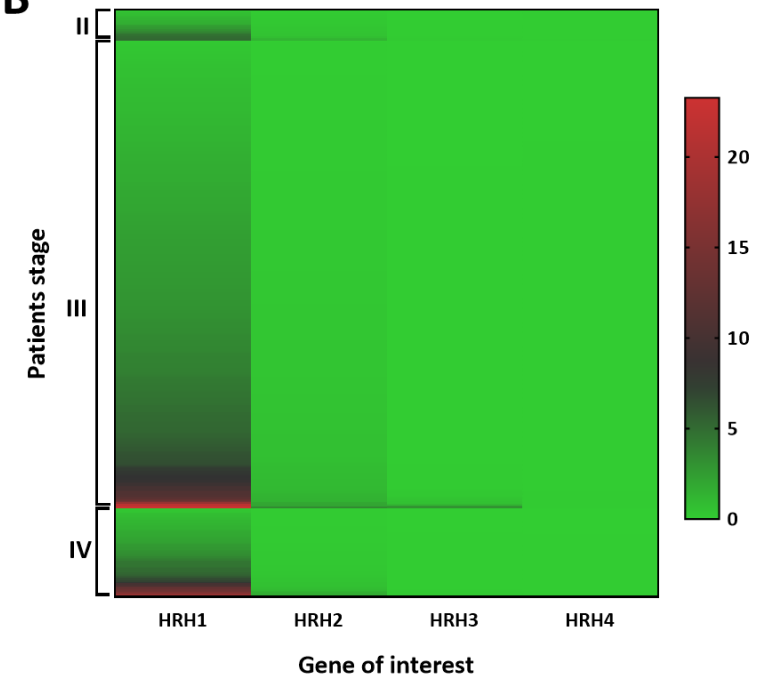

C

	Median value of histamine receptors expression			Fold change		P value	
Gene	Stage II	Stage III	Stage IV	IV/II	IV/III	II v IV	III v IV
HRH1	2.34	2.65	3.12	**1.336**	**1.179**	**0.003**	**0.054**
HRH2	0.29	0.26	0.21	0.71	0.786	0.56	0.7152
HRH3	0.01	0.01	0.010				
HRH4	0.01	0.009	0.008				

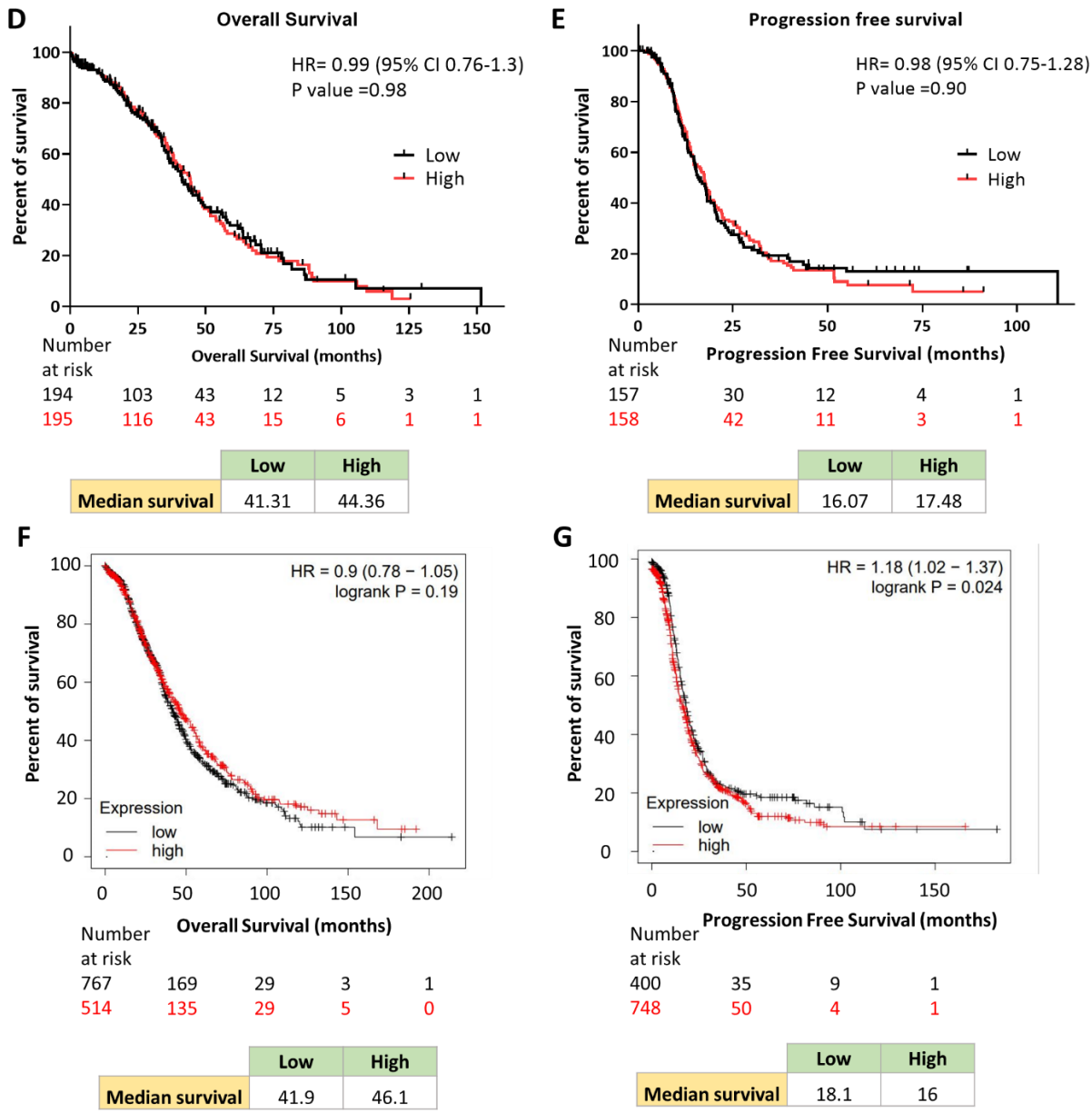

Figure 3.2: mRNA expression of histamine receptors in clinical samples of OC and their correlation with overall and progression free survival.

Microarray data of 403 OC clinical samples were obtained from the TCGA database A) Age and stage information of the patients included in the analysis. B) Heat-map showing mRNA expression of HRH1, HRH2, HRH3 and HRH4 in OC clinical samples ranked by stage (from top to bottom: stage II to IV). The colours range is proportionated to gene expression values (green for expression values between 0 and 8, black for expression values between 8 and 15, red for expression values between 15 to 25). C) The mRNA expression median value of the four different histamine receptors was calculated for each stage of the disease. Fold change of expression between stage IV and II or stage IV and III was calculated and P-values reported through a t-test. Kaplan-Meier curves were calculated between high expression patients (red) and low expression patients (black) for D) overall survival and E) progression free survival. Additional Kaplan-Meier plots were obtained from the online database "The Kaplan-Meier plotter" (http://kmplot.com/analysis/) and show percent of survival for F) patients' overall survival and G) patients' progression free survival. The numbers at the bottom of each Kaplan-Meier graph indicates the numbers of patients at low (black) and high (red) risk still alive at each of the time points reported on the graph.

3.3.3. HRH1 is expressed in SKOV3, OVCAR3 and OVCAR5 at both RNA and protein level

The findings so far have shown that of the four histamine receptors, HRH1 has the highest expression in both ovarian cancer cell lines and ovarian cancer clinical samples, and that its expression seems to be related with invasion and migration *in vitro*. To evaluate HRH1 expression in the three OC cell lines used in this project, an RT-qPCR analysis was carried out on SKOV3, OVCAR3 and OVCAR5. As show in figure 3.3 A, HRH1 mRNA expression, reported as fold change compared to β-Actin (and normalized to HRH1 expression in HME (immortalised epithelial breast) cells), was measured in all the cell lines, and SKOV3 showed its highest expression, with more than a two-fold increase compared to OVCAR3 ($p=0.026$; SKOV3 mean=2.35 ± SD=1.06; OVCAR3 mean=0.89 ± SD=0.80) (Figure 3.3 A). These data are in agreement with what was previously shown in the microarray analysis (section 3.2.1). HRH1 was also quantified at the protein level in the three cell lines by using both western blot and immunofluorescence analysis (Figure 3.3 B, D, respectively). Western blot analysis, reported as fold change against GAPDH, displayed the presence of HRH1 (band around 56 KDa) and GAPDH (band at 37 KDa), confirming the presence of HRH1 in the three cell lines (Figure 3.3 B, C). SKOV3, OVCAR3 and OVCAR5 were also immunolabelled with α-HRH1 antibody (Figure 3.3 D) and total HRH1 immunopositivity was calculated as corrected total cell fluorescence (CTCF) through the imaging software Fiji (Figure 3.3 E). CTCF, normalised to CTCF of HME (immortalised epithelial breast cells, used as control to normalise RNA and protein data) cells, showed that HRH1 was present in all three OC cell lines and although no statistically significant differences were found among them ($p=0.43$), a small trend towards an increase in SKOV3 cells was seen. Overall, the data presented here show that HRH1 is expressed by three different ovarian cancer cell lines, and while mRNA levels seem to be higher in SKOV3, the three cell lines seem to present the same level of the protein.

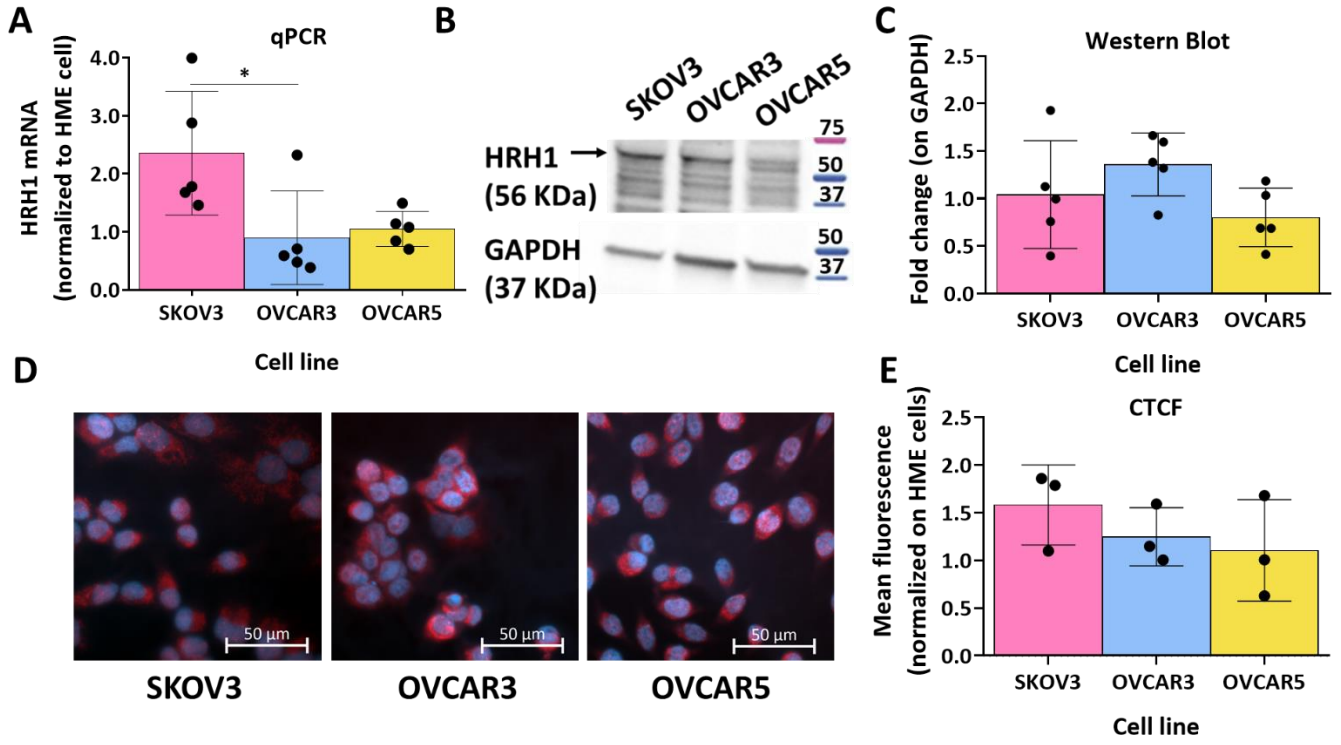

Figure 3.3: HRH1 expression was evaluated in SKOV3, OVCAR3 and OVCAR5 at both mRNA and protein level

HRH1 expression was assessed in SKOV3, OVCAR3 and OVCAR5 with different techniques. A) RT-qPCR analysis showing the relative quantity of HRH1 (normalised on relative levels of HRH1 in HME cells) in the three different cell lines. The mean values of 5 independent experiments were combined for statistical analysis. B) Representative western blot showing HRH1 (56 KDa) and GAPDH (37 KDa, endogenous control) protein levels in SKOV3, OVCAR3 and OVCAR5. C) HRH1 fold change relative to GAPDH was measured by western blot analysis in the three OC cell lines. The mean values of five independent experiments were combined for statistical analysis. D) Representative immunofluorescence images of HRH1 (red) and DAPI (blue) in the three OC cell lines; scale bar 50 µm. E) Cell total corrected fluorescence (CTCF) was used to quantify HRH1 protein level by immunofluorescence. Data were normalized to HRH1 expression in HME cells. The mean values of three independent experiments were combined for statistical analysis. One-way ANOVA, followed by Tukey post-hoc test was used to quantify statistical differences. Bars show 1X SD; * P<0.05.

3.3.4. SKOV3 cells invade more than OVCAR3 through a Matrigel® layer

So far, the results obtained have shown that HRH1 is expressed by SKOV3, OVCAR3 and OVCAR5 and that its mRNA expression correlates with their invasion and migration *in vitro*. As the invasion data used for the correlation analysis were generated by Mulcahy (2016), *in vitro* invasion rates of SKOV3 and OVCAR3 (the most and least invasive cell lines according to Mulcahy (2016) data, respectively) were explored through a Matrigel® invasion assay. Cells were plated on top of the Matrigel® layer, allowed to invade for 48 h and then stained with crystal violet, imaged and counted (see section 2.14 for further details) (Figure 3.4 A). The percentage of invading SKOV3 (mean=10.22 ± SD=4.44) was 3.5-fold higher than OVCAR3 (p=0.035; mean=2.87 ± SD=2.66), confirming that SKOV3 have a higher invasion potential than OVCAR3 (Figure 3.4 B).

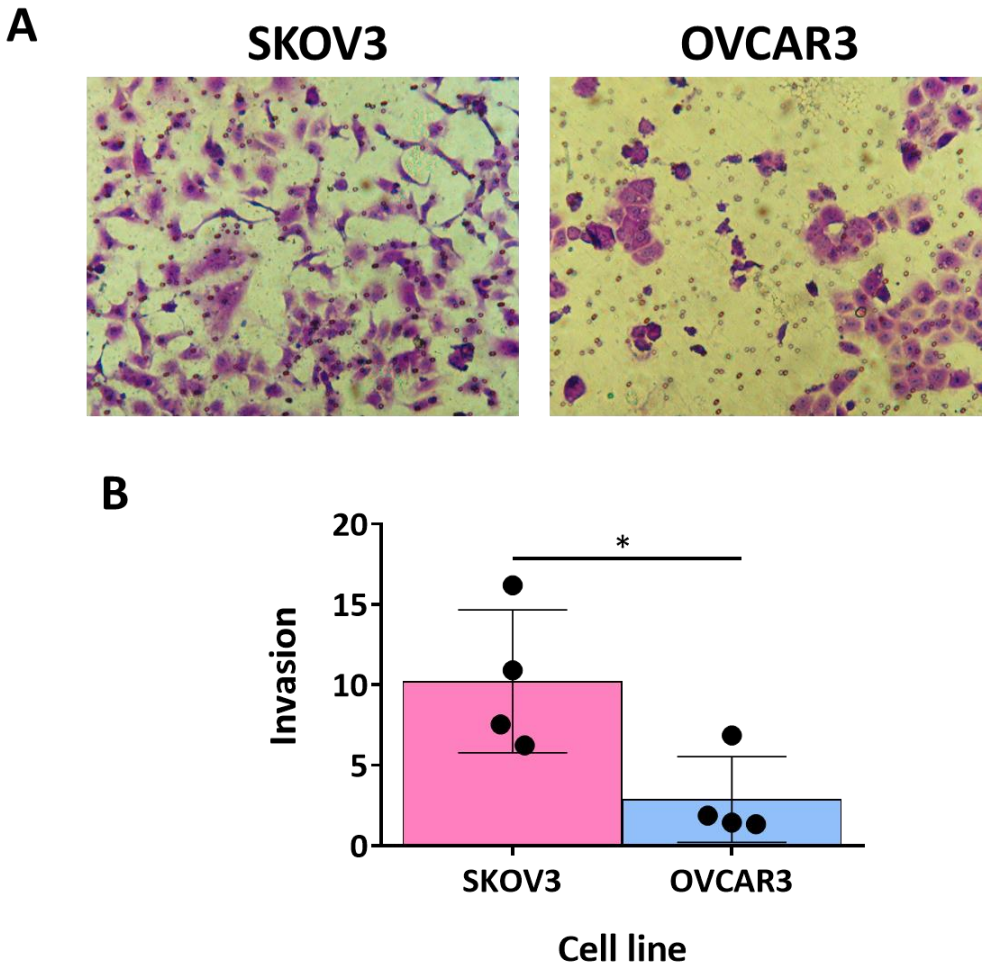

Figure 3.4: SKOV3 cells invade more than OVCAR3 through a Matrigel® layer.
A) Representative images of a Matrigel® invasion assay on SKOV3 and OVCAR3. Cells were stained with crystal violet. B) Percentage of invading cells through a Matrigel® layer. T-test followed with Welch's correction was used to quantify any statistical differences. Bars showing 1X SD; * P<0.05.

3.4 Discussion

The aim of the work described in this chapter was to test if there was an association between histamine receptors expression and the behaviour of OC cells in assays modelling aspects of metastatic behaviour *in vitro* and in clinical samples. To test the former, a Pearson correlation analysis was carried out between gene expression data of six OC cell lines (IGROV1, OVCAR3, OVCAR4, OVCAR5, OVCAR8, SKOV3) obtained from the Cell Miner database (Reinhold et al. 2012) and their *in vitro* migration and invasion rates previously estimated by Mulcahy (2016). Amongst the four histamine receptors, HRH1 gene expression levels were different across the six OC cell lines and there was a positive correlation between HRH1 gene expression and the migration and invasion rates of the cell lines *in vitro*. SKOV3 showed the highest HRH1 expression and the highest invasion and migration rates *in vitro*. Both HRH2 and HRH3 had a very low expression level in the cell lines and no correlation was found with their invasion or migration; HRH4 levels were too low to be detectable. Similarly, mRNA expression analysis of the histamine receptors in a subset of OC clinical samples showed that HRH1 was the only receptor expressed in OC samples in stage II, III and IV. Moreover, HRH1 highest expression was found in specimens obtained from patients in late stages of the diseases (stage IV), showing a fold-change increase of HRH1 mRNA of 1.3 and 1.2 when compared with samples obtained from patients in stage II or III, respectively. These finding suggest that HRH1 might be involved in, or associated with, disease progression. HRH2 displayed a low expression in OC clinical samples and in the *in vitro* data, and its expression was not correlated with disease stage; HRH3 and HRH4 mRNA were expressed at low levels in OC clinical samples. These findings together indicate the presence of HRH1 in both clinical samples of OC and in OC cell lines, and are consistent with its potential involvement in cancer progression and metastasis. Only six OC cell lines were used for correlation analysis, and such a small number of data points is not ideal for generating reliable results. Although the six OC cell lines considered in the presented analysis are the only OC cells contained in the NCI60 panel, other dataset available online, like the one generated by Schaner et al. (2003), include a larger dataset of OC cell lines and could have been integrated into the analysis to further implement the results. Therefore, the presented correlation analyses are consistent with the possibility that HRH1 plays a role in OC invasion and migration, but further experiments are necessary to confirm this.

Similarly, only one dataset comprising gene expression information of 403 HGSOC clinical samples was used to investigate the clinical correlation between histamine receptors gene expression and disease progression. More than half of the patients were classified at stage III (n=319) of the disease while the number of patients presenting early stage of OC (stage II) or late stage (Stage IV) was very small (n=21, n=61, respectively). A multitude of datasets, containing different cohorts of patients (FireHouse Legacy, PanCancer atlas http://www.cbioportal.org/), are available online and could have been

integrated into the analysis, although such an extensive bioinformatic analysis lies beyond the scope of this thesis. However, a brief exploration of these datasets gives further insight into the potential involvement of HRH1 in OC. For example, the online tool UALCAN, generated by Chandrashekar and colleagues (Chandrashekar et al. 2017) includes the analysis of 302 ovarian serous cystadenocarcinoma clinical samples and confirmed the overexpression of HRH1 in patients presenting with stage IV disease (median of HRH1 expression= 6.406) compared with stage II (HRH1 median of expression= 6.05) and III (HRH1 median of expression= 4.804), further supporting the case for a role of HRH1 in OC progression.

Survival analysis showed no correlation between HRH1 gene expression and patients' overall survival. Actually, although not significant, it was curious to observe that patients expressing high level of HRH1 had a slightly higher median survival time (≈ 44 months) than patients with low levels of HRH1 (≈ 41 months). This data was further confirmed by using the online tool "The Kaplan-Meier plotter", a database which included overall survival data of a much larger patient cohort (1,281). These findings pinpoint to the possibility that the higher expression of HRH1 in clinical samples of stage IV OC may to an extent be beneficial for patients and might lead to a small increase of survival. Correlation of HRH1 gene expression and TCGA patients' progression free survival data showed no differences in time to relapse. Surprisingly, by using "The Kaplan-Meier plotter" database, the same analysis showed that patients with low level of HRH1 had longer survival time (2 months more) than patients with high level of HRH1. The discrepancy between these results might be related to the dataset itself and to the parameters chosen for the analysis. First of all, "The Kaplan-Meier plotter" uses a much larger database of patients (1,281 OC) compared to the 315 obtained from TCGA and therefore might provide a more representative analysis. Second, the TCGA dataset contains information of patients affected by HGSOC while "The Kaplan-Meier plotter" includes patients affected by serous (both HGS and LGS) and endometrioid OC. The presence of different OC subtypes might therefore explain the differences between the results here presented. Moreover, for both databases, a follow-up time of more than 100 months was used for overall and progression free survival analysis. By month 50, more than three quarters of patients were dead or censored, and the remaining survival time was calculated on a very small number of patients that was not anymore representative of the overall population. This might have led to generation of misleading results that should be interpreted with caution. Indeed, Kaplan-Meier analyses are most accurate at the time point when most patients are still present in the study (Rich et al. 2010). Overall, while HRH1 does not seem to be a good prognostic marker for patients' survival, it seems to play a potential role in disease progression and further studies are needed to elucidate this mechanism.

Few studies are available regarding the expression of HRH1 and its role in ovarian cancer patients, but both its mRNA and protein have been already identified in a variety of cancer patients' samples including liver, colorectal, ovarian, endometrial, breast, urothelial cancers and melanoma, (The protein atlas, access in May 2021). Moreover, the role of HRH1 in cancer progression and its association with a poorer prognosis and overall survival has been already demonstrated in pancreatic, colorectal and breast cancer studies, as already described in sections 1.4.3 and 3.1 (Fernández-Nogueira et al. 2016; Fernández-Nogueira et al. 2018; Rodriguez et al. 2018; Salmeron et al. 2020; Zhao et al. 2020) and the idea of repurposing antihistaminic drugs as promising novel therapeutics for cancer treatment has gained a lot of attention (Medina and Rivera 2010; Faustino-Rocha et al. 2017).

The expression of HRH1 was further analysed in SKOV3, OVCAR3 and OVCAR5 both at the mRNA and protein level. All the cell lines express HRH1 mRNA, with SKOV3 exhibiting the highest expression, which is in agreement with what was shown by the NCI60 microarray. Similar to the mRNA expression analysis, the three OC cell lines investigated expressed HRH1 at the protein level. Although the western blot analysis revealed similar levels of HRH1 across samples, the technique did not seem to be sensitive enough for quantify HRH1 protein levels. The HRH1 western blot band appeared as a strong band at the correct molecular weight (56 KDa), but additional bands with molecular weights ranging between 10 to 60 KDa were detected each time, potentially indicating a low specificity of the antibody. Unfortunately, even though two different antibodies were tested and the protocol was implemented to ensure the highest possible resolution, the same additional bands were observed across different replicates. Perhaps, the use of alternative antibodies would have produced more specific and clean results, although it is widely recognise in literature that western blot are high variable technique, and several parameters can influence their reproducibility such as protein sample handling, gel composition, blocking buffers and others (Ghosh et al. 2014; Gilda et al. 2015). If available, a blocking peptide would have been used to run pre-adsorption tests and validate antibody specificity. During the 'pre-absorption test', the antibody is pre-incubated with an excess of blocking peptide (the immunogen used to generate the antibody). If the antibody binds specifically to the immunizing peptide, the pre-adsorption steps will decrease the intensity of the protein staining; if the antibody binds to other proteins, the intensity of the signal will be unvaried (Pillai-Kastoori et al. 2020). This method has several limitations: for example, binding of the blocking peptide with the antibody might reduce off-target binding to other antigens presenting the same epitope, producing a 'false specificity' (Pillai-Kastoori et al. 2020).

To complement the western blot data, HRH1 protein level was evaluated by immunolabelling analysis; CTCF quantification of HRH1 labelling confirmed the presence of the protein in SKOV3, OVCAR3 and OVCAR5 cells and indicated a similar level of immunopositivity across the samples. Curiously, while RT-

qPCR analysis show SKOV3 to bear higher level of HRH1 compared to the other two cell lines, protein levels appeared to be similar in the three cell lines. These differences could be attributed to the low specificity of the antibodies used for western blot and immunolabelling analyses. Nevertheless, several mechanisms like post-translational modification, ribosome occupancy, protein half-life and degradation, and technical noise could explain the poor correlation between mRNA and protein expression (Greenbaum et al. 2003; Abreua et al. 2009; Maier et al. 2009). In addition, preliminary investigation of the *in vitro* invasive potential of OC cells shows that SKOV3 invaded significantly more than OVCAR3 through a Matrigel® layer, confirming what previously identified by Mulcahy (2016). This evidence together with the finding that SKOV3 bears higher level of HRH1 mRNA could suggest a potential implication of HRH1 in OC invasiveness *in vitro*.

3.5 Key findings

- HRH1 is expressed in three OC cell lines, and it is correlated with OC invasion and migration *in vitro*
- HRH1 is expressed at higher levels in clinical samples of stage IV OC than stages II or III
- SKOV3, OVCAR3 and OVCAR5 express HRH1 at both RNA and protein level, with SKOV3 showing the highest mRNA expression
- SKOV3 invasion rate through a Matrigel® layer is higher than OVCAR3, and this could be possibly related with SKOV3 bearing the highest expression of HRH1 mRNA

Chapter 4

The role of HRH1 in metastatic mechanisms

4. The role of HRH1 in metastatic mechanisms

4.1. Background

Metastasis is the result of a multi-stage process that leads to the development of a secondary tumour in a part of the body distant from the primary one (Fares et al. 2020). Histamine and its four receptors have been implicated in different steps of tumour growth and progression, highlighting the dual role that this amine plays in cancer biology (Kahlson and Rosengren 1968). For example, histamine decreases tumour proliferation through HRH1 activation and promotes tumour growth by exerting an immune-inhibitory effect through the stimulation of HRH2 on T lymphocytes (Burtin et al. 1982). Early *in vitro* and *in vivo* studies on the role of HRH1 antagonists in cancer were inconclusive, with some studies showing no effects on tumour growth (Kurokawa et al. 1995), some displaying decreased mice survival and tumour growth promotion (Burtin et al. 1982; Brandes et al. 1994) and others revealing anti-tumour effects (Urdiales et al. 1992; Gómez-Fabre et al. 1997). Since then, several studies have been published supporting the idea that HRH1 might play a role in cancer progression. A recent paper by Fernández-Nogueira and colleagues (2018) show that selective chemical inhibition of HRH1 reduces the migration of MDA-MD-231 and BT-549 (breast cancer) cell lines in a wound-healing model, potentially by decreasing the expression of the mesenchymal marker vimentin. In addition, HRH1 inhibition induces accumulation of cells in sub-G0 phase, with consequent suppression of cell proliferation, and triggers activation of the mitochondrial pathway via ERK activation (Fernández-Nogueira et al. 2018). Similarly, by using both wound-healing and transwell migration assays, Zhao et al. (2020) demonstrate that SNU368 and HLE (hepatocellular carcinoma) cell lines migrate more slowly than control cells when HRH1 is knocked down, while their migratory ability increases when HRH1 is overexpressed. Similar results were obtained in a Matrigel® invasion assay. Furthermore, the authors validate the *in vitro* findings by injecting into the lateral tail vein of nude mice SNU368 cells with HRH1 knocked down, or HLE cells with HRH1 overexpressed. By assessing the number of metastatic nodules in the lung, Zhao and colleague demonstrated that HRH1 knockdown drastically decreases the metastatic potential of SNU368 cells while HRH1 overexpression in HLE cells significantly increases the incidence of lung metastasis (Zhao et al. 2020). Thus, although there is some evidence for the involvement of HRH1 in different aspects of the metastatic cascade, little is known about its role in metastatic spread of OC.

4.1.1. Methods to study the different steps of the metastatic process *in vitro*

Three ovarian cancer cell lines with different aggressiveness profiles (section 2.1.1) were used as a model to study the involvement of HRH1 in aspects of ovarian cancer metastasis. These cells were employed in different assays to test individual steps of the metastatic cascade *in vitro.*

Epithelial to mesenchymal transition

EMT is a reversible transformation during which cells lose their epithelial phenotype and acquire a mesenchymal one (Hay 1995) (see section 1.2.1 for further details). During this process, epithelial cells lose epithelial features, such as their polarity, and reduce cell adhesion structures by downregulating adhesive molecules, including E-cadherin (CDH1), claudins, cytokeratin and others. Classical epithelial molecules are replaced by mesenchymal markers such as vimentin, catenins, N-cadherin allowing cells to collectively acquire mesenchymal features and increase their motility and invasive ability (Kalluri and Weinberg 2010). In this project, EMT was investigated by quantification of CDH1 and vimentin through RT-qPCR analysis (Yang et al. 2020), as described in section 2.5.5.

Cellular adhesion to endothelial cells

After invasion into surrounding tissue, cancer cells reach lymphatic or blood vessels, enter them (intravasation) and are transported to distant organs, where they can exit the vessels (extravasation) and colonise new sites (further details can be found in section 1.2). In order to intravasate and later extravasate from blood vessels, cancer cells need to adhere to them and survive several stresses they will face during their transit in the bloodstream (see section 1.2 for further details) (Gupta and Massagué 2006).

In this project, a static adhesion assay was employed to investigate the ability of OC cells to adhere to endothelial cell monolayers, under different conditions (for details regarding the protocol see section 2.12). Endothelial cells were grown until confluency and activated with a pro-inflammatory cytokine. Cancer cells were labelled with a fluorescent dye and introduced onto the endothelial cell monolayer then allowed to interact for a short time. Non adherent cells were eluted, and adherent cells were quantified.

Cellular invasion

Cell invasion is a 'hallmark' of cancer (Krakhmal et al. 2015); during cancer invasion, cells detach from the main tumour, adhere to the ECM, degrade it and bypass physical barriers like the basement membrane (BM) to access other sites (for further details see section 1.2) (Sahai 2005). The BM, a

specialised extracellular matrix (ECM), is a network of macromolecules that encloses cells in a specific tissue or organ.

A Matrigel® invasion assay was used to test the involvement of HRH1 in OC cells invasion, as described in section 2.14. The system employed in this assay is made of two compartments divided by a porous membrane permeable to cells (Hall and Brooks 2014); the size of each pore is smaller than the diameter of a cell, ensuring that passage of any cell through it is due to active cell-migration processes. This assay is based on the transwell invasion assay method (Boyden 1962) with the addition of a layer of extracellular matrix-like substance (Matrigel®) on top of the transwell. Cells are plated on top of the Matrigel® in serum-free media and placed into a well containing media supplemented with a chemoattractant (FBS in this project). Cells able to migrate and invade, will hydrolyse the Matrigel® layer, move through the membrane's pores and attach to the underside of the membrane. Non invading cells remain on the upper side of the membrane. Invading cells are stained and quantified.

Cell motility

Cell migration describes the movement of cells on a surface. Cell migration is a process that occurs during normal physiological process like embryogenesis (Keller 2006) and wound healing (Friedl and Wolf 2009) and pathological process including cancer metastasis (Clark and Vignjevic 2015). Cancer cells are particularly able to adapt to the surrounding environment, assuming disparate morphology and migration characteristics that allow them to stay motile (for more information see section 1.2) (Friedl et al. 2012). Cells can migrate both as individual single cells (through amoeboid-like migration or fibroblast-like migration) or as an organised group of cells (Krakhmal et al. 2015). A variety of *in vitro* techniques are available to study cell motility, including the transwell chamber migration assay, cell exclusion zone assay, wound healing assay and others (Decaestecker et al. 2007; Paul et al. 2017).

In this project, a wound healing assay was used to study the motility of OC cells treated with different compounds (section 2.13). Cells are plated and grown to confluency and the monolayer is 'wounded' by scratching with a pipette tip. 'Wound' closure is imaged over time and cell migration is assessed by measuring the reduction in the size of the 'wound' area at different time point.

4.2. Aim and objectives

Histamine can influence cancer cells proliferation and alter their invasion, migration and adhesion, via activation of its receptors but its role has not yet been studied in ovarian cancer. The aim of the work described in this chapter was to investigate the role of HRH1 in the different steps of the metastatic cascade of ovarian cancer cells *in vitro*. The specific objectives were:

1. To study if HRH1 could modify the expression of EMT-key genes such as CDH1 and vimentin

2. To explore if HRH1 is involved in the adhesion of different OC cell lines to a monolayer of endothelial cells
3. To test if HRH1 pharmacological activation (through histamine treatment) or inactivation (via chlorpheniramine treatment) or its knockdown (siRNA HRH1) is involved in the invasion process of OC cell lines
4. To investigate the involvement of HRH1 in the motility of OC cell line

4.3. Results

4.3.1. HRH1 knockdown does not alter the expression of the EMT markers CDH1 and Vimentin

To study if HRH1 could influence EMT of OC cells, SKOV3 OVCAR3 and OVCAR5 cells were treated with siRNAs to knockdown HRH1. As HRH1 transfection did not work for OVCAR5 cells, they were not used for further analysis and only SKOV3 and OVCAR3 were further analysed. Forty-eight h post transfection, mRNA expression of HRH1, CDH1, a marker of epithelial phenotype, and vimentin, a marker of mesenchymal phenotype, were quantified by RT-qPCR. mRNA expression levels were normalised to the "non-transfected" cells group (cells that were treated only with transfection reagent and did not receive any siRNA). HRH1 knockdown was confirmed in both SKOV3 and OVCAR3, with HRH1 mRNA level decreasing by 60% in SKOV3 ($p=0.03$; siRNA control mean=0.83 ± SD=0.13; siRNA HRH1 mean=0.37 ± SD=0.14) (Figure 4.1 A) and 50% in OVCAR3 ($p=0.029$; siRNA control mean=1.07 ± SD=0.21; siRNA HRH1 mean=0.45 ± SD=0.22) (Figure 4.1 B) compared to control cells. CDH1 and vimentin were quantified by RT-qPCR and no difference in their expression was found upon HRH1 knockdown in neither SKOV3 ($p>0.99$, $p=0.68$, respectively) nor OVCAR3 cells ($p>0.99$; $p=0.2$, respectively) (Figure 4.1 A, B). These results suggest that reduction of expression of HRH1 mRNA does not trigger differences in the expression of EMT- key related genes in OC cells and that this transition is independent from HRH1 expression.

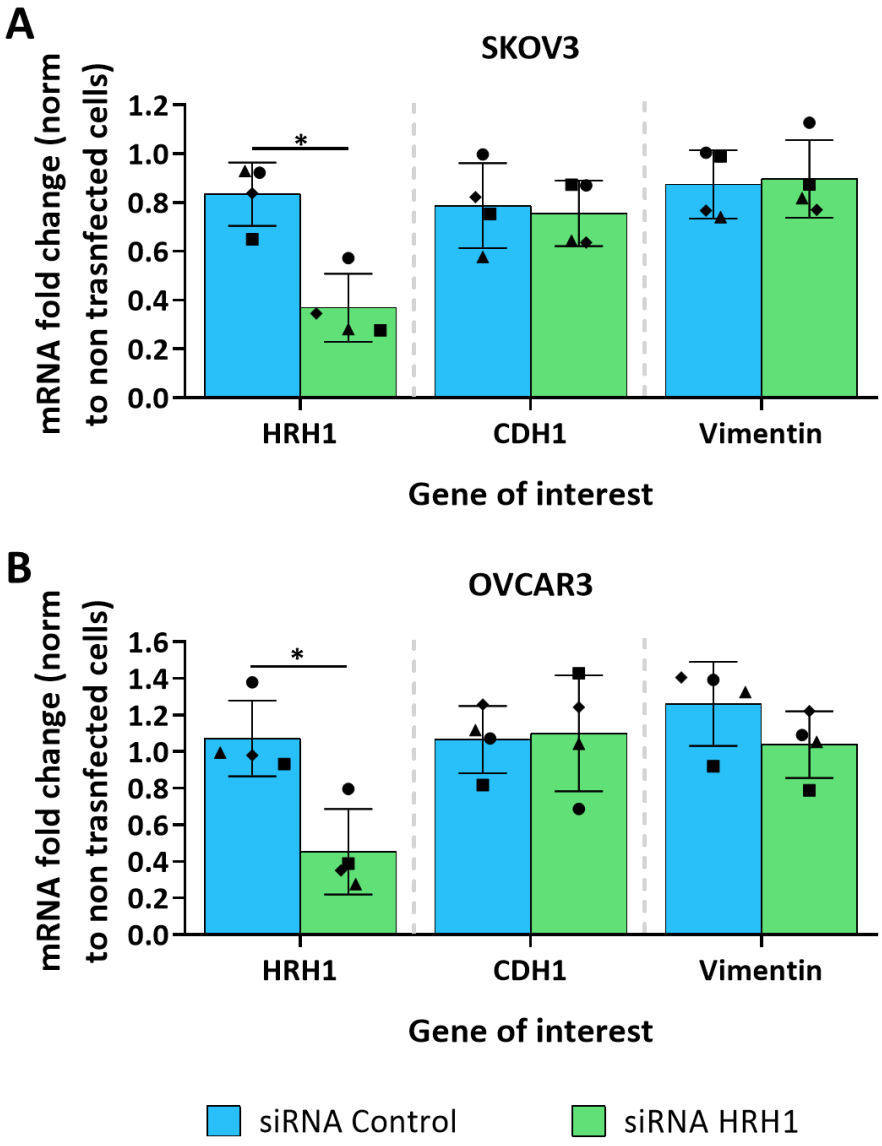

Figure 4.1: The effect of HRH1 knockdown on EMT markers.

SKOV3 and OVCAR3 cells were treated with siRNA control or specific for HRH1 for 48 h. The expression level of HRH1, CDH1 and vimentin were measured by RT-qPCR in A) SKOV3 and B) OVCAR3. β-Actin was used as endogenous control. Expression levels were normalised to 'non-transfected' cells control group. The mean values of four independent experiments were combined for statistical analysis. Mann-Whitney test was used to quantify differences between control cells and transfected cells for each gene of interest. Bars show, 1X SD. *P<0.05.

4.3.2. HRH1 knockdown does not alter the adhesion ability of OC cells to a monolayer of endothelial cells

To investigate the role of HRH1 in OC adhesion to an endothelial cell monolyer, a static adhesion assay was carried out using SKOV3, OVCAR3 and OVCAR5. In brief, OC cell lines were transfected with control or HRH1 siRNAs. Knockdown efficiency was measured by RT-qPCR 24 h after transfection. mRNA level of HRH1 decreased by 50% in SKOV3 HRH1 knockdown (p=0.006, siRNA control mean=1.15 ± SD=0.13; siRNA HRH1 mean=0.57 ± SD=0.14) (Figure 4.2 A) while no differences were seen in OVCAR3 and OVCAR5 (p=0.072, p=0.37, respectively) (Figure 4.2 B,C). Cells were stained with CFSE and then introduced onto a confluent HUVEC monolayer and allowed to interact for 15 or 30 minutes (Figure 4.2 D,E,F). No differences in adhesion were found when SKOV3 (15 min p=0.26; 30 min p=0.41), OVCAR3 (15 min p=0.63; 30 min p=0.28) and OVCAR5 (15 min p=0.47; 30 min p=0.92) were treated with HRH1 siRNAs at both 15 and 30 minutes post-adhesion (Figure 4.2 G, H, I). These data suggest that when level of expression of HRH1 is lowered, the ability of OC cells to adhere to HUVECs is unaffected.

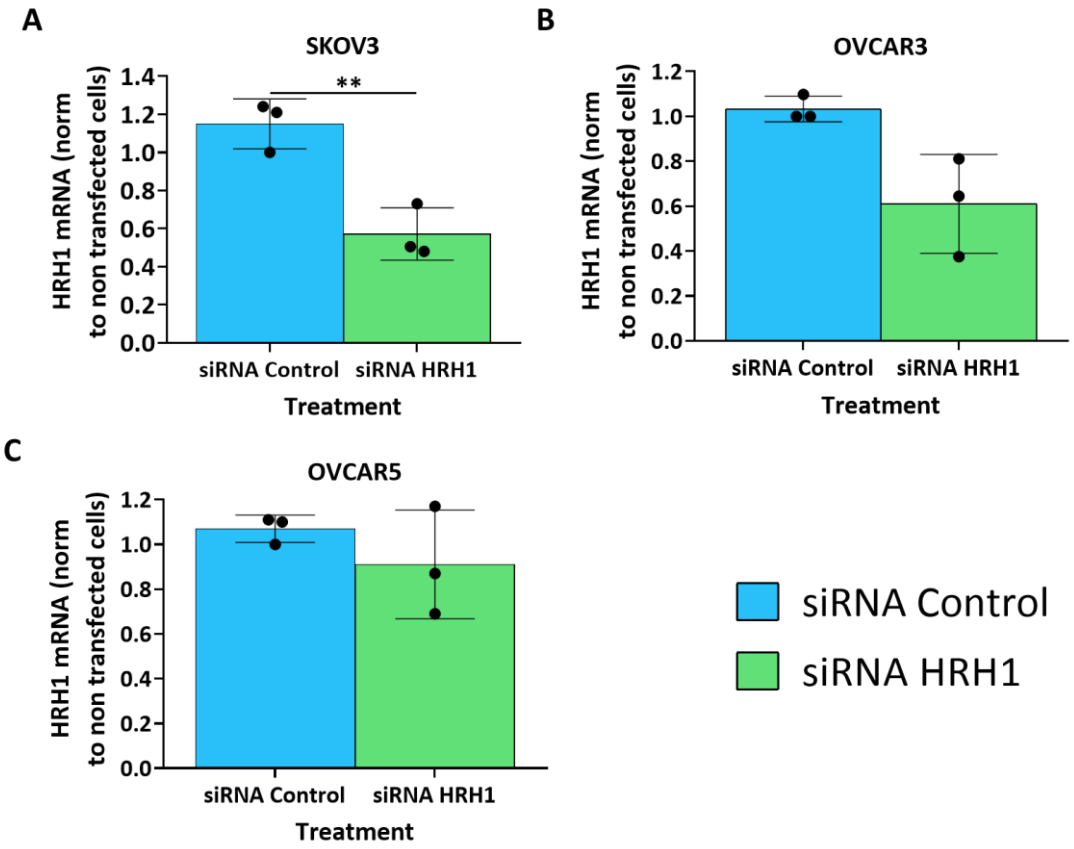

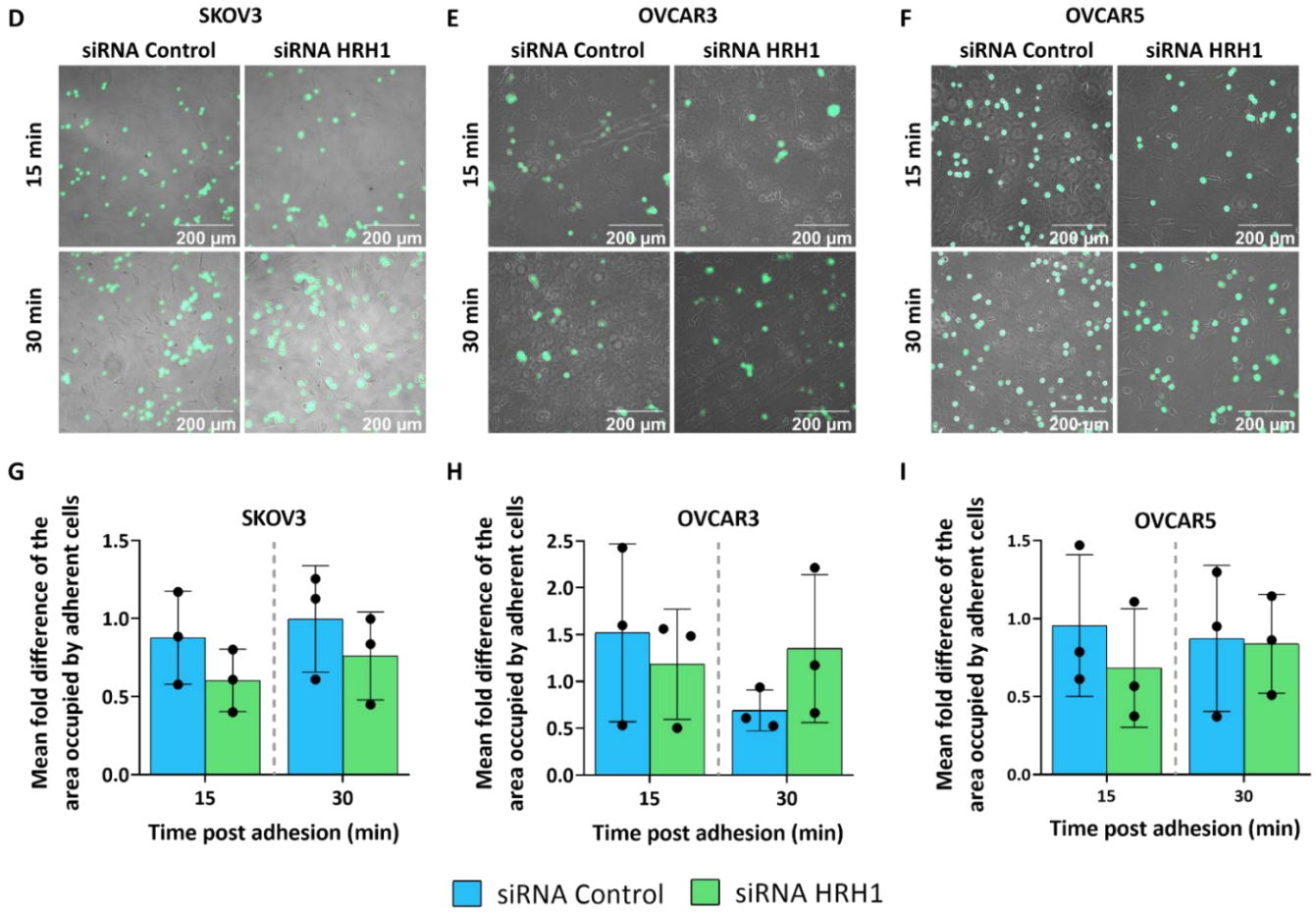

Figure 4.2: Effect of HRH1 knockdown on the adhesion ability of OC cell lines.

RT-qPCR was used to confirm HRH1 knockdown in A) SKOV3, B) OVCAR3 and C) OVCAR5 cell lines. β-Actin was used as endogenous control. Expression levels were normalised to 'non-transfected' cells control group. Representative images of a static adhesion assay on D) SKOV3, E) OVCAR3 and F) OVCAR5 cells. Cells were stained with CFSE (green) and plated onto a monolayer of HUVEC cells (brightfield) for 15 or 30 minutes. Scale bar 200 µm The area occupied by adherent cells was mesured at both 15 and 30 minutes for G) SKOV3, H) OVCAR3 and I) OVCAR5 and was normalized to the area occupied by 'non transfected' cells control group. The mean of three biological replicates, each one containing three technical replicates, were used for the analysis. T-test followed by Welch's correction was used for statistical analysis. Bars show, 1X SD. **P<0.01.

4.3.3. Histamine or antihistamine treatment does not alter the adhesion ability of OC cells to a HUVEC monolayer

To further explore if HRH1 was involved in OC cells adhesion to an endothelial cell monolayers, a static adhesion assay was carried out using SKOV3, OVCAR3 and OVCAR5 treated with control media, histamine or chlorpheniramine. Prior to undertaking the experiment, an MTT assay was used to generate IC50 curves and identify a sub-lethal dose of both compounds to treat the cell with. A concentration of 250 µM chlorpheniramine was used for subsequent experiments (Appendix 1, Figure 7.1). As histamine treatment did not affect cell viability at all the concentrations tested (Appendix 1, Figure 7.2), a concentration of 100 µM was used, as previously described in other studies (Verweij et al. 2018). Briefly, SKOV3, OVCAR3 and OVCAR5 were treated with control media, 100 µM histamine or 250 µM chlorpheniramine for 24 h. CFSE-stained cells were introduced onto the HUVEC monolayer and allowed to interact for 15 or 30 minutes; adherent cells were then fixed, imaged, and counted (Figure 4.3 A). The ability of SKOV3 (15 min $p=0.84$; 30 min $p=0.51$), OVCAR3 (15 min $p=0.30$; 30 min $p=0.19$) and OVCAR5 (15 min $p=0.059$; 30 min $p=0.24$) to adhere to HUVECs was not affected by either histamine treatment or antihistamine treatment (Figures 4.3 B, C, D). These findings suggest that histamine and chlorpheniramine do not affect the adhesion of OC cell lines to a monolayer of HUVEC cells.

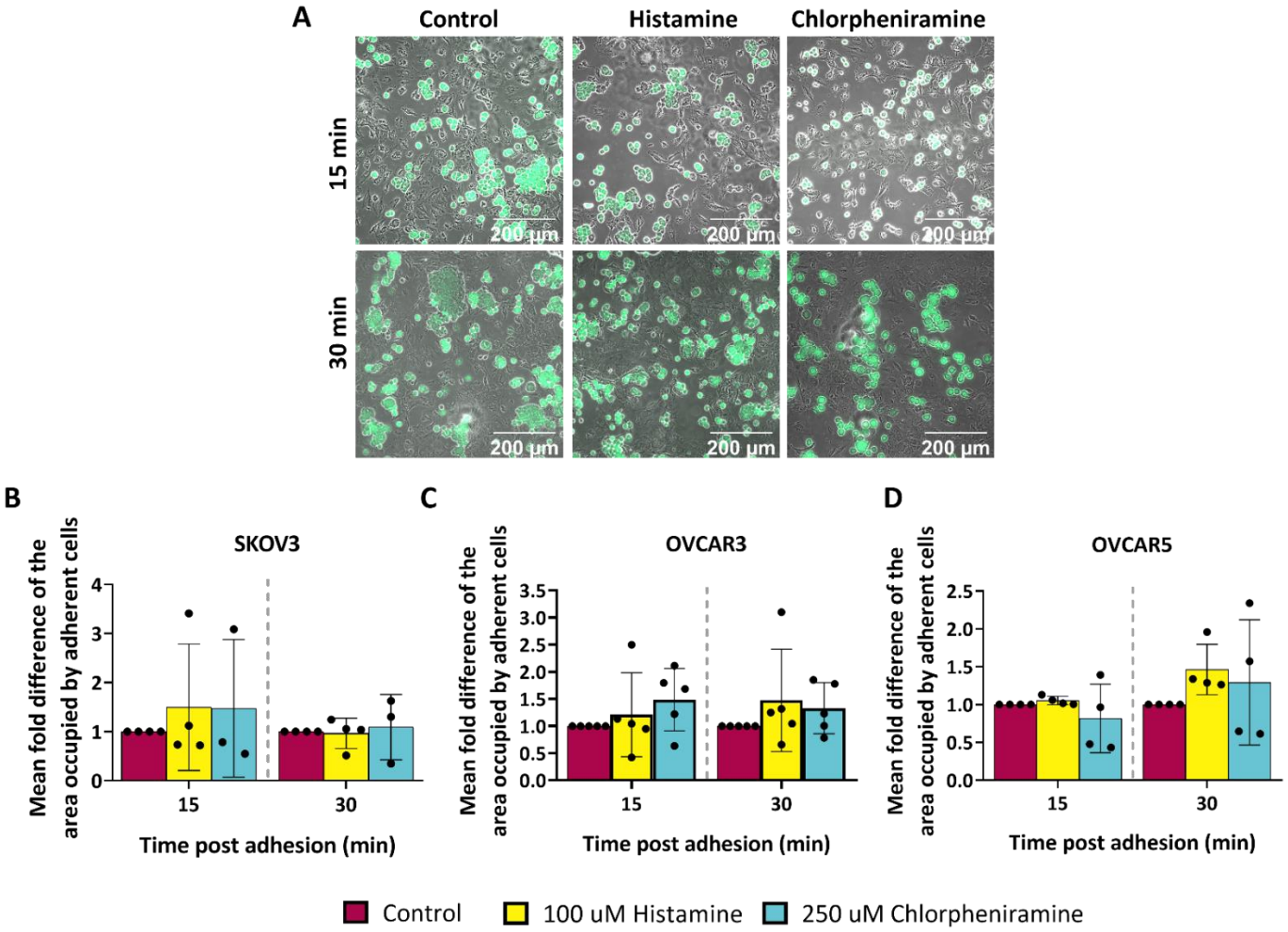

Figure 4.3: The effect of histamine and chlorpheniramine treatment on OC cells adhesion.

A) Representative images of CFSE (green) stained SKOV3 adhering to a HUVEC monolayer (brightfield) under different pharmacological treatments (control, histamine and chlorpheniramine) after 15- or 30-minutes incubation. Scale bar 200 µm. The area occupied by adherent cells was calculated for B) SKOV3 C) OVCAR3 and D) OVCAR5. Data were normalized to the control cells. The mean of at least four independent experiments, each one containing at least three technical replicates, were used for the analysis. Statistical differences were calculated for each time point by using a Kruskal-Wallis test, followed by a Dunn multiple comparison test. Bars show, 1X SD.

4.3.4. Transient knockdown of HRH1 decreases the invasion of OC cells

From the data presented thus far, it appears that HRH1 is not implicated in the adhesion or EMT of OC cells. Thus, another aspect of the metastatic cascade was investigated. A Matrigel® invasion assay was performed using SKOV3, OVCAR3 and OVCAR5 cells in which HRH1 was knocked down. Briefly, cells were transfected with siRNA control or siRNA specific for HRH1 for 24 h and knockdown was measured by RT-qPCR. HRH1 was successfully knocked down in SKOV3 (p=0.0335; siRNA control mean=1.00 ± SD=0.012; siRNA HRH1 mean=0.69 ± SD=0.10) (Figure 4.4 A) and OVCAR3 (p=0.009; siRNA control mean=1.00 ± SD=0.012; siRNA HRH1 mean=0.68 ± SD=0.061) (Figure 4.4 B) while there was no effect on HRH1 expression in OVCAR5 (p=0.20) (Figure 4.4 C). Transfected cells were then plated onto a Matrigel® insert and allowed to invade for 24 h or 48 h. Invaded cells were stained, imaged and counted to estimate the percentage of invasion (Figure 4.4 D, E, F). HRH1 knockdown significantly reduced the invasion of SKOV3; there was a 40% reduction in invading cells at 24 h (p=0.007; siRNA control mean=1 ± SD=0.334; siRNA HRH1 mean=0.57 ± SD=0.21) and a 60% reduction after 48 h (p=0.002; siRNA control mean=1 ± SD=0.49; siRNA HRH1 mean=0.39 ± SD=0.14) (Figure 4.4 G). Knockdown of HRH1 led to a reduction of OVCAR3 invasion that was not statistically significant at 24 h (p=0.06) but reached significance at 48 h (p=0.049; siRNA control mean=1.0 ± SD=0.49; siRNA HRH1 mean=0.48 ± SD=0.39) (Figure 4.4 H). OVCAR5 cells treated with HRH1 siRNA were more invasive than OVCAR5 control cells after 24 h (p=0.7), while there was a reduction in the average of invading cells of 50% after 48 h, although this did not reach significance (p=0.18) (Figure 4.4 I). Taken together, these data indicate that HRH1 affects the invasive capacity of SKOV3 and OVCAR3 cell lines, and when its expression is reduced, cells become less invasive.

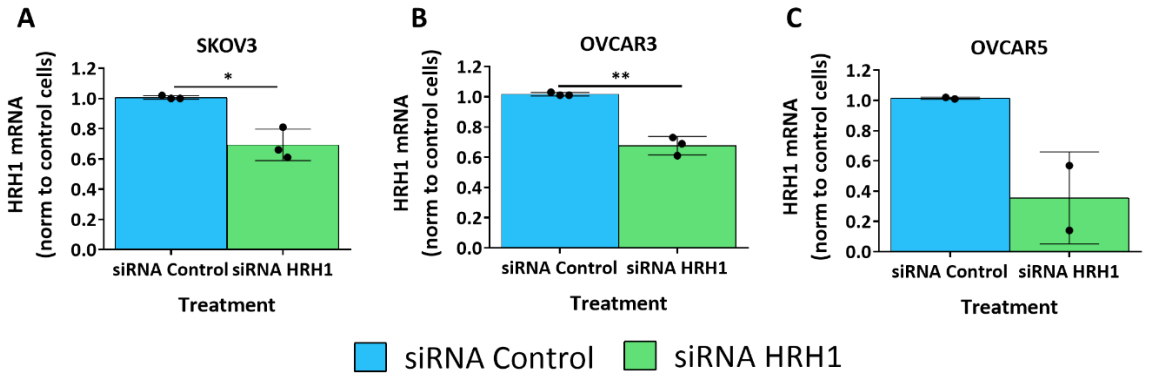

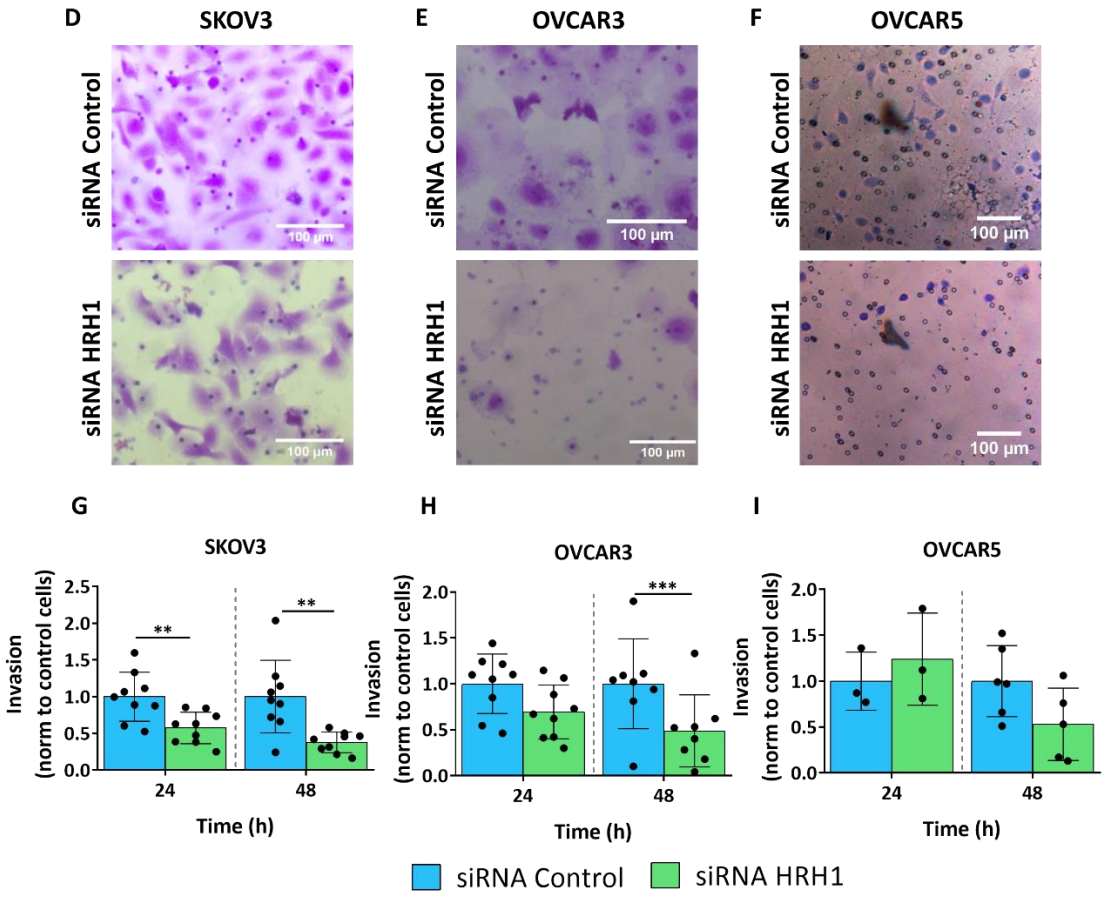

Figure 4.4: Quantification of the invasion ability of SKOV3, OVCAR3 and OVCAR5 through the Matrigel® invasion assay.

HRH1 knockdown efficiency in A) SKOV3, B) OVCAR3 and C) OVCAR5. β-Actin was used as endogenous control. Expression levels were normalised to control cells. Representative images of Matrigel® membranes analysed to assess cells (purple) invasion for D) SKOV3, E) OVCAR3 and F) OVCAR5. Scale bar 100 µm. Percentage of invasion was calculated at both 24 h and 48 h for G) SKOV3, H) OVCAR3 and I) OVCAR5. Invasion levels were normalized to control cells. Mann-Whitney test was used for statistical analysis. Three independent experiments were used for analysis of SKOV3 and OVCAR3. For OVCAR5 analysis, one experiment was used to assess 24 h invasion while two biological replicates were used to assess 48 h invasion. Bars show, 1X SD. *P<0.05, **P<0.01, ***P<0.001.

4.3.5. Histamine treatment increases invasion of SKOV3 cell line

In order to confirm the involvement of HRH1 in the invasion of OC cells, a Matrigel® assay was repeated on SKOV3 cells treated with control medium, 100 µM histamine or 250 µM chlorpheniramine. These additional Matrigel® assays were performed only on SKOV3 cells, as they were demonstrated to be the most invasive cell lines amongst those used in this project (section 3.2.4). In brief, cells were plated onto the Matrigel® and control media, histamine or chlorpheniramine were added. Cells were allowed to invade for 48 h and the experiment proceeded as described in section 2.14.1.3 (Figure 4.5 A). Histamine addition showed an 80% increase in the number of invading SKOV3 compared to control cells (p=0.022; control mean=1 ± SD=0.29; histamine mean=1.82 1 ± SD=0.55) (Figure 4.5 B), as well as more than 3-fold increase in the number of invading cells when compared to chlorpheniramine treated cells (p<0.0001; chlorpheniramine mean=0.66 1 ± SD=0.16) (Figure 4.5 B). Chlorpheniramine addition

decreased the number of invading SKOV3 by 30% when compared with the control group, although it did not reach significance (p=0.077) (Figure 4.5 B). These results confirm previous findings, that when HRH1 is activated via histamine, it increases the ability of cells to invade through a Matrigel® layer, although its pharmacological inhibition did not modify SKOV3 invasion rate.

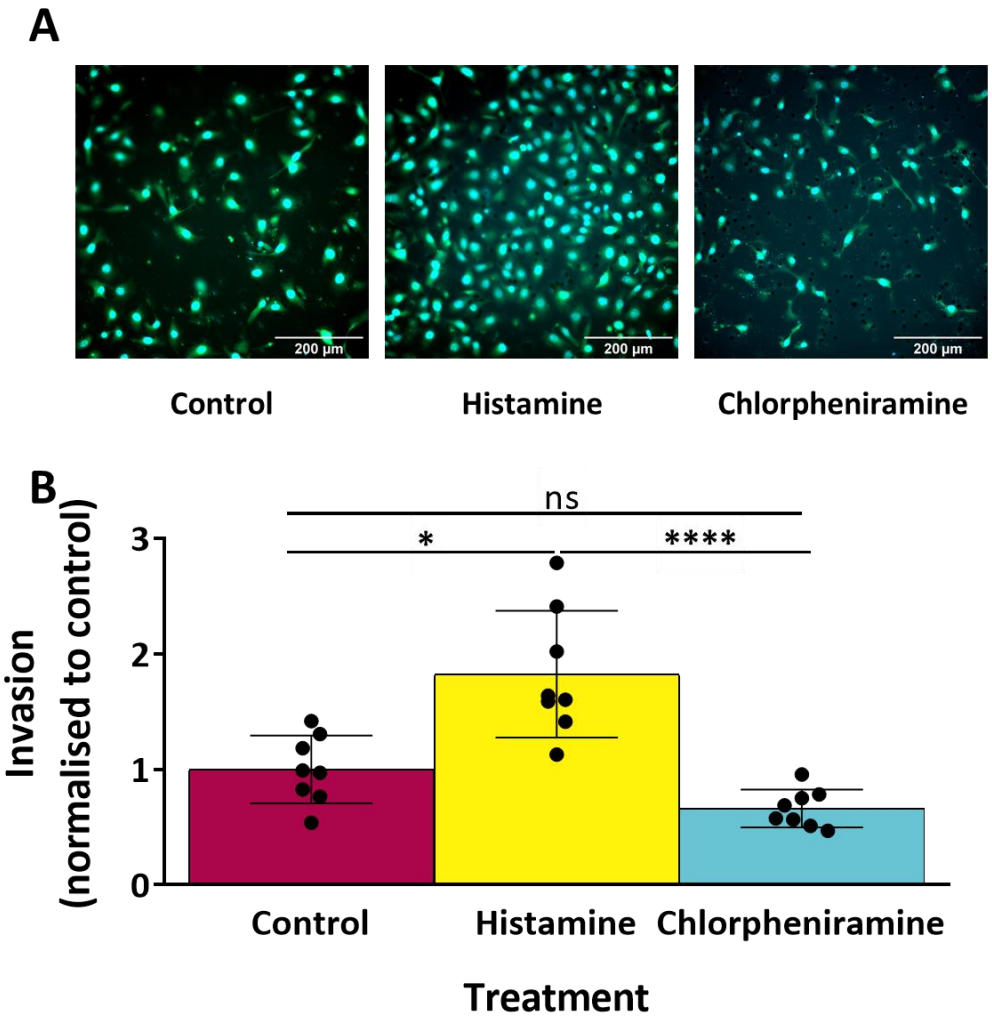

Figure 4.5: Matrigel® assay was used on SKOV3 treated with control media, histamine or chlorpheniramine to assess their invasion.
A) Representative images of Matrigel® membranes used for quantifying SKOV3 invasion. Cells were stained with DAPI (blue) and CFSE (green). Scale bare 200 µm. B) Percentage of invasion was calculated for SKOV3 control, treated with histamine or chlorpheniramine. Two independent experiments were combined, each one with four technical replicates. Kruskal-Wallis test followed by Dunn's correction was used for statistical analysis. Bars show 1X SD; *P<0.05, ****P<0.0001.

4.3.6. HRH1 KD does not affect the migration rate of ovarian cancer cells

The findings so far provide no evidence for HRH1 being involved in regulation of EMT nor in the adhesion of OC cells to endothelial cell monolayers but show that it can alter the invasive ability of OC

cells through a Matrigel® layer. This could be achieved through modification of cell motility, cell-cell interactions or ECM breakdown. To test if HRH1 could affect the motility of OC cells, a wound healing assay was performed using SKOV3, OVACR3 and OVCAR5 cells transfected with siRNA control or siRNA for HRH1 (Figure 4.6 A). HRH1 knockdown was quantified by RT-qPCR, confirming a successful reduction of HRH1 expression by 50% in SKOV3 ($p=0.006$; siRNA control mean=1.15 ± SD=0.13; siRNA HRH1 mean=0.57 ± SD=0.14) (Figure 4.6 B). Knockdown efficiency did not reach significance in OVCAR3 ($p=0.075$) (Figure 4.6 C; siRNA control mean=1.03 ± SD=0.058; siRNA HRH1 mean=0.63 ± SD=0.22). In OVCAR5 cells, HRH1 was successfully knocked down, with mRNA expression decreasing by 20% ($p=0.019$; siRNA control mean=1.037 ± SD=0.064; siRNA HRH1 mean=0.76 ± SD=0.094) (Figure 4.6 D). Twenty-four hours after the transfection, the cell monolayer was 'wounded', and gap closure monitored at 0, 4, 8, 12 and 24 h. No differences in the percentage of open 'wound' were observed after knocking down HRH1 in SKOV3 ($p=0.080$) (Figure 4.6 E), OVCAR3 ($p=0.59$) (Figure 4.6 F) and OVCAR5 ($p=0.94$) (Figure 4.6 G), with control cells showing the same rate of motility as transfected cells. Taken together, these data suggest that HRH1 silencing does not affect cell motility.

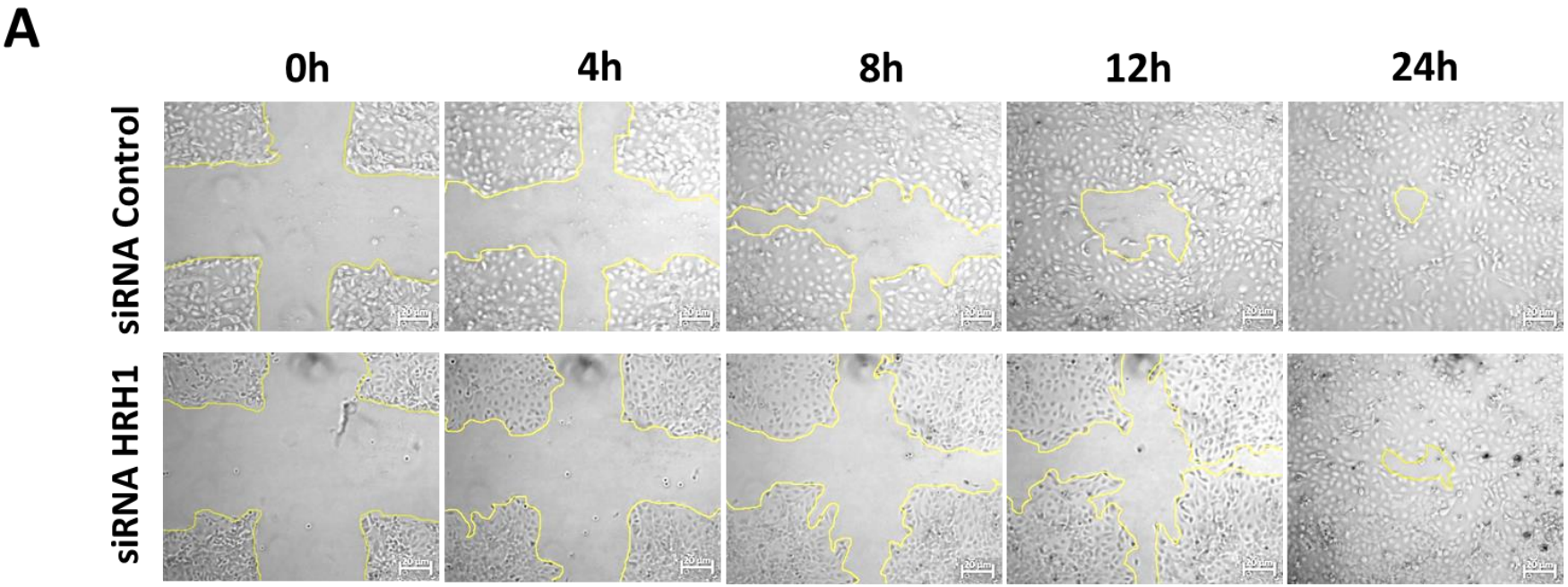
A
0h
4h
8h
12h
24h
siRNA Control
siRNA HRH1

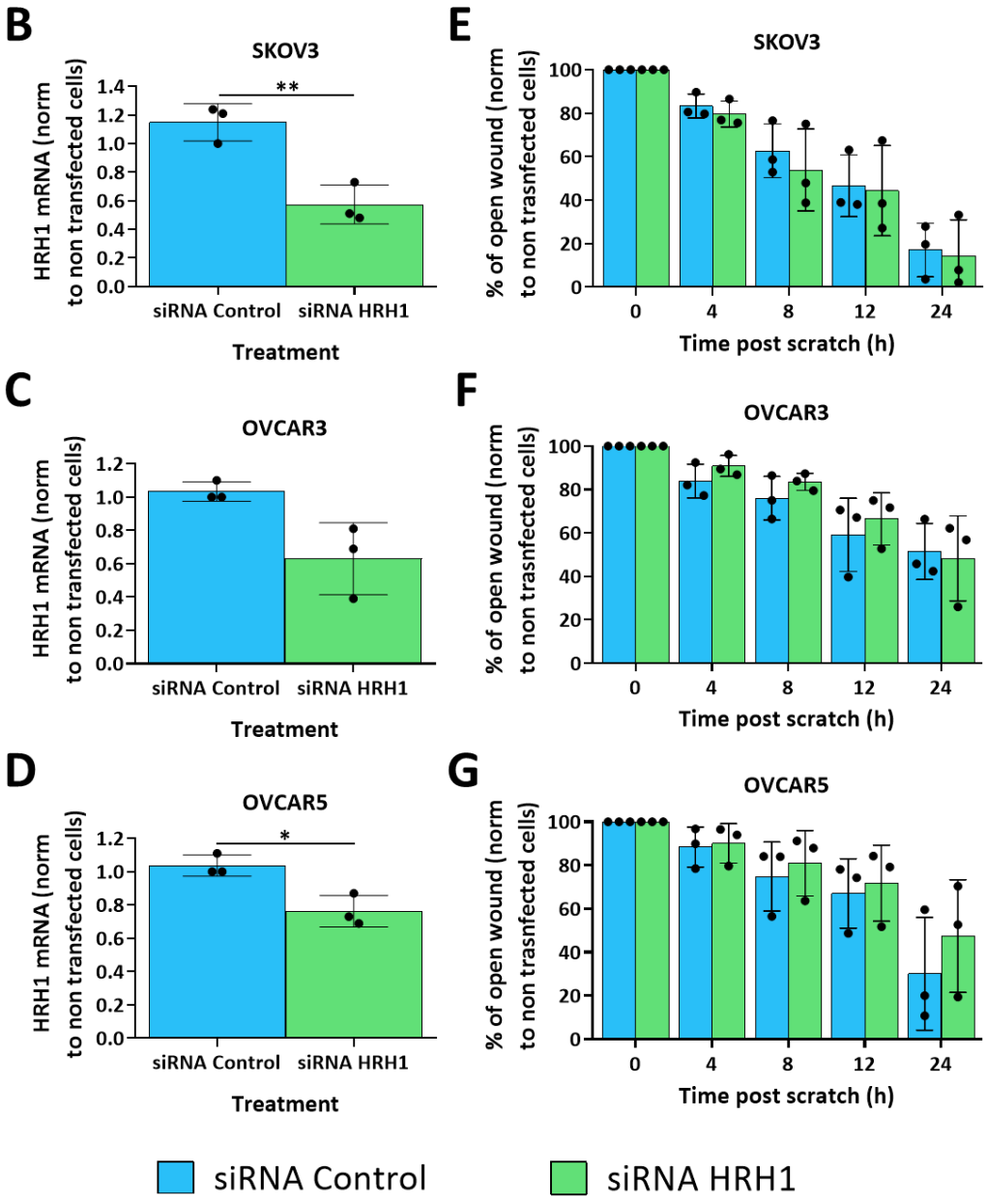

Figure 4.6: Testing HRH1 involvement in the motility of OC cells.

A) Representative images of a wound healing assay on SKOV3 cells control or knocked down for HRH1. The 'wounded area' is highlighted in yellow. Scale bar 20 µm. Quantification of HRH1 knockdown by RT-qPCR on B) SKOV3, C) OVCAR3 and D) OVCAR5. β-Actin was used as endogenous control. Expression levels were normalised to 'non-transfected' cells control group. The 'wound' closure was monitored and quantified over time. The percentage of open 'wound' was calculated for E) SKOV3, F) OVCAR3 and G) OVCAR5. Data were normalised to 'non-transfected' cells control group. The means of three independent experiments, each one containing four technical replicates, were combined for analysis. Data were normalised to the 'non transfected' cells control group. A t-test followed by a Welch's correction was used to identify statistical differences in the mRNA expression of HRH1 between different siRNA treatments groups. Two-way ANOVA, followed by Tukey's post-hoc test, was applied to identify statistical differences in the wound healing assay. Bars show, 1X SD. *P<0.05, **P<0.01.

4.3.7. Administration of chlorpheniramine reduces migration in SKOV3 and OVCAR5

As previously demonstrated in section 4.3.6, HRH1 knockdown does not alter the motility of OC cells. To verify these results, a wound healing assay was performed on SKOV3, OVCAR3 and OVCAR5 treated with media control, 100 µM histamine or 250 µM chlorpheniramine (Figure 4.7 A). The effects on both compounds on cell proliferation was previously tested, resulting in neither histamine nor chlorpheniramine influencing the proliferation rate of SKOV3, OVCAR3 and OVCAR5 (Appendix 1, Figure 7.3). At 8 h post 'wounding', chlorpheniramine-treated SKOV3 cells had closed the 'wound' significantly less than histamine-treated cells ($p=0.022$; histamine mean= 55.14 ± SD=2.81; chlorpheniramine mean=67.15 ± SD=11.65), with chlorpheniramine treated cells closing only 35% of the 'wounded' area compared with the 50% covered by histamine-treated cells (Figure 4.7 B). Neither treatment affected the motility of OVCAR3 during the 24 h period ($p=0.80$) (Figure 4.7 C). Chlorpheniramine-treated OVCAR5 cells closed the 'wound' slower than either control cells ($p=0.014$; control mean=44.26 ± SD=7.38; chlorpheniramine mean=55.16 ± SD=0.51) or histamine treated cells ($p=0.009$; histamine mean=43.56 ± SD=8.63) (Figure 4.7 D) at 24 h post 'wound'. These results show that chlorpheniramine can modify the motility of OC cells, but that its effect is variable depending on cell type. Whilst chlorpheniramine administration decreases the 'wound' closure speed of SKOV3 and OVCAR5 at late time points, it does not modulate motility of OVCAR3.

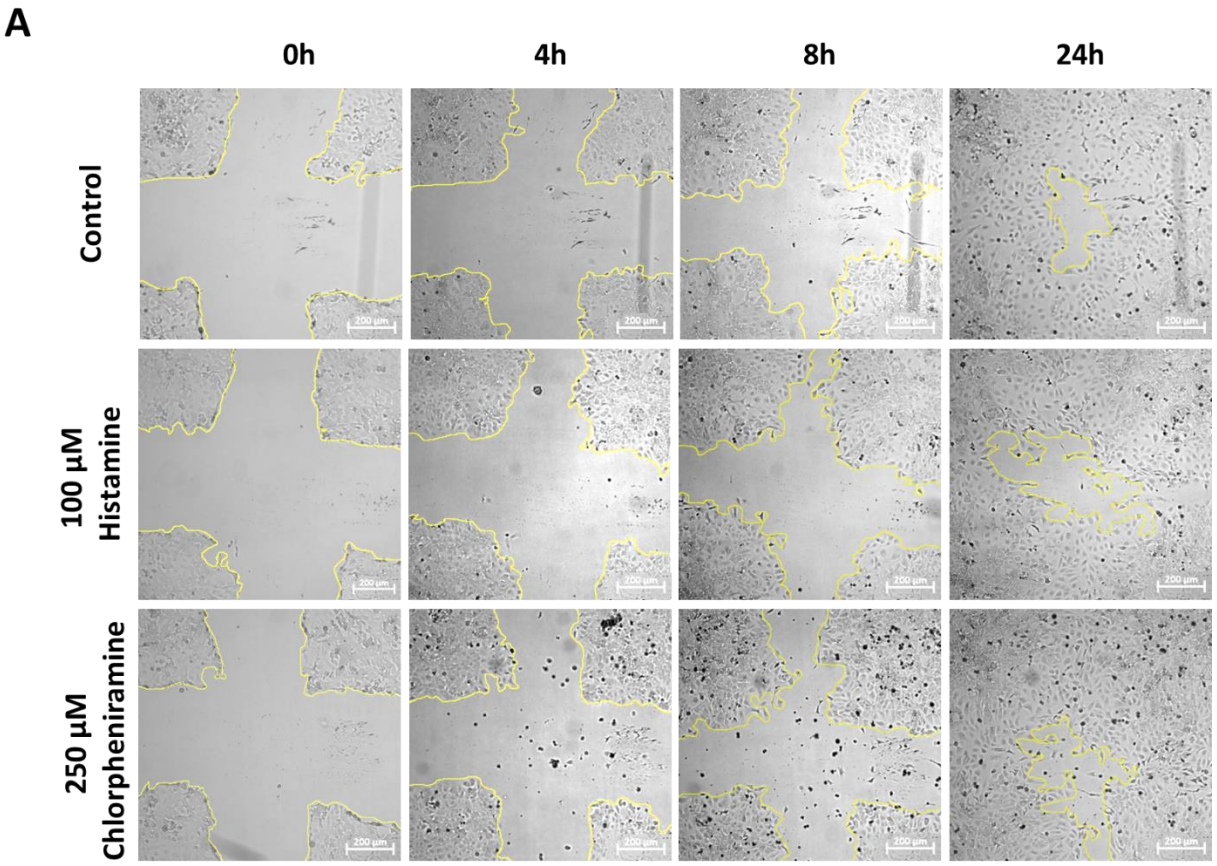
A
0h
4h
8h
24h
Control
100 µM Histamine
250 µM Chlorpheniramine

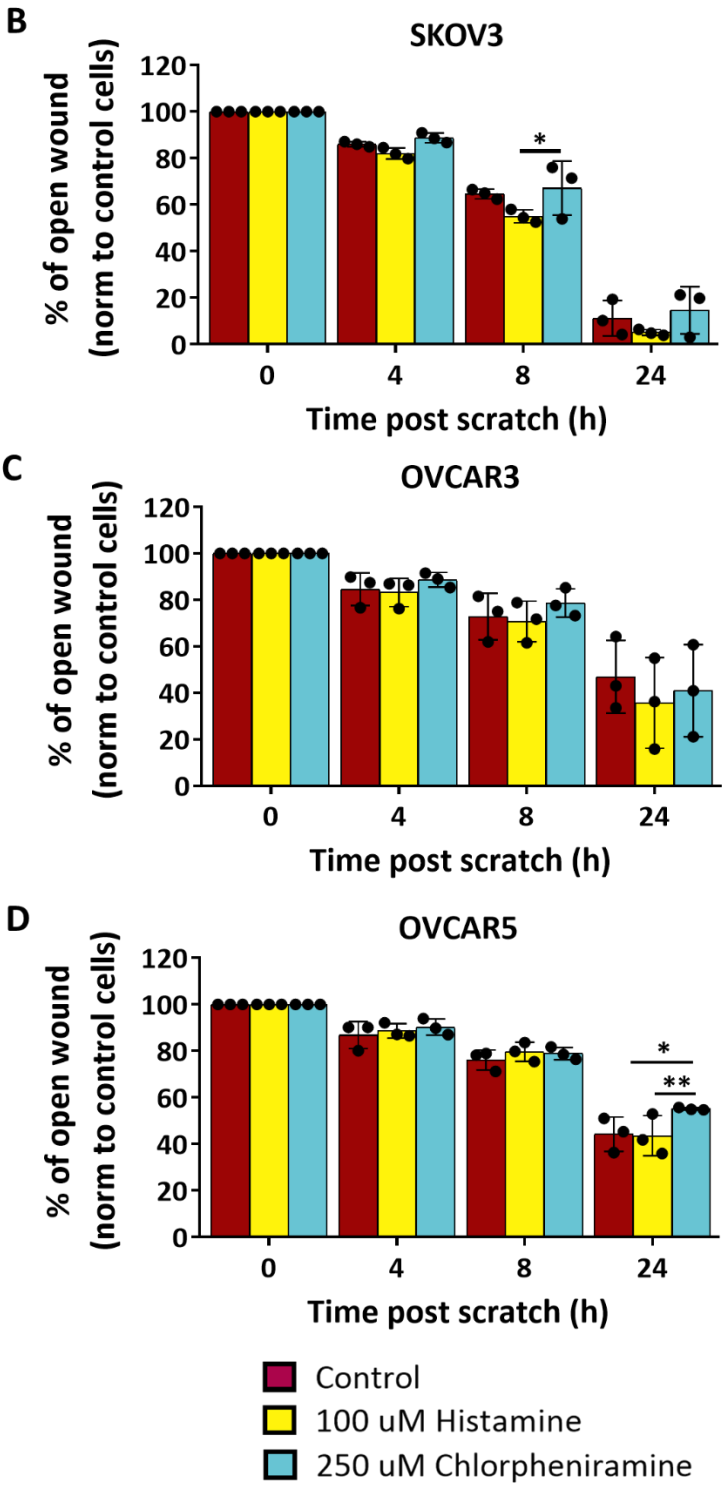

Figure 4.7: Effect of histamine and chlorpheniramine on OC cells motility.

A) Representative pictures of a wound healing assay on SKOV3 cells treated with media control, 100 µM histamine or 250 µM chlorpheniramine. The 'wound' area (highlighted in yellow) was monitored over time and quantified. Scale bar 200 µm. The percentage of 'wound' opening was calculated for B) SKOV3 C) OVCAR3 and D) OVCAR5. Data were normalised to control cells. Three biological replicates, each one containing 4 technical replicates, were used for the analysis. Two-way ANOVA followed by Tukey's post hoc was used for statistical analysis. Bars show, 1X SD. *P<0.05, **P<0.01.

4.4. Discussion

The aim of the work described in this chapter was to assess whether HRH1 is involved in different steps of the metastatic cascade of OC using a range of *in vitro* assays. The results presented in chapter 3 revealed an inverse correlation between HRH1 and ovarian cancer aggressiveness, with OC samples obtained from patients with stage IV of the disease presenting a higher amount of HRH1 mRNA when compared with ovarian cancer samples obtained from patients in stage II or III. Histamine and its involvement in cancer growth and metastasis have been previously studied, but its role still remains controversial (Faustino-Rocha et al. 2017). In this project three different OC cell lines, SKOV3, OVCAR3 and OVCAR5 were used and HRH1 expression was modulated in two ways: a) by transient transfection of HRH1 and b) by administration of histamine or chlorpheniramine. Different *in vitro* assays were then used to investigate characteristics involved in individual steps of the metastatic cascade.

EMT

EMT is a key process in cancer metastasis, as it allows cancer cells to change their morphology and behaviour and acquire a more aggressive phenotype, giving them the ability to detach from the primary tumour and travel to distant sites of the body. In order to study if HRH1 could regulate the EMT process, SKOV3 and OVCAR3 were treated with HRH1 siRNA and mRNA expression levels of CDH1 and vimentin were quantified by RT-qPCR. Although HRH1 was successfully knocked down in both cell lines, no differences in CDH1 or vimentin expression were identified, indicating that HRH1 knockdown does not change the expression of EMT-related genes. There are some data in the literature on the role of HRH1 in OC EMT, and most of the studies exploring the role of histamine in the EMT process have shown that all four histamine receptors can regulate this process. For example, a study published by Kennedy and colleagues (2018) demonstrated that, upon chemical inhibition of HRH1 and HRH2, CDH1 levels were upregulated in cholangiocarcinoma tumours from mice while vimentin levels were dramatically reduced (Kennedy et al. 2018). This might be due to the different type of cancer investigated in the two studies, as Kennedy and colleagues (2018) used a model of cholangiocarcinoma and studied this process *in vivo*. Moreover, it cannot be discarded that more cell types may act synergistically to induce EMT or that EMT might not definitely be necessary for metastasis (Fischer et al. 2015).

The data obtained in this project show that HRH1 does not modify the expression of two key- EMT genes in two OC cell lines. To further study this, the same experiment could be repeated upon chemical activation or inhibition of HRH1 and the expression of other key EMT markers (e.g., β-catenin, SNAI1, SNAI2, ZO1, ZEB, N-cadherin) should be evaluated to have a more comprehensive view. It is well established that during the EMT not all the markers change, therefore by testing only CDH1 and

vimentin, it cannot be discounted that other marker of EMT are affected. In addition other cellular characteristics such as cell morphology or polarity could have been integrated in the study (Pantazi et al. 2020). Moreover, another endogenous control should be used for RT-qPCR instead of β-actin. As one of the major components of the cytoskeleton, β-actin changes during the EMT process, hence other housekeeping genes, such as the 18S ribosomal RNA, might have been a more appropriate control in this context, as it is widely expressed in the cell but not regulated by EMT. Although this study revealed no evidence that direct histamine treatment induced changes in expression of key EMT-related markers in OC cell lines, histamine administration to the surrounding environment (e.g., stromal fibroblast, ECM) could indirectly modify OC behaviour and induce changes in EMT regulators. As shown by Porretti et al (2014), addition of conditioned media obtained from histamine-treated fibroblast (10 μM) to MDA-MB-231 (breast cancer) cell lines induced upregulation of α-SMA level, a shift of β-catenin localization (from membrane to cytoplasm) and increased of Slug mRNA. These changes reverted when MDA-MB-231 were treated with conditioned media from fibroblasts treated with 20 μM of histamine (Porretti et al. 2014). These results also indicate how different doses of histamine can trigger different cellular behaviour; hence, different concentrations of histamine could be analysed to further clarify HRH1 involvement in the EMT process.

Cell adhesion

A static adhesion assay was employed to study whether HRH1 was involved in the adhesion of OC cells to an endothelial cell monolayer. When cells were treated with siRNAs no differences in their adhesive behaviour were observed. Similar results were observed when adding histamine or chlorpheniramine to the three cell lines. Even though the data presented here suggests that HRH1 does not play a role in OC adhesion to endothelial cell monolayers, it is important to highlight that the static adhesion assay produced very variable data, with a high discrepancy across biological replicates, making the data somewhat inconclusive. More replicates should be repeated to be able to draw conclusion from it.

Several studies focusing on the adhesion of different cancer cells to plastic surfaces have shown different results from what presented in this thesis. For instance, Genre and colleagues (2009) highlight a dual role of histamine in the modulation of cell adhesion in a normal epithelial breast cell (HBL-100) and invasive breast cancer cell (MDA-MB 231) lines. The authors observed that histamine administration increased the adhesion of HBL-100 cells and reduced the adhesion of MDA-MB 213 cells to plastic, possibly due to a reduction of E-Cadherin expression (Genre et al. 2009). It is important to consider that the mechanisms involved in cell adhesion to plastic are completely different from mechanisms involved in cell–cell adhesion or cell-ECM adhesion. In the former process, plastic surfaces are chemically treated and negatively charged molecules are formed; these negative reactive ions

stimulate cell adhesion by either direct binding to positively charged adhesive molecule on the cell surface or by absorbing serum proteins contained within the media, potentially mediating cell adhesion (Martin and Rubin 1974; Lerman et al. 2018). Cell-cell and cell-ECM adhesion involves more complex mechanisms where several adhesive proteins of one cell need to adhere and form stable bonds with receptors expressed by other cells or by ECM components. These differences could explain why the results obtained in this project are in contrast with previous literature data.

Conversely, histamine is known to directly act on the endothelial barrier and induce modification of adhesive molecule expressed by endothelial cells (Shimamura et al. 2004); therefore, this could potentially be a way by which histamine could influence cancer adhesion to the endothelium. In fact, the administration of cimetidine, an HRH2 antagonist, to HUVECs has been reported to decrease E-selectin (an adhesion molecule) expression and consequently reduced HT-29 (colorectal cancer) cells adhesion to them (Kobayashi et al. 2000). These findings might lead to the hypothesis that although HRH1 appears not to be directly involved in OC cells adhesion to the endothelium, its activation or inhibition in endothelial cells could lead to subsequent regulation of adhesion molecule expression, thus indirectly altering OC adhesion. Therefore, an adhesion assay in which HUVEC cells are treated either with HRH1 siRNAs or with chemical activator or inhibitors of HRH1 could further elucidate HRH1 role in the adhesion process.

Another factor that could explain why the results presented in this project differ from some reports in the literature is that OC cells normally spread predominantly into the peritoneal cavity rather than through the hematogenous route (Motohara et al. 2019). By expressing several adhesive molecules such as β-integrin, CD44 and CA125, OC preferably attach to the mesothelium of peritoneal organs and passively move towards proximal site of the abdominal tract. Therefore, an adhesion assay using peritoneal mesothelial cells could better mimic the adhesion process of OC cells.

Cell invasion

Cells in which HRH1 was knocked down showed a significant decrease in invasion through Matrigel® in an invasion assay system. This change in the behaviour was observed in SKOV3 cells after 24 h, and in both SKOV3 and OVCAR3 after 48 h. OVCAR5 treated with siRNA for HRH1 showed a 50% reduction in the average number of invading cells after 48 h incubation, although this decrease was not statistically significant. This could be explained by the high variability of the data points within each group. While the Matrigel® experiment was repeated three times for SKOV3 and OVCAR3, only two replicates were used for OVCAR5 and moreover, the cells did not show a significant knockdown of HRH1 when treated with siRNA, a factor that could also explain the different cell behaviour. Therefore, at least one more replicate should be repeated before drawing conclusion regarding HRH1 role in OVCAR5 invasion.

These data might also be explained by considering that the three cell lines used in this project have a different origin: OVCAR3 cells are of HGSC origin, SKOV3 is derived from a non-serous carcinoma (Domcke et al. 2013; Beaufort et al. 2014; Haley et al. 2016), while there is still controversy regarding the derivation of OVCAR5 (they have always been thought to be derived from HGSC, but recent literature findings highlight the possibility that OVCAR5 may be derived from the gastrointestinal tract (Blayney et al. 2016)). Hence the different histopathological origin of the cells could possibly explain why OVCAR5 does not show the same trend as the other two cell lines. Another possible explanation is that as SKOV3 express a higher level of HRH1 mRNA (section 3.2.3), knocking it down may have a greater biological effect on cell behaviour than in the other cell lines. Taken together, these findings are the first to indicate that HRH1 could play a role in the invasive behaviour of OC cells.

These findings are supported by a recent study investigating the role of HRH1 in hepatocellular carcinoma (HCC) (Zhao et al 2020). By employing the same systems used in this project (Matrigel® and wound healing assays), Zhao and colleagues found that HRH1 knockdown was able to reduce both invasion and migration of HCC *in vitro*; similarly, injection in the lateral tail vain of HCC cells knocked down for HRH1 in nude mice show a decreased metastatic behaviour *in vivo*, with a reduction in the number of lung metastatic lesions when compared with mice injected with control HCC cells (Zhao et al. 2020).

In the work presented in this thesis, the potential involvement of histamine signalling in OC cell invasion was further validated by a Matrigel® assay employing SKOV3 cells treated with chemical activators or inhibitors of HRH1. Histamine treatment led to an increase of SKOV3 invasion compared to control cells and chlorpheniramine treated cells. As the invasion assay was performed only twice, more replicates should be done to validate the data. Additionally, increasing the number of replicates might clarify whether chlorpheniramine addition reduces OC invasion, as the data obtained in this experiment indicates that upon chlorpheniramine administration, SKOV3 decreases their invasion by 30% but this change did not reach statistical significance. Indeed, this finding is in contrast with the study of Kim et al. (2014) regarding the effect of ketotifen (a selective HRH1 antagonist) on MDA-MB-231 and HT-1080 (breast cancer and fibrosarcoma cell lines, respectively) cells. Ketotifen administration caused a dose-dependent suppression of invasion through a Matrigel® layer and migration from the edge of the wound of both cell lines, and also reduced the expression of MMP9 in MDA-MB-231 (Kim et al. 2014). Different cell lines and different drugs were used in the two studies, fact that might explain the controversy of the data obtained. This is an important parameter to consider when comparing different studies, as different drugs might exert different actions on distinct cell lines.

These results further confirm the involvement of the histamine signalling in the invasion process, although this might not only be due to HRH1 activation, but it could be the result of a more complex process involving the other histamine receptors. More invasion assays employing a specific HRH1 activator, and a panel of antagonists could be used to further verify HRH1 involvement in the invasion of OC cells.

Cell migration

To test HRH1 involvement in cell motility, a wound healing assay was performed on a) cells treated with siRNAs and b) cells treated with histamine and anti-HRH1. While transient transfection of HRH1 did not modify the motility rate of SKOV3, OVCAR3 and OVCAR5 cells, histamine and chlorpheniramine administration resulted in different behaviours depending on the cell line. Chlorpheniramine treatment significantly decreased SKOV3 motility when compared with histamine treated cells at 8 h post- "wound". OVCAR5 receiving chlorpheniramine showed slower rates of motility 24 h post-"wound", when compared with histamine-treated and control cells. OVCAR3 motility was not affected by histamine or anti-HRH1 treatment, suggesting a distinct role of these compounds on OVCAR3 migration.

Various publications claim diverse roles of histamine and its antagonist in cancer cell motility. For instance, by using a wound healing assay, Rudolph and colleagues (2008) revealed that a combination of histamine and pyrilamine, an HRH1 antagonist, significantly inhibits motility rate of SW756 (endometrial cancer) cells while combination of histamine with HRH3 or HRH4 antagonists increased it (Rudolph et al. 2008). Moreover, addition of 100 µM histamine to three different melanoma cell lines (HT144, A375, B16F10) significantly increases their motility through a transwell membrane (Blaya et al. 2010). On the contrary, Fernández-Nogueira and colleagues (2018) study found that HRH1 inhibition can increase breast cancer (MDA-MB-231 and BT-549) cells motility *in vitro* (Fernández-Nogueira et al. 2018).

The different behaviour of the three cell lines used in this project could reflect intrinsic differences between the cell lines used in the experiments or their different sensitivity to histamine and chlorpheniramine. In addition, the reduction in motility due to administration of chlorpheniramine to SKOV3 and OVCAR5 could be also linked to off-target effects inducing activation of pathways independent from HRH1 inhibition. This could explain why differences in motility are observed when using pharmacological treatments but not in the knockdown experiment. Although the wound healing assay is widely accepted for the study of cell motility, it does not consider the motility of individual cells, the effect of chemoattractant presented in the media or distinguish between cell division or motility. Even though cells were serum starved 24 h prior the experiment (to suppress cell division), it

cannot be excluded that cell proliferation might have occurred abrogating potential motility difference due to HRH1 knockdown. Hence, the wound healing assay should be repeated and drugs able to inhibit cell division like Mitomycin C should be incorporated in the media as a control for cell proliferation (Varankar and Bapat 2018). In addition, the wound healing assay can often produce very variable results: confluence at the time of the "wound", maintaining a healthy cell status, the width of the "wound" are all factors that are difficult to control and that can vary across independent samples, influencing cell behaviour. Therefore, a transwell migration assay or single cells tracking analysis could have been implemented in the work to improve result power, meanwhile obtaining additional information regarding cell behaviour in the presence of a chemoattractant and information on single cell locomotion.

Additionally, 2D migration assays are not fully representative of the migratory ability of cells in the body and often cells cultured in a 3D environment exhibit completely different types of behaviour in terms of gene expression, locomotion, proliferation and shape (Friedl et al. 1998). Therefore, three-dimensional migration assays using collagen or another component of the extracellular matrix, a spheroid migration assay or co-culture models (including cells belonging to the tumour microenvironment) could better mimic the tumour solid microenvironment.

Technical issues and future directions

Overall, transfection efficiency has been inconsistent across the different experiments presented in this project. Prior to performing the experiments, siRNA length of transfection was optimized for the three cell lines used in the project. Knockdown efficiency was measured at 24, 48 and 72h post-transfection, confirming a significant reduction of HRH1 level of expression in most of the cell lines at each time point (Appendix 1, Figure 7.4). Despite the optimization failure in knocking down HRH1 was observed in several experiments (adhesion assay, wound healing assay). The inability of consistently knocking down HRH1 led sometimes to difficulties in interpretation of the data. Indeed, HRH1 knockdown failed for OVCAR3 and OVCAR5 used for the adhesion assay (section 4.3.2) and in OVCAR3 used for the wound healing assay (section 4.3.6). In both assays it was concluded that HRH1 was not involved nor in the adhesion nor in the migration of OC cell lines. Even though this might be the case, there is a possibility that HRH1 plays a role in the adhesion and migration of OC cell lines, but this was not visible due to insufficient reduction of HRH1 level of expression. Several factors can impact siRNA transfection efficiency such as cell viability, seeding density, quality of the siRNAs and RNA contamination. Ideally, generating cell line stably expressing lower level of HRH1 or using different siRNA targeting different region of HRH1 would have ensure a higher reproducibility across experiments and helped drawing more conclusive results.

To date, there are no data available regarding the level of native HRH1 activity in the OC cell lines used in this project. This measure should have been tested in the current project in order to evaluate whether the doses of histamine or chlorpheniramine used to treat OC cell lines were effective in inducing or reducing the receptor's activity. This could have been done by measuring the level of soluble messengers downstream the HRH1 pathway (e.g. Ca^{2+} levels) or by using FRET imaging (as further discussed in section 6.4).

To further explore HRH1 role in OC metastatic cascade, other aspects of this process could be evaluated. For example, OC cells adhesion to different component of the ECM (like collagen, laminin, fibronectin, vitronectin or gelatine) could be tested. A range of different techniques could be employed to study such processes. For example, coverslips could be coated with one or more ECM components and cell adhesion to them assessed (Varol 2020). Alternatively, a ECM protein microarray could be used, as in the study by Kuschel et al. (2006). Moreover, another aspect to investigate would be to determine if HRH1 can regulate the degradation of ECM components. A zymography assay, where cells are plated on coverslips coated with ECM-fluorescent labelled components would be useful to visualise ECM breakdown and assess histamine signalling in matrix degradation (Yamaguchi et al. 2009; Díaz 2013).

4.5. Key findings

- Knockdown of HRH1 does not influence the expression of CDH1 and vimentin, two genes related to the EMT process
- HRH1 knockdown, or the administration of its activator or inhibitors does not alter the ability of SKOV3, OVCA3 and OVCAR5 to adhere to an endothelial cell monolayer, suggesting that HRH1 is not involved in the adhesion process of OC cells in this context
- Invasion by SKOV3 and OVCAR3 through a Matrigel® layer decreases upon HRH1 knockdown; similarly, the addition of histamine to SKOV3 cells increases their invasive potential, suggesting HRH1 involvement in the invasion of OC cells
- The motility of OC cells in a wound healing assay is not impaired by HRH1 knockdown, while chlorpheniramine treatment slows down the motility of SKOV3 and OVCAR5, suggesting either complex underlying biology, or limitations in the methods employed

Chapter 5

HRH1 in EVs biogenesis and their role in OC cell invasion in vitro

5. HRH1 in EV biogenesis and their role in OC cell invasion *in vitro*

5.1. Background

Local and distant intracellular communication is a key factor for cancer progression. Not only can cells communicate with each other through local signalling, they can also send "messages" to future metastasis sites generating favourable 'premetastatic niches' (Peinado et al. 2013; Wortzel et al. 2019). Extracellular vesicles (EVs) have been extensively studied in the past decade and have been proposed by numerous researchers to play a fundamental role in tumour dissemination (Li et al. 2018). EVs can influence several cell behaviours like migration (McCready et al. 2010), invasion (Castellana et al. 2009), EMT (Chen et al. 2018), adhesion (Skog et al. 2008) and vascular permeability (Di Modica et al. 2017). Moreover, EVs bear an essential role in driving ECM degradation through both releasing of their cargo of MMPs (Shan et al. 2018), or by stimulating the expression of MMPs in recipient cells (Purushothaman et al. 2016).

Histamine has been studied for its involvement in cancer invasion and progression, as extensively reviewed by Massari and colleagues (2020). Indeed, results from chapter 4, highlight a potential role of histamine and its receptor HRH1 in OC invasion and migration *in vitro.* However, very little is known regarding the involvement of histamine in EV biology. A recent publication from Verweij and colleagues (2018) demonstrated that histamine stimulation can increase EV biogenesis in a panel of cells lines (HeLa and SiHa (cervical carcinoma), primary human umbilical vein endothelial (HUVEC) and mesenchymal stem cells (MSC)) (Verweij et al. 2018). For the purpose of the experiments, the authors generated HeLa cells stably transfected with a CD63 pHluorin construct. The CD63-pHluorin reporter consists of a tetraspanin (TSPAN) (CD63) based optical reporter cloned with a pH sensitive GFP (pHluorin) molecule, with the pHluorin normally located in the outer membrane of ILVs where it does not emit fluorescence due to the acidic pH (5.5). Upon fusion of MVBs with the PM, ILVs are released in the extracellular space and the sudden change of pH from acidic to neutral (pH 7.4) activates the pHluorin, generating fluorescent flashes (Figure 5.1). By employing TIRF microscopy, the authors observed that stimulation of CD63 positive Hela cells with histamine immediately induced an increase in the number of multivesicular bodies (MVBs) fusing with the plasma membrane (PM). Similar results were also obtained when treating SiHa, HUVEC and MSC cells with histamine (Verweij et al. 2018).

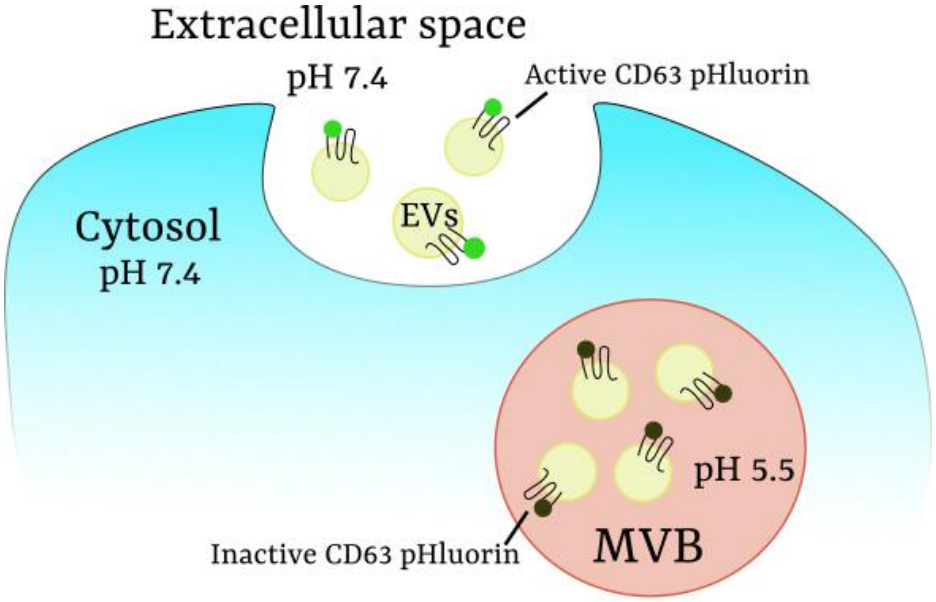

Figure 5.1: Schematic representation of the working mechanisms of the CD63-pHluroin reporter.
CD63-pHluorin is sorted on the membrane of intraluminal vesicles (ILVs) inside the MVB and it is quenched (therefore inactive) when facing the acidic compartment of the MVB (pH 5.5). When the MVB fuses with the plasma membrane, ILVs are released in the extracellular space characterised by a neutral pH (7.4). The sudden neutralisation of the pH activates the pHluorin reporter that emits fluorescence, resulting in a sudden increase of fluorescence intensity.

As most G protein coupled receptors (GPCRs) use calcium as a second messenger (Dickenson and Hill 1993), the authors investigated whether histamine- induced MVB-PM fusion events were linked to an increase of intracellular calcium. With the same experimental method, Verweij and colleagues ruled out the involvement of calcium signalling in the histamine- induced MVB-PM fusion event, as the use of both an intracellular or extracellular calcium chelator (BAPTA-AM and EGTA-AM, respectively) did not reduce the number of histamine- induced MVB-PM fusion events (Verweij et al. 2018). Interestingly, phosphoproteomic analysis showed that the rise in EV release was due to the activation of a protein network starting with HRH1 and ending with activation of synaptosomal-associated protein 23 (SNAP23), a member of the SNARE protein family involved in membrane fusion processes. Subsequent molecular analysis revealed that HRH1 mediates phosphorylation (and therefore activation) of SNAP23 through calcium-independent protein kinase Cα activation. This is the first publication linking histamine, and particularly HRH1, with EV biogenesis. The same year, another paper was published by Khan et al. (2018), showing that the use of 10 µM ketotifen (a selective antagonist of HRH1) reduces EV release in cervical (HeLa) and breast (MCF7 and BT549) cancer cell lines. Collectively, although only a small amount of literature is available, these publications indicate that histamine could positively modulate EV biogenesis in several cell lines through HRH1 activation, and that the inhibition of the latter reduces EV release. It also raises the possibility that the effect of histamine on invasion

that was observed in OC cells (presented in section 4.3.4 and 4.3.5) is mediated through the action of EVs.

5.2. Aim and Objectives

As histamine can increase EV production in different cell types (cervical cancer, endothelial and mesenchymal cell lines), the aim of the investigations described in this chapter is to test if histamine could increase EV production in OC cell lines through HRH1 activation and investigate their potential involvement in OC cell invasion *in vitro*. The specific objectives were:

- To determine whether treatment of SKOV3 with histamine and chlorpheniramine may influence EV characteristics like size, morphology, and expression of protein markers
- To investigate the effects of histamine and chlorpheniramine on EV release in SKOV3 cells
- To test whether EVs extracted from intact SKOV3 could rescue the loss of invasion of SKOV3 cells knocked down for HRH1
- To analyse if histamine and several inhibitors of EV biogenesis can modify the invasive ability of SKOV3 cells
- To explore if EVs released by SKOV3 cells following histamine stimulation can contribute to invasive ability of OC cells by degrading components of the ECM
- To study whether histamine treatment could modify the protein content of EVs

5.3. Results

5.3.1. Characterisation of EVs obtained from SKOV3 under different treatments

The EVs used in this project were extracted by size exclusion chromatography (SEC) (described in section 2.15), so the first step was to identify the "EV-containing fractions" and validate collection conditions. EVs were extracted from 48 h serum-free conditioned media (SFM) obtained from SKOV3 cells treated with control media, 100 µM histamine or 250 µM chlorpheniramine and fractions 1 to 15 (500 µl each) were collected individually. Because long incubation with SFM might reduce cell proliferation and induce cell death, SKOV3 were counted and stained for Annexin V and their proliferation and apoptosis were quantified, respectively. Indeed, experiments performed by a current member of the lab showed that even though incubation with SFM slightly decreased cell proliferation, it did not alter SKOV3 viability, showing suitability of SFM for EV extraction (Appendix 2, Figure 7.5). Protein concentration and particle concentration were measured for each single fraction by BCA assay and NTA, respectively. As reported in figure 5.2 A, B, C, no particles were detected in fractions 1-6, with particles starting to appear at fraction 7 independently of the treatment type (filled bars). The three samples showed a peak in particle number at fraction 9, followed by a steady decrease. Protein concentration was below 1 µg/µl up to fraction 10 (indicated by dots on the graphs) followed by a sharp increase in later fractions. The combination of particle size and protein quantification identified SEC fractions 7-10 as those containing the highest amount of EVs and the least contaminating proteins. Therefore, these fractions were combined for all the following experiments involving EVs.

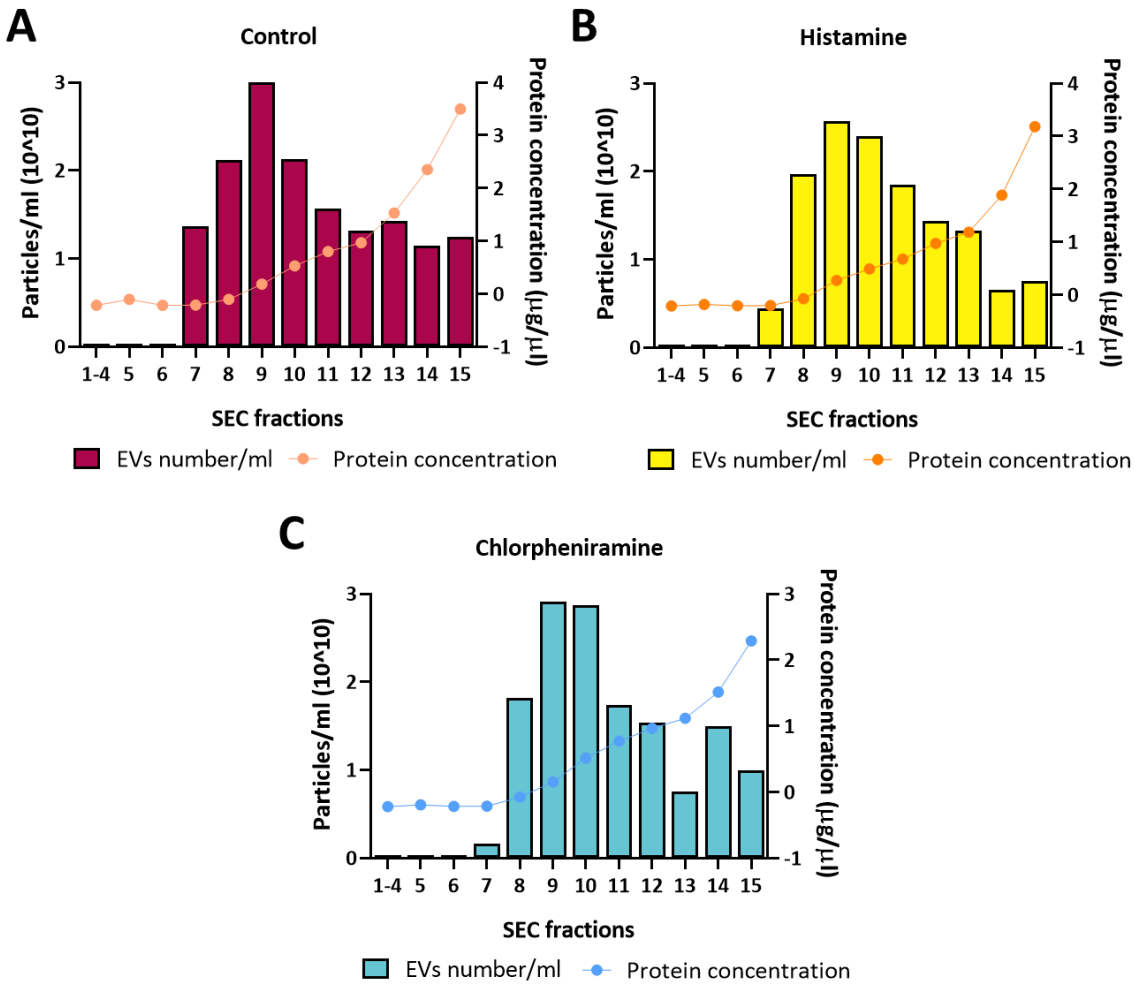

Figure 5.2: Particle number and protein concentration of EVs extracted from conditioned SFM, with SKOV3 that were untreated or treated with histamine or chlorpheniramine.

Fractions 1 to 15 were analysed for particles number and protein concentration by NTA and BCA assay. EVs were derived from A) control SFM, B) 100 µM histamine or C) 250 µM chlorpheniramine. Filled bars represent number of EVs per ml solution (x 10^10) while the dots graphs indicate protein concentration (µg/µl) for the corresponding fraction. One biological replicate.

Absolute purification of EVs from cell culture (or other sources) is an unrealistic goal, therefore it is necessary to verify the origin and the characteristics of any extracted EVs prior to their use. Several techniques should be used, to analyse EV morphology (TEM), their size (NTA and TEM) and their enrichment in specific biomarkers (western blot, flow cytometry and others) (Théry et al. 2018). At the same time, in order to ensure a high purity of the preparation, the absence of organelle markers (such as mitochondria, endoplasmic reticulum and Golgi) should be validated (Théry et al. 2018).

Therefore, to further characterise the EV, their size, morphology, and protein enrichment were investigated. EV size was first measured through NTA analysis (described in section 2.16.1). EVs extracted from control, histamine or chlorpheniramine treated cells after 48 h conditioning showed a size distribution between 50 to 200 nm, as expected (Figure 5.3 A). Curiously, chlorpheniramine treatment seemed to increase the number of particles with size between 75-150 nm, although this increase was not significant ($p=0.63$). EV morphology was then assessed through TEM (described in section 2.16.2); EVs derived from cells treated with control media, histamine and chlorpheniramine showed the typical cup shaped EV structure surrounded by a lipid bilayer (Figure 5.3 B), with a size ranging between 50 to 200 nm. Enrichment in the classical EV markers (ALIX, HSP70, CD63, TSG101, β-Actin, CD81) and the absence of cellular contaminants (Golgi apparatus (GM130) and mitochondria (cytochrome C)) was investigated through western blot (described in section 2.16.3). Western blot analysis (Figure 5.3 C) showed that all three EV samples were enriched in CD63 (smear from 65-40 kDa), TSG101 (43 kDa) and CD81 (25 kDa) but did not show the presence of ALIX (96 kDa), HSP70 (70 kDa) and β-Actin (42 kDa), although these proteins were expressed in the corresponding cells. The absence of GM130 (a Golgi apparatus marker) and cytochrome C (a mitochondrial marker) in the EV samples confirmed the lack of cellular contamination in the EV preparations. Interestingly, the level of CD81, CD63 and Tsg101 appeared to be higher in EVs derived from chlorpheniramine-treated cells compared to both EVs derived from control and histamine-treated cells (Figure 5.3 C), suggesting that chlorpheniramine treatment either increases the enrichment of these biomarkers in the EVs, or increases the number of EVs. The absence of bands in the non-conditioned media sample (NCM) indicates that the samples extracted by SEC were enriched in EVs and did not contain free proteins derived from other sources.

EV surface antigens were further analysed by flow-cytometry with the MACSplex assay (described in section 2.16.4). In this qualitative assay, EV samples were mixed with beads coated with monoclonal antibodies directed against 37 potential EV surface antigens and were analysed through flow cytometry. MACSplex assay results (Figure 5.3 D, reported as mean fluorescence intensity values normalised to CD9) confirmed that the three EV samples were enriched in the classical EV markers CD81, CD9 and CD63. Additionally, all the samples showed strong labelling for CD29 (integrin β1), SSEA-1 (Stage-specific

embryonic antigen 1) and moderate labelling for CD133.1 (prominin-1) and ROR1 (tyrosine-protein kinase transmembrane receptor). A weak signal was also observed for CD24, CD86, and CD142 (platelet tissue factor). A full list of the 37 EV surface antigens used in the experiment can be found in Appendix 2, Figure 7.6. Taken together, the data show that EVs extracted from control, histamine and chlorpheniramine treated cells present the typical EV size and morphology and were immunopositive for the classical EV biomarkers, CD63, TSG101 and CD81.

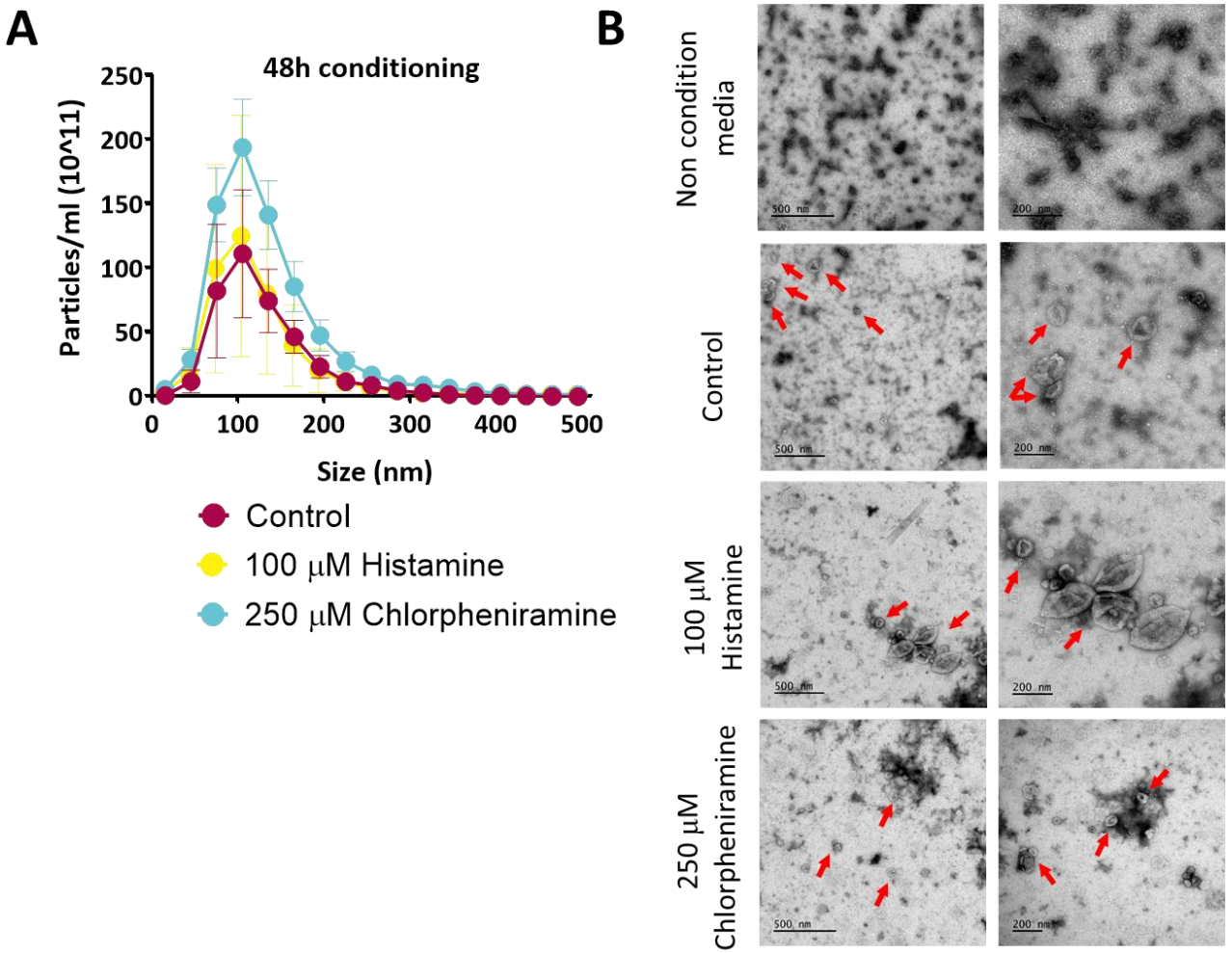
A
48h conditioning
Particles/ml (10^11)
250
200
150
100
50
0
0
100
200
300
400
500
Size (nm)
Control
100 μM Histamine
250 μM Chlorpheniramine
B
Non condition media
Control
100 μM Histamine
250 μM Chlorpheniramine
500 nm
200 nm

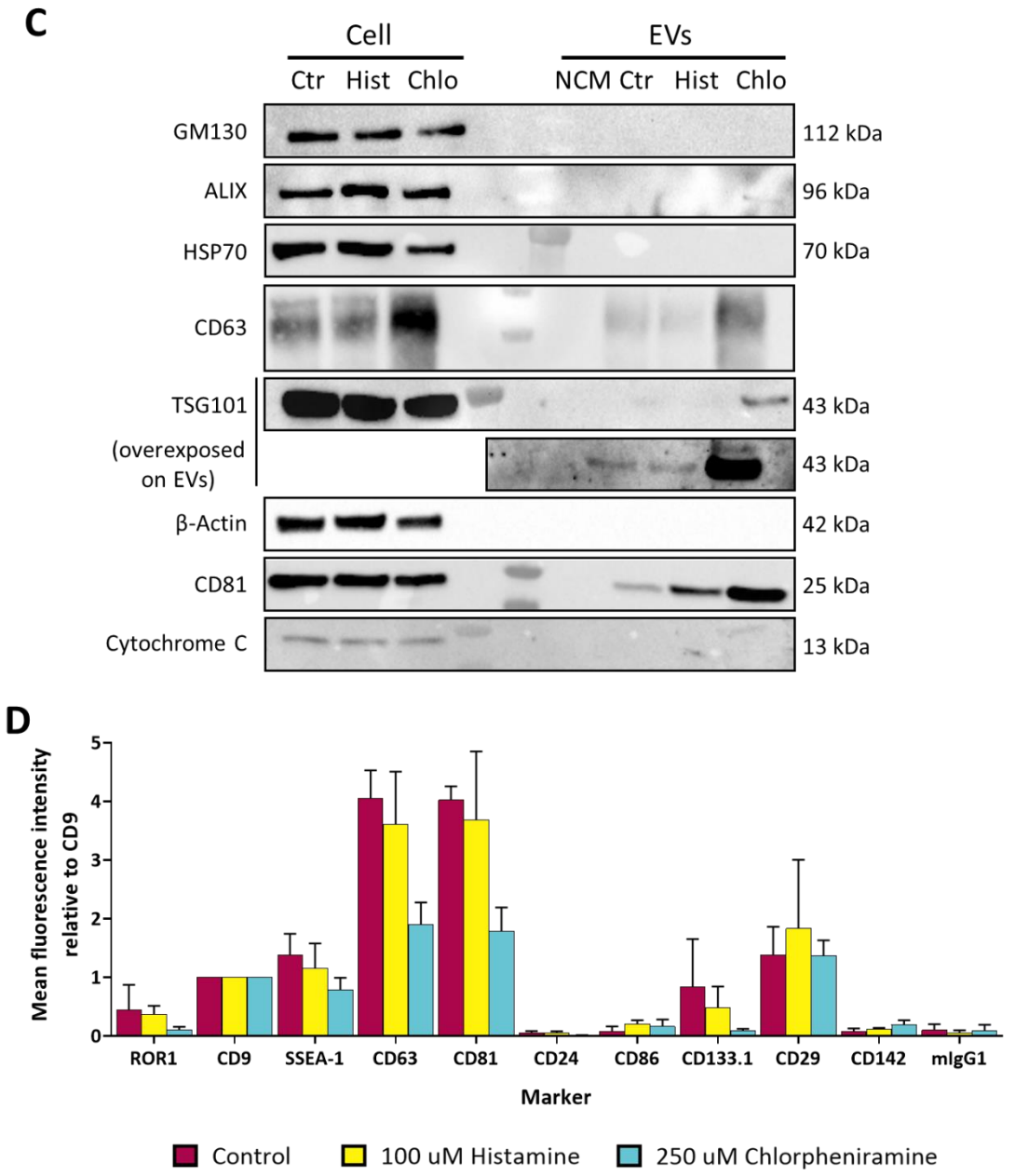

Figure 5.3: Characterization of size, morphology and protein markers of EVs derived from SKOV3 treated with control SFM, 100 µM histamine and 250 µM chlorpheniramine.

A) NTA results showing particle-size distribution for EVs extracted after 48 h conditioning from SKOV3 control (red) or treated with 100 µM histamine (yellow) or 250 µM chlorpheniramine (blue). Eight biological replicates. B) Representative TEM images of EVs obtained from non-conditioned media, histamine or chlorpheniramine treated cells, or control (untreated) cells. EVs are indicated with red arrows in both lower magnification images (left side, scale bar 500 nm) and high magnification images (right side, scale bar 200 nm). One biological replicate. C) Representative western blot images of cell (left side) and EV (right side) samples probed for six EV biomarkers: ALIX (96 kDa), HSP70 (70 kDa), CD63 (40-65 kDa), TSG101 (43 kDa), β-Actin (42 kDa), CD81 (25 kDa) and markers for the Golgi apparatus and the mitochondria: GM1303 (112 kDa), cytochrome C (13 kDa). D) MACSplex data showing mean fluorescence intensity of 10 different EV surface antigens on EVs extracted from cells treated with control media (red bars), 100 µM histamine (yellow bars) or 250 µM chlorpheniramine (blue bars). Data are reported as mean fluorescence intensity normalised to CD9. Three biological replicates were used for both western blot and MACSplex analysis. Bars show, 1X SD.

5.3.2. Histamine or antihistamine treatment do not modify EV concentration

It is known from the literature that histamine, through activation of HRH1, is an inducer of EV biogenesis in a plethora of cell lines (Verweij et al. 2018), while HRH1 inhibition can reduce EV release (Khan et al. 2018). To investigate if this mechanism was retained in OC cell lines, EVs were extracted from control, histamine- or chlorpheniramine-treated SKOV3 cells after 48 h conditioning, their concentration per cell measured through NTA (Figure 5.4 A) and the number of EVs/cell calculated for each condition and normalised to control. Curiously, chlorpheniramine-treated cells produced 60% more EVs than control cells and twice as many EVs/cell than histamine-receiving cells, although this increase was not significant ($p=0.13$; control set as 1; mean histamine=0.85 ± SD=0.54; chlorpheniramine mean=1.69 ± SD=1.01) (Figure 5.4 A). As these results were in contrast to that previously reported in the literature (Khan et al. 2018; Verweij et al. 2018), the same experiment was repeated but this time with EVs extracted after 4 h conditioning. Normally, EVs are constantly released and taken up by cells and this "release/uptake balance" is quantified when measuring EV concentration through NTA. If a compound affects EV release in a short time point, its effect may to an extent be covered by the "release/uptake balance", especially if conditioning the media for a long time (48 h). Therefore, a shorter time points was used for the following experiments. As illustrated in Figure 5.4 B, control, histamine- or chlorpheniramine-treated SKOV3 produced a similar number of EVs/cell and these EV populations had a similar size, with most of the particles falling in the size range between 75 and 200 nm (Figure 5.4 C). In summary, histamine or chlorpheniramine treatment of SKOV3 does not appear to modify the total output of EVs, nor their size.

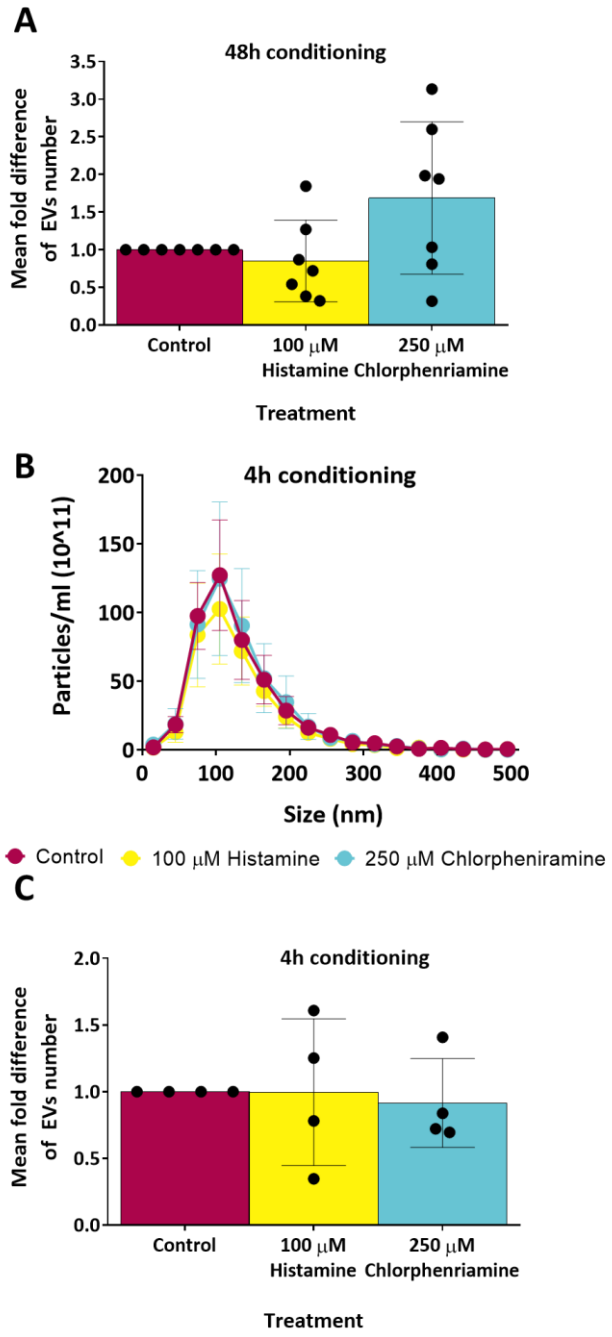

Figure 5.4: Size and concentration of EVs extracted from control, histamine or chlorpheniramine treated cells.

A) The mean number of EVs produced by one cell was measured for control, histamine and chlorpheniramine-derived EVs after 48 h conditioning. Data were normalised to control. B) NTA results showing particle-size distribution for EVs extracted after 4 h from cells treated with control media (red), 100 μM histamine (yellow) or 250 μM chlorpheniramine (blue). C) The mean number of EVs produced by one cell was measured for EVs derived from control, histamine and chlorpheniramine-treated cells after 4 h conditioning. Data were normalised to control. Seven biological replicates were used for quantification of 48 h conditioned EVs while four biological replicates were used for 4 h conditioning EVs. Error bar, 1X SD.

5.3.3. Histamine increases the rate of MVB-PM fusion events

The experiments reported in section 5.3.2 did not yield the expected increase in EV release following treatment with histamine. This could be due to biological or technical reasons as will be discussed later in section 5.4. Therefore, a second method was employed to test whether histamine induces EV release in a model of OC. SKOV3 were transiently transfected with a plasmid containing a CD81 pHluorin reporter (see section 2.4 for protocol details), treated with control media or media supplemented with 100 μM histamine and 5 minutes-long videos were immediately recorded with a TIRF microscope (described in section 2.18). Twelve cells were imaged in total for each condition. Analysis of the videos showed that both control and histamine treated cells had MVB-PM fusion events (Figure 5.5 A, green circles). Histamine-treated cells exhibited twice as many fusion events compared to control cells ($p=0.02$, control mean=3.17 ± SD=2.95; histamine mean=6.67± SD=4.92) (Figure 5.5 B). The analysis also revealed no differences in the features of the fusion events, such as brightness and size. Violin plots in figure 5.5 C indicate that MVB-PM fusions events had a similar brightness, with distribution of fluorescence being comparable across samples ($p=0.97$, control median=8328, histamine median=9201,) (Figure 5.5 C). Fluorescence of the MVB-PM fusion events of both control and histamine treated cells also exhibited a similar size, ranging between 0.3 to 0.9 μm, with most events falling in the range between 0.4 and 0.6 μm (Figure 5.5 D). Taken together, these results show that histamine significantly increases MVB-PM fusion events in SKOV3 cells in the 5 minutes frame following treatment administration.

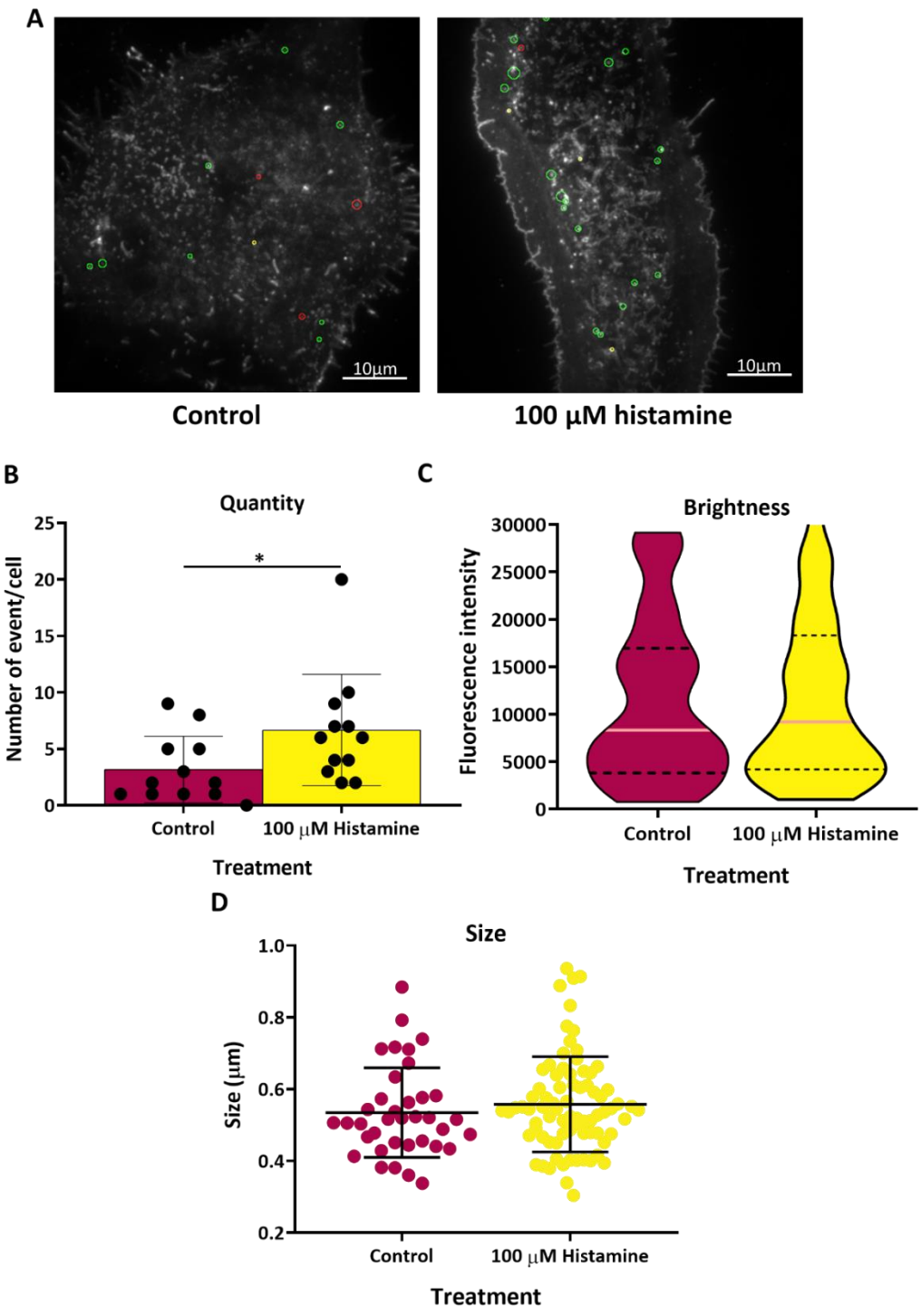

Figure 5.5: Quantification and analysis of MVB-PM fusion events in SKOV3 cells treated with control media or 100 µM histamine.

A) Representative images of total projected MVB-PM fusion events on a control cells (left side) and histamine treated cell (right side). Positive events that were further analysed are circled in green; yellow and red circles indicate events that did not satisfy one or more parameters used in the analysis, respectively (for further information see section 2.18). Scale bar 10 µm. B) Quantity of CD81 MVB-PM fusion events per cell in cells treated with control media or 100 µM histamine (n=12). C) Brightness (mean fluorescence) and D) Size (µm) of single MVB-PM fusion events (control n=37, histamine n=78) in control or histamine-treated cells. Statistical differences were calculated with the Mann-Whitney test. Bars show, 1X SD. * P<0.05.

5.3.4. High dose of chlorpheniramine reduces MVB-PM fusion events

To investigate if HRH1 chemical inhibition could impair MVB fusion to the PM, SKOV3 were treated with two different concentrations of chlorpheniramine: 10 μM (low dose) or 250 μM (high dose) and imaged by TIRF microscopy at 5 minutes intervals over a 35-minute time frame (as described in section 2.18). Two cells were imaged for each time point. Figure 5.6 A shows that, even though the number of samples was too small (n=2) to assess statistical significance, cells treated with 250 μM chlorpheniramine exhibited half the MVB-PM fusion events compared to cells receiving 10 μM chlorpheniramine; this effect was retained throughout the time-interval considered, with an exception at the 15-20 minutes time point where both concentrations showed similar fusion rates (Figure 5.6 A). To better understand whether different concentrations of chlorpheniramine could differently regulate MVB-PM fusion rates, the time variable was excluded from the analysis. Hence, all cells receiving the same treatment were combined and the total number of events per cell considered for further analysis. SKOV3 treated with 10 μM chlorpheniramine exhibited the same number of MVB-PM fusion events as control cells ($p=0.85$), while cells treated with a high dose of the drug showed significantly less MVB-PM fusion events than both control cells ($p=0.04$, control mean=3.17 ± SD=2.95, 250 μM mean=1.21 ± SD=1.58) and cells receiving low doses of the drug ($p=0.02$, 10 μM mean=3.29 ± SD=2.67) (Figure 5.6 B). Treatment with 10 μM chlorpheniramine increased the brightness of MVB-PM fusion events compared to control cells ($p=0.02$, control mean=11,553 ± SD=8,698, 10 μM mean=18,570 ± SD=13,425) (Figure 5.6 C) while administration of high doses of chlorpheniramine did not impair the brightness of fusion events compared to control cells ($p=0.05$). Finally, neither low doses nor high doses of chlorpheniramine modified the size of MVB-PM fusion events, with both treatments retaining events with a size between 0.3 to 1 μm, similarly to control samples ($p>0.99$. $p=0.2$, respectively). As a body of evidence, treatment with 250 μM chlorpheniramine reduced the number of fusion events compared to both control cells and cells receiving low dose of chlorpheniramine; low doses of the drug significantly increased the fluorescence of the fusion events but did not modify their size. Taken together these data suggest that HRH1 inhibition impairs EV biogenesis only when using high concentration of chlorpheniramine.

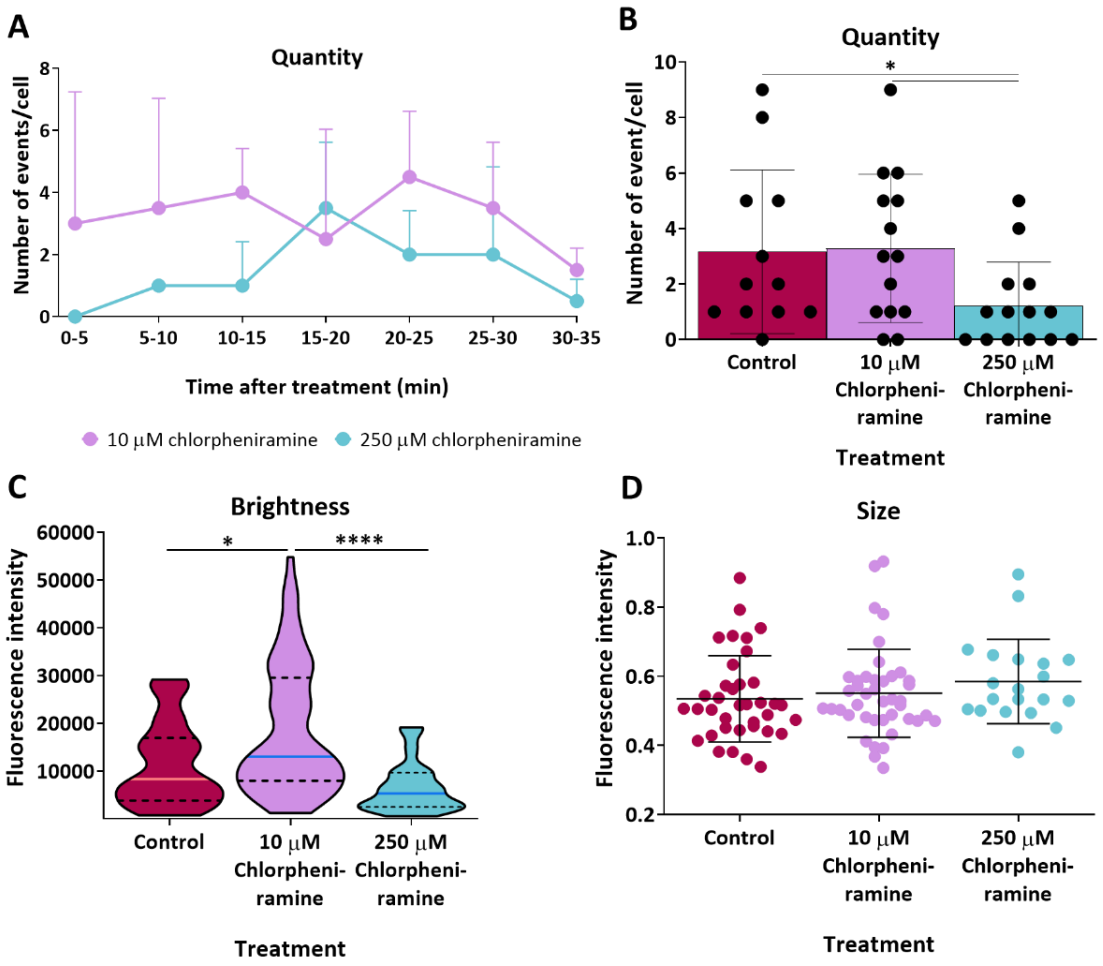

Figure 5.6: Quantification and analysis of MVB-PM fusion events of cells treated with low or high doses of chlorpheniramine.

A) Quantity of CD81 MVB-PM fusion events per cell over time in cells receiving 10 or 250 µM chlorpheniramine. Cells were imaged for 5 minutes in a time frame of 35 minutes post treatment. Two cells were imaged for each time point for each condition. B) CD81 MVB-PM fusion events per cell were quantified in cell treated with control media (n=12), 10 or 250 µM chlorpheniramine (n=14 for both). C) Brightness (mean fluorescence) and D) size (µm) were calculated for single fusion event (Control n= 37, 10 µM chlorpheniramine n=42; 250 µM chlorpheniramine n=20). Statistical differences were calculated with the Kruskal-Wallis test, followed by a Dunn's multiple comparison test. Bars show, 1X SD. * P<0.05, **** P<0.0001.

5.3.5. EVs extracted from SKOV3 cells rescue the HRH1 knockdown-induced loss of invasion

EVs have been extensively studied for their role in cancer progression and several papers have shown their involvement in cell invasion and migration (Becker et al. 2016; Dai et al. 2020; Xavier et al. 2020). The data reported in section 4.3.4 indicates that HRH1 knockdown reduces SKOV3 invasion through a Matrigel® layer. In addition, data reported in section 5.3.3 and 5.3.4 highlighted a potential involvement of HRH1 in regulating EV biogenesis. This pointed towards the idea that HRH1 knockdown could reduce the invasion of OC cell lines by reducing the number of released EVs. To test this

hypothesis, and check if EVs could restore the invasiveness of SKOV3 knocked down for HRH1, a rescue experiment was performed. EVs were extracted from non-treated SKOV3 cells and either EVs or PBS were added to SKOV3 cells receiving HRH1 or control siRNAs, following which invasion through a Matrigel® layer was measured (Figure 5.7 A). RT-qPCR analysis revealed that knocked down cells expressed half the amount of HRH1 than cells receiving control siRNA, confirming successful knockdown of HRH1 ($p=0.02$, control mean=1.008 ± SD=0.18, HRH1 mean=0.45 ± SD=1.04) (Figure 5.7 B). Image analysis of Matrigel® membranes confirmed data reported previously in chapter 4, that is that SKOV3 cells in which HRH1 was knocked down (siRNA HRH1 + PBS) (siRNA HRH1 + PBS mean= 0.57 ± SD=0.25) invaded 40 % less than cells receiving siRNA control + PBS (siRNA control + PBS mean= 1.0 ± SD=0.29) ($p=0.023$) (Figure 5.7 C). Interestingly, addition of EVs to the HRH1 knockdown SKOV3 (siRNA HRH1 + EVs) rescued their phenotype, resulting in these cells invading as much as the SKOV3 receiving siRNA control + PBS ($p=0.90$, siRNA control + PBS mean=1.0 ± SD=0.29, siRNA HRH1 + EVs mean= 1.05 ± SD=0.34). Indeed, the HRH1 knockdown SKOV3 receiving EVs invaded twice as much as HRH1 knockdown SKOV3 receiving PBS ($p=0.017$, siRNA HRH1 + EVs mean=1.056 ± SD=0.34) (Figure 5.7 C). These data demonstrate that while HRH1 knockdown decreases the invasion of SKOV3, addition of EVs, extracted from non-treated SKOV3, leads to a significant rescue of invasion, consistent with a mechanism whereby reduced invasion in HRH1 knocked down cells is caused by reduced EV release.

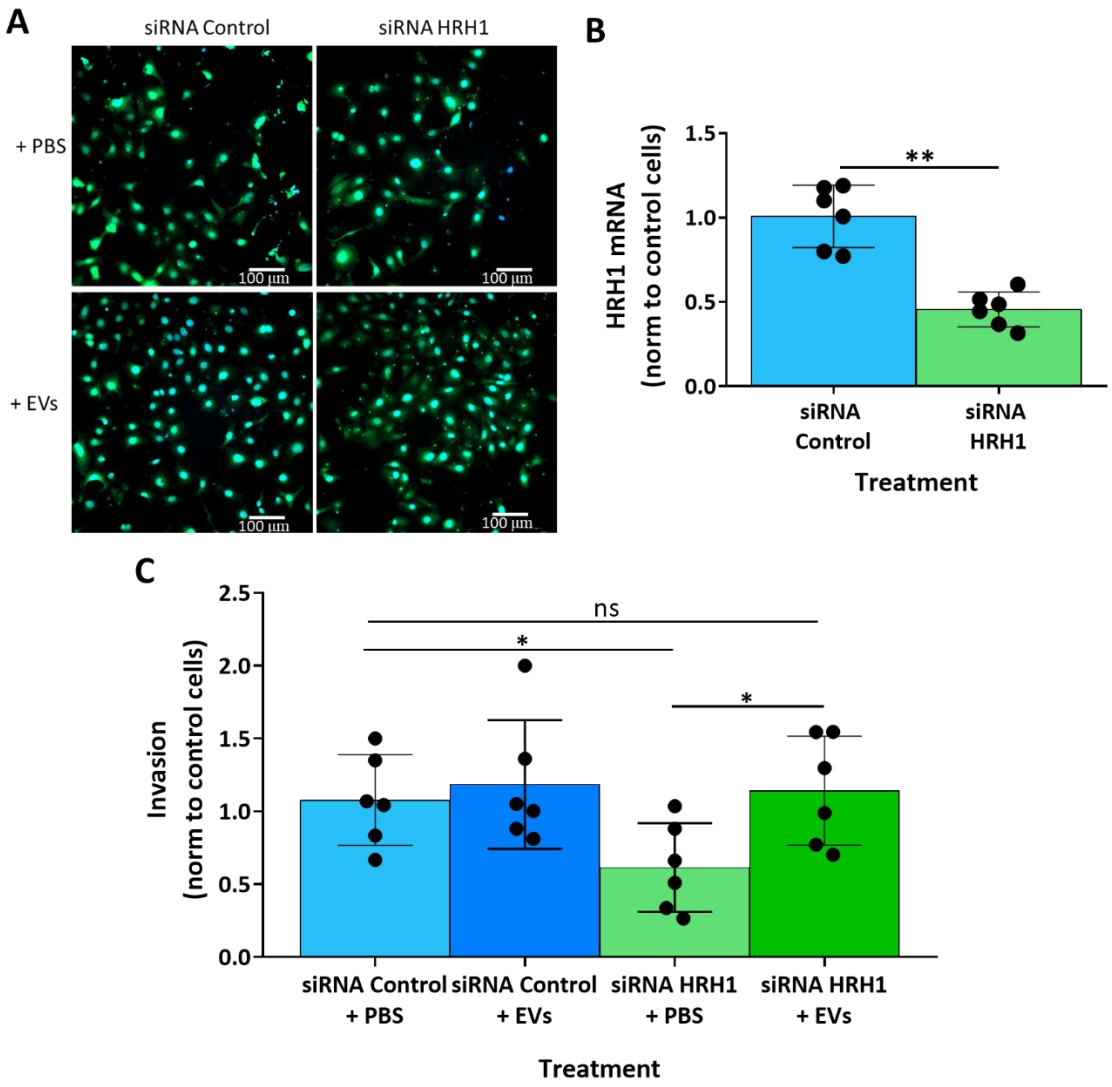

Figure 5.7: Matrigel® invasion assay on SKOV3 control or knocked down for HRH1 with or without addition of exogenous EVs.

A) Representative images of SKOV3 invading through a Matrigel® layer under different conditions. Cells were stained with DAPI (blue) and CFSE (green). Scale bar 100 µm. B) RT-qPCR analysis was used to evaluate transfection efficiency. HRH1 mRNA level are reported as fold change on β-actin (used as endogenous control). C) Percentage of invasion was calculated for SKOV3 under different conditions. Data were normalised to control cells. Two biological replicates, each one containing three technical replicates (n=6 in total) were used for statistical analysis. Statistical differences between two groups were identified by using the Mann-Whitney test while Kruskal-Wallis test, followed by a Dunn's post-hoc test was used for comparing three or more groups. Bars show, 1X SD. * $P<0.05$, ** $P<0.01$.

5.3.6. GW4869 does not alter SKOV3 invasion through a Matrigel® layer

The data presented thus far are consistent with the hypothesis that HRH1 can regulate EV biogenesis, and this can influence SKOV3 invasiveness *in vitro*. It has been reported that inhibition of different molecules involved in EV biogenesis (including neutral sphingomyelinase and Rab27a) and subsequent decrease of EV production, can lead to reduction of cancer growth and spread *in vitro* and *in vivo* (Fabbri et al. 2012; Peinado et al. 2013; Guo et al. 2019). Here it was investigated whether inhibition

of EV biogenesis through administration of GW4869, a neutral sphingomyelinases inhibitor, could affect SKOV3 invasion, and if histamine administration could rescue the effect.

Firstly, SKOV3 were treated with one of the following treatments: 1) DMSO (control), 2) 100 μM histamine, 3) 10 μM GW4869 or 4) 100 μM histamine and 10 μM GW4869 and their invasion through a Matrigel® layer was measured (Figure 5.8 A). Prior the experiment, GW4869 IC50 in SKOV3 was measured through and MTT assay and the concentration of 10 μM was chosen for subsequent experiments (Appendix 2, figure 7.7). Image analysis revealed that SKOV3 treated with histamine (mean =2.52 ± SD=1.21) show a 40% increase in the average number of invading cells compared to control cells (mean =1.76 ± SD=0.3,), although this was not significant due to high variability of data (p=0.46) (Figure 5.8 B). At the same time, neither administration of GW4869 nor the combination of both drugs modified the invasion of SKOV3 cells (Figure 5.8 B). Interestingly, NTA quantification of EV concentration per cells revealed that, while histamine-treated SKOV3 produced as many EVs as control cells (p=0.84), treatment with GW4869 induced a 2-fold increase in the number of EVs per cell compared with both SKOV3 control (control set as 1, GW4869 mean= 2.79 ± SD=1.6) (p=0.03) and cells receiving 100 μM histamine (mean= 1.09 ± SD=0.56) (p=0.04) (Figure 5.8 C). Collectively, the results presented here suggest that GW4869 does not alter SKOV3 invasion, and this could be linked to the finding that this treatment does not reduce EV biogenesis in SKOV3 cells.

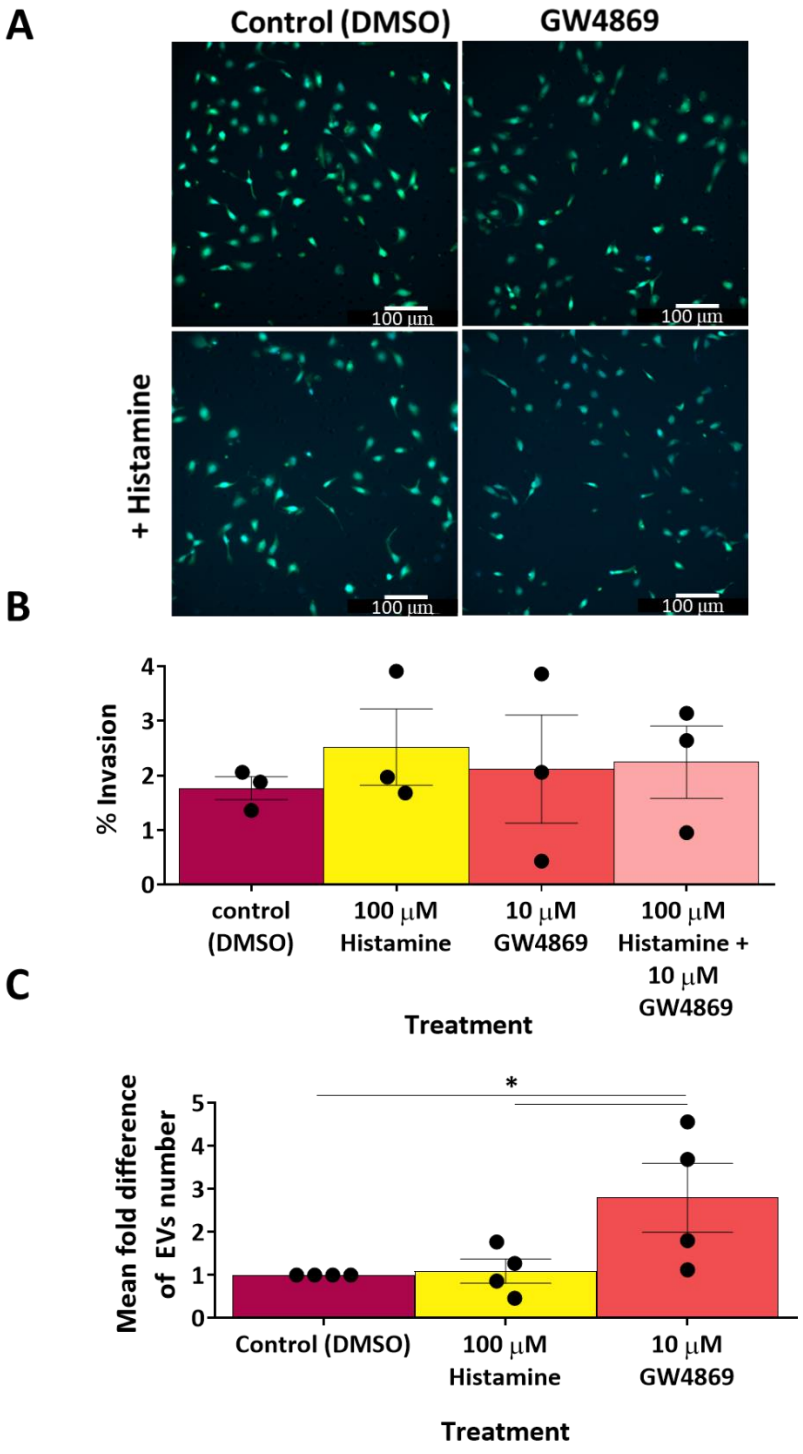

Figure 5.8: Matrigel® invasion assay on SKOV3 control or treated with 100 µM histamine, 10 µM GW4869 or a combination of both drugs.

A) Representative images of a Matrigel® invasion assay on SKOV3 under different conditions. Cells were stained with DAPI (blue) and CFSE (green). Scale bar 100 µm. B) Percentage of invasion of SKOV3 treated with DMSO, 100 µM histamine, 10 µM GW4869 or with a combination of the two compounds. One biological replicate with three technical replicates. C) Quantification of EV number per cells in SKOV3 treated with control media, 100 µM histamine or 10 µM GW4869. Data were normalised on control. Four biological replicates were combined for statistical analysis. Statistical differences were calculated with a Kruskal-Wallis test followed by Dunn's post-hoc test. Bars show, 1X SD. * P<0.0.5.

5.3.7. Rab27a knockdown impairs SKOV3 invasion and histamine administration does not rescue it

Another well-established mechanism associated with EV biogenesis involves the protein Rab27a (Ostrowski et al. 2010) (see section 1.3.2). Therefore, the effect of Rab27a knockdown on SKOV3 invasion, with or without addition of histamine, was investigated. Rab27a transfection conditions were optimised (Appendix 2, Figure 7.8), then SKOV3 cells were transfected with either siRNA control or siRNA for Rab27a and allowed to invade through a Matrigel® layer for 48 h, with or without addition of 100 μM histamine (Figure 5.9 A). Cells transfected for Rab27a showed a decrease of its mRNA of more than 80% compared to cell control (p=0.002; siRNA control mean=1.33 ± SD=0.16; siRNA Rab27 mean=0.19 ± SD=0.077), as reported through RT-qPCR analysis, thus indicating a successful Rab27a knockdown (Figure 5.9 B). Analysis of the Matrigel® membranes revealed that the average number of invading histamine-treated SKOV3 cells was 40% higher that control cells, although this increase was not significant (p=0.37; siRNA control mean=1 ± SD=0.16; siRNA control + histamine mean=1.40 ± SD=0.39) (Figure 5.9 C). Silencing of Rab27a lowered the average number of invading cells by 40% compared to control cells (siRNA Rab27a mean=0.58 ± SD=0.26) (although this was not significant) (p=0.10) (Figure 5.9 C), and significantly decreased it compared to histamine-treated cells (p=0.012; siRNA control + histamine mean=1.40 ± SD=0.39). Histamine addition to Rab27a knocked down cells failed to rescue their invasion, further decreasing the number of invading cells (p=0.55). Interestingly, SKOV3 knocked down for Rab27a receiving histamine invaded 60% less than control cells (p=0.026; siRNA Rab27a + histamine mean=0.40 ± SD=0.11) and less than cells receiving histamine alone (p=0.0018) (Figure 5.9 C). Overall, these data suggest that the histamine- induced increase in SKOV3 cell invasion is mediated via Rab27a-mediated EV release.

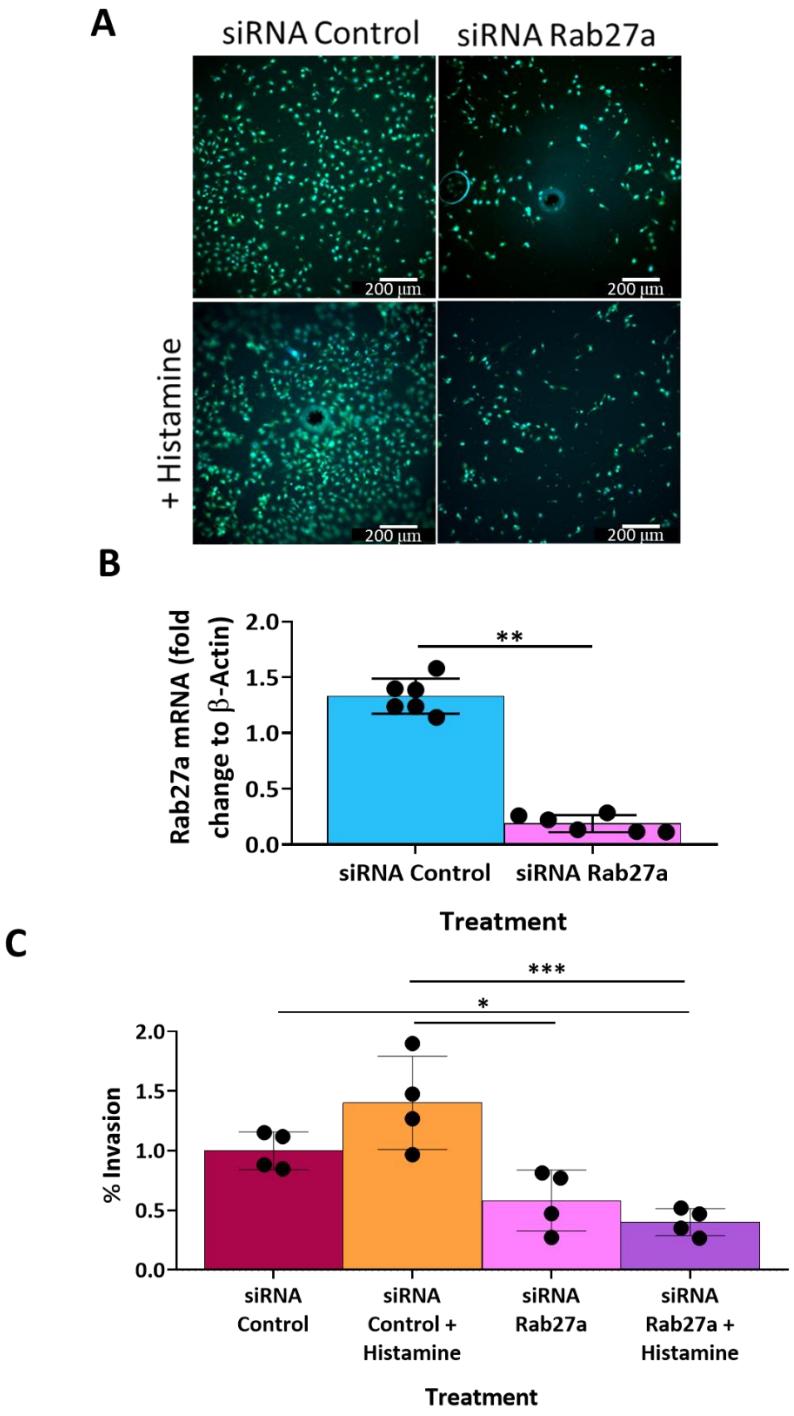

Figure 5.9: Invasion assay on SKOV3 transfected for Rab27a with or without histamine addition.

A) Representative images of a Matrigel® invasion assay on SKOV3 under different conditions. Cells were stained with DAPI (blue) and CFSE (green). Scale bar 200 µm. B). RT-qPCR analysis showing level of Rab27a mRNA in SKOV3 treated with siRNA control or siRNA for Rab27a. Data are expressed as fold change on β-actin (endogenous control). Data were normalised on cell receiving only transfection reagent. Two biological replicates, each one containing three technical replicates were used for the analysis (n=6) C) Percentage of invasion of SKOV3 treated with either siRNA control or siRNA for Rab27a with or without addition of 100 µM histamine. Data were normalised to control. Two biological replicates, containing two technical replicates each were combined for statistical analysis (n=4). Statistical differences were identified with a Mann-Whitney test when comparing two groups. Kruskal-Wallis test followed by Dunn's post-hoc test was used to compare three or more conditions. Bars show, 1X SD. *P<0.0.5, ** P<0.01, ***P<0.001.

5.3.8. EVs derived from histamine treated SKOV3 show enhanced proteolytic activity than control or chlorpheniramine-induced EVs

Thus far, the finding that EVs can rescue the reduction of invasion of SKOV3 following HRH1 knockdown (section 5.3.5) indicates that EVs could play a functional role during cell invasion. Cell invasion is a complex process where cells need to adhere to a surface, degrade the ECM and migrate through it. Hence, EVs could act at several points of this process by either influencing cell migration, modifying their proteolytic activity or behaving as a "facilitator" of invasion, by priming the metastatic sites (Hoshino et al. 2015; Sung et al. 2015). As histamine and chlorpheniramine administration to SKOV3 modify EV release (section 5.3.3 and 5.3.4), it was investigated if both treatments could also modify EV functions. Therefore, EVs were extracted from SKOV3 treated with either SFM, or SFM supplemented with 100 µM histamine or 250 µM chlorpheniramine and their ability to degrade collagen was tested through a collagen degradation assay (see section 2.17 for further details). FITC-quenched collagen was plated in a 96-well plate together with the different EV samples; collagen degradation induced release of the FITC molecule with subsequent release of fluorescence, which was detected using a spectrophotometer at time point 0, 2, 6, 12, 18 and 24 h. Figure 5.10 A shows the efficacy of the assay, as several collagenase dilutions degraded collagen over time in a dose-dependent manner. Overall, equal number of EVs derived from control cells, histamine or chlorpheniramine treated cells degraded collagen to some extent, but no differences were identified between treatments among different time points ($p=0.066$) (Figure 5.10 B). However, when data from the different time points were combined to consider the overall effect, EVs derived from histamine-treated cells (mean=4.51 ± SD=2.56) appeared to have an enhanced proteolytic activity and degraded the collagen substrate significantly more than control EVs ($p=0.016$, mean=2.02 ± SD=0.97) or EVs extracted from chlorpheniramine treated cells ($p=0.0026$, mean=1.39 ± SD=0.42). In sum, all the EV samples used in this experiment can degrade collagen, with EVs- induced by HRH1 chemical activation (via histamine) showing a greater ability to degrade collagen compared to EVs extracted from control or chlorpheniramine treated cells.

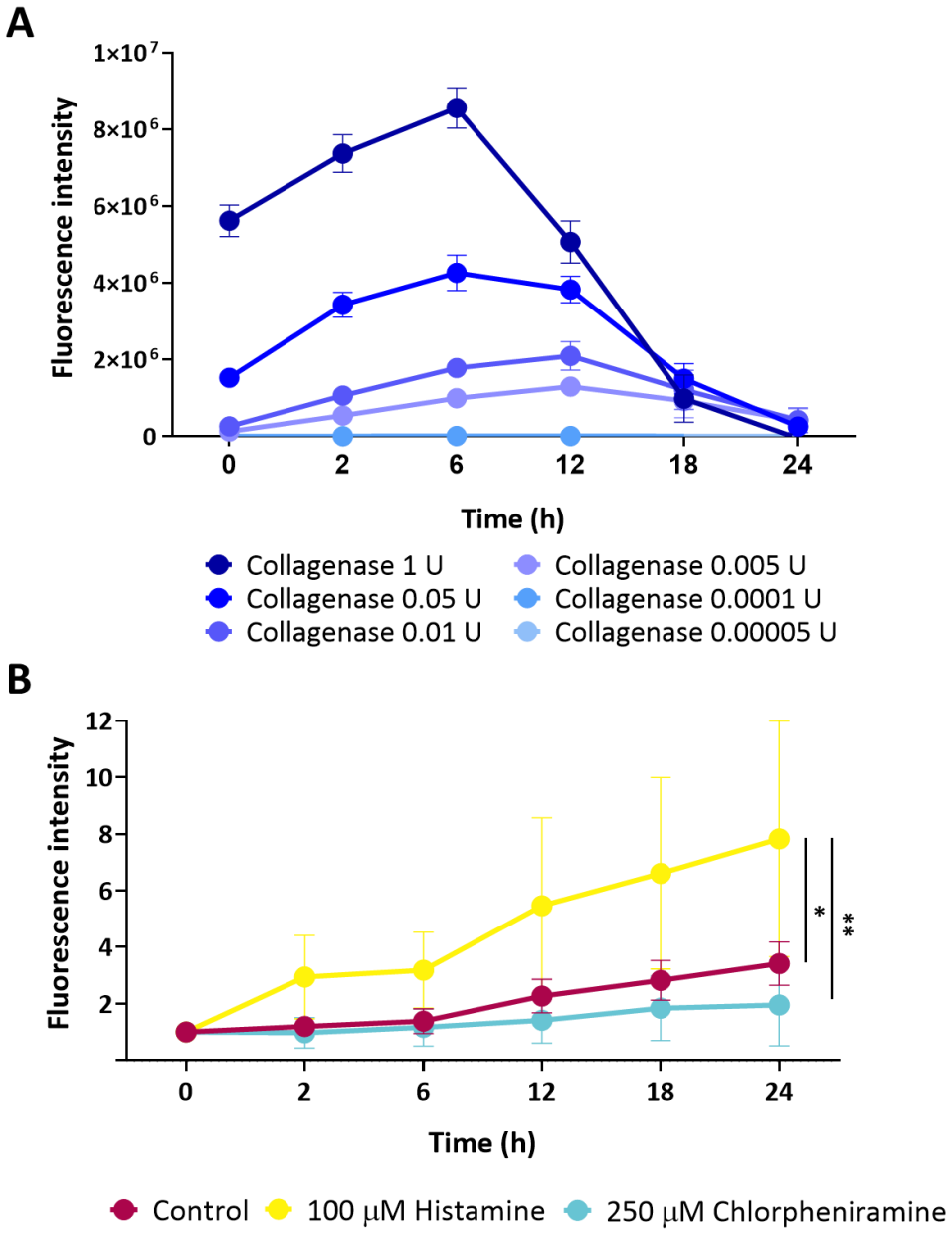

Figure 5.10: Collagen degradation assay on EVs derived from cell treated with control media, 100 µM histamine or 250 µM chlorpheniramine.

A) Fluorescence intensity of six different dilutions of collagenase were used as positive control. One biological replicate containing four technical replicates. B) Fluorescence intensity of collagen degradation following treatment with EVs derived from cells treated with SFM, or with SFM supplemented with 100 µm histamine or 250 µM chlorpheniramine. One hundred time "EVs per surface" were added to each well for each condition, as described in section 2.17.1. To calculate the dilution factor, the surface area of 5 t175 cm^2 flasks (number of flasks used to extract EVs) was divided by the surface area of one well of a 96-well plate (recipient well). The dilution factor was then multiplied by 100 to obtain the final concentration of EVs to add to each experimental well. Data were normalised to time 0 h for each treatment. The average of three biological replicates, each one containing four technical replicates, were combined for statistical analysis. Statistical differences were calculated with a one-way ANOVA followed by a Tukey's post hoc. Bars show, 1X SD. * P<0.05, ** P<0.01.

5.3.9. Identification of the protein content of EVs control and EVs derived from histamine treated SKOV3

The data reported above (section 5.3.3) indicates that administration of 100 μM histamine to SKOV3 cells increases the number of MVB-PM fusion events and overall improves EV ability to degrade collagen (section 5.3.8). In order to understand if histamine treatment modified the EV protein content, EVs were extracted from SKOV3 control cells or cells treated with 100 μM histamine after 4 h conditioning, and their protein content was analysed through mass-spectrometry. The total number of proteins identified in control and histamine treated EVs is illustrated in figure 5.11 A, and the total number of proteins identified in each of the four biological replicates for each treatment group is shown in figure 5.11 B, C. In total, 888 proteins were identified, of which 546 were shared between control EVs and EVs derived from histamine treated cells, 82 were unique to control EVs, and 260 were found only in histamine induced-EVs (Figure 5.11 A). For control cell derived EVs, although most of the proteins were shared between the four biological replicates, some proteins were present in only one of the replicates, with 81 out of the 628 total proteins being expressed only in replicate 1, 51 in replicate 2 and 35 in replicate 3 (Figure 5.11 B). A similar situation was found for EVs derived from histamine treated cells, with replicate 1 expressing 108 of the 806 total proteins, replicate 3 expressing 74, replicates 2 expressing 45 and replicate 4 33 (Figure 5.11 C). Due to the low overlap of protein expression across biological samples, only proteins contained in at least three replicates of at least one condition were used for further analysis.

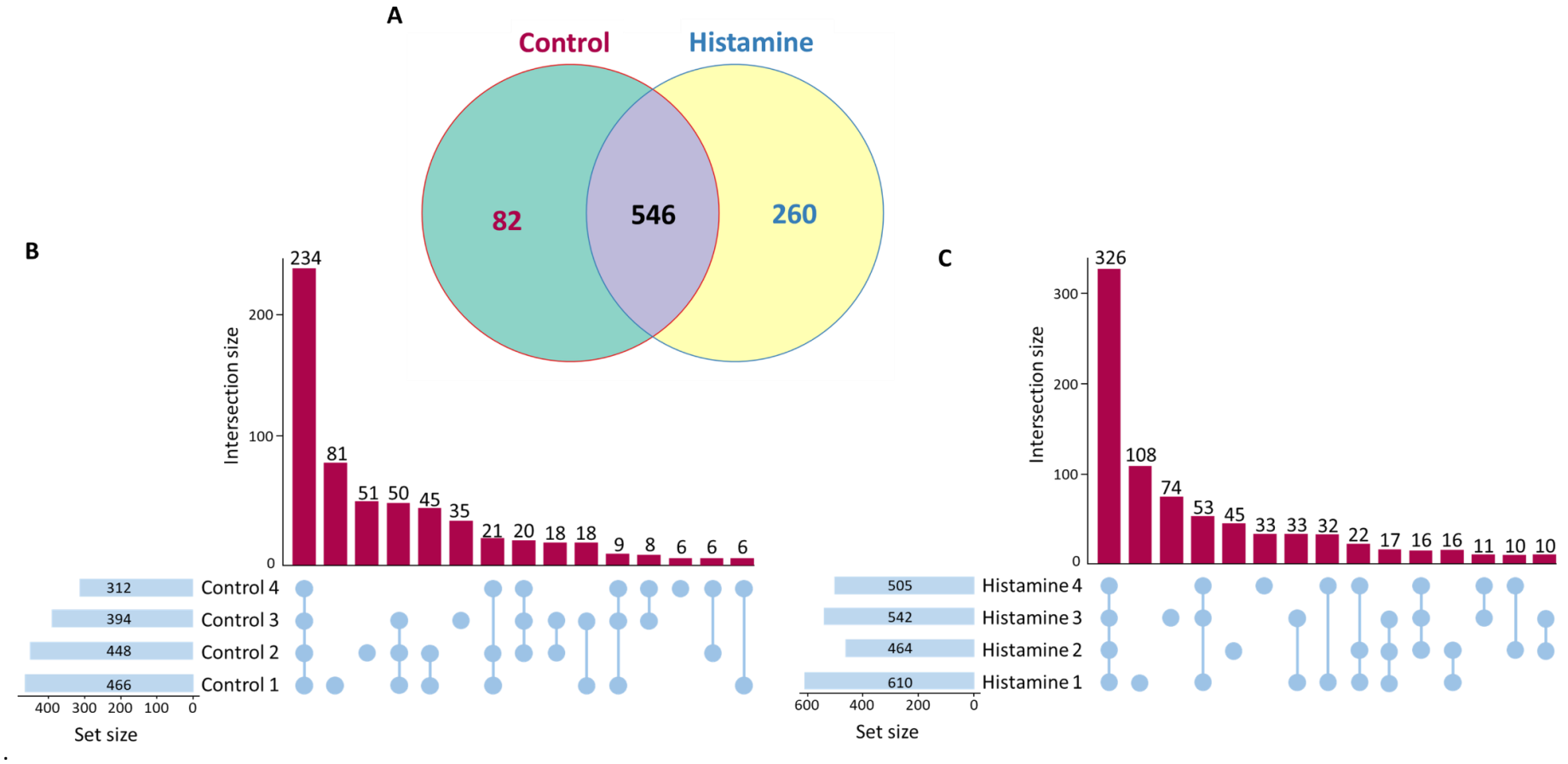

Figure 5.11: Protein content of EVs extracted from SKOV3 treated either with control media or with 100 µM histamine.

A) Venn diagram showing the total number of proteins identified in control and histamine- induced EVs. UpSet plots of proteins identified in B) control and C) histamine- induced EVs show the distribution of proteins across biological replicates.

The Venn diagram in figure 5.12 A shows the proteins found in at least three replicates of at least one treatment group. Overall, 461 proteins were identified, with 321 being shared between the two samples, 21 expressed only in control EVs and 119 only present in EVs derived from histamine treated cells (Figure 5.12 A). For non-overlapping proteins, a read was only counted if it was identified in three or more replicates of one treatment and in less than three replicates for the other treatment group. UpSet plots show the protein distribution across biological replicates of the same treatment group (Figure 5.12 B, C). Interestingly, when comparing the content of the SKOV3 EVs with the 100 most abundant proteins identified in EV (list obtained from ExoCarta, accessed May 2021), 81% of top EV marker proteins were present in EVs derived from histamine treated cells and 79% in control EVs (Appendix 2, Figure 7.9). In further support of this, gene ontology (GO) analysis on the total protein content of both EV samples showed that the most enriched term for cellular components was “extracellular exosomes”, for both control EVs and histamine- induced EVs (Figure 5.12 D), suggesting that the proteins analysed through mass-spectrometry are truly derived from EVs and not from other sources.

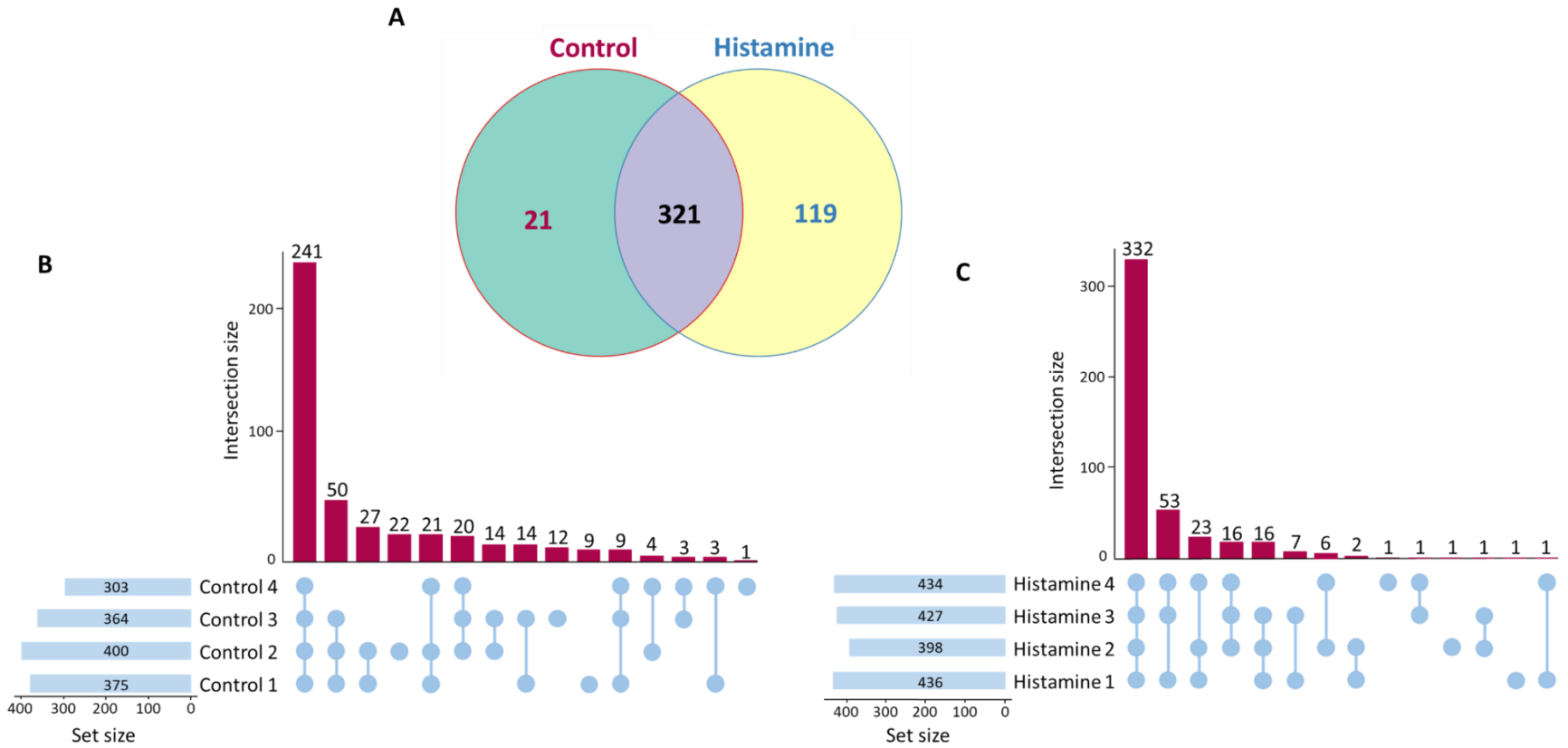
A
Control
Histamine
21
321
119
B
Intersection size
241
50
27
22
21
20
14
14
12
9
9
4
3
3
1
303
364
400
375
Control 4
Control 3
Control 2
Control 1
400 300 200 100 0
Set size
C
Intersection size
332
53
23
16
16
7
6
2
1
1
1
1
1
1
434
427
398
436
Histamine 4
Histamine 3
Histamine 2
Histamine 1
400 300 200 100 0
Set size

D

EVs derived from control cells			
Cellular component	Fold enrichment	P-value	Benjamini
Extracellular exosome	83.3	4.0E-174	1.8E-171
Focal adhesion	27.9	8.7E-79	2.0E-76
Membrane	49.0	9.9E-64	1.5E-61
Extracellular matrix	22.0	9.2E-63	1.1E-60
Cytosol	58.4	3.4E-62	3.1E-60
Cell-cell adherens junction	19.4	1.8E-48	1.4E-46
Melanosome	10.6	2.8E-35	1.9E-33
Proteasome complex	7.9	1.6E-29	9.5E-28
Ribosome	10.3	8.7E-26	4.5E-24
Cytosolic large ribosomal subunit	7.0	2.9E-23	1.4E-21
EVs derived from histamine treated cells			
Cellular component	Fold enrichment	P-value	Benjamini
Extracellular exosome	77.8	2.7E-190	1.4E-187
Focal adhesion	25.0	1.3E-85	3.3E-83
Membrane	49.5	5.3E-84	9.0E-82
Cytosol	59.2	1.1E-82	1.4E-80
Extracellular matrix	19.0	1.8E-64	1.8E-62
Cell-cell adherens junction	15.8	9.9E-45	8.5E-43
Melanosome	9.2	3.7E-37	2.7E-35
Proteasome complex	7.1	4.8E-33	3.1E-31
Ribosome	10.1	1.8E-32	1.0E-30
Myelin sheath	8.5	7.3E-26	3.7E-24

Figure 5.12: Protein content of EVs extracted from SKOV3 treated either with control media or with 100 µM histamine.

A) Venn diagram showing proteins identified in at least three biological replicates of control and histamine-induced EVs. UpSet plots of proteins identified in B) control and C) histamine EVs show the distribution of proteins across biological replicates. D) GO-term analysis showing the 10 most enriched cellular component in control EVs and EVs derived from histamine treated cells. Cellular components are sorted for p-value after Benjamini-Hochberg correction.

5.3.10. Deregulated protein identification and GO term analysis

EV cargo can change due to the conditions within their parent cells, such as stress and disease, and this can influence their function (Melo et al. 2015). To assess what changes were occurring to the proteome of EVs derived from histamine-treated cells, the Log_2 of the mean fold change (Log_2 LFQ intensity histamine – Log_2 LFQ intensity control) of each protein following histamine treatment, and p-

value of this change, was calculated. Log_2 fold change of each protein was plotted against – Log_{10} of the p-value obtained from the t-test and a volcano plot was generated, initially, a permutation-based false discovery rate (FDR) (Bonferroni correction) approach was used; but when applying an FDR value of 0.01 or 0.05 to the analysis, no differences were found in the content of histamine – induced EVs, meaning than none of the proteins identified in EVs derived from histamine treated cells had a fold change higher than 2 and a significant p-value (Figure 5.13 A, B). Therefore, the analysis was repeated, and p-values were calculated without applying FDR correction. The volcano plot in figure 5.13 C shows all the identified proteins (black dots): proteins in orange had a 2-fold change either up (right side) or down (left side), proteins in red had a p-value lower than 0.05 and proteins in green had both (Figure 5.13 C). Of all the proteins, 11 were upregulated (2-fold increase or more) in histamine treated EVs while 4 were downregulated (more than 2-fold decrease). Out of these, 6 of the upregulated proteins had a significant p-value and are listed in figure 5.13 D, while none of the downregulated proteins had a significant p-value. A full list of all the proteins with a significant p-value can be find in Appendix 2, Figure 7.10 A, together with the 10 most up and down-regulated proteins (Appendix 2, Figure 7.10 B, C).

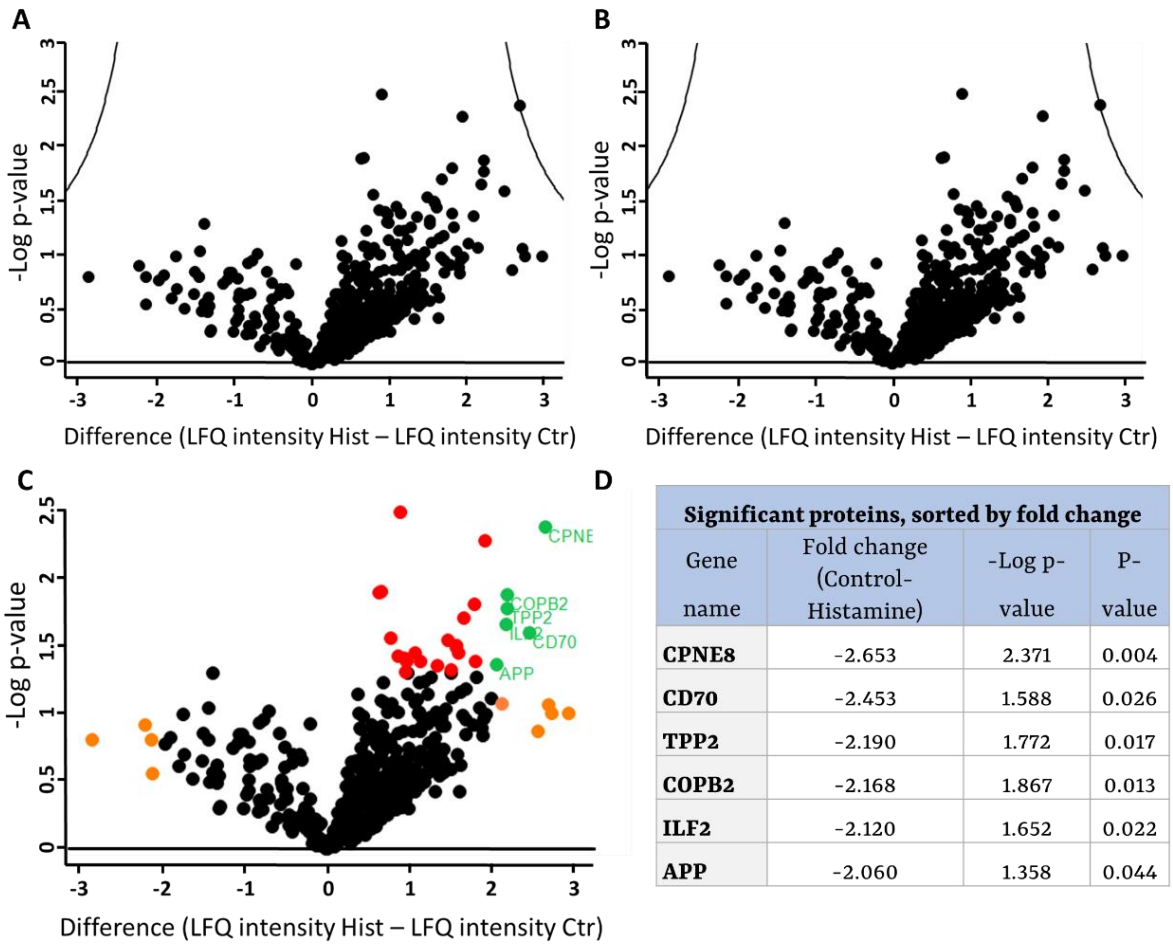

Significant proteins, sorted by fold change			
Gene name	Fold change (Control-Histamine)	-Log p-value	P-value
CPNE8	-2.653	2.371	0.004
CD70	-2.453	1.588	0.026
TPP2	-2.190	1.772	0.017
COPB2	-2.168	1.867	0.013
ILF2	-2.120	1.652	0.022
APP	-2.060	1.358	0.044

Figure 5.13: Fold change of proteins identified in EVs from control and histamine treated SKOV3.
The Log_2 of the mean fold change of each protein was plotted against $-Log_{10}$ of the p value obtained from the t test. Initially p-values were corrected for the Bonferroni FDR and volcano plots were calculated when applying A) a 0.01 FDR and B) a 0.05 FDR. C) P-values were calculated without applying Bonferroni FDR correction and a volcano plot was generated. Proteins with a fold change <= 2 or >= 2 are coloured orange, proteins with a p-value of < 0.05 are coloured in red and proteins that have both are coloured in green. D) List of proteins showing more than 2-fold increase and a p-value lower than 0.5.

In order to understand whether the combination of the six upregulated proteins was linked to enrichment of a particular biological pathway or molecular function in EVs derived from histamine treated cells, gene ontology (GO) analysis was carried out through DAVID and enriched GO terms for cellular compartment, biological process and molecular function were found. The most enriched term for cellular component was “extracellular exosome” as further confirmation of the origin of the samples used for mass-spectrometry (Figure 5.14 A). Only one term was reported for both biological process (“viral entry into host cell”) and molecular function (“protein binding”) (Figure 5.14 A) making it difficult to conclude which pathways were enriched in histamine- induced EVs. Thus, the GO term analysis was repeated but this time all proteins that were increased or decreased by 1.5 -fold or more were included. Overall, the name list of the upregulated proteins returned 15 terms for cellular component, 18 for biological process and 7 for molecular function (Figure 5.14 B). The downregulated proteins returned 6 terms for cellular component, 16 for biological process and 6 for molecular function (Figure 5.14 C). As expected, the most enriched cellular component term for both up and down regulated protein was again “extracellular exosomes”. Following Benjamini-Hoechberg correction, none of the biological process terms was significant for upregulated proteins. Similarly, the only significant molecular function term was “protein binding”. Interestingly, although not statistically significant, other molecular function terms that resulted from the analysis were “endopeptidase activity”, “serin-type endopeptidase inhibitor activity”, “integrin binding” and “laminin binding”, all pathways related with cancer dissemination and metastasis (Givant-Horwitz et al. 2005; Ramovs et al. 2017; Su et al. 2020) (Figure 5.14 B). On the other hand, the most significant biological process terms of downregulated proteins were “keratinocyte differentiation” “complement activation classical pathway”, “innate immune response” and “negative regulation of endopeptidase activity”. Again, although non-significant, “negative regulation of peptidase activity” and “negative regulation of proteolysis” appeared as deregulated pathways in the biological process list (Figure 5.14 B). As was found for upregulated proteins, zero terms were significant among the molecular functions. Even if there was not a conclusive difference in the proteome of constitutive and histamine- induced EVs, that could explain the effect of the latter on invasion, though some insights have been generated that should be explored in future work.

A

Six significant upregulated proteins			
Cellular component	Fold enrichment	P-value	Benjamini
Extracellular exosome	54.5	0.01	0.670
Integral component of plasma membrane	36.4	0.037	1
Intracellular ribonucleoprotein complex	18.2	0.072	1
Biological process	Fold enrichment	P-value	Benjamini
Viral entry into host cell	18.2	0.042	1
Molecular function	Fold enrichment	P-value	Benjamini
Protein binding	81.8	0.026	1

B

Upregulated proteins			
Cellular component	Fold enrichment	P-value	Benjamini
Extracellular exosome	65.8	1.4E-11	1.8E-9
Membrane	50	5.0E-8	3.3E-6
Focal adhesion	23.7	9.4E-7	4.2E-5
Cytosol	47.4	9.7E-5	3.2E-3
Cell surface	18.4	7.1E-4	1.9E-2
Extracellular matrix	13.2	3.0E-3	6.5E-2
Biological process	Fold enrichment	P-value	Benjamini
Translational initiation	10.5	3.10E-3	9.8E-1
Ephrin receptor signalling pathway	7.9	1.5E-2	9.8E-1
SRP-dependent cotranslational protein targeting to membrane	7.9	1.7E-2	9.8E-1
Cellular response to low-density lipoprotein particle stimulus	5.3	1.9E-2	9.8E-1
Neuron remodelling	5.3	2.1E-2	9.8E-1
Viral transcription	7.9	2.4E-2	9.8E-1
Notch signalling pathway	7.9	2.5E-2	9.8E-1
Tumour necrosis factor-mediated signalling pathway	7.9	2.6E-2	9.8E-1
Nuclear-transcribed mRNA catabolic process, nonsense-mediated decay	7.9	2.7E-2	9.8E-1
Negative regulation of endopeptidase activity	7.9	2.8E-2	9.8E-1
Molecular function	Fold enrichment	P-value	Benjamini
Protein binding	78.9	3.8E-4	4.2E-2
Endopeptidase activity	7.9	5.9E-3	3.3E-1
Poly(A) RNA binding	21.1	8.9E-3	3.3E-1
Serine-type endopeptidase inhibitor activity	7.9	1.8E-2	4.7E-1
Integrin binding	7.9	2.1E-2	4.7E-1
Receptor binding	10.5	3.9E-2	7.2E-1
Laminin binding	5.3	5.2E-2	8.2E-1

C

Downregulated proteins			
Cellular component	Fold enrichment	P-value	Benjamini
Extracellular exosome	100	7.5E-9	2.3E-7
Blood microparticle	36.4	6.5E-5	9.8E-4
Extracellular space	54.5	4.0E-4	4.0E-3
Extracellular region	45.5	8.3E-3	6.2E-2
Extracellular matrix	27.3	1.1E-2	6.5E-2
Biological process	Fold enrichment	P-value	Benjamini
Keratinocyte differentiation	27.3	8.9E-4	6.1E-2
Complement activation, classical pathway	27.3.	1.5E-3	6.1E-2
Innate immune response	36.4	1.7E-3	6.1E-2
Negative regulation of endopeptidase activity	27.3	2.2E-3	6.1E-2
Negative regulation of peptidase activity	18.2	1.0E-2	2.2E-1
Negative regulation of proteolysis	18.2	1.5E-2	2.3E-1
Positive regulation of B cell activation	18.2	1.7E-2	2.3E-1
Phagocytosis, recognition	18.2	2.1E-2	2.3E-1
Phagocytosis, engulfment	18.2	2.8E-2	2.5E-1
Keratinization	18.2	2.9E-2	2.8E-1
Molecular function	Fold enrichment	P-value	Benjamini
RAGE receptor binding	18.2	6.5E-3	2.2E-1
Immunoglobulin receptor binding	18.2	1.5E-2	2.3E-1
Cysteine-type endopeptidase inhibitor activity	18.2	2.0E-2	2.3E-1
Protease binding	18.2	5.8E-2	3.7E-1
Antigen binding	18.2	5.9E-2	3.7E-1
Calcium ion binding	27.3	6.5E-2	3.7E-1

Figure 5.14: GO term analysis of deregulated cellular protein following histamine treatment.
All the EVs proteins that were A) upregulated by 2 fold or greater – B) up or C) down-regulated by 1.5-fold or greater following histamine treatment were analysed using the DAVID tool and the GO terms from cellular component, biological function and molecular function were recorded. P-value represents EASE score. Fold enrichment is the number of genes annotated with that term divided by the number of genes expected by the software to be annotated with that term.

5.4. Discussion

The aim of this chapter was to investigate the role of histamine and chlorpheniramine in EV biogenesis and understand whether EVs played a functional role in SKOV3 invasion *in vitro*. The results presented in chapter 4 (section 4.3.4 and 4.3.5) suggested that HRH1 could somehow modulate OC cells invasion *in vitro.* Considering that previous studies have linked HRH1 activation with EV biogenesis and its inhibition with a reduction of released EVs (Khan et al. 2018; Verweij et al. 2018), here it was contemplated the idea that HRH1 could modulate OC invasion by regulating EV biogenesis. Therefore, EVs were extracted from control cells or cells receiving histamine or chlorpheniramine and their size, morphology and enrichment in protein biomarker was investigated. After that, the effect of histamine and chlorpheniramine on EV biogenesis was investigated through NTA and TIRF microscopy. Finally, the involvement of EVs in SKOV3 invasion was tested under different conditions and the protein content of control EVs or histamine- induced EVs was analysed to identify any potential difference.

EV extraction and characterization

Several techniques are today available for EV isolation such as ultracentrifugation, density gradient centrifugation, SEC and precipitation using different chemicals (immunoaffinity, polyethylene glycol and others); each one of these techniques is based on different physical or molecular processes and has different advantages and disadvantages (Witwer et al. 2013; Carnino et al. 2019). In this project, SEC was employed to extract EV and the purity of the extraction and different EV features were investigated. The EVs/protein ratio demonstrates that SEC is able to separate the majority of the EVs in the media from the free protein also found in the media. NTA analysis revealed the presence of a mix population of EVs in the samples, as particles size ranged between 50 to 200 nm. This might indicate that SEC enables the extraction of not only small EVs (like exosomes, with size ranging between 40 to 100 nm) but also of larger EVs (like microvesicles, with size ranging between 100 to 1000 nm). Indeed, TEM imaging confirmed the presence of small and large EVs with the typical cup shaped structure surrounded by a lipid bilayer. Particularly, histamine- induced EVs exhibit bigger structures with a size over 200 nm. If possible, it would be interesting to repeat the TEM by using immunolabelling with either CD63 or CD81 to further characterise the EV population.

In EV research, western blot analysis is normally used to confirm the presence of EVs in the sample; this is achieved by confirming the presence of proteins that are thought to be commonly contained in all EVs, regardless their origin (Yoshioka et al. 2013). In the present study, western blot analysis showed enrichment of typical EV biomarkers such as TSG101, CD81 and CD63 and the absence of markers indicative of cellular contamination (GM103 and cytochrome C), confirming the origin of the samples. However, the EVs were immunonegative for Alix, HSP70 and β-actin, proteins that belong to the panel

normally used to identify EVs. This could be explained by the finding that not all EV subpopulations retain all classical EV markers (Yoshioka et al. 2013; Kowal et al. 2016) or that the antigenic epitope targeted by the antibodies was either not expressed on the EVs or not accessible, resulting in absence of the band (Belov et al. 2016). Chlorpheniramine-induced EVs showed more intense bands for CD63, CD81 and TSG101, suggesting that either chlorpheniramine treatment enriches the loading of these proteins into EVs or perhaps it increases the biogenesis of a specific subpopulation of EV (Kowal et al. 2016). Alternatively, the higher concentration of these proteins in EVs might be caused by a pipetting error during sample preparation due to low concentration of EV protein. Increasing the number of starting flasks and consequently increase the EVs yield could solve this issue. The same EV samples used for western blot analysis were also characterised via flow cytometry through a MACSPlex assay. This led to the identification of CD9, CD63 and CD81 on all samples together with a variety of additional proteins including the integrin CD29, glycolipid SSEA-1, glycoprotein CD133.1 and the transmembrane receptor ROR1.

Collectively, EV samples were successfully characterised and analysis provided assurance that the SEC extraction produced a relatively pure population of EV with the typical features that are reported in the literature (Cheng et al. 2017).

Histamine and chlorpheniramine involvement in EV biogenesis

Very few studies focus on the involvement of agonists or antagonists of HRH1 in EV biogenesis. Only two groups previously demonstrated that histamine administration to different cell subtypes induces MVB-PM fusion through the activation of a protein network that involves HRH1 (Verweij et al. 2018) and that inhibition of HRH1 via administration of ketotifen (an HRH1 antagonist) reduces EV release in a dose dependent manner (Khan et al. 2018). In the work described in this thesis, the effect of histamine and chlorpheniramine to induce/reduce EV release was tested in two ways: 1) SKOV3 cells were treated with the compounds and EV concentration was measured via NTA, 2) the number, brightness and size of MVB-PM fusion events in SKOV3 expressing a CD81-pHluorin reporter was quantified via TIRF microscopy. EV quantification through NTA revealed that cells treated with chlorpheniramine for 48 h released twice the amount of EVs compared to both histamine and control cells, although this did not reach statistical significance due to the high spread of the data points. This effect was abrogated when cells were treated with the same drugs for a shorter time (4 h). These findings suggest that chlorpheniramine-mediated EV release might be a consequence of the length of time of the treatment applied to the cells.

It has been previously demonstrated that HRH1 antagonists induce cell death through apoptosis (Jangi et al. 2008; Blaya et al. 2010; Fernández-Nogueira et al. 2018; Matsumoto et al. 2021). It is also well

established that dying cells release apoptotic bodies, or apoptotic microvesicles: particles with size ranging between 50 to 5000 nm formed by separation of the plasma membrane from the cytoskeleton (Doyle and Wang 2019; Kakarla et al. 2020). In the current project, MTT analysis demonstrated the ability of chlorpheniramine to kill OC cells. Although a concentration lower than the sub-lethal dose was used throughout the project, it is not possible to exclude the possibility that the concentration chosen might initiate cell death and therefore induce release of apoptotic bodies. This could explain why longer exposure with chlorpheniramine resulted in SKOV3 cells releasing double the amount of EVs, and why this effect was lost when reducing time of exposure. This effect could be further studied by quantifying annexin V immunolabelling on both chlorpheniramine treated cells and EVs via flow cytometry or by immunolabelling key components of the apoptotic pathway such as caspase 3 or caspase 9 (Théry et al. 2001). Notably, EV concentration was measured through NTA, a good technique for roughly estimate the mean of EV size and concentration. However, it is not very accurate and reliable when it comes to actually comparing EV concentration across different treatments (Filipe et al. 2010; Bachurski et al. 2019).

To further elucidate the role of histamine and anti-HRH1 in EV release, TIRF microscopy was used and live video of SKOV3 treated with control media, 100 µM histamine or two different doses of chlorpheniramine (250 µM or 10 µM) were recorded to quantify the fusion rate of MVB with the PM. Multiple localised increases in fluorescence were identified in SKOV3 cells under all conditions, suggesting fusion of CD81-pHluorin positive vesicles with the PM. Moreover, the average size of the MVB-PM events analysed was between 0.4-0.7 µm for all conditions, as previously reported by Verweij and colleagues (Verweij et al. 2018), whom confirmed by electron microscopy that 75% of the CD63-pHluorin event had a size ranging between 0.4-0.6 µm. All the events with no decrease of fluorescence, with an irregular decrease of fluorescence, or with lateral movement of the fluorescence signal after fusion were not included in the analysis as this suggested that there is none or incomplete fusion of the MVB with the PM (Bebelman et al. 2020). Histamine addition to SKOV3 cells significantly increased the number of MVB-PM fusion events, demonstrating that histamine induced EV release in an OC cell line. Histamine- induced MVB-PM fusion events retained the same brightness and size as MVB-PM fusion events in control cells, suggesting that histamine treatment does not largely modify their features. Previous unpublished work done in the laboratory revealed that histamine induces MVB-PM fusion events immediately after its addition to SKOV3 and that the effect lasts for about 20 minutes, by which time MVB-PM fusion rate falls back to normal level. This could potentially explain the discrepancy between data obtained from NTA and TIRF microscopy analysis. As histamine effects on MVB-PM fusion rate seems “immediate”, conditioning the media for longer time (4 h and 48 h) might abrogate the differences observed by TIRF microscopy. Indeed, the amount of EVs in conditioned

media is the net overall equilibrium between how many EVs the cell release and how many EVs those same cells internalise. If histamine effect lasts for only 20 minutes, it might be that all the EVs produced are quickly internalised by cells leading to no differences in EVs number after 4 or 48 h media conditioning.

As histamine appears to induce EV release through activation of HRH1 (section 5.3.3), inhibition of HRH1 was achieved via treatment of SKOV3 cells with 10 or 250 µM chlorpheniramine and the effect on CD81 positive MVB-PM fusion events was analysed. Cells were imaged every 5 minutes in a time frame of 35 minutes. Overall, no differences were found between the number of fusion events across time points, although a visible trend suggests that SKOV3 cells receiving the higher dose of chlorpheniramine release a smaller number of EVs. To provide a partial analysis of how these two treatments could affect MVB-PM fusion, the data from different time points were combined. The combination of all fusion events of SKOV3 cells treated with the higher or lower doses of chlorpheniramine showed that administration of 250 µM chlorpheniramine to SKOV3 cells significantly decreases the number of MVB-PM fusion events compared to cells receiving the lower dose of the drug and to control cells. This is in line with what previously reported by Khan et al (2018). Higher doses of the drug might completely inhibit HRH1 activity, therefore impairing EV release while lower concentration of drug might not be enough to fully inhibit HRH1 activity resulting in no differences in EV release. It is important to state that HRH1 activation or inhibition upon histamine and chlorpheniramine treatment has not been investigated and this should be integrated in the project to fully validate the efficacy of the treatments. Moreover, administration of 10 µM chlorpheniramine also increased the overall brightness of the fusion events, while it did not modify their size. It is possible that inhibition of HRH1 can alter the composition of MVBs, resulting in a increase of the fluorescent signal. As previously mentioned, there is also a possibility that chlorpheniramine might induce cell death in SKOV3 and therefore increase the number of apoptotic bodies released. If that is the case, the TIRF settings used in this project would have not been able to pick up this event as cells were only exposed to chlorpheniramine for 35 minutes.

EVs involvement in invasion

EVs have been extensively implicated in cancer cell invasion and migration. Through delivery of their RNAs, miRNAs, proteins and DNAs content they can change recipient cells fate and behaviour. Results reported in chapter 4 indicate that HRH1 knockdown reduces OC cell invasion while histamine treatment increases it; in addition, histamine treatment induces EV release in SKOV3 cells while antihistamine administration reduces it (section 5.3.3 and 5.3.4). Thus, it was hypothesised that the reduced invasive capacity due to HRH1 knockdown was a consequence of a decrease of EV release.

Hence, intact EVs were used to investigate whether their addition to cells with low expression of HRH1 could rescue this phenotype. Indeed, SKOV3 cells knocked down for HRH1 showed a reduced invasiveness that was restored by the addition of intact EVs extracted from the same cell line. This is a first indication that HRH1, potentially by regulating EV release rate, can modulate invasion of OC cell lines through a matrix layer. Previous studies have shown that EV can increase the number of metastatic foci *in vivo* and that addition of autologous EV is sufficient to increase invasiveness of recipient cell *in vitro* (Luga et al. 2012; Beckler et al. 2013; O'Brien et al. 2013). Also, multiple studies have shown that EVs can support cancer progression by conferring metastatic characteristics to less invasive cell (Lima et al. 2013; Zhou et al. 2014; Zomer et al. 2015; Schillaci et al. 2017).

To further evaluate whether HRH1 stimulation of EV release, via histamine administration, could influence SKOV3 cell invasion, EV release was inhibited by either treatment of SKOV3 cells with GW4869 (an inhibitor of neutral sphingomyelinase) or via knockdown of Rabb27a, and then histamine was added to the same cells and their invasion through a Matrigel® assay was tested. 48 h treatment with 10 µM GW4869 did not suppress EV release but on the contrary, it significantly increased the number of secreted EVs per cell. This effect led to SKOV3 cells that had received GW4869 to invade as much as control cells; histamine addition did not further increase their invasion. Few reports have previously shown that GW4869 either did not modified EV release (Phuyal et al. 2014) or it increased their release (Cashikar and Hanson 2019). It was hypothesised that this was due or to different time of exposure and concentration of the drug used or to the fact that nSMase was not involved in EV biogenesis (Phuyal et al. 2014; Cashikar and Hanson 2019). In the project presented here, cells were incubated with the drug for 48 h, a much longer time if compared with the 16 h previously reported (Trajkovic 2008; Menck et al. 2017). One possibility is that GW4869 did inhibit EV biogenesis but that during the long incubation time the cells activated compensatory mechanisms to restore EV biogenesis. On the other hand, SKOV3 may not relay on the nSMase pathway to produce EVs as much as other cell types, explaining the results presented in this thesis. Nonetheless, neutral sphingomyelinases are present in different cellular compartments where they are linked to small vesicles generation and to microvesicles (MVs) shedding. In fact, whilst GW4869 has been shown to decrease release of small vesicles, it increased the secretion of microvesicles from the plasma membrane (Menck et al. 2017). This could explain the increased number of EVs observed in this project. Moreover, this experiment was only repeated once and therefore the data should be carefully considered before drawing any conclusion.

As the GW4869 experiment was inconclusive, further invasion assays were carried out on cells knocked down for Rab27a, with or without addition of histamine. Histamine failed to significantly increase SKOV3 cell invasion, although it increased the mean number of invading cells by 40%. Moreover,

SKOV3 cells knocked down for Rab27a also showed a reduction of 40% in the number of invading cells, although this was not significant. The combination of both treatments significantly decreased the invasiveness of SKOV3, with histamine failing to rescue this phenotype. Rab27a has been previously shown to control EV biogenesis; specifically, its knockdown decreases EV production and consequently reduces cancer growth and metastatic niche formation. Indeed, Rab27a knockdown reduces invasion of melanoma (WM164, WM983C and 1205Lu) and bladder cancer (T24, FL3) cell lines *in vitro* (Ostenfeld et al. 2014; Guo et al. 2019) and increases lung metastasis of tumours derived from human melanoma cells (SK-Mel-28) and murine melanoma cells (B16-F10) *in vivo* (Peinado et al. 2013). Rab27a has been shown to act on munc13-4 to regulate release of secretory granules in platelets (Shirakawa et al. 2004; Neeft et al. 2005). At the same time, muc13-4 has been hypothesised to interact through its C terminus with SNAP23 (Elstak et al. 2011), a protein previously reported to mediate EV release upon HRH1 activation (Verweij et al. 2018). Moreover, the implication of muc13-4 in EV release has been previously suggested (Ostrowski et al. 2010), and a recent report has identified muc13-4 to be involved in a calcium dependent-stimulated EV pathway (Messenger et al. 2018). These results are consistent with the hypothesis that the effects of histamine on invasion are mediated through EV biogenesis involving the function of Rab27a. This could be a possible explanation to why histamine addition to cells where Rab27a was knocked down did not rescue their invasiveness. Further experiments should be performed to test this hypothesis and better elucidate the role of histamine in OC cell lines invasion.

EVs and collagen degradation

As histamine and chlorpheniramine act on EV biogenesis, it was investigated whether they could also affect the function of EV. For this reason, EVs extracted from control, histamine or chlorpheniramine treated cells were tested for their ability to degrade collagen through a time-point collagen degradation assay. The data obtained showed that all EV samples degraded collagen at a similar rate. However, when combining the data, histamine- induced EVs expressed a higher collagen degradation rate compared to the other two treatments. Early attempt of the experiment showed that low concentration of EVs (1X or 10X “EVs per surface”, see section 2.17.1 for details) did not produce any fluorescence, due to high absorbance values of the background sample (PBS). To be able to visualise an effect, a high concentration of EVs (100X “EVs per surface” see section 2.17.1 for details) was used for the experiment. By employing this normalization method, EVs are normalized by volume but their number will differ across conditions and biological experiments. Therefore, the increased proteolytic activity exhibited by histamine- induced EVs might be related to the experimental conditions used rather than to a biological effect. A different normalization method that could have been used for this assay is to calculate the number of EVs produced by one cell and add an equivalent number of EVs to

the recipient well. This normalization method would have allowed to keep constant the number of EVs across different conditions and to obtain more robust results. However, the lack of appropriate technologies for studying EV behaviour *in vivo* makes difficult to understand what a "physiological" concentration of EV is and how to translate this to *in vitro* settings. Nevertheless, this is a first indication that histamine might induce changes in the EV cargo allowing them to better degrade collagen and therefore acting as "priming factors" for metastatic dissemination. HRH1 has been reported to regulate production of several components of the metalloproteinase family, including MMP2, MMP3, MMP8, MMP9 and MMP13, in a variety of cell types such as chondrocytes, astrocytes and keratinocytes (Tetlow and Woolley 2002; Tetlow and Woolley 2004; Patel et al. 2016). HRH1 exerts a stimulatory effect on MMP9 production and promotes collagen IV degradation in the basement membrane (Gschwandtner et al. 2008). Similarly, EVs have been demonstrated to carry on both their surface and their lumen a variety of proteolytic enzymes that facilitate matrix remodelling and cell movement. For example, EVs have been reported to mediate the secretion of the matrix degrading proteinase MT1-MMP to invadopodia and increase matrix degradation and cell invasion (Hoshino et al. 2013; Clancy et al. 2015). Moreover, MT1-MMP in EVs derived from tumour cells (melanoma, pancreatic, human fibrosarcoma) are involved in activation of MMP2 and degradation of both collagen type I and gelatine (Hakulinen et al. 2008; Han et al. 2015). Interestingly, EVs extracted from ascitic fluid of OC patients have also been shown to contain gelatinolytically active MMP2 and MMP9 (Wei et al. 2017). In future, it would be interesting to validate the content of EVs derived from histamine or chlorpheniramine treated cells and study whether they differ in their composition of MMPs or other proteolytic enzymes. For example, an in-gel zymography assay could be useful to identify the presence of MMPs and to verify if they are expressed in their active or pro-active form (Leber and Balkwill 1997; Snoek-van Beurden et al. 2005; Vandooren et al. 2013; Inanc et al. 2017).

Proteomic analysis of EV cargo

A total of 888 proteins were identified in control EVs and EVs derived from histamine treated cells; of these, 461 were identified in at least three samples of one treatment group only. This means that half of the proteins identified in the EVs were only seen in one or two of the samples tested of one or both treatment groups, suggesting that these proteins may not commonly be found in EVs and their presence might be related to technical issues due to the extraction procedure.

Only six proteins were significantly enriched (p-value < 0.05, two-fold increase) in histamine – induced EVs, while no proteins were significantly downregulated; to note, none of these proteins was significantly enriched in EVs samples after applying FDR correction. This could suggest that histamine administration does not induce substantial differences in the EV protein cargo and perhaps the effects

seen so far are a result of the RNA or lipid cargo or of a combination of the three. The six upregulated proteins were: CPNE8, CD70, TPP2, COPB2, ILF2 and APP. Consultation with Exocarta and Vesiclepedia databases (accessed May 2021) and research of current literature reveal that all the six proteins have been previously identified in EVs from various sources. Moreover, extensive literature review did not reveal any relationship between the six up-regulated genes in regard of both EVs function, cancer metastasis or histamine signalling pathways nor any relationship between the different genes among them.

CPNE8 (Copine-8) is a calcium-dependent phospholipid-binding protein (Tomsig and Creutz 2002). Its gene expression has been identified as a characteristic signature for ovarian clear cell carcinoma and its downregulation can repress SKOV3 cell growth (Nagasawa et al. 2019). Moreover, in breast cancer cells lines (MCFDCIS, HCC1313), CPNE8 has been found to cooperate with SNAI2 and AX1 to promote cell motility (Dang et al. 2016). CPNE8 has been found to be enriched in small EVs of the metastatic breast cancer cell line MDA-MB-231 (Risha et al. 2021).

CD70 is a cytokine belonging to the tumour necrosis factor (TNF) ligand family and it is generally expressed in highly activated lymphocytes (Denoeud and Moser 2011). While CD70 expression is normally very limited in non-lymphoid organs, its presence has been found in several tumours such as renal, pancreatic, colon, brain and ovarian cancers (Adam et al. 2006; Ryan et al. 2010). Particularly, CD70 expression in OC cell lines and OC clinical samples has been associated with increase resistance to cisplatin (Aggarwal et al. 2009; Liu et al. 2013). CD70 has been identified as a tumour-specific marker on EVs derived from clear cell renal cell carcinoma cell line (786-O, Caki1, Caki2, and RCC53) and in clear cell renal cell carcinoma human tissue (Himbert et al. 2020).

TPP2 (tripeptidyl peptidase II) is an enzyme acting in the ubiquitin-proteasome pathway and shows both endopeptidase and exopeptidase activity (Tomkinson 2019). TPP2 expression has been found to correlate with tumour size in human oral squamous cell carcinoma and to regulate cellular proliferation in oral squamous cell carcinoma cell lines (Ca9-22, HSC-2, HSC-3, HSC-4 and HO1N1) (Usukura et al. 2013). TPP2 has been reported to be upregulated in EVs derived from serum of patients with chronic obstructive pulmonary disease (Koba et al. 2021).

COPB2 (Coatomer subunit beta) belongs to the Golgi apparatus coatomer complex, a protein complex involved in the coating of non clathrin-coated vesicles, and it is essential for Golgi apparatus budding and vesicular trafficking (Waters et al. 1991; Orci et al. 1993). COPB2 upregulation has been identified in OC tissue and in different subtypes of breast cancer tissues (Claerhout et al. 2012) and it has been associated with promotion of cell proliferation and tumorigenesis in breast, lung, gastric and colorectal cancers cell lines (Pu et al. 2018; An et al. 2019; Bhandari et al. 2019; Wang et al. 2020). COPB2 has

been identified in the proteome of EVs derived from OC cell lines (IGROV, OVCAR3, OVCAR5, SKOV3) (Liang et al. 2013; Sinha et al. 2014; Hurwitz et al. 2016).

ILF2 (interleukin enhancer-binding factor 2) is a transcription factor required for T-cell expression of the interleukin 2 gene (Kiesler et al. 2010). By forming a complex with ILF3, it binds to mRNA and redistributes it from the nucleus to the cytoplasm, thereby regulating gene expression (Reichman et al. 2002). ILF2 has been extensively studied in tumours and it has been found to be overexpressed in glioma, non-small cell lung cancer, oesophageal and liver cancers (Huang et al. 2014; Ni et al. 2015a; Ni et al. 2015b; Cheng et al. 2016). Moreover, its protein levels in pancreatic ductal adenocarcinoma clinical samples has been associated with poor survival (Wan et al. 2015).As for COPB2, ILF2 has been previously identified in the proteome of EVs derived from OC cell lines (Liang et al. 2013; Sinha et al. 2014; Hurwitz et al. 2016).

APP (amyloid beta precursor protein) is a membrane protein principally expressed in the synapse of neurons, and it is normally involved in synapse formation, neural plasticity, and iron export. Its proteolysis generates the amyloid beta plaques found in the brain of Alzheimer's patients (Müller and Zheng 2012). In the OC cell line OVCAR3, APP was found to be the target of miRNA 20a; through its downregulation, APP promoted proliferation and invasion of these cell lines (Fan et al. 2010). Similarly, APP was found to promote cell proliferation and motility in an invasive breast cancer cell line (MDA-MB-231) (Lim et al. 2014; Tsang et al. 2018). Proteomic profiling of EVs extracted from OC cell lines have shown the presence of APP (Liang et al. 2013; Sinha et al. 2014; Hurwitz et al. 2016).

GO term analysis did not highlight any known associations of these six proteins with cancer progression or metastasis. The only biological process identified through DAVID analysis was "viral entry into host cell" and only the molecular function "protein binding" was obtained; none of these terms was significant after Benjamini correction. As described above, each of the six upregulated proteins is involved in very diverse molecular pathways and although all of them have been involved in different aspects of cancer progression (motility, cell growth, cisplatin resistance) GO terms analysis did not report any association with cell invasion, migration or ECM degradation pathways. Therefore, a less stringent analysis was performed, and all the proteins that showed a 1.5-fold increase or decrease in histamine- induced EVs were subjected to GO terms analysis.

The most enriched cellular component term for both up and down regulated proteins was "extracellular exosomes", further confirming the origin of the samples. Very few terms were significantly enriched for biological process or molecular function for both up and down regulated proteins. Upregulated proteins were enriched for the molecular function "protein binding" while none of the biological process terms were significantly different. Downregulated proteins were enriched for

the biological process “keratinocyte differentiation”, “complement activation, classical pathway”, “innate immune response” and “negative regulation of endopeptidase activity” while zero terms of the molecular function were significant. The term “negative regulation of endopeptidase activity” refers to any process that decreases the frequency, rate or extent of endopeptidase activity, the endohydrolysis of peptide bonds within proteins. Several endopeptidases like asparaginyl endopeptidase or prolyl endopeptidase have been shown to favour cancer metastasis and dissemination in gastric and breast cancer *in vivo* (Cui et al. 2016; Qi et al. 2018) and to be expressed in the serum of patients with advanced colorectal cancers (Larrinaga et al. 2014). This indicates that histamine treatment might decrease the loading into EVs of negative regulators of endopeptidases, therefore potentially enhancing their proteolytic activity. Indeed, although not significantly enriched, other terms that appeared in the biological process of downregulated proteins were “negative regulation of peptidase activity” and “negative regulation of proteolysis”, further supporting the theory that histamine treatment increases the proteolytic activity of EVs.

Further experiments will be needed to validate this assumption. In this project, EVs were extracted after only 4 h incubation with histamine; the short time used might be not enough to capture changes in the EV content. Extending the length of the treatment might have led to different results. On the other hand, TIRF microscopy data indicated that histamine has an instant effect on EV biogenesis; ongoing work in the lab indicates that EV biogenesis is boosted during the 10 minutes following addition of histamine to SKOV3 cells, and that this effect declines after this time. Considering this, 4 h incubation time may be long enough to capture potential changes in the EV cargo; once secreted, some of the EVs might degrade, some will be taken up by nearby cells and the effect of histamine treatment might be lost. If available, an infusion pump would have been used to ensure a steady infusion of histamine throughout the incubation time that might have helped to enrich the histamine- induced EV population.

5.5. Key findings

- EVs extracted by SEC from control, histamine or chlorpheniramine treated SKOV3 cells retained the classical EV size and morphology, had low protein contamination (compare to non-conditioned media) and expressed some of the classical EVs markers such as CD81, CD63 and TSG101
- NTA analysis showed no difference in the concentration of EVs derived from control, histamine or chlorpheniramine treated SKOV3 cells

- Histamine treatment increased the number of CD81 positive MVB-PM fusion events in SKOV3 cells, quantified via TIRF microscopy. High doses of chlorpheniramine decreased CD81 positive MVB-PM fusion events in SKOV3 cells
- EVs extracted from intact SKOV3 cells rescue the loss of invasion of SKOV3 cells knocked down for HRH1
- GW4869 increased the number of EVs produced per SKOV3 cell. Histamine, GW4869, or a combination of both compounds did not modify SKOV3 cell invasiveness
- Transient transfection with Rab27a did not impair SKOV3 invasion through a Matrigel® layer, but addition of histamine to the same cells significantly reduced it
- Histamine – induced EVs degraded collagen more than control and chlorpheniramine-induced EVs
- A proteomic screen of EV content revealed that EVs derived from histamine treated cells might contain a lower number of proteins involved in negative regulation of endopeptidases

Chapter 6

General discussion

6. General discussion

Despite research over the last decade has led to improved understanding of molecular events underlying cancer dissemination, and to the availability of improved surgical techniques and novel therapeutic strategies, OC survival has barely improved (Oikonomopoulou et al. 2008). This is mostly related to the fact that OC is diagnosed when metastatic spread has already occurred. Metastasis is the culmination of neoplastic progression. Even though, many molecular mechanisms underlying the metastatic process are today known, our understanding of this process is not yet complete (Eccles and Welch 2007). Indeed, more effort should be done to clarify the contributions of several soluble factors or genetic mutation to the "seed cells" and to the tumour microenvironment (Eccles and Welch 2007). A better understanding of the different cellular and molecular participants involved in tumour progression may ultimately lead to the development of new therapy aiming to block metastasis and overall might improve cancer survival (Park and Choi 2016). In this project the role of HRH1 in OC progression and EV biogenesis was investigated. As the role of antihistamine and histamine in modulating EV release and their potential effect on OC spread has been barely studied, a better understanding of its biology can open avenues for future treatment options.

6.1. Histamine receptors and OC

In this project, the gene expression of histamine receptors was investigated in both OC cell lines and in OC clinical samples. Correlation analysis between histamine receptors gene expression and *in vitro* invasion and migration rates of six OC cell lines demonstrated that HRH1 was strongly correlated with both invasion and migration of the cell lines investigated. The other histamine receptors showed either no correlation with cellular behaviours (HRH2 and HRH3) or were not detected in the samples (HRH4). Similarly, analysis of microarray data on OC specimens showed that HRH1 and HRH2 were the only histamine receptors expressed in OC clinical samples, and while no association between HRH2 and tumour stage was found, HRH1 appeared to be associated with tumour stage. Indeed, OC samples obtained from patients with stage IV tumour presented a higher level of expression of HRH1 compared with tumour at stage II and III. Interestingly, no association between HRH1 expression and patients' overall survival was found while low level of HRH1 were associated with a little improvement of patients' progression free survival (2 months increase). This is not the first situations in which proteins deregulated in cancer tissues have no association with overall and progression free survival of cancer patients. For example, by studying correlation between gene expression and EOC survival, Gui et al. (2021) reported that both CDC5 and KLF4A were overexpressed in advanced EOC compared to normal ovarian tissues, but had no correlation with patient's overall or progression free survival. In colorectal cancer, CDC6, CDC45 and ORC6 mRNA levels were found to be higher expressed in cancerous samples

than adjacent mucosa samples; however patients that had a low expression of CDC6 and CDC45 in the tumour samples had a worst prognosis while no association was found for ORC6 (Hu et al. 2019). Therefore, HRH1 might be biologically relevant to oncogenic processes in OC but its expression alone is not representative of disease outcome. This could be due to HRH1 being implicated in a more complex biological mechanisms, yet to be identified, that could regulate OC progression. To date, this is the first study analysing the correlation of histamine receptors, particularly HRH1, with OC migration and invasion *in vitro* and with disease progression in clinical samples. So far, only one publication from Wang and colleagues (2014) has investigated the prognostic values of HRH1 in different cancer types. From their genomic analysis, the authors identified that out of 153 clinical samples analysed only 23 showed a correlation between HRH1 and cancer prognosis. Particularly, 2 cases of OC out of 18 total cases show that lower expression of HRH1 was related with poorer patients survival (Wang et al. 2014). The difference between the study from Wang and colleagues and the data presented in this thesis, may be related to the type of analysis conducted on the clinical samples. Whilst Wang and colleagues directly compared the expression of HRH1 with the survival rate of each single patient, in this project the overall impact of HRH1 with overall and progression free survival was analysed, and the data were segregated according to the expression levels of HRH1, using the median value of the dataset as threshold. As the relationship between the expression of HRH1 and prognosis varies among cancers and also in the same cancer, it can be hypothesised that HRH1 plays a more complex role in tumours and cannot be simply classified as tumour suppressor or oncogene.

Another factor to consider is that antihistamines have been shown to downregulate HRH1 level at the mRNA level (Pype et al. 1998; Mizuguchi et al. 2012). For this reason, information regarding patients' intake of antihistamine should have been taken into account if available, potentially leading to more informative results. Indeed, in their clinical study regarding the use of antihistamine and the risk of OC incidence Verdoodt et al. (2019) did not find an overall association between antihistamine use and the risk of EOC but they did identify an inverse association between antihistamine use and EOC risk in pre-menopausal woman and between antihistamine use and risk of mucinous ovarian cancer (Verdoodt et al. 2019). The current lack of knowledge regarding the role of histamine receptors in ovarian cancer urges additional clinical studies and moving forward a more extensive bioinformatic analysis should be carried out to further validate HRH1 role in this disease.

Another possibility could be that HRH1 level of expression in OC clinical samples is not directly correlated with OC stage, but it is actually related to their 'therapy resistance status'. Indeed, *in* vitro studies demonstrated a higher expression of HRH1 at both the mRNA and protein level in therapy resistant breast cancer (T-474 and MDA-MB453 lapatinib-resistant and MDA-MB453 trastuzumab-resistant cell lines), lung (cisplatin-resistant A549) and cisplatin-resistant HeLa cells (Fernández-

Nogueira et al. 2018; Matsumoto et al. 2021). Inoculation of trastuzumab- and lapatinib-resistant MDA-MB-453 cells into the mammary fat pad of athymic nude mice demonstrated that HRH1 upregulation is also retained in resistant tumours *in vivo* (Fernández-Nogueira et al. 2018). Moreover, administration of histamine to therapy-resistant cell lines increases their viability and promotes their proliferation without influencing the therapy sensitive counterpart (Fernández-Nogueira et al. 2018; Matsumoto et al. 2021). These data points toward the idea that HRH1 upregulation in resistant tumour might favour their proliferation and survival. In fact, the use of several HRH1 antagonists selectively induces apoptosis in trastuzumab-resistant MDA-MB453 and in cisplatin resistant Hela and A549 cell lines *in vitro* and dramatically reduces the growth of trastuzumab-resistant MDA-MB453 in athymic nude mice (Fernández-Nogueira et al. 2018; Matsumoto et al. 2021). One of the suggested mechanisms through which antihistamine could re-sensitise cancer cells to chemotherapy is by decreasing the expression of multidrug resistance (MDR)-associated P-glycoprotein 1. In fact, administration of loratadine, ebastine and astemizole (all antagonists of HRH1) to a MDR-variant of A549 (lung cancer) cell line significantly re-sensitised A549-MDR cells to vinorelbine (Ellegaard et al. 2016). Based on these findings it will be interesting to analyse the clinical data used in this thesis in relation to patients' therapy status. It could be that the higher expression of HRH1 in stage IV tumour specimens identified in this project is due to these patients been resistant to chemotherapy and not to their disease stage. Inhibition of HRH1 might lead to sensitization of OC to therapy and therefore open a new scenario for the use of antihistamine in cancer therapeutic.

6.2. The role of HRH1 in the metastatic phenotype of OC *in vitro*

HRH1 has been previously studied for its ability to promote several aspects of the metastatic cascade and induce cancer cells apoptosis. Indeed, as described in sections 1.4.3 and 4.1, HRH1 is involved in several steps of the metastatic cascade in different cancer subtypes (Cricco et al. 2006; Genre et al. 2009; Fernández-Nogueira et al. 2018; Kennedy et al. 2018; Zhao et al. 2020).

Before subsequent experiments, the expression of HRH1 was firstly validated in three OC cell lines. HRH1 was detected in SKOV3, OVCAR3 and OVCAR5 at both the mRNA and protein level, indicating the presence of this histamine receptors in OC cell lines. Secondly, HRH1 levels were modulated by either transient transfection with siRNA of via chemical activation or inhibition, and its role in EMT, adhesion, migration and invasion of OC cell lines was tested *in vitro*. The results obtained indicated that HRH1 modulates only some aspects of cell behaviour, that could be implicated in the metastatic cascade. Particularly, HRH1 does not impair the expression of E-cadherin and vimentin, two key EMT-related genes, and does not change the adhesion of SKOV3, OVCAR3 and OVCAR5 to a monolayer of endothelial cells. HRH1 inhibition significantly slowed down the invasion ability of SKOV3 and OVCAR3

through a Matrigel® layer and the motility of SKOV3 and OVCAR5 from the edge of a 'wound'. This is the first study investigating the role of HRH1 in metastasis-related properties of OC cells and suggests that HRH1 might be involved in invasion and migration of OC cells *in vitro*. Similar results have been previously obtained when studying the role of this receptor in invasion and migration of breast and hepatocellular carcinoma cell lines *in vitro* (Fernández-Nogueira et al. 2018; Zhao et al. 2020).

Interestingly, the different modality used in this project to downregulate/inhibit HRH1 did not lead to the same results. For instance, HRH1 knockdown reduced the number of invasive SKOV3 and OVCAR3 through a Matrigel® layer but its pharmacological inhibition did not produce the same effect in SKOV3 cells. Similarly, motility of SKOV3 and OVCAR5 cells in a 'wound healing' assay was not modified following HRH1 transfection but it decreased following chlorpheniramine administration. The variability of the data indicates that either the approaches used in this project to modulate HRH1 activity were not ideal or that there might be off-target effects leading to the results seen. Indeed, transfection efficiency has been variable across the project, thus influencing the outcome of the downstream experiment. Going forward, a cellular model either expressing no HRH1 or overexpressing HRH1 should be developed and used to elucidate HRH1 role in OC invasion. Similarly, although concentration of histamine and antihistamine and time of incubation were chosen based on the MTT assay and on previous literature findings, translating the mode of action of a compound from the human body to a cellular model is not easy to do. Probably, different concentrations or longer/shorter exposure time to the drug might have led to different results.

Several reports have also indicated that administration of HRH1 antagonists to cancer cell lines could lead to biological effects independent from HRH1 activation. For example, administration of terfenadine, astemizol, diphenhydramine and triprolidine induces apoptosis of human melanoma cell lines (A375, HT144, HSs294T) through modulation of Ca^{2+} homeostasis and activation of tyrosine kinase and PLC-dependent apoptotic pathways, independently from HRH1 activation (Jangi et al. 2006; Jangi et al. 2008). Therefore, it is not possible to exclude that the effect seen in this project following chlorpheniramine or histamine administration might be due either to off target effects of the compounds or also to activation of different histamine receptors. The latter is supported by several publications that have highlighted the dual role of the other histamine receptors (HRH2, HRH3, HRH4) in modulating cancer invasion. Ranitidine (a HRH2 antagonist) treated 4T1 (mouse epithelial breast carcinoma cell line) tumour bearing Bulb-c mice showed a reduction of the number of lung metastasis compared to control mice (Vila-Leahey et al. 2016). HRH3 pharmacological inhibition or knockdown inhibits U87MG (glioblastoma) cells growth, EMT, their invasion through a Matrigel® layer and motility from the edge of a 'wound'; indeed, HRH3 inhibition reduced tumour growth in a nude mouse model xenografted with the same cell line (Lin et al. 2015). Contrarily, clobenpropit (an HRH4 agonist)

administration to CCA (cholangiocarcinoma) cells has been reported to decrease their EMT, ECM breakdown, migration and invasion (Meng et al. 2011). Interestingly, Cricco and colleagues (2011) have demonstrated that histamine exerts a dual action on the invasion rate of MDA-MB 231 (breast cancer) cells by employing an *in vitro* Matrigel® assay; low doses of histamine (lower than 1 µM) induce cancer cell invasion, while high doses of histamine (more than 10 µM) diminish it, emphasizing the dual role of histamine in an invasive breast cancer cell line (Cricco et al. 2011). Going ahead with this project, a panel of activators and inhibitors of the four different histamine receptors should be tested to effectively rule out the involvement of HRH2, HRH3 and HRH4 in different metastatic mechanisms of OC *in vitro* and further clarify the role of HRH1.

Numerous studies have focused on elucidating the effect of HRH1 antagonists on cell cycle and apoptosis in cancer cells. Loratadine stimulates G2/M cell cycle arrest in human colon cancer (COLO 205) cells lines and induces their apoptosis *in vitro,* and also inhibits growth of tumours derived from human colon cancer (COLO 205) cells *in vivo* (Chen et al. 2006). In addition, loratadine enhances the DNA damage induced by ionizing radiation and induces G2/M cell cycle arrest in HT29 (human colon carcinoma), DU145 (human prostate carcinoma) and SF295 (human glioblastoma) cell lines (Soule et al. 2010). Meclizine, another HRH1 selective antagonist, induces apoptosis of human colon cancer cell lines (COLO 205 and HT 29) in a dose-dependent manner by inducing G0/G1 cell cycle arrest and upregulating p53 and p21 (Lin et al. 2007). The fact that HRH1 inhibitors can induce cell-cycle arrest and consequent apoptosis suggests that a similar effect might occur also in the model used in this thesis. Chlorpheniramine treatment, rather than selectively inhibit mechanisms associated with cell movement or invasion, could induce cytotoxic effects on OC cells. In future, Annexin V and PI staining could be used to check the viability of the three OC cell lines following chlorpheniramine or histamine treatment. Moreover, DNA could be stained with a fluorescent dye and flow-cytometry used to quantify cell cycle progression after histamine and chlorpheniramine administration. These analyses would not only further elucidate the role of HRH1 in OC cells but could also potentially explain the discrepancy between the results obtained after HRH1 knockdown and HRH1 chemical inhibition.

6.3. HRH1 in EV biogenesis and cargo modulation and their effect on OC invasion *in vitro*

Histamine has been identified as an inducer of EV biogenesis (Verweij et al. 2018) via activation of HRH1 and subsequent phosphorylation of SNAP23. At the same time, HRH1 inhibition via ketotifen administration has been related with a reduction of the number of EVs in HeLa (cervical cancer cell), MCF7 and BT549 (breast cancer) cell lines (Khan et al. 2018). This knowledge, together with the

findings that HRH1 knockdown decreased OC cell invasion while its activation via histamine increased it, suggested that the reduced invasion due to HRH1 knockdown was due to a reduction of EV release; conversely, an enhanced invasion of SKOV3 cells upon histamine activation was related to an increase in EV production. Therefore, EV biogenesis following histamine and chlorpheniramine administration was tested through NTA and TIRF microscopy. These two techniques produced equivocal results: NTA showed no difference in the number of EVs released after histamine or chlorpheniramine treatment, whilst TIRF microscopy revealed that SKOV3 treated with histamine presented a higher number of MVB-PM fusion events than control cells. In addition, SKOV3 treated with high doses of chlorpheniramine showed an overall decrease in the number of CD81 positive-MVB-PM fusion events.

These data are in agreement with the literature regarding the involvement of histamine and HRH1 antagonists in EV biogenesis and indicate that histamine induces EV biogenesis while HRH1 antagonists reduce it. Although this might be the case, it cannot be excluded that histamine and antihistamine might favour/inhibit the release of only a specific subpopulation of EVs. Indeed, studies on several EVs inducers/inhibitors have highlighted how they can influence the release of specific EV subpopulations. For instance, administration of GW4869, an inhibitor of neutral sphingomyelinase, inhibits the release of small EVs (50-100 nm) while increasing the release of bigger EVs (100-200 nm) (Menck et al. 2017). Due to the technical limitation of the NTA and to the way TIRF microscopy was used in this project (visualization exclusively of CD81 positive MVB population), it was not possible to study if histamine and antihistamine controlled the overall release of EVs or preferentially induced/inhibited a specific EV subtype. Going forward, dual-labelling TIRF microscopy, either using different tetraspanins or with a combination of tetraspanin and cargo proteins, could be employed to further elucidate the mechanisms underpinning histamine and antihistamine involvement in EV biogenesis.

Due to the ability of histamine and chlorpheniramine to modulate EV biogenesis and to the previous finding highlighting a role of HRH1 in OC invasion *in vitro*, the participation of EVs in OC invasion was tested. Initially, endogenous EVs were added to control cells and cells knocked down for HRH1 and their invasion assessed in a Matrigel® assay. As expected, EV addition rescued the loss of invasion of SKOV3 following HRH1 knockdown, indicating that EVs are actively involved in OC cell invasion and may act downstream of HRH1. Other studies have shown that incubation with endogenous EVs enhances the tumorigenic characteristics of recipient cells (Menck et al. 2015; Raimondo et al. 2015; You et al. 2015b). For example, incubation of MCF7 and SK-BR-3 cells (both breast cancer cell lines) with autologous (derived from the same cell lines) or heterologous (derived from a different cell lines) MVs showed enhanced invasive potential, while the same effect was not observed upon incubation with MVs derived from immortalised mammary epithelial cell line (hTERT-HME1) (Menck et al. 2015). This demonstrates how the effect of EVs to mediate cellular invasion is dependent on the type of cells

used in each study, as the content of EVs released by cells with a metastatic phenotype differs from that of non-metastatic cells (Jeppesen et al. 2014). Proteomic analysis of EVs extracted from metastatic bladder cancer (FL3 and SLT4) cells lines revealed an enrichment of proteins related to metastatic propensity. Most of these proteins, such as vimentin, Casein kinase II, Hepatoma-derived growth factor, annexin 2 and moesin are related to EMT and were not present in the proteome of nonmetastatic cell (T24)-derived exosomes (Jeppesen et al. 2014). Therefore, it cannot be excluded that the ability of EVs to rescue the invasion of SKOV3 with reduced HRH1 is solely due to EVs being derived from highly metastatic cells (SKOV3). Therefore, future rescue experiments should be performed using EVs obtained from less invasive OC cell lines like OVCAR3; this would clarify to which extent the EV content (therefore their origin) affect metastatic activity, compared to the effect solely induced by the receptor.

The ability of histamine in regulating EV biogenesis and EVs effect on OC cell invasion was further investigated via inhibition of EV biogenesis through GW4869 treatment or by transient transfection of Rab27a. Histamine was added to the same cells and invasion was measured via a Matrigel® invasion assay. GW4869 did not impair SKOV3 invasion while Rab27a knockdown together with histamine administration significantly slowed down SKOV3 invasion with histamine failing to rescue this phenotype. These data suggest that histamine function in OC cell invasion is mediated by EV biogenesis through a mechanism requiring Rab27a. Rab27a has been previously linked with cancer invasion as its reduction was shown to attenuate the invasive potential of metastatic breast cancer cells lines (MDA-MD-435 and MDA-MD-231) *in vitro* (Wang et al. 2008). With regards to the effect of Rab27a on EV biogenesis, knockdown of Rab27a and consequent reduction of EV release reduced the invasive potential of bladder cancer (T24, FL3) cell lines *in vitro* (Ostenfeld et al. 2014) and of melanoma (WM164, WM983C and 1205Lu) cell lines *in vitro* and *in vivo* (Peinado et al. 2013; Guo et al. 2019). However, Rab27a has also been linked to the secretion of non-exosomal associated protein that could stimulate/reduce cancer cell invasion. Bobrie and colleagues (2012) showed that stable transfection of Rab27a in 4T1 (mammary carcinoma) cells decreases exosome secretion and reduces tumour growth and lung metastasis in Balb-c mice subcutaneously injected with the same cells. Rab27a knockdown also impairs the level of released soluble proteins; in particular, MMP9 was mostly released as a soluble form and its levels were lower in conditioned media of Rab27a knockdown 4T1 cells than in conditioned media of control cells. The concentration of other soluble factors like cytokines and chemokines was also modulated by Rab27a (Bobrie et al. 2012). The fact that Rab27a can regulate soluble factors that can modify tumour microenvironment and favour cancer spread suggests that the effect seen on SKOV3 invasion might be mediated by soluble factors and not by EVs. In the future, the interplay between Rab27a and HRH1 in EV biogenesis should be tested. For example, TIRF microscopy

could be used to quantify the number of MVB-PM fusion events in cells transfected with Rab27a siRNA before and after histamine addition. Also, downstream effectors of Rab27a, like muc13-4, could be used in functional experiments to further elucidate if Rab27a and histamine pathways cooperate in regulating EV biogenesis and OC invasion.

Finally, EVs were extracted from control cells or cells treated with histamine or antihistamine and their ability to degrade a collagen substrate was quantified. Overall, EVs derived from histamine treated cells showed a higher proteolytic activity compared to EVs control or EVs derived from chlorphenamine treated cells. This finding suggests that histamine treatment might change the composition of EVs, and particularly of factors involved in ECM degradation and proteolysis. As ECM degradation is a necessary step of cancer cell invasion, addition of histamine-induced EVs to OC cell lines might further enhance their invasion through a matrix, confirming the previous result showed in chapter 4 and 5. Indeed, histamine increases the MVB-PM fusion rates and consequently induces release of EVs (section 5.3.3). Addition of histamine increase the invasion of SKOV3 through a Matrigel® layer (section 4.5.3) and rescues the loss of invasion through a Matrigel® layer of SKOV3 knocked down for HRH1 (section 5.3.5). Taken together these findings point towards the idea that by enhancing EVs release and potentially modifying their content, histamine can increase the ability of OC cells to breakdown the ECM and enhance their ability to invade through a Matrigel® layer.

Proteomic analysis did not reveal upregulation of any specific molecule related to matrix degradation or metastatic behaviour in EVs derived from histamine treated cells. Nevertheless, GO-term analysis of downregulated proteins (1.5-fold change) in histamine- induced EVs revealed the presence of the term “negative regulation of endopeptidase activity”. This further support the idea that histamine might modify the EV cargo probably by reducing the presence of negative regulators of peptidase, therefore enhancing their proteolytic activity. Indeed, several endopeptidase inhibitors have been previously identified in EVs through proteomic analysis. For instance, TIMP (tissue inhibitor of metalloproteinases) 1,2 and 3 have been identified in cancer-derived EVs (Beckler et al. 2013; Chan et al. 2015; He et al. 2015; Minciacchi et al. 2015). Going forward, the proteolytic content of EVs could be assessed via zymography and in situ zymography. Depending on the result obtained, selected component of the MMP family and other proteases could be knocked down or inhibited in cell lines and EVs proteolytic activity could be tested again. These experiments might help understanding the specific molecular pathways involved in matrix degradation and OCs invasion following histamine administration.

6.4. Future directions and novel contributions

In future, this project could be expanded to identify the specific molecular mechanism underpinning the results herein discussed. Firstly, as OC is a complex disease characterised by many subtypes, different cell lines representative of each OC subtype should be used to understand whether HRH1 role in OC invasion and migration is conserved across them, or it is just specific to one subtype of OC. Secondly, it should be verified whether the concentration of histamine and chlorpheniramine used in this project do activate/inhibit HRH1. This could be achieved by performing FRET experiments or by quantification of downstream effectors like inositol 1,4,5-triphosphate (IP_3)/IP_2 or calcium (Zhang and Xie 2012). Thirdly, it will be important to validate if the effects of histamine on OC invasion and EV biogenesis are solely due to HRH1 activation and not to activation of the other histamine receptors. Therefore, a panel of specific HRH1 agonists should be used and both Matrigel® invasion assays and TIRF microscopy analysis should be repeated. Fourthly, it would be interesting to understand whether HRH1 is involved in cell cycle and apoptosis of OC. This could illuminate potential cytotoxic effects that together with the preliminary work presented in this thesis supports the idea of repurposing antihistamine for cancer treatment. Moreover, considering that HRH1 modulates several aspects of inflammation (chemotaxis of eosinophils and neutrophils and functional capacity of antigen-presenting cells) and of the immune system (activation of Th1 lymphocytes and decrease of humoral immunity), it would be important to assess HRH1 toxicity in vivo at different concentration, in both wild type and immune compromised mice. Together, these experiments could provide new insights to the field of cancer biology and pave the way to antihistamine application for cancer treatment in the future.

Finally, the novel contributions (Figure 6.1) of the work presented here are:

- Demonstration that HRH1 mRNA is highly expressed in OC samples from patients with advance stage of cancer (stage IV) and its expression in OC cell lines correlates with their invasiveness and motility *in vitro*
- Indication that HRH1 might play a role in OC invasion and motility *in vitro* but does not regulate expression of two EMT genes nor modulate the adhesion of OC cells to an endothelial cell monolayer
- Prove that HRH1 modulates EV release and that its activation (via histamine) boost CD81-positive MVB-PM fusion rate in SKOV3 cells, while its inhibition (via chlorpheniramine) decreases them
- Demonstration that histamine- induced EVs have an enhanced proteolytic activity

- Indication that histamine effects on OC cell invasion might be a result of reduced EV biogenesis and this could be mediated by an interplay between HRH1 and Rab27a

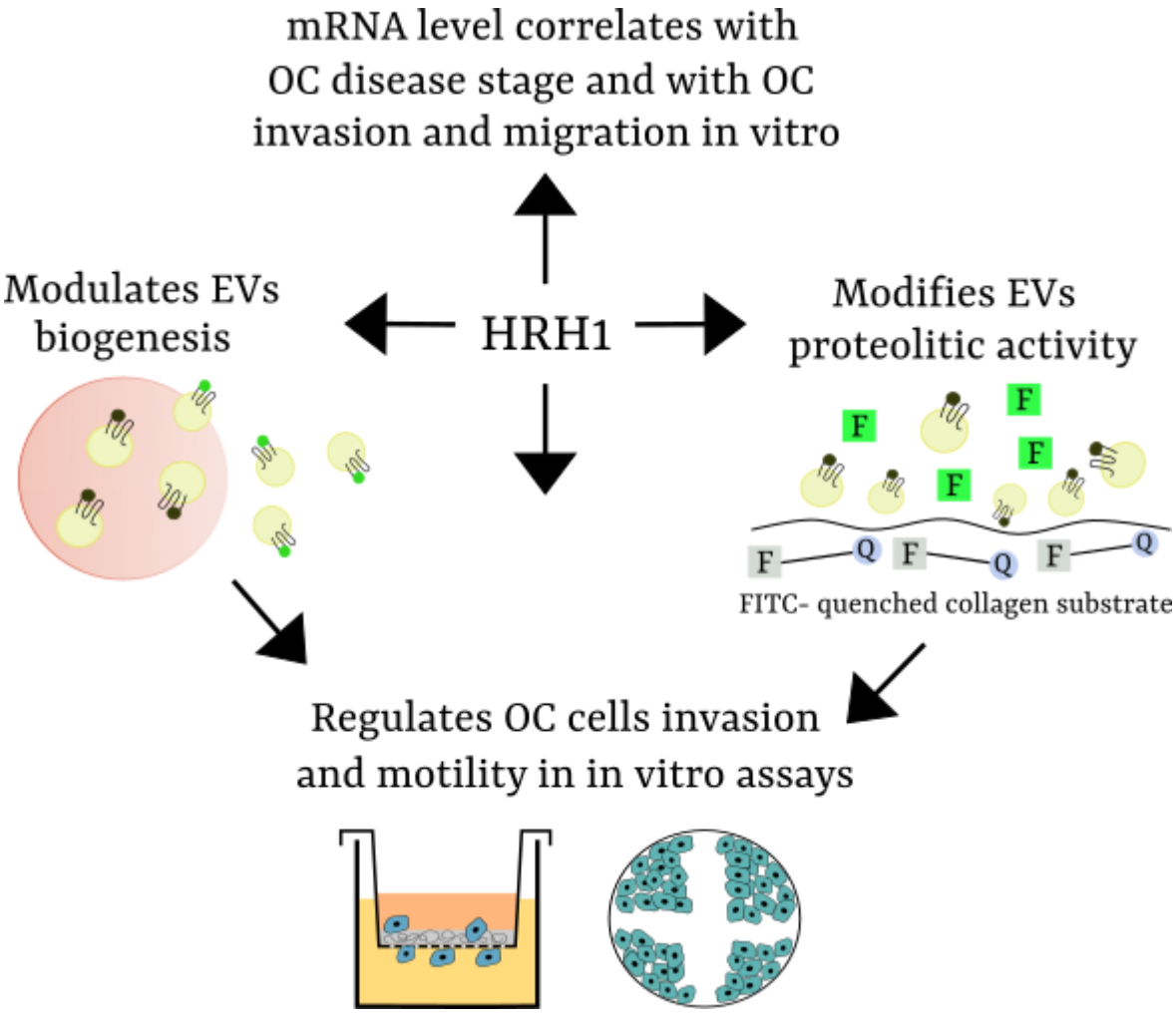

Figure 6.1: The proposed model for HRH1 role in OC progression and EV biogenesis.
HRH1 mRNA expression is upregulated in OC clinical samples of patients in stage IV and it correlates with invasion and migration rates of six OC cell lines *in vitro* suggesting a potential involvement of this receptor in OC progression. HRH1 modulates EV release, particularly its activation increases the number of MVB-PM fusion events while its inhibition decreases them. Moreover, HRH1 activation via histamine increases the proteolytic activity of EV to degrade a collagen substrate. Reduction of expression of HRH1 or its pharmacological inhibition reduces invasion and migration of OC cell *in vitro*, in line with a mechanism in which HRH1, by modulating EV release and their proteolytic activity can affect pro-metastatic properties of OC cell lines.

Appendices

7. Appendices

Appendix 1: Supplementary material for chapter 4

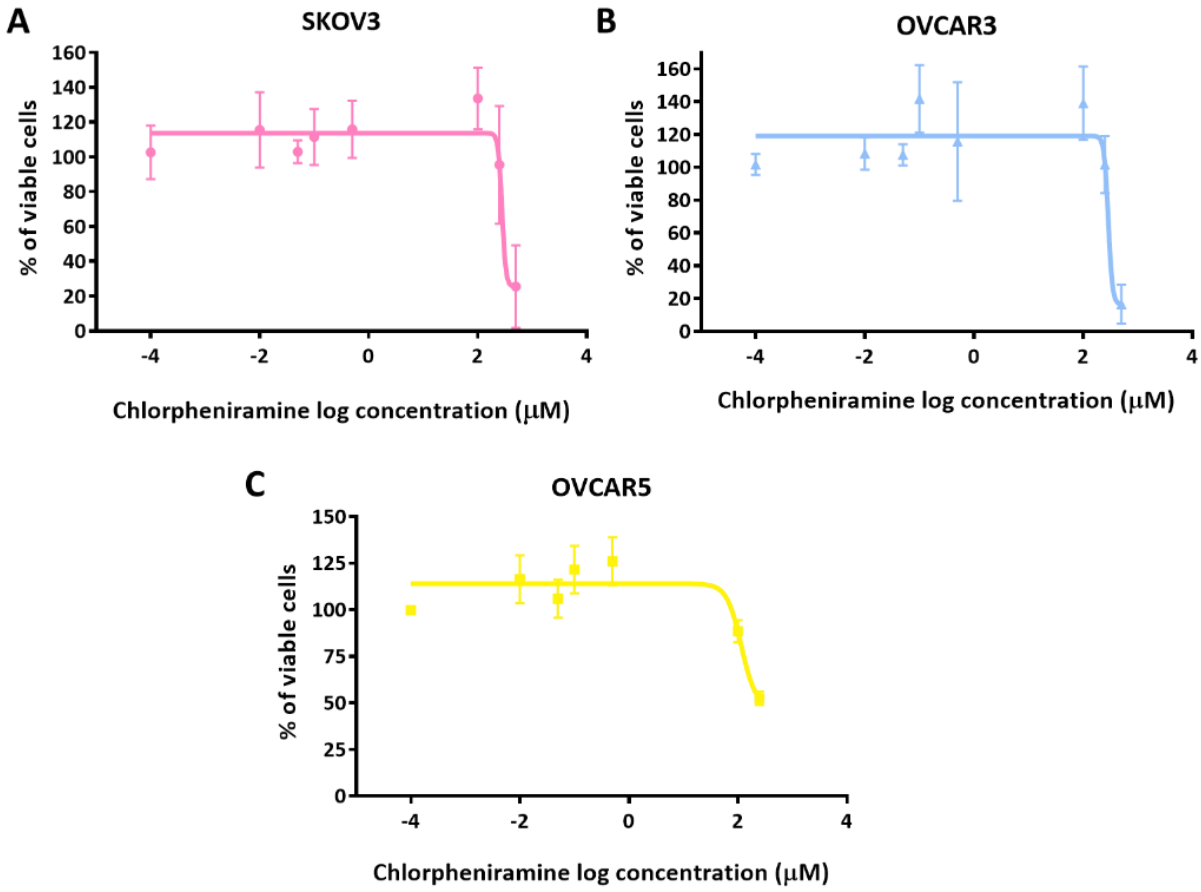

Figure 7.1: Dose response of SKOV3, OVCAR3 and OVCAR5 to chlorpheniramine.
SKOV3, OVCAR3 and OVCAR5 were treated with increasing concentrations of chlorpheniramine (ranging from 10 nM to 1 mM) for 48 h and then an MTT assay was performed to assess cell viability The four parameters regression model was employed to generate the sigmoidal curves and calculate chlorpheniramine IC50 for A) SKOV3, B) OVCAR3 and C) OVCAR5. IC50 curves resulted in the following concentrations: 420.9 µM for SKOV3, 371.1 µM for OVCAR3 and 250.7 µM for OVAR5. Three biological replicates, each one containing four technical replicates were combined for IC50 calculation. Bars show 1X SD.

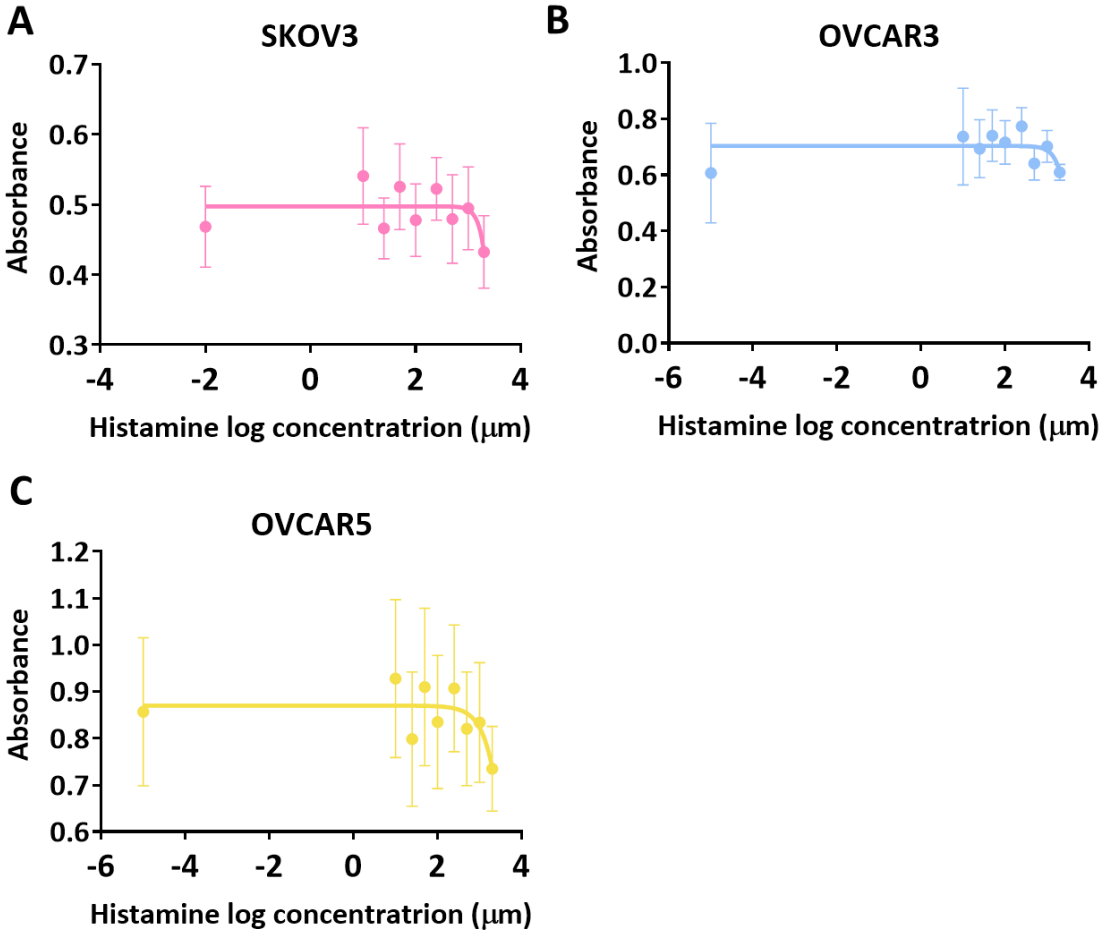

Figure 7.2: Dose response curves of SKOV3, OVCAR3 and OVCAR5 to histamine.

SKOV3, OVCAR3 and OVCAR5 were treated with increasing concentrations of histamine (ranging from 10 nM to 2 mM) for 48 h and then an MTT assay was performed to assess cell viability The four parameters regression model was employed to generate the sigmoidal curves and calculate chlorpheniramine IC50 for A) SKOV3, B) OVCAR3 and C) OVCAR5. Histamine did not affect cells viability therefore a concentration of 100 µM was used, as previously described in other studies (Verweij et al. 2018). Three biological replicates, each one containing four technical replicates were combined for IC50 calculation. Bars show 1X SD.

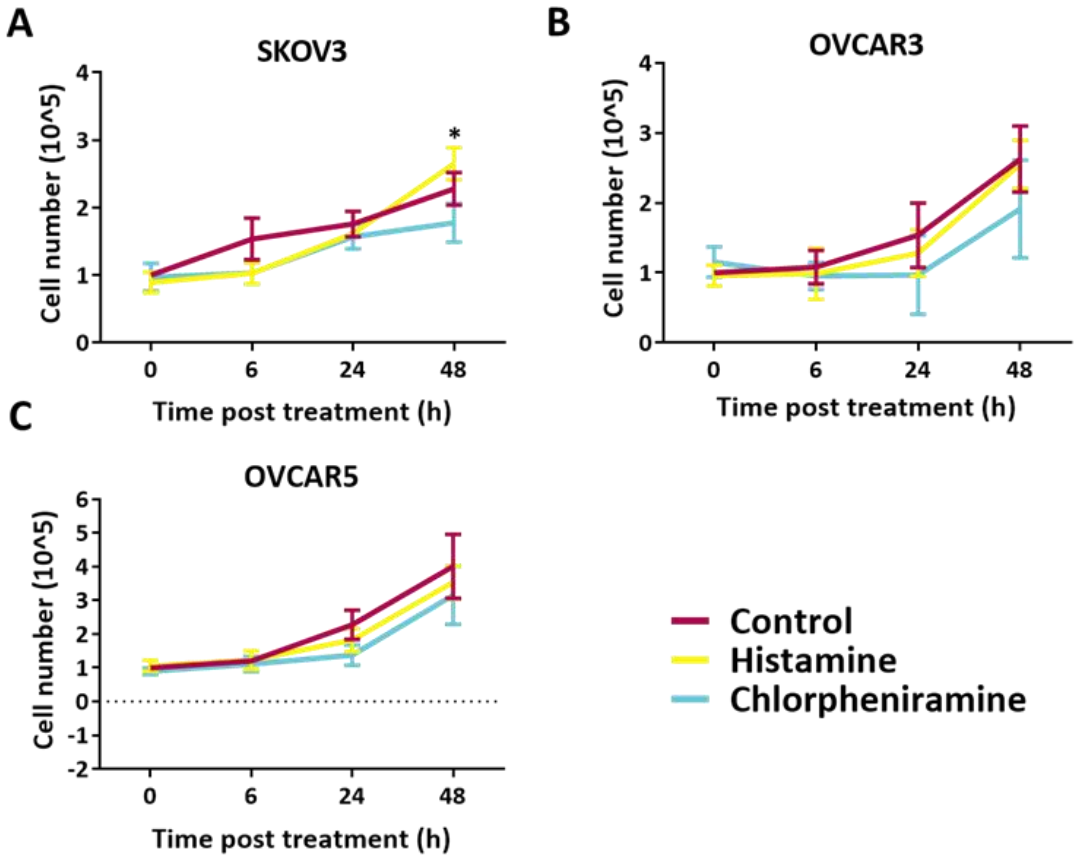

Figure 7.3: SKOV3, OVCAR3 and OVCAR5 proliferation under histamine and chlorpheniramine treatment.

SKOV3, OVCAR3 and OVCAR5 were plated is 6-well plates and treated with control media, 100 µM histamine or 250 µM chlorpheniramine and their proliferation was measured at time 0, 6. 24 and 48 h. Data were normalised to number of cells at time 0 h for each treatment. Cell proliferation for A) SKOV3, B) OVCAR3 and C) OVCAR5. Three biological replicates were combined. Statistical differences were calculated through a two-way ANOVA, followed by a Tuckey's post hoc test. Bars show 1X SD.

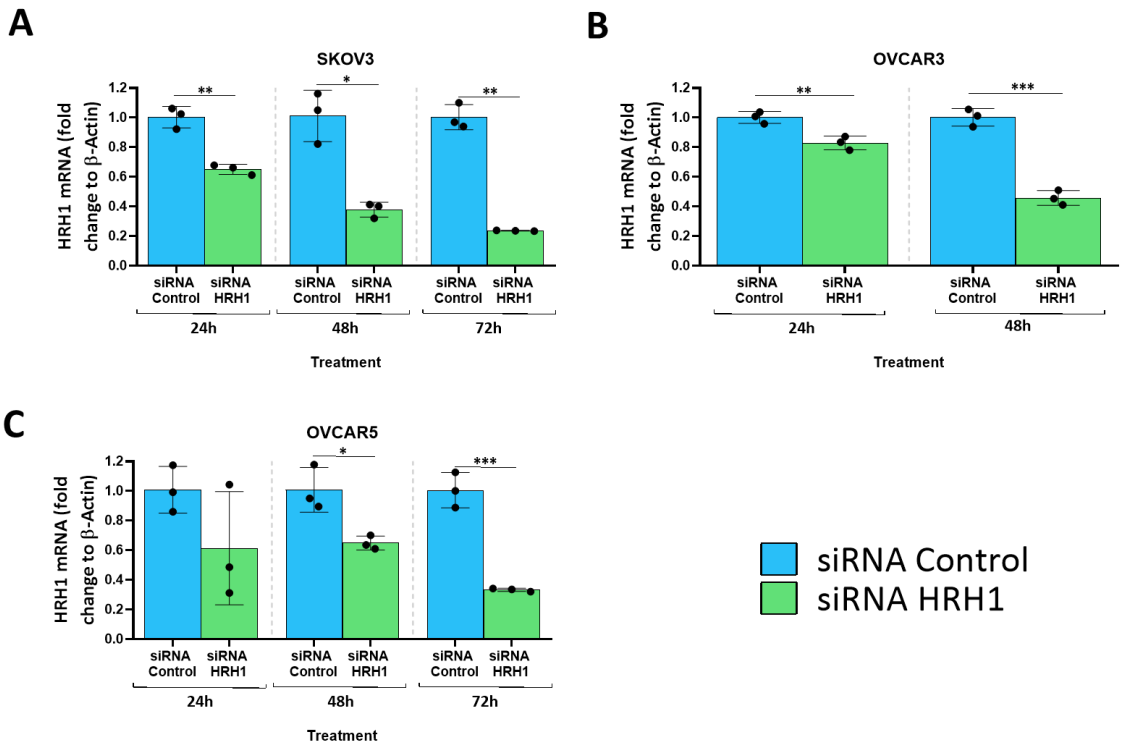

Figure 7.4: Transfection efficiency of HRH1.

HRH1 transfection conditions were validated prior to downstream experiments. RT-qPCR was used to measure knockdown efficiency for A) SKOV3, B) OVCAR3 and C) OVCAR5 after 24, 48 and 72 h transfection with siRNA control or siRNA specific for HRH1. Data for OVCAR3 are only available at 24 and 48 h. One biological replicate containing three technical replicates was used for the analysis. Statistical differences were quantified by using a t-test followed by Welch's correction. Bars show, 1X SD. *P<0.05, **P<0.01, ***P<0.001.

Appendix 2: Supplementary material for chapter 5

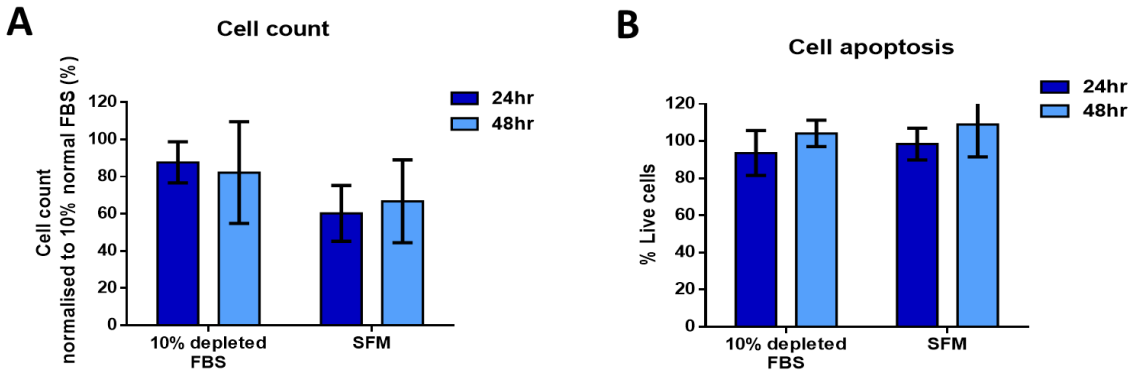

Figure 7.5: Cell count and cell apoptosis of SKOV3 incubated with 10% FBS depleted media or with SFM.
A) Percentage of SKOV3 cell count after 24 and 48 h incubation in 10% FBS depleted media or SFM. B) Percentage of live cell of SKOV3 cultured in 10% FBS depleted media or SFM for 24 and 48 h. Data were normalised to cell count in complete media. Three biological replicates. These data were kindly provided by Elise Padbury, a current PhD student in the lab.

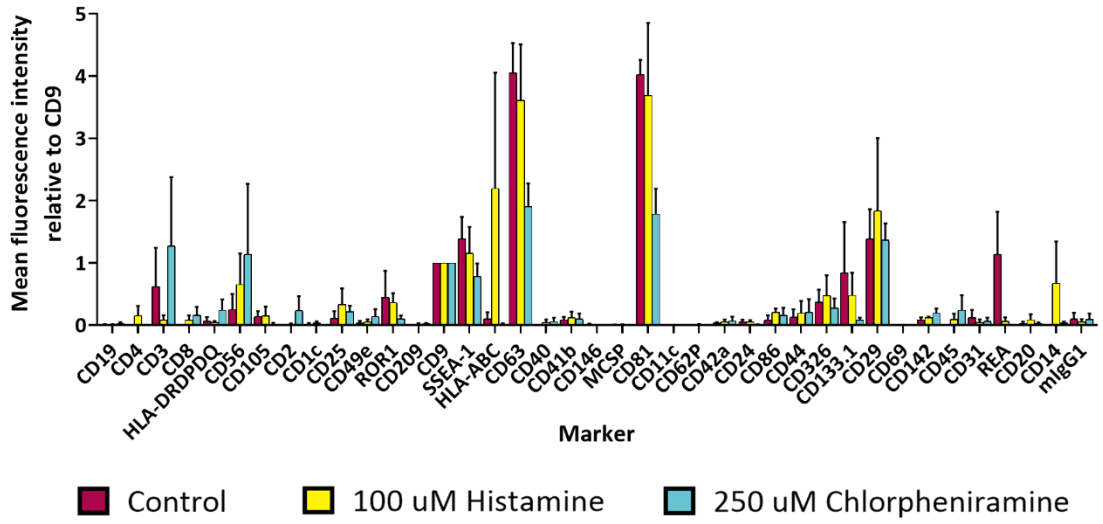

Figure 7.6: Full list of antibodies used for the MACSPlex assay.
Flow cytometry data showing mean fluorescence intensity of 37 different EV surface epitopes on EVs extracted from control media (red bars), 100 µM histamine (yellow bars) or 250 µM chlorpheniramine (blue bars). Data are reported as mean fluorescence intensity normalised on CD9. Three biological replicates were used. Bars show 1X SD.

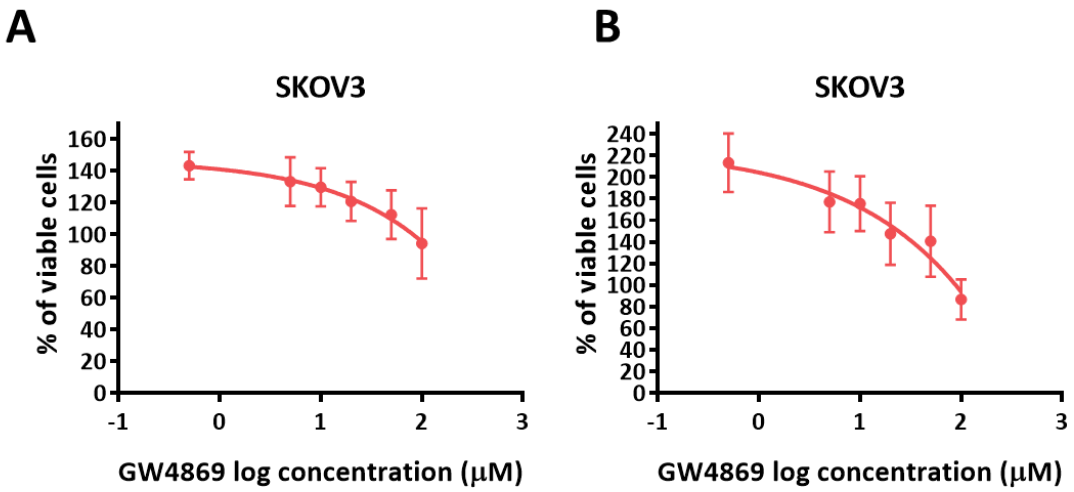

Figure 7.7: Dose response of SKOV3 to GW4869.

SKOV3 were treated with increasing concentrations of GW4869 (ranging from 500 nM to 100 µM) for 24 and 48 h and then an MTT assay was performed to assess cell viability The four parameters regression model was employed to generate the sigmoidal curves and calculate GW4869 IC50 for SKOV3 at A) 24 h and B) 48 h post-treatment. IC50 curves resulted in the following concentrations 0.9 M for 24 h and 53 M for 48 h. Three biological replicates, each one containing six technical replicates were combined for IC50 calculation. Bars show 1X SD.

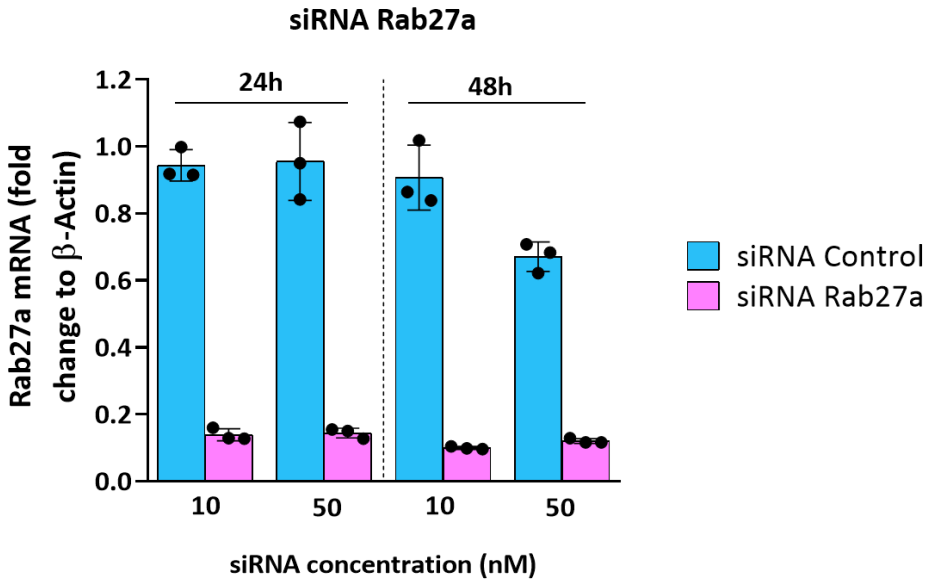

Figure 7.8: Validation of Rab27a transient transfection on SKOV3.

RT-qPCR analysis showing Rab27a mRNA expression in SKOV3 transfected with 10 or 50 nm of Rab27a 24 and 48 h post transfection. β-Actin was used as endogenous control. Data are normalised to siRNA control for each condition and time point. One independent experiment with three technical replicates. Bars show 1X SD.

Gene symbol	Number of times identified (ExoCarta)	Identified in control derived EVs
PDCD6IP	399	All samples
GAPDH	377	All samples
HSPA8	363	All samples
ACTB	350	All samples
ANXA2	337	All samples
CD9	328	All samples
PKM	327	All samples
HSP90AA1	327	All samples
ENO1	327	None
ANXA5	313	None
HSP90AB1	306	None
CD63	306	All samples
YWHAZ	301	All samples
YWHAE	300	All samples
EEF1A1	295	All samples
PGK1	291	All samples
CLTC	283	All samples
PPIA	278	All samples
SDCBP	277	All samples
ALDOA	275	All samples
EEF2	274	All samples
ALB	274	None
TPI1	270	All samples
VCP	269	All samples
CFL1	268	All samples
MSN	266	All samples
ATP1A1	266	All samples
PRDX1	263	All samples
MYH9	262	All samples
EZR	262	All samples
CD81	262	All samples
ANXA6	260	All samples
FLOT1	259	All samples
YWHAB	258	All samples
LDHB	258	All samples
SLC3A2	257	All samples
GNB1	257	All samples
PFN1	256	All samples
TSG101	255	All samples
YWHAQ	254	Histamine only
GNAI2	252	All samples
CLIC1	251	All samples
ANXA1	251	All samples
ITGB1	250	All samples
LDHA	249	All samples
FASN	248	All samples
CDC42	248	Histamine only
RAP1B	242	All samples
CCT2	242	All samples
YWHAG	240	All samples

Gene symbol	Number of times identified (ExoCarta)	Identified in control derived EVs
GNB2	240	None
ACTN4	240	All samples
RAB5C	239	All samples
C3	239	None
RAB10	236	All samples
HIST1H4A	234	All samples
KRT1	233	None
FN1	233	All samples
AHCY	233	All samples
A2M	232	None
BSG	230	All samples
ACTN1	229	All samples
ANXA7	228	All samples
ACLY	228	All samples
HIST1H4B	227	None
GDI2	227	All samples
FLNA	227	All samples
UBA1	226	All samples
GNAS	226	All samples
GSN	225	None
CCT4	225	All samples
RAN	222	All samples
PRDX2	222	All samples
RHOA	220	All samples
CCT3	220	All samples
RAC1	219	None
LGALS3BP	219	All samples
TCP1	218	All samples
KRT10	218	None
CAP1	218	All samples
RAB7A	217	All samples
TUBB4B	216	All samples
HSPA5	215	All samples
IQGAP1	214	All samples
GPI	214	All samples
RALA	213	All samples
KPNB1	212	All samples
HIST1H4I	212	None
TFRC	211	All samples
EIF4A1	211	All samples
HIST4H4	210	None
CCT8	210	All samples
TLN1	209	All samples
HIST1H4K	209	None
HIST1H4H	209	None
CCT6A	209	All samples
ANXA11	209	All samples
HIST1H4J	208	None
HIST1H4F	208	None
HIST1H4D	208	None

Figure 7.9: Top 100 EVs proteins.

Full list of the 100 most enriched proteins identified into EVs through mass-spec. This list was retrieved from the Vesiclepedia website accessed in June 2021 (http://microvesicles.org/extracellular_vesicle_markers).

A

Significant proteins, sorted by fold change			
Gene name	Fold change (Control- Histamine)	-Log p-value	P-value
CPNE8	-2.653	2.371	0.004
CD70	-2.453	1.588	0.026
TPP2	-2.190	1.772	0.017
COPB2	-2.168	1.867	0.013
ILF2	-2.120	1.652	0.022
APP	-2.060	1.358	0.044
SDC4	-1.796	1.383	0.041
PSMC6	-1.790	1.799	0.016
NCSTN	-1.662	1.695	0.020
CAD	-1.595	1.440	0.036
MYOF	-1.572	1.479	0.033
SERPINE2	-1.565	1.494	0.032
LMAN2	-1.509	1.318	0.048
PTK7	-1.473	1.536	0.029
APLP2	-1.344	1.351	0.044
EIF3B	-1.192	2.269	0.005
PLXNB2	-1.132	1.380	0.042
CTNND1	-1.075	1.444	0.036
NME1-NME2	-0.964	1.377	0.042
PSMB6	-0.954	1.303	0.049
ALCAM	-0.938	1.401	0.040
GOLM1	-0.896	2.476	0.003
CAV1	-0.861	1.415	0.035
ALDH16A1	-0.780	1.554	0.028
PGM1	-0.659	1.893	0.013
PSMA6	-0.630	1.885	0.013

B

10-most upregulated proteins, sorted by fold change			
Gene name	Fold change (Control- Histamine)	-Log p-value	P-value
CD81	-2.936	0.995	0.101
LGALS1	-2.722	0.995	0.101
RPL13a	-2.684	1.063	0.086
CPNE8	-2.653	2.371	0.004
CLDN1	-2.562	0.869	0.135
CD70	-2.453	1.588	0.026
TPP2	-2.190	1.772	0.017
COPB2	-2.168	1.867	0.013
ILF2	-2.120	1.652	0.022
PYGB	-2.060	1.068	0.085

C

10-most downregulated proteins sorted by fold change			
Gene name	Fold change (Control- Histamine)	-Log p-value	P-value
SERPINB3	2.849	0.806	0.156
C3	2.203	0.909	0.123
IGHA1	2.125	0.807	0.156
S100A7	2.115	0.554	0.279
S100A9	1.957	0.774	0.168
TGM1	1.893	0.821	0.151
CSTA	1.789	0.609	0.246
S100A16	1.739	0.993	0.102
CASP14	1.723	0.697	0.201
IGHG1	1.622	0.514	0.306

Figure 7.10: List of significant proteins identified in histamine- induced EVs and top 10 up and down regulated proteins.

A) List of proteins presented in histamine- induced EVs with a p-value< 0.05. Proteins are sorted by fold-change expressed as Intensity LFQ histamine – Intensity LFQ control. B) Top 10 upregulated protein in histamine- induced EVs. C) top 10 downregulated proteins identified in histamine- induced EVs. Proteins are sorted by fold change.

References

8. Bibliography

Abreua, R. de S. et al. 2009. Global signatures of protein and mRNA expression levels. *Mol Biosyst* 5(12), pp. 1512–1526. doi: doi:10.1039/b908315d. Global.

Adam, P.J. et al. 2006. CD70 (TNFSF7) is expressed at high prevalence in renal cell carcinomas and is rapidly internalised on antibody binding. *British Journal of Cancer* 95(3), pp. 298–306. doi: 10.1038/sj.bjc.6603222.

Afify, A.M. et al. 1999. HER-2/neu oncogene amplification in stage I and stage III ovarian papillary serous carcinoma. *Experimental and Molecular Pathology* 66(2), pp. 163–169. doi: 10.1006/exmp.1999.2255.

Aggarwal, S. et al. 2009. Immune modulator CD70 as a potential cisplatin resistance predictive marker in ovarian cancer. *Gynecologic Oncology* 115(3), pp. 430–437. Available at: http://dx.doi.org/10.1016/j.ygyno.2009.08.031.

Ahmed, A.A. et al. 2010. Driver mutations in TP53 are ubiquitous in high grade serous carcinoma of the ovary. *Journal of Pathology* 221(1), pp. 49–56. doi: 10.1002/path.2696.

Akers, J.C. et al. 2013. Biogenesis of extracellular vesicles (EV): exosomes, microvesicles, retrovirus-like vesicles, and apoptotic bodies. *J Neurooncol* 113(1), pp. 1–11. doi: 10.1007/s11060-013-1084-8.

Al-Alem, L. and Jr, T.E.C. 2015. Ovarian cancer: involvement of the matrix metalloproteinases. *Reproduction* 150(2). doi: 10.1530/REP-14-0546.

Al-Nedawi, K. et al. 2009. Endothelial expression of autocrine VEGF upon the uptake of tumor-derived microvesicles containing oncogenic EGFR. *Proceedings of the National Academy of Sciences of the United States of America* 106(10), pp. 3794–3799. doi: 10.1073/pnas.0804543106.

Alitalo, A. and Detmar, M. 2012. Interaction of tumor cells and lymphatic vessels in cancer progression. *Oncogene* (October 2011), pp. 4499–4508. doi: 10.1038/onc.2011.602.

Alonso, N. et al. 2016. PI3K pathway is involved in ERK signaling cascade activation by histamine H2R agonist in HEK293T cells. *BBA - General Subjects* 1860(9), pp. 1998–2007. Available at: http://dx.doi.org/10.1016/j.bbagen.2016.06.016.

An, C. et al. 2019. Silencing of COPB2 inhibits the proliferation of gastriccancer cells and induces apoptosis via suppression of the RTK signaling pathway. *International Journal of Oncology* 54(4), pp. 1195–1208. doi: 10.3892/ijo.2019.4717.

El Andaloussi, S. et al. 2013. Extracellular vesicles: Biology and emerging therapeutic opportunities. *Nature Reviews Drug Discovery* 12(5), pp. 347–357. Available at: http://dx.doi.org/10.1038/nrd3978.

Arya, M. et al. 2005. Basic principles of real-time quantitative PCR. *Expert Review of Molecular Diagnostics* 5(2), pp. 209–219. doi: 10.1586/14737159.5.2.209.

Asara, J.M. et al. 2008. A label-free quantification method by MS/MS TIC compared to SILAC and spectral counting in a proteomics screen. *Proteomics* 8(5), pp. 994–999. doi: 10.1002/pmic.200700426.

Au Yeung, C.L. et al. 2016. Exosomal transfer of stroma-derived miR21 confers paclitaxel resistance in ovarian cancer cells through targeting APAF1. *Nature Communications* 7

Aykul, S. and Martinez-Hackert, E. 2016. Determination of half-maximal inhibitory concentration using biosensor-based protein interaction analysis. *Anal Biochem* 508, pp. 97–103. doi:

10.1016/j.ab.2016.06.025.

Babst, M. et al. 1998. The Vps4p AAA ATPase regulates membrane association of a Vps protein complex required for normal endosome function. *EMBO Journal* 17(11), pp. 2982–2993. doi: 10.1093/emboj/17.11.2982.

Babst, M. et al. 2002. Escrt-III an endosome associated heterooligomeric protein complex required for MVB sorting.pdf. *Developmental Cell* 3, pp. 271–282.

Bachurski, D. et al. 2019. Extracellular vesicle measurements with nanoparticle tracking analysis–An accuracy and repeatability comparison between NanoSight NS300 and ZetaView. *Journal of Extracellular Vesicles* 8(1). Available at: https://doi.org/10.1080/20013078.2019.1596016.

Bakker, R.A. et al. 2001. Histamine H 1 -Receptor Activation of Nuclear Factor-kB: Roles for Gβγ and Gαq/11 - Subunits in Constitutive and Agonist- Mediated Signaling. *Molecular Pharmacology* 60(5), pp. 1133–1142. doi: https://doi.org/10.1124/mol.119.117564.

Barakat, A. et al. 2019. Understanding survival analysis: Actuarial life tables and the Kaplan–Meier plot. *British Journal of Hospital Medicine* 80(11), pp. 642–646. doi: 10.12968/hmed.2019.80.11.642.

Bates, R.C. et al. 2000. Spheroids and cell survival. *Critical Reviews in Oncology/Hematology* 36(2–3), pp. 61–74. doi: 10.1016/S1040-8428(00)00077-9.

Batlle, E. et al. 2000. The transcription factor Snail is a repressor of E-cadherin gene expression in epithelial tumour cells. *Nature Cell Biology* 2(2), pp. 84–89. doi: 10.1038/35000034.

Batra, S. and Fadeel, I. 1994. Release of intracellular calcium and stimulation of cell growth by ATP and histamine in human ovarian cancer cells (SKOV-3). *Cancer Letters* 77(94), pp. 57–63. doi: 10.1016/0304-3835(94)90348-4.

Beaufort, C.M. et al. 2014. Ovarian cancer cell line panel (OCCP): Clinical importance of in vitro morphological subtypes. *PLoS ONE* 9(9). doi: 10.1371/journal.pone.0103988.

Bebelman, M.P. et al. 2020. Real-time imaging of multivesicular body–plasma membrane fusion to quantify exosome release from single cells. *Nature Protocols* 15(1), pp. 102–121. Available at: http://dx.doi.org/10.1038/s41596-019-0245-4.

Becker, A. et al. 2016. Extracellular Vesicles in Cancer: Cell-to-Cell Mediators of Metastasis. *Cancer Cell* 30(6), pp. 836–848. doi: 10.1016/j.ccell.2016.10.009.

Beckler, M.D. et al. 2013. Proteomic analysis of exosomes from mutant KRAS colon cancer cells identifies intercellular transfer of mutant KRAS. *Molecular and Cellular Proteomics* 12(2), pp. 343–355.

Belov, L. et al. 2016. Extensive surface protein profiles of extracellular vesicles from cancer cells may provide diagnostic signatures from blood samples. *Journal of Extracellular Vesicles* 5(1), pp. 1–12. doi: 10.3402/jev.v5.25355.

Bendas, G. and Borsig, L. 2012. Cancer cell adhesion and metastasis: Selectins, integrins, and the inhibitory potential of heparins. *International Journal of Cell Biology* 2012. doi: 10.1155/2012/676731.

Beral, V. et al. 2012. Ovarian cancer and body size: Individual participant meta-analysis including 25,157 women with ovarian cancer from 47 epidemiological studies. *PLoS Medicine* 9(4). doi: 10.1371/journal.pmed.1001200.

Bergers, G. and Benjamin, L.E. 2003. Tumorigenesis and the angiogenic switch. *Nature Reviews Cancer* 3(6), pp. 401–410. doi: 10.1038/nrc1093.

Best, C.H. et al. 1927. The nature of the vaso-dilator constituents of certain tissue extracts. *J Physiol* 62(4), pp. 397–417. doi: 10.1113/jphysiol.1927.sp002369.

Bhandari, A. et al. 2019. COPB2 is up-regulated in breast cancer and plays a vital role in the metastasis via N-cadherin and Vimentin. *Journal of Cellular and Molecular Medicine* 23(8), pp. 5235–5245. doi: 10.1111/jcmm.14398.

Black, J. et al. 1972. Definition and antagonism of histamine H2 receptors. *Nature* 236, pp. 385–390.

Black, J. and Shankley, N. 1985. The isolated stomach preparation of the mouse : a physiological unit for pharmacological analysis. *Br J Pharmac* 86, pp. 571–579.

Blanc, L. and Vidal, M. 2018. New insights into the function of Rab GTPases in the context of exosomal secretion. *Small GTPases* 9(1–2), pp. 95–106. doi: 10.1080/21541248.2016.1264352.

Blaya, B. et al. 2010. Histamine and histamine receptor antagonists in cancer biology. *Inflammation and Allergy - Drug Targets* 9(3), pp. 146–157. doi: 10.2174/187152810792231869.

Blayney, J.K. et al. 2016. Prior knowledge transfer across transcriptional data sets and technologies using compositional statistics yields new mislabelled ovarian cell line. *Nucleic Acids Research* 44(17). doi: 10.1093/nar/gkw578.

Bobrie, A. et al. 2012. Rab27a supports exosome-dependent and -independent mechanisms that modify the tumor microenvironment and can promote tumor progression. *Cancer Research* 72(19), pp. 4920–4930. doi: 10.1158/0008-5472.CAN-12-0925.

Bowtell, D.D. et al. 2016. Rethinking ovarian cancer II: reducing mortality from high-grade serous ovarian cancer. *Nature Reviews Cancer* 15(11), pp. 668–679. doi: 10.1038/nrc4019.Rethinking.

Boyden, S. 1962. The chemotactic effect of mixtures of antibody and antigen on polymorphonuclear leucocytes. *Journal of Experimental Medicine* 115(3), pp. 453–466.

Brandes, L.J. et al. 1994. Enhanced cancer growth in mice administered daily human equivalent doses of some H1 antihistamines: predictive in vitro correlates. *Journal of the National Cancer Institute* 86(10), pp. 770–775.

Bray, F. et al. 2018. Global cancer statistics 2018: GLOBOCAN estimates of incidence and mortality worldwide for 36 cancers in 185 countries. *CA: A Cancer Journal for Clinicians* 68(6), pp. 394–424. doi: 10.3322/caac.21492.

Brooks, S.A. et al. 2010. Molecular interactions in cancer cell metastasis. *Acta Histochemica* 112(1), pp. 3–25. Available at: http://dx.doi.org/10.1016/j.acthis.2008.11.022.

Brown, M. et al. 2018. Lymph node blood vessels provide exit routes for metastatic tumor cell dissemination in mice. *Science* 359(6382), pp. 1408–1411. doi: 10.1126/science.aal3662.

Brügger, B. and Bankaitis, V.A. 2012. Lipids and vesicular transport. *Biochimica et Biophysica Acta - Molecular and Cell Biology of Lipids* 1821(8), p. 1039. Available at: http://dx.doi.org/10.1016/j.bbalip.2012.05.005.

Bruno, S. et al. 2012. Microvesicles derived from mesenchymal stem cells enhance survival in a lethal model of acute kidney injury. *PLoS ONE* 7(3). doi: 10.1371/journal.pone.0033115.

Burtin, C. et al. 1982. Decrease in tumour growth by injections of histamine or serotonin in fibrosarcoma bearing mice: influence of H1 and H2 histamine receptors. *British Journal of Cancer* 45(54), pp. 54–60.

Buschauer, A. et al. 2015. Histamine H1- and H4-receptor signaling cooperatively regulate MAPK activation. *Biochemical Pharmacology* 98(3), pp. 432–9. Available at: doi: 10.1016/j.bcp.2015.09.011.

Cai, J. et al. 2016. Functional transferred DNA within extracellular vesicles. *Experimental Cell Research* 349(1), pp. 179–183. Available at: http://dx.doi.org/10.1016/j.yexcr.2016.10.012.

Cannistra, S.A. 2004. Cancer of the Ovary. *The New England journal of medicine* 351, pp. 2519–2529. doi: 10.1136/bmj.312.7025.258a.

Cano, A. et al. 2000. The transcription factor Snail controls epithelial-mesenchymal transitions by repressing E-cadherin expression. *Nature Cell Biology* 2(2), pp. 76–83. doi: 10.1038/35000025.

Carnino, J.M. et al. 2019. Isolation and characterization of extracellular vesicles from Broncho-Alveolar lavage fluid: A review and comparison of different methods. *Respiratory Research* 20(1), pp. 1–11. doi: 10.1186/s12931-019-1210-z.

Cashikar, A.G. and Hanson, P.I. 2019. A cell-based assay for CD63-containing extracellular vesicles. *PLoS ONE* 14(7), pp. 1–19. doi: 10.1371/journal.pone.0220007.

Castellana, D. et al. 2009. Membrane microvesicles as actors in the establishment of a favorable prostatic tumoral niche: A role for activated fibroblasts and CX3CL1-CX3CR1 axis. *Cancer Research* 69(3), pp. 785–793. doi: 10.1158/0008-5472.CAN-08-1946.

Cathcart, J. et al. 2015. Targeting matrix metalloproteinases in cancer: Bringing new life to old ideas. *Genes and Diseases* 2(1), pp. 26–34. Available at: http://dx.doi.org/10.1016/j.gendis.2014.12.002.

Cavallaro, U. and Christofori, G. 2004. Cell adhesion and signalling by cadherins and Ig-CAMs in cancer. *Nature Reviews Cancer* 4(2), pp. 118–132. doi: 10.1038/nrc1276.

Chaffer, C.L. et al. 2016. EMT, cell plasticity and metastasis. *Cancer and Metastasis Reviews* 35(4), pp. 645–654. Available at: http://dx.doi.org/10.1007/s10555-016-9648-7.

Chambers, A.F. et al. 2002. Dissemination and growth of cancer cells in metastatic sites. *Nature Reviews Cancer* 2(8), pp. 563–572. doi: 10.1038/nrc865.

Chan, J.K. et al. 2006. Ovarian cancer in younger vs older women: A population-based analysis. *British Journal of Cancer* 95(10), pp. 1314–1320. doi: 10.1038/sj.bjc.6603457.

Chan, Y.K. et al. 2015. Proteomic analysis of exosomes from nasopharyngeal carcinoma cell identifies intercellular transfer of angiogenic proteins. *International Journal of Cancer* 137(8), pp. 1830–1841. doi: 10.1002/ijc.29562.

Chanda, R. and Ganguly, A.K. 1987. Diamineoxidase activity and tissue histamine content of human skin, breast and rectal carcinoma. *Cancer Letters* 34(2), pp. 207–212.

Chanda, R. and Ganguly, A.K. 1995. Diamine-oxidase activity and tissue di- and poly-amine contents of human ovarian, cervical and endometrial carcinoma. *Cancer Letters* 89(1), pp. 23–28. doi: 10.1016/0304-3835(95)90153-1.

Chandrashekar, D.S. et al. 2017. UALCAN: A Portal for Facilitating Tumor Subgroup Gene Expression and Survival Analyses. *Neoplasia (United States)* 19(8), pp. 649–658. Available at: http://dx.doi.org/10.1016/j.neo.2017.05.002.

Chen, J.S. et al. 2006. Checkpoint kinase 1-mediated phosphorylation of Cdc25C and bad proteins involved in antitumor effects of loratadine-induced G2/M phase cell-cycle arrest and apoptosis. *Molecular Carcinogenesis* 45(7), pp. 461–478. doi: 10.1002/mc.20165.

Chen, L. et al. 2018. HCC-derived exosomes elicit HCC progression and recurrence by epithelial-mesenchymal transition through MAPK/ERK signalling pathway article. *Cell Death and Disease* 9(5). Available at: http://dx.doi.org/10.1038/s41419-018-0534-9.

Chen, V.W. et al. 2003. Pathology and classification of ovarian tumors. *Cancer* 97(S10), pp. 2631–2642. doi: 10.1002/cncr.11345.

Chen, Y. et al. 2017. Aberrant low expression of p85α in stromal fibroblasts promotes breast cancer cell metastasis through exosome-mediated paracrine Wnt10b. *Oncogene* . doi: 10.1038/onc.2017.100.

Cheng, L. et al. 2017. A comprehensive overview of exosomes in ovarian cancer: Emerging biomarkers and therapeutic strategies. *Journal of Ovarian Research* 10(1), pp. 1–9. doi: 10.1186/s13048-017-0368-6.

Cheng, S. et al. 2016. Expression and critical role of interleukin enhancer binding factor 2 in Hepatocellular Carcinoma. *International Journal of Molecular Sciences* 17(8)

Cho, J. et al. 2011. Exosomes from ovarian cancer cells induce adipose tissue-derived mesenchymal stem cells to acquire the physical and functional characteristics of tumor-supporting myo fi broblasts. *Gynecologic Oncology* 123(2), pp. 379–386. Available at: http://dx.doi.org/10.1016/j.ygyno.2011.08.005.

Cho, K.R. and Shih, I. 2009. Ovarian cancer. *Annu Rev Pathol* (4), pp. 287–313. doi: 10.1146/annurev.pathol.4.110807.092246.OVARIAN.

Cianchi, F. et al. 2008. Histamine in cancer: The dual faces of the coin. *Cancer Biology and Therapy* 7(1), pp. 36–37. doi: 10.4161/cbt.7.1.5706.

Claerhout, S. et al. 2012. Abortive autophagy induces endoplasmic reticulum stress and cell death in cancer cells. *PLoS ONE* 7(6). doi: 10.1371/journal.pone.0039400.

Clancy, J.W. et al. 2015. Regulated delivery of molecular cargo to invasive tumour-derived microvesicles. *Nature Communications* 6, pp. 1–11. doi: 10.1038/ncomms7919.

Clark, A. and Vignjevic, D. 2015. Modes of cancer cell invasion and the role of the microenvironment. *Current Opinion in Cell Biology* 36, pp. 13–22. Available at: http://dx.doi.org/10.1016/j.ceb.2015.06.004.

Clark, E.A. and Hill, S.J. 1996. Sensitivity of histamine H3 receptor agonist-stimulated [35S]GTPγ[S] binding to pertussin toxin. *European Journal of Pharmacology* 296, pp. 223–225.

Colangelo, N.W. and Azzam, E.I. 2020. Extracellular vesicles originating from glioblastoma cells increase metalloproteinase release by astrocytes: The role of CD147 (EMMPRIN) and ionizing radiation. *Cell Communication and Signaling* 18(1), pp. 1–14. doi: 10.1186/s12964-019-0494-4.

Colombo, M. et al. 2013. Analysis of ESCRT functions in exosome biogenesis, composition and secretion highlights the heterogeneity of extracellular vesicles. *Journal of Cell Science* 126(24), pp. 5553–5565. doi: 10.1242/jcs.128868.

Colombo, M. et al. 2014. Biogenesis, Secretion, and Intercellular Interactions of Exosomes and Other Extracellular Vesicles. *Annual Review of Cell and Developmental Biology* 30(1), pp. 255–289. doi: 10.1146/annurev-cellbio-101512-122326.

Comijn, J. et al. 2001. The two-handed E box binding zinc finger protein SIP1 downregulates E-cadherin and induces invasion. *Molecular cell* 7(6), pp. 1267–1278. Available at: http://eutils.ncbi.nlm.nih.gov/entrez/eutils/elink.fcgi?dbfrom=pubmed&id=11430829&retmode=ref

&cmd=prlinks%5Cnpapers2://publication/uuid/3754EFCC-BFDE-4761-9C4E-FF3529B10C78.

Cortez, A.J. et al. 2018. Advances in ovarian cancer therapy. *Cancer Chemotherapy and Pharmacology* 81(1), pp. 17–38. Available at: http://dx.doi.org/10.1007/s00280-017-3501-8.

Costa-Silva, B. et al. 2015. Pancreatic cancer exosomes initiate pre-metastatic niche formation in the liver Bruno. *Nat Cell Biol* 17(6), pp. 816–826. doi: 10.1038/ncb3169.Pancreatic.

Cox, J. et al. 2014. Accurate proteome-wide label-free quantification by delayed normalization and maximal peptide ratio extraction, termed MaxLFQ. *Molecular and Cellular Proteomics* 13(9), pp. 2513–2526. doi: 10.1074/mcp.M113.031591.

De Craene, B. et al. 2005. The transcription factor snail induces tumor cell invasion through modulation of the epithelial cell differentiation program. *Cancer Research* 65(14), pp. 6237–6244. doi: 10.1158/0008-5472.CAN-04-3545.

Craene, B. De and Berx, G. 2013. Regulatory networks defining EMT during cancer initiation and progression. *Nature Reviews Cancer* 13(2), pp. 97–110. Available at: http://dx.doi.org/10.1038/nrc3447.

Cricco, G. et al. 2006. Histamine modulates cellular events involved in tumour invasiveness in pancreatic carcinoma cells. *Inflammation Research* 55(SUPPL. 1), pp. 83–84. doi: 10.1007/s00011-005-0054-9.

Cricco, G. et al. 2011. Histamine and Breast Cancer: A New Role for a Well Known Amine. *Breast Cancer - Carcinogenesis, Cell Growth and Signalling Pathways* . doi: 10.5772/20633.

Cui, Y. et al. 2016. Asparaginyl endopeptidase promotes the invasion and metastasis of gastric cancer through modulating epithelial-to-mesenchymal transition. *Oncotarget* 7(23), pp. 34356–34370. doi: 10.18632/oncotarget.8879.

Dai, J. et al. 2020. Exosomes: key players in cancer and potential therapeutic strategy. *Signal Transduction and Targeted Therapy* 5(1). Available at: http://dx.doi.org/10.1038/s41392-020-00261-0.

Dang, T.T. et al. 2016. ΔNp63α induces the expression of FAT2 and Slug to promote tumor invasion. *Oncotarget* 7(19), pp. 28592–28611. doi: 10.18632/oncotarget.8696.

Dean, M. et al. 2017. *Activin A stimulates migration of the fallopian tube epithelium, an origin of high-grade serous ovarian cancer, through non-canonical signaling*. Elsevier Ireland Ltd. Available at: http://dx.doi.org/10.1016/j.canlet.2017.01.011.

Decaestecker, C. et al. 2007. Can anti-migratory drugs be screened in vitro? A review of 2D and 3D assays for the quantitative analysis of cell migration. *Medicinal Research Reviews* 27(2), pp. 149–176. doi: 10.1002/med.20078.

Denoeud, J. and Moser, M. 2011. Role of CD27/CD70 pathway of activation in immunity and tolerance. *Journal of Leukocyte Biology* 89(2), pp. 195–203. doi: 10.1189/jlb.0610351.

Desgrosellier, J.S. and Cheresh, D.A. 2010. Integrins in cancer: Biological implications and therapeutic opportunities. *Nature Reviews Cancer* 10(1), pp. 9–22. Available at: http://dx.doi.org/10.1038/nrc2748.

Díaz, B. 2013. Invadopodia Detection and Gelatin Degradation Assay Begoña. *Bio Protoc.* 3(24). doi: 10.21769/BioProtoc.997.

Dickenson, J.M. and Hill, S.J. 1993. Adenosine A1-receptor stimulated increases in intracellular calcium in the smooth muscle cell line, DDT1MF-2. *British Journal of Pharmacology* 108(1), pp. 85–92. doi: 10.1111/j.1476-5381.1993.tb13444.x.

Domcke, S. et al. 2013. Evaluating cell lines as tumour models by comparison of genomic profiles. *Nature Communications* 4, pp. 1–10. Available at: http://dx.doi.org/10.1038/ncomms3126.

Dongre, A. and Weinberg, R.A. 2019. New insights into the mechanisms of epithelial–mesenchymal transition and implications for cancer. *Nature Reviews Molecular Cell Biology* 20(2), pp. 69–84. Available at: http://dx.doi.org/10.1038/s41580-018-0080-4.

Dötsch, M.M. et al. 2015. Low expression of ITIH5 in adenocarcinoma of the lung is associated with unfavorable patients' outcome. *Epigenetics* 10(10), pp. 903–912. doi: 10.1080/15592294.2015.1078049.

Doyle, L.M. and Wang, M.Z. 2019. Overview of Extracellular Vesicles, Their Origin, Composition, Purpose, and Methods for Exosome Isolation and Analysis. *Cells* 8(727). doi: doi:10.3390/cells8070727.

Drexler, H.G. et al. 1999. False human hematopoietic cell lines: Cross-contaminations and misinterpretations. *Leukemia* 13(10), pp. 1601–1607. doi: 10.1038/sj.leu.2401510.

Drexler, H.G. and Uphoff, C.C. 2002. Mycoplasma contamination of cell cultures: Incidence, sources, effects, detection, elimination, prevention. *Cytotechnology* 39(2), pp. 75–90. doi: 10.1023/A:1022913015916.

Drutel, G. et al. 2001. Identification of Rat H 3 Receptor Isoforms with Different Brain Expression and Signaling Properties. *Molecular Pharmacology* 59(1), pp. 1–8.

Dvorak, H.F. et al. 1988. Identification and characterization of the blood vessels of solid tumors that are leaky to circulating macromolecules. *American Journal of Pathology* 133(1), pp. 95–109.

Easton, D.F. et al. 1995. Breast and Ovarian Cancer Incidence in BRCA I -Mutation Carriers. *American Journal of Medical Genetics* 56(3), pp. 265–271. doi: 10.1002/ajmg.1320560305.

Eccles, S.A. and Welch, D.R. 2007. Metastasis: recent discoveries and novel treatment strategies. *Lancet* 369(9574), pp. 1742–1757. doi: 10.1016/S0140-6736(07)60781-8.

Elias, K.M. et al. 2015. Beyond genomics: critical evaluation of cell line utility for ovarian cancer research. *Gynecologic Oncology* 139(1), pp. 97–103. doi: 10.1016/j.ygyno.2015.08.017.

Ellegaard, A.M. et al. 2016. Repurposing Cationic Amphiphilic Antihistamines for Cancer Treatment. *EBioMedicine* 9, pp. 130–139. Available at: http://dx.doi.org/10.1016/j.ebiom.2016.06.013.

Elstak, E.D. et al. 2011. The munc13-4-rab27 complex is specifically required for tethering secretory lysosomes at the plasma membrane. *Blood* 118(6), pp. 1570–1578. doi: 10.1182/blood-2011-02-339523.

Escola, J.M. et al. 1998. Selective enrichment of tetraspan proteins on the internal vesicles of multivesicular endosomes and on exosomes secreted by human B-lymphocytes. *Journal of Biological Chemistry* 273(32), pp. 20121–20127. doi: 10.1074/jbc.273.32.20121.

Fabbri, M. et al. 2012. MicroRNAs bind to Toll-like receptors to induce prometastatic inflammatory response. *Proceedings of the National Academy of Sciences of the United States of America* 109(31). doi: 10.1073/pnas.1209414109.

Fan, X. et al. 2010. MiR-20a promotes proliferation and invasion by targeting APP in human ovarian

cancer cells. *Acta Biochimica et Biophysica Sinica* 42(5), pp. 318–324. doi: 10.1093/abbs/gmq026.

Fang, T. et al. 2018. Tumor-derived exosomal miR-1247-3p induces cancer-associated fibroblast activation to foster lung metastasis of liver cancer. *Nature Communications* 9(1), pp. 1–13. doi: 10.1038/s41467-017-02583-0.

Fares, J. et al. 2020. Molecular principles of metastasis: a hallmark of cancer revisited. *Signal Transduction and Targeted Therapy* 5(1). Available at: http://dx.doi.org/10.1038/s41392-020-0134-x.

Farnsworth, R.H. et al. 2018. The evolving role of lymphatics in cancer metastasis. *Current Opinion in Immunology* 53, pp. 64–73. Available at: https://doi.org/10.1016/j.coi.2018.04.008.

Fathalla, M.F. 1971. Incessant ovulation - a factor in ovarian neoplasia? *Lancet* 2(163)

Faustino-Rocha, A.I. et al. 2017. Antihistamines as promising drugs in cancer therapy. *Life Sciences* 172, pp. 27–41. Available at: http://dx.doi.org/10.1016/j.lfs.2016.12.008.

Feki, A. et al. 2009. Dissemination of intraperitoneal ovarian cancer: Discussion of mechanisms and demonstration of lymphatic spreading in ovarian cancer model. *Critical Reviews in Oncology/Hematology* 72(1), pp. 1–9. doi: 10.1016/j.critrevonc.2008.12.003.

Feng, Q. et al. 2017. A class of extracellular vesicles from breast cancer cells activates VEGF receptors and tumour angiogenesis. *Nature Communications* 8, pp. 1–17. doi: 10.1038/ncomms14450.

Fernández-Nogueira, P. et al. 2016. Differential expression of neurogenes among breast cancer subtypes identifies high risk patients. *Oncotarget* 7(5), pp. 5313–5326. doi: 10.18632/oncotarget.6543.

Fernández-Nogueira, P. et al. 2018. Histamine receptor 1 inhibition enhances antitumor therapeutic responses through extracellular signal-regulated kinase (ERK) activation in breast cancer. *Cancer Letters* 424, pp. 70–83. doi: 10.1016/j.canlet.2018.03.014.

Ferrandina, G. et al. 2007. Ovarian cancer patients with “node-positive-only” Stage IIIC disease have a more favorable outcome than Stage IIIA/B. *Gynecologic Oncology* 107, pp. 154–158. doi: 10.1111/j.1440-1673.2000.00863.pp.x.

Filipe, V. et al. 2010. Critical evaluation of nanoparticle tracking analysis (NTA) by NanoSight for the measurement of nanoparticles and protein aggregates. *Pharmaceutical Research* 27(5), pp. 796–810. doi: 10.1007/s11095-010-0073-2.

Fischer, K.R. et al. 2015. EMT is not required for lung metastasis but contributes to chemoresistance. *Nauture* 527(7579), pp. 472–476. doi: 10.1038/nature15748.EMT.

Fitzner, D. et al. 2011. Selective transfer of exosomes from oligodendrocytes to microglia by macropinocytosis. *Journal of Cell Science* 124(3), pp. 447–458. doi: 10.1242/jcs.074088.

Fleming, J.S. et al. 2006. Incessant ovulation, inflammation and epithelial ovarian carcinogenesis: Revisiting old hypotheses. *Molecular and Cellular Endocrinology* 247(1–2), pp. 4–21. doi: 10.1016/j.mce.2005.09.014.

Fontana, F. et al. 2021. Extracellular vesicles: Emerging modulators of cancer drug resistance. *Cancers* 13(4), pp. 1–16. doi: 10.3390/cancers13040749.

Fouad, Y.A. and Aanei, C. 2017. Revisiting the hallmarks of cancer. *American Journal of Cancer Research* 7(5), pp. 1016–1036.

Frankel, A. et al. 2001. Induction of anoikis and suppression of human ovarian tumor growth in vivo by down-regulation of Bcl-XL. *Cancer Research* 61(12), pp. 4837–4841.

Friedl, P. et al. 1998. Cell migration strategies in 3-D extracellular matrix: Differences in morphology, cell matrix interactions, and integrin function. *Microscopy Research and Technique* 43(5), pp. 369–378. doi: 10.1002/(SICI)1097-0029(19981201)43:5<369::AID-JEMT3>3.0.CO;2-6.

Friedl, P. et al. 2012. Classifying collective cancer cell invasion. *Nature Cell Biology* 14(8), pp. 777–783. doi: 10.1038/ncb2548.

Friedl, P. and Wolf, K. 2009. Plasticity of cell migration : a multiscale tuning model. *Journal of Cell Biology* 188(1), pp. 11–19. doi: 10.1083/jcb.200909003.

Fritz, I. et al. 2020. Desloratadine and loratadine stand out among common H1-antihistamines for association with improved breast cancer survival. *Acta Oncologica* 59(9), pp. 1103–1109. Available at: https://doi.org/10.1080/0284186X.2020.1769185.

Fukui, H. et al. 1994. Molecular cloning of the human histamine H1 receptor gene. *Biochemical and Biophysical Research Communications* 201(2), pp. 894–901. doi: 10.1006/bbrc.1994.1786.

Galindo-Hernandez, O. et al. 2014. Extracellular vesicles from MDA-MB-231 breast cancer cells stimulated with linoleic acid promote an EMT-like process in MCF10A cells. *Prostaglandins Leukotrienes and Essential Fatty Acids* 91(6), pp. 299–310. Available at: http://dx.doi.org/10.1016/j.plefa.2014.09.002.

Galluzzi, L. et al. 2012. Molecular mechanisms of cisplatin resistance. *Oncogene* 31(15), pp. 1869–1883. doi: 10.1038/onc.2011.384.

Gantner, F. et al. 2002. Histamine H4 and H2 Receptors Control Histamine-Induced Interleukin-16 Release from Human CD8+T Cells. *The Journal of Pharmacology and Experimental Therapuetics* 303(1), pp. 300–307. doi: 10.1124/jpet.102.036939.acid.

Garnier, D. et al. 2012. Cancer cells induced to express mesenchymal phenotype release exosome-like extracellular vesicles carrying tissue factor. *Journal of Biological Chemistry* 287(52), pp. 43565–43572. doi: 10.1074/jbc.M112.401760.

Gayarre, J. et al. 2016. The NER-related gene GTF2H5 predicts survival in high-grade serous ovarian cancer patients. *Journal of Gynecologic Oncology* 27(1), pp. 1–13. doi: 10.3802/jgo.2016.27.e7.

Genre, F. et al. 2009. Effect of histamine on the expression of metalloproteinases and cell adhesion in breast cancer cell lines. *Inflammation Research* 58(SUPPL. 1), pp. 55–56. doi: 10.1007/s00011-009-2006-2.

Gershenson, D.M. et al. 2006. Clinical Behavior of Stage II-IV Low-Grade Serous Carcinoma of the Ovary. *Obstetrics and gynecology* 108(2), pp. 361–368.

Ghosh, R. et al. 2014. The necessity of and strategies for improving confidence in the accuracy of western blots. *Expert Review of Proteomics* 11(5), pp. 549–560. doi: 10.1586/14789450.2014.939635.

Giaccone, G. 2000. Clinical perspectives on platinum resistance. *Drugs* 59(SUPPL. 4), pp. 9–17. doi: 10.2165/00003495-200059004-00002.

Gilda, J.E. et al. 2015. Western blotting inaccuracies with unverified antibodies: Need for a Western Blotting Minimal Reporting Standard (WBMRS). *PLoS ONE* 10(8), pp. 1–18. doi: 10.1371/journal.pone.0135392.

Givant-Horwitz, V. et al. 2005. Laminin-induced signaling in tumor cells. *Cancer Letters* 223(1), pp. 1–10. doi: 10.1016/j.canlet.2004.08.030.

Goff, B.A. et al. 2004. Frequency of Symptoms of Ovarian Cancer in Women Presenting to Primary Care Clinics. *Journal of American Medical Association* 291(22), pp. 2705–2712.

Gómez-Fabre, P.M. et al. 1997. Polyamine contents of human breast cancer cells treated with the cytotoxic agents chlorpheniramine and dehydrodidemnin B. *Cancer Letters* 113(1–2), pp. 141–144. doi: 10.1016/S0304-3835(96)04591-0.

Gonzalez-Avila, G. et al. 2019. Matrix metalloproteinases participation in the metastatic process and their diagnostic and therapeutic applications in cancer. *Critical Reviews in Oncology/Hematology* 137(October 2018), pp. 57–83. Available at: https://doi.org/10.1016/j.critrevonc.2019.02.010.

Gould, G.W. and Lippincott-Schwartz, J. 2009. New roles for endosomes: from vesicular carriers to multi-purpose platforms. *Nature Review of Molecular Cell Biology* 10(4), pp. 287–292.

Graves, L.E. et al. 2004. Proinvasive properties of ovarian cancer ascites-derived membrane vesicles. *Cancer Research* 64(19), pp. 7045–7049. doi: 10.1158/0008-5472.CAN-04-1800.

Greenbaum, D. et al. 2003. Comparing protein abundance and mRNA expression levels on a genomic scale. *Genome Biology* 4(9). doi: 10.1186/gb-2003-4-9-117.

Greening, D.W. et al. 2015. Emerging roles of exosomes during epithelial-mesenchymal transition and cancer progression. *Seminars in Cell and Developmental Biology* 40, pp. 60–71. Available at: http://dx.doi.org/10.1016/j.semcdb.2015.02.008.

Grotegut, S. et al. 2006. Hepatocyte growth factor induces cell scattering through MAPK/Egr-1-mediated upregulation of Snail. *EMBO Journal* 25(15), pp. 3534–3545.

Gschwandtner, M. et al. 2008. Histamine upregulates keratinocyte MMP-9 production via the histamine H1 receptor. *Journal of Investigative Dermatology* 128(12), pp. 2783–2791. doi: 10.1038/jid.2008.153.

Gui, T. et al. 2021. Identification and analysis of genes associated with epithelial ovarian cancer by integrated bioinformatics methods. *PLoS ONE* 16(6 June), pp. 1–18. Available at: http://dx.doi.org/10.1371/journal.pone.0253136.

Guo, D. et al. 2019. RAB27A promotes melanoma cell invasion and metastasis via regulation of pro-invasive exosomes. *International Journal of Cancer* 144(12), pp. 3070–3085. doi: 10.1002/ijc.32064.

Gupta, G.P. and Massagué, J. 2006. Cancer Metastasis : Building a Framework. *Cell* , pp. 679–695. doi: 10.1016/j.cell.2006.11.001.

Gupta, P.B. et al. 2019. Phenotypic plasticity as a driver of cancer formation, progression and resistance to therapy. *Cell Sten Cell* 24(1), pp. 65–78. doi: 10.1016/j.stem.2018.11.011.

Gutowski, S. et al. 1991. Antibodies to the α(q) subfamily of guanine nucleotide-binding regulatory protein α subunit attenuate activation of phosphatidylinositol 4,5-bisphosphate hydrolysis by hormones. *Journal of Biological Chemistry* 266(30), pp. 20519–20524. doi: 10.1016/s0021-9258(18)54955-3.

Gyorffy, B. et al. 2012. Implementing an online tool for genomewide validation of survival-associated biomarkers in ovarian-cancer using microarray data from 1287 patients. *Endocrine-Related Cancer* 19(2), pp. 197–208. doi: 10.1530/ERC-11-0329.

Györffy, B. et al. 2010. An online survival analysis tool to rapidly assess the effect of 22,277 genes on breast cancer prognosis using microarray data of 1,809 patients. *Breast Cancer Research and Treatment* 123(3), pp. 725–731. doi: 10.1007/s10549-009-0674-9.

Hajra, K.M. et al. 2002. The SLUG zinc-finger protein represses E-cadherin in breast cancer. *Cancer Research* 62(6), pp. 1613–1618.

Hakulinen, J. et al. 2008. Secretion of active membrane type 1 matrix metalloproteinase (MMP-14) into extracellular space in microvesicular exosomes. *Journal of Cellular Biochemistry* 105(5), pp. 1211–1218. doi: 10.1002/jcb.21923.

Haley, J. et al. 2016. Functional characterization of a panel of high-grade serous ovarian cancer cell lines as representative experimental models of the disease. *Oncotarget* 7(22), pp. 32810–32820. doi: 10.18632/oncotarget.9053.

Hall, D.M.S. and Brooks, S.A. 2014. *In Vitro Invasion Assay Using Matrigel™: A Reconstituted Basement Membrane Preparation*. doi: 10.1007/978-1-4614-8244-4.

Hallas-potts, A. et al. 2019. Ovarian cancer cell lines derived from non-serous carcinomas migrate and invade more aggressively than those derived from high-grade serous carcinomas. *Scientific Reports* (January), pp. 1–10. Available at: http://dx.doi.org/10.1038/s41598-019-41941-4.

Han, K.Y. et al. 2015. Evidence for the involvement of MMP14 in MMP2 processing and recruitment in exosomes of corneal fibroblasts. *Investigative Ophthalmology and Visual Science* 56(9), pp. 5323–5329. doi: 10.1167/iovs.14-14417.

Hanson, P.I. and Cashikar, A. 2012. Multivesicular body morphogenesis. *Annual Review of Cell and Developmental Biology* 28, pp. 337–362. doi: 10.1146/annurev-cellbio-092910-154152.

Al Harbi, R. et al. 2021. Ovarian sex cord-stromal tumors: An update on clinical features, molecular changes, and management. *International Journal of Gynecological Cancer* 31(2), pp. 161–168. doi: 10.1136/ijgc-2020-002018.

Harding, C. and Stahl, P. 1983. Transferrin recycling in reticulocytes: pH and iron are important determinants of ligand binding and processing. *Biochemical and Biophysical Research Communications* 113(2), pp. 650–658.

Harrap, K.R. 1985. Preclinical studies identifying carboplatin as a viable cisplatin alternative. *Cancer Treatment Reviews* 12(SUPPL. A), pp. 21–33. doi: 10.1016/0305-7372(85)90015-5.

Hay, E. 1995. An overview of epithelio-mesenchymal transformation. *Acta Anatomica* 154(1), pp. 8–20. doi: 10.1159/000147748.

He, M. et al. 2015. Hepatocellular carcinoma-derived exosomes promote motility of immortalized hepatocyte through transfer of oncogenic proteins and RNAs. *Carcinogenesis* 36(9), pp. 1008–1018. doi: 10.1093/carcin/bgv081.

Heijnen, H.F.G. et al. 2014. Activated platelets release two types of membrane vesicles : Microvesicles by surface shedding and exosomes derived from exocytosis of multivesicular bodies and alpha-granules Activated Platelets Release Two Types of Membrane Vesicles : Microvesicles by S. (May). doi: 10.1182/blood.V94.11.3791.423a22.

Henne, W.M. et al. 2013. Molecular Mechanisms of the Membrane. Sculpting ESCRT Pathway. *Cold Spring Harbour Perpectives in Biology* 5, p. a016766.

Hescheler, J. et al. 1987. On the mechanism of histamine induced enhancement of the cardiac Ca 2 + current. *European Journal of Physiology* 410, pp. 23–29.

Hewitt, R.E. et al. 1997. Laminin and collagen IV subunit distribution in normal and neoplastic tissues of colorectum and breast. *British Journal of Cancer* 75(2), pp. 221–229. doi: 10.1038/bjc.1997.37.

Himbert, D. et al. 2020. Characterization of CD147, CA9, and CD70 as Tumor-Specific Markers on Extracellular Vesicles in Clear Cell Renal Cell Carcinoma. *Diagnostics* 10(12), p. 1034. doi: 10.3390/diagnostics10121034.

Hofstra, C.L. et al. 2003. Histamine H 4 Receptor Mediates Chemotaxis and Calcium Mobilization of Mast Cells. *The Journal of Pharmacology and Experimental Therapuetics* 305(3), pp. 1212–1221. doi: 10.1124/jpet.102.046581.tor.

Hong, C.Q. et al. 2015. Elevated C1orf63 expression is correlated with CDK10 and predicts better outcome for advanced breast cancers: A retrospective study. *BMC Cancer* 15(1), pp. 1–12. Available at: http://dx.doi.org/10.1186/s12885-015-1569-2.

Hood, J.D. and Cheresh, D.A. 2002. Role of integrins in cell invasion and migration. *Nature Reviews Cancer* 2(2), pp. 91–100. doi: 10.1038/nrc727.

Hoshino, A. et al. 2015. Tumour exosome integrins determine organotropic metastasis. *Nature* 527(7578), pp. 329–335. doi: 10.1038/nature15756.

Hoshino, D. et al. 2013. Exosome secretion is enhanced by invadopodia and drives invasive behavior. *Cell rep* 5(5). doi: 10.1016/j.celrep.2013.10.050.

Hsu, Y.L. et al. 2017. Hypoxic lung cancer-secreted exosomal MIR-23a increased angiogenesis and vascular permeability by targeting prolyl hydroxylase and tight junction protein ZO-1. *Oncogene* 36(34), pp. 4929–4942. doi: 10.1038/onc.2017.105.

Hu, Y. et al. 2017. TWEAK-stimulated macrophages inhibit metastasis of epithelial ovarian cancer via exosomal shuttling of microRNA. *Cancer Letters* (February), pp. 1–8. Available at: http://dx.doi.org/10.1016/j.canlet.2017.02.009.

Hu, Y. et al. 2019. Potential prognostic and diagnostic values of CDC6, CDC45, ORC6 and SNHG7 in colorectal cancer. *OncoTargets and Therapy* 12, pp. 11609–11621. doi: 10.2147/OTT.S231941.

Huang, D.W. et al. 2009a. Bioinformatics enrichment tools: Paths toward the comprehensive functional analysis of large gene lists. *Nucleic Acids Research* 37(1), pp. 1–13. doi: 10.1093/nar/gkn923.

Huang, D.W. et al. 2009b. Systematic and integrative analysis of large gene lists using DAVID bioinformatics resources. *Nature Protocols* 4(1), pp. 44–57. doi: 10.1038/nprot.2008.211.

Huang, Q. et al. 2014. Expression of NF45 correlates with malignant grade in gliomas and plays a pivotal role in tumor growth. *Tumor Biology* 35(10), pp. 10149–10157. doi: 10.1007/s13277-014-2310-5.

Hurley, J.H. 2008. ESCRT complexes and the biogenesis of multivesicular bodies. *Current Opinion in Cell Biology* 20(1), pp. 4–11. doi: 10.1016/j.ceb.2007.12.002.

Hurley, J.H. and Hansin, P.I. 2010. Membrane budding and scission by the ESCRT machinery: it's all in the neck. *Nature Review of Molecular Cell Biology* 11(8), pp. 556–566. doi: 10.1038/nrm2937.Membrane.

Hurwitz, S.N. et al. 2016. Proteomic profiling of NCI-60 extracellular vesicles uncovers common protein cargo and cancer type-specific biomarkers. *Oncotarget* 7(52), pp. 86999–87015. doi: 10.18632/oncotarget.13569.

Hutagalung, A.H. and Novick, P.J. 2011. Role of Rab GTPases in membrane traffic and cell physiology. *Physiological Reviews* 91(1), pp. 119–149. doi: 10.1152/physrev.00059.2009.

Ichikawa, A. et al. 2012. Histamine Biosynthesis and Function., pp. 1–8. doi:

10.1002/9780470015902.a0001404.pub2.

Inanc, S. et al. 2017. An improved collagen zymography approach for evaluating the collagenases MMP-1, MMP-8, and MMP-13. *BioTechniques* 63(4), pp. 174–180. doi: 10.2144/000114597.

Jangi, S.M. et al. 2006. H1 histamine receptor antagonists induce genotoxic and caspase-2-dependent apoptosis in human melanoma cells. *Carcinogenesis* 27(9), pp. 1787–1796. doi: 10.1093/carcin/bgl021.

Jangi, S.M. et al. 2008. Terfenadine-induced apoptosis in human melanoma cells is mediated through Ca2+ homeostasis modulation and tyrosine kinase activity, independently of H1 histamine receptors. *Carcinogenesis* 29(3), pp. 500–509. doi: 10.1093/carcin/bgm292.

Jayson, G.C. et al. 2014. Ovarian cancer. *The Lancet* 384(9951), pp. 1376–1388. Available at: http://dx.doi.org/10.1016/S0140-6736(13)62146-7.

Jeppesen, D.K. et al. 2014. Quantitative proteomics of fractionated membrane and lumen exosome proteins from isogenic metastatic and nonmetastatic bladder cancer cells reveal differential expression of EMT factors. *Proteomics* 14(6), pp. 699–712. doi: 10.1002/pmic.201300452.

Johnstone, R.M. et al. 1987. Vesicle Formation during Reticulocyte Maturation Association of Plasma Membrane Activities Wirh Released Vesicles (Exosomes). *The Journal of Biological Chemistry* 262(1), pp. 9412–9420.

Jones, S. et al. 2011. Frequent Mutations of Chromatin Remodeling Gene ARID1A in Ovarian Clear Cell Carcinoma. *Science* 330(6001), pp. 228–231. doi: 10.1126/science.1196333.Frequent.

Jutel, M. et al. 2009. Histamine , histamine receptors and their role in immune pathology Clinical & Experimental Allergy. *Cliniucal and experimental allergy* 39, pp. 1786–1800. doi: 10.1111/j.1365-2222.2009.03374.x.

Kahlson, G. and Rosengren, E. 1968. New approaches to the physiology of histamine. *Physiol Rev* 48(1), pp. 155–196. doi: 10.1152/physrev.1968.48.1.155.

Kaiser, H.E. 1989. Characteristics and Pattern of Direct Tumor Spreading. *Local Invasion and Spread of Cancer* 1857(33), pp. 1–16. doi: 10.1007/978-94-009-1093-5_1.

Kajimoto, T. et al. 2013. Ongoing activation of sphingosine 1-phosphate receptors mediates maturation of exosomal multivesicular endosomes. *Nature Communications* 4. doi: 10.1038/ncomms3712.

Kakarla, R. et al. 2020. Apoptotic cell-derived exosomes : messages from dying cells. *Experimental & Molecular Medicine* 52, pp. 1–6. Available at: http://dx.doi.org/10.1038/s12276-019-0362-8.

Kalluri, R. and Neilson, E.G. 2003. Epithelial-mesenchymal transition and its implications for fibrosis. *Journal of Clinical Investigation* 112(12), pp. 1776–1784.

Kalluri, R. and Weinberg, R.A. 2010. The basics of epithelial-mesenchymal transition. *Physics of Plasmas* To be subm(May), pp. 1420–1428. doi: 10.1172/JCI39104.1420.

Keller, R. 2006. Mechanisms of elongation in embryogenesis. *Development* 133(12), pp. 2291–2302. doi: 10.1242/dev.02406.

Kennedy, L. et al. 2018. Blocking H1/H2 histamine receptors inhibits damage/fibrosis in Mdr2−/− mice and human cholangiocarcinoma tumorigenesis. *Hepatology* 68(3), pp. 1042–1056. doi: 10.1002/hep.29898.

Khan, F.M. et al. 2018. Inhibition of exosome release by ketotifen enhances sensitivity of cancer cells to doxorubicin. *Cancer Biology and Therapy* 19(1), pp. 25–33. Available at:

https://doi.org/10.1080/15384047.2017.1394544.

Kidani, Y. et al. 1978. Antitumor Activity of 1,2-Diaminocyclohexane-Platinum Complexes against Sarcoma-180 Ascites Form. *Journal of Medicinal Chemistry* 21(12), pp. 1315–1318.

Kiesler, P. et al. 2010. NF45 and NF90 regulate HS4-dependent interleukin-13 transcription in T cells. *Journal of Biological Chemistry* 285(11), pp. 8256–8267. Available at: http://dx.doi.org/10.1074/jbc.M109.041004.

Kim, H. et al. 2014a. Novel suppressive effects of ketotifen on migration and invasion of MDA-MB-231 and HT-1080 cancer cells. *Biomolecules and Therapeutics* 22(6), pp. 540–546. doi: 10.4062/biomolther.2014.081.

Kim, H.S. et al. 2014b. Risk and prognosis of ovarian cancer in women with endometriosis: A meta-analysis. *British Journal of Cancer* 110(7), pp. 1878–1890. doi: 10.1038/bjc.2014.29.

Kim, J.S. et al. 2017a. Epidemiologic factors that predict long-term survival following a diagnosis of epithelial ovarian cancer. *British Journal of Cancer* 116(7), pp. 964–971. Available at: http://dx.doi.org/10.1038/bjc.2017.35.

Kim, K.M. et al. 2017b. RNA in extracellular vesicles. *Wiley Interdiscip Rev RNA* 8(4). doi: 10.1002/wrna.1413.

King, H.W. et al. 2012. Hypoxic enhancement of exosome release by breast cancer cells. *BMC Cancer* 12. doi: 10.1186/1471-2407-12-421.

Koba, T. et al. 2021. Proteomics of serum extracellular vesicles identifies a novel COPD biomarker, fibulin-3 from elastic fibres. *ERJ Open Research* 7(1), pp. 00658–02020. Available at: http://dx.doi.org/10.1183/23120541.00658-2020.

Kobayashi, K.I. et al. 2000. Cimetidine inhibits cancer cell adhesion to endothelial cells and prevents metastasis by blocking E-selectin expression. *Cancer Research* 60(14), pp. 3978–3984.

Köberle, B. et al. 2010. Cisplatin resistance: Preclinical findings and clinical implications. *Biochimica et Biophysica Acta - Reviews on Cancer* 1806(2), pp. 172–182. Available at: http://dx.doi.org/10.1016/j.bbcan.2010.07.004.

Kobilka, B.K. 2007. G protein coupled receptor structure and activation ☆. *Biochimica et Biophysica Acta* 1768, pp. 794–807. doi: 10.1016/j.bbamem.2006.10.021.

Kori, M. et al. 2016. Molecular signatures of ovarian diseases: Insights from network medicine perspective. *Systems Biology in Reproductive Medicine* 62(4), pp. 266–282. Available at: http://dx.doi.org/10.1080/19396368.2016.1197982.

Kosaka, N. et al. 2013. Neutral sphingomyelinase 2 (nSMase2)-dependent exosomal transfer of angiogenic micrornas regulate cancer cell metastasis. *Journal of Biological Chemistry* 288(15), pp. 10849–10859. doi: 10.1074/jbc.M112.446831.

Koulouris, C.R. and Penson, R.T. 2009. Ovarian Stromal and Germ Cell Tumors. *Seminars in Oncology* 36(2), pp. 126–136. Available at: http://dx.doi.org/10.1053/j.seminoncol.2008.12.004.

Kowal, J. et al. 2014. Biogenesis and secretion of exosomes. *Current Opinion in Cell Biology* 29(1), pp. 116–125. doi: 10.1016/j.ceb.2014.05.004.

Kowal, J. et al. 2016. Proteomic comparison defines novel markers to characterize heterogeneous populations of extracellular vesicle subtypes. *Proceedings of the National Academy of Sciences of the*

United States of America 113(8), pp. E968–E977. doi: 10.1073/pnas.1521230113.

Krakhmal, N. V. et al. 2015. Cancer invasion: Patterns and mechanisms. *Acta Naturae* 7(2), pp. 17–28. doi: 10.32607/20758251-2015-7-2-17-28.

Kroeger Jr, P.T. and Drapkin, R. 2017. Pathogenesis and heterogeneity of ovarian cancer. *Curr Opin Obstet Gynecol* 29(1), pp. 26–34. doi: 10.1097/GCO.0000000000000340.

Kuo, K.T. et al. 2009a. Analysis of DNA copy number alterations in Ovarian serous tumors identifies new molecular genetic changes in low-grade and high-grade carcinomas. *Cancer Research* 69(9), pp. 4036–4042. doi: 10.1158/0008-5472.CAN-08-3913.

Kuo, K.T. et al. 2009b. Frequent activating mutations of PIK3CA in ovarian clear cell carcinoma. *American Journal of Pathology* 174(5), pp. 1597–1601. doi: 10.2353/ajpath.2009.081000.

Kurman, R.J. and Shih, I. 2011. Molecular pathogenesis and extraovarian origin of epithelial ovarian cancer — Shifting the paradigm. *Human Pathology* 42(7), pp. 918–931. Available at: http://dx.doi.org/10.1016/j.humpath.2011.03.003.

Kurman, R.J. and Shih, I.M. 2016. The dualistic model of ovarian carcinogenesis revisited, revised, and expanded. *American Journal of Pathology* 186(4), pp. 733–747. doi: 10.1016/j.ajpath.2015.11.011.

Kurokawa, M. et al. 1995. Enhanced cancer growth in mice administered daily human equivalent doses of some H1 antihistamines: predictive in vitro correlates. *Journal of the National Cancer Institute* 87(21), pp. 1638–1639.

Kuschel, C. et al. 2006. Cell adhesion profiling using extracellular matrix protein microarrays. *BioTechniques* 40(4), pp. 523–531. doi: 10.2144/000112134.

Lambert, A.W. et al. 2017. Emerging Biological Principles of Metastasis. *Cell* 168(4), pp. 670–691. Available at: http://dx.doi.org/10.1016/j.cell.2016.11.037.

Larrinaga, G. et al. 2014. Prolyl endopeptidase activity is correlated with colorectal cancer prognosis. *International Journal of Medical Sciences* 11(2), pp. 199–208. doi: 10.7150/ijms.7178.

Latifi, A. et al. 2012. Isolation and Characterization of Tumor Cells from the Ascites of Ovarian Cancer Patients: Molecular Phenotype of Chemoresistant Ovarian Tumors. *PLoS ONE* 7(10). doi: 10.1371/journal.pone.0046858.

Läubli, H. and Borsig, L. 2010. Selectins promote tumor metastasis. *Seminars in Cancer Biology* 20(3), pp. 169–177.

Laulagnier, K. et al. 2004. Mast cell- and dendritic cell-derived display a specific lipid composition and an unusual membrane organization. *Biochemical Journal* 380(1), pp. 161–171. doi: 10.1042/BJ20031594.

Le, M.T.N. et al. 2014. MiR-200-containing extracellular vesicles promote breast cancer cell metastasis. *Journal of Clinical Investigation* 124(12), pp. 5109–5128. Available at: http://www.embase.com/search/results?subaction=viewrecord&from=export&id=L600716297%0Ahttp://dx.doi.org/10.1172/JCI75695.

Leber, T.M. and Balkwill, F.R. 1997. Zymography: A single-step staining method for quantitation of proteolytic activity on substrate gels. *Analytical Biochemistry* 249(1), pp. 24–28. doi: 10.1006/abio.1997.2170.

Lee, J.M. et al. 2019. New strategies in ovarian cancer treatment. *Cancer* 125(S24), pp. 4623–4629. doi:

10.1002/cncr.32544.

Lengyel, E. 2010. Ovarian cancer development and metastasis. *American Journal of Pathology* 177(3), pp. 1053–1064. Available at: http://dx.doi.org/10.2353/ajpath.2010.100105.

Lerman, M.J. et al. 2018. The Evolution of Polystyrene as a Cell Culture Material. *Tissue Engineering - Part B: Reviews* 24(5), pp. 359–372. doi: 10.1089/ten.teb.2018.0056.

Leurs, R.O.B. et al. 1991. Histamine H1 receptor mediated cyclic GMP production in guinea pig lung tissue is an L-arginine dependent process. *Biochemical Pharmacology* 42(2), pp. 271–277.

Lheureux, S. et al. 2019. Epithelial ovarian cancer: Evolution of management in the era of precision medicine. *CA: A Cancer Journal for Clinicians* , pp. 280–304. doi: 10.3322/caac.21559.

Li, J. et al. 2011. Tubal origin of ovarian low-grade serous carcinoma. *Modern Pathology* 24(11), pp. 1488–1499. doi: 10.1038/modpathol.2011.106.

Li, K. et al. 2018. Exosomes play roles in sequential processes of tumor metastasis. *International Journal of Cancer* 144(7), pp. 1486–1495. doi: 10.1002/ijc.31774.

Li, Y.L. et al. 2009. Identification of suitable reference genes for gene expression studies of human serous ovarian cancer by real-time polymerase chain reaction. *Analytical Biochemistry* 394(1), pp. 110–116. Available at: http://dx.doi.org/10.1016/j.ab.2009.07.022.

Liang, B. et al. 2013. Characterization and proteomic analysis of ovarian cancer-derived exosomes. *Journal of Proteomics* 80, pp. 171–182. Available at: http://dx.doi.org/10.1016/j.jprot.2012.12.029.

Liang, C. et al. 2007. In vitro scratch assay : a convenient and inexpensive method for analysis of cell migration in vitro. *Nature Protocols* 2(2), pp. 329–333. doi: 10.1038/nprot.2007.30.

Lim, S. et al. 2014. Amyloid-β precursor protein promotes cell proliferation and motility of advanced breast cancer. *BMC Cancer* 14(1), pp. 1–12. doi: 10.1186/1471-2407-14-928.

Lima, L.G. et al. 2013. Intercellular transfer of tissue factor via the uptake of tumor-derived microvesicles. *Thrombosis Research* 132(4), pp. 450–456. Available at: http://dx.doi.org/10.1016/j.thromres.2013.07.026.

Lin, J.C. et al. 2007. Induction of apoptosis and cell-cycle arrest in human colon cancer cells by meclizine. *Food and Chemical Toxicology* 45(6), pp. 935–944. doi: 10.1016/j.fct.2006.11.016.

Lin, J.J. et al. 2015. Inhibition of histamine receptor 3 suppresses glioblastoma tumor growth, invasion, and epithelial-to-mesenchymal transition. *Oncotarget* 6(19), pp. 17107–17120.

Ling, P. et al. 2004. Histamine H 4 receptor mediates eosinophil chemotaxis with cell shape change and adhesion molecule upregulation. *British Journal of Pharmacology* 142, pp. 161–171. doi: 10.1038/sj.bjp.0705729.

Liu, N. et al. 2013. Increased CD70 expression is associated with clinical resistance to cisplatin-based chemotherapy and poor survival in advanced ovarian carcinomas. *OncoTargets and Therapy* 6, pp. 615–619. doi: 10.2147/OTT.S44445.

Liu, Z. et al. 2006. Role of H 1 receptors in histamine-mediated up-regulation of STAT4 phosphorylation. *International Immunopharmacology* 6, pp. 485–493. doi: 10.1016/j.intimp.2005.09.014.

Llorente, A. et al. 2013. Molecular lipidomics of exosomes released by PC-3 prostate cancer cells. *Biochimica et Biophysica Acta - Molecular and Cell Biology of Lipids* 1831(7), pp. 1302–1309. doi: 10.1016/j.bbalip.2013.04.011.

Loh, S.Y. et al. 1992. Reduced drug accumulation as a major mechanism of acquired resistance to cisplatin in a human ovarian carcinoma cell line: Circumvention studies using novel platinum (ii) and (iv) ammine/amine complexes. *British Journal of Cancer* 66(6), pp. 1109–1115. doi: 10.1038/bjc.1992.419.

Lokman, N.A. et al. 2012. Chick Chorioallantoic Membrane (CAM) Assay as an In Vivo Model to Study the Effect of Newly Identified Molecules on Ovarian Cancer Invasion and Metastasis. *Journal of Molecular Science* 13, pp. 9959–9970. doi: 10.3390/ijms13089959.

Lovenberg, T.W. et al. 1999. Cloning and Functional Expression of the Human Histamine H 3 Receptor. *Molecular Pharmacology* 1107, pp. 1101–1107.

Lu, Y. et al. 2015. Shared genetics underlying epidemiological association between endometriosis and ovarian cancer. *Human Molecular Genetics* 24(20), pp. 5955–5964. doi: 10.1093/hmg/ddv306.

Luga, V. et al. 2012. Exosomes mediate stromal mobilization of autocrine Wnt-PCP signaling in breast cancer cell migration. *Cell* 151(7), pp. 1542–1556. Available at: http://dx.doi.org/10.1016/j.cell.2012.11.024.

Lukanova, A. and Kaaks, R. 2005. Endogenous hormones and ovarian cancer: Epidemiology and current hypotheses. *Cancer Epidemiology Biomarker and Prevention* 14(1), pp. 98–107.

Luo, T. et al. 2013. Histamine H2 receptor activation exacerbates myocardial ischemia / reperfusion injury by disturbing mitochondrial and endothelial function. *Basic Research in Cardiology* 108(342). doi: 10.1007/s00395-013-0342-4.

Ma, J. et al. 2020. Desloratadine, a Novel Antigrowth Reagent for Bladder Cancer. *Technology in Cancer Research and Treatment* 19(1), pp. 1–9. doi: 10.1177/1533033820926591.

von Mach-Szczypiński, J. et al. 2009. Metabolism of histamine in tissues of primary ductal breast cancer. *Metabolism: Clinical and Experimental* 58(6), pp. 867–870. doi: 10.1016/j.metabol.2009.02.011.

Mahmood, N. et al. 2018. Multifaceted role of the urokinase-type plasminogen activator (uPA) and its receptor (uPAR): Diagnostic, prognostic, and therapeutic applications. *Frontiers in Oncology* 8(FEB). doi: 10.3389/fonc.2018.00024.

Maier, T. et al. 2009. Correlation of mRNA and protein in complex biological samples. *FEBS Letters* 583(24), pp. 3966–3973. Available at: http://dx.doi.org/10.1016/j.febslet.2009.10.036.

Mani, S.A. et al. 2007. Mesenchyme Forkhead 1 (FOXC2) plays a key role in metastasis and is associated with aggressive basal-like breast cancers. *Proceedings of the National Academy of Sciences of the United States of America* 104(24), pp. 10069–10074. doi: 10.1073/pnas.0703900104.

Martin, G.R. and Rubin, H. 1974. Effects of cell adhesion to the substratum on the growth of chick embryo fibroblasts. *Experimental Cell Research* 85(2), pp. 319–333. doi: 10.1016/0014-4827(74)90133-5.

Maslinski, C. and Fogel, W.A. 1991. Catabolism of histamine. *Handbook of experimental pharmacology* 97, pp. 165–189.

Matsumoto, N. et al. 2021. Histamine H1 receptor antagonists selectively kill cisplatin - resistant human cancer cells. *Scientific Reports* , pp. 1–16. Available at: https://doi.org/10.1038/s41598-021-81077-y.

Mattheyses, A.L. et al. 2010. Imaging with total internal reflection fluorescence microscopy for the cell

biologist. *Journal of cell SCi* 123, pp. 3621–3628.

Matulonis, U.A. et al. 2016. Ovarian cancer. *Nature Reviews Disease Primers* 2, pp. 1–22. doi: 10.1038/nrdp.2016.61.

McCready, J. et al. 2010. Secretion of extracellular hsp90α via exosomes increases cancer cell motility: A role for plasminogen activation. *BMC Cancer* 10. doi: 10.1186/1471-2407-10-294.

Mcguire, W.P. et al. 1996. Cyclophosphamide and cisplatin compared with paclitaxel and cisplatin in patients with stage III and stage IV ovarian cancer. *The New England journal of medicine* 334(1), pp. 1–6.

McMahon, H.T. and Boucrot, E. 2015. Membrane curvature at a glance. *Journal of Cell Science* 128(6), pp. 1065–1070. doi: 10.1242/jcs.114454.

Medina, V.A. et al. 2011. Histamine Receptors as Potential Therapeutic Targets for Cancer Drug Development. *Drug Development - A Case Study Based Insight into Modern Strategies* . doi: 10.5772/27773.

Medina, V.A. and Rivera, E.S. 2010. Histamine receptors and cancer pharmacology. *British Journal of Pharmacology* 161(4), pp. 755–767. doi: http://dx.doi.org/10.1111/bph.2009.157.issue-1.

Melin, A. et al. 2006. Endometriosis and the risk of cancer with special emphasis on ovarian cancer. *Human Reproduction* 21(5), pp. 1237–1242. doi: 10.1093/humrep/dei462.

Mellish, K.J. et al. 1993. In vitro platinum drug chemosensitivity of human cervical squamous cell carcinoma cell lines with intrinsic and acquired resistance to cisplatin. *British Journal of Cancer* 68(2), pp. 240–250. doi: 10.1038/bjc.1993.322.

Melo, S.A. et al. 2015. Cancer Exosomes Perform Cell-Independent MicroRNA Biogenesis and Promote Tumorigenesis. *Cancer Cell* 26(5), pp. 707–721. doi: 10.1016/j.ccell.2014.09.005.Cancer.

Menck, K. et al. 2015. Tumor-derived microvesicles mediate human breast cancer invasion through differentially glycosylated EMMPRIN. *Journal of Molecular Cell Biology* 7(2), pp. 143–153. doi: 10.1093/jmcb/mju047.

Menck, K. et al. 2017. Neutral sphingomyelinases control extracellular vesicles budding from the plasma membrane. *Journal of Extracellular Vesicles* 6(1). Available at: https://doi.org/10.1080/20013078.2017.1378056.

Meng, F. et al. 2011. The H4 histamine receptor agonist, clobenpropit, suppresses human cholangiocarcinoma progression by disruption of epithelial mesenchymal transition and tumor metastasis. *Hepatology* 54(5), pp. 1718–1728. doi: 10.1002/hep.24573.

Messenger, S.W. et al. 2018. A Ca2+-stimulated exosome release pathway in cancer cells is regulated by Munc13-4. *Journal of Cell Biology* 217(8), pp. 2877–2890. doi: 10.1083/jcb.201710132.

Minciacchi, V.R. et al. 2015. Large oncosomes contain distinct protein cargo and represent a separate functional class of tumor-derived extracellular vesicles. *Oncotarget* 6(13). Available at: http://www.oncotarget.com/fulltext/3598.

Mitra, A.K. 2016. Ovarian Cancer Metastasis: A Unique Mechanism of Dissemination. *Tumor Metastasis* . doi: 10.5772/64700.

Mizuguchi, H. et al. 2012. Inverse agonistic activity of antihistamines and suppression of histamine H1 receptor gene expression. *Journal of Pharmacological Sciences* 118(1), pp. 117–121. doi:

10.1254/jphs.11177SC.

Di Modica, M. et al. 2017. Breast cancer-secreted miR-939 downregulates VE-cadherin and destroys the barrier function of endothelial monolayers. *Cancer Letters* 384, pp. 94–100. Available at: http://dx.doi.org/10.1016/j.canlet.2016.09.013.

Molloy, T. and van 't Veer, L.J. 2008. Recent advances in metastasis research. *Current Opinion in Genetics and Development* 18(1), pp. 35–41. doi: 10.1016/j.gde.2008.01.019.

Momenimovahed, Z. et al. 2019. Ovarian cancer in the world: Epidemiology and risk factors. *International Journal of Women's Health* 11, pp. 287–299. doi: 10.2147/IJWH.S197604.

Monczor, F. and Fernandez, N. 2016. Current knowledge and perspectives on histamine H1 and H2 receptor pharmacology: Functional selectivity, receptor crosstalk, and repositioning of classic histaminergic ligands. *Molecular Pharmacology* 90(5), pp. 640–648. doi: 10.1124/mol.116.105981.

Moreno-Bueno, G. et al. 2006. Genetic profiling of epithelial cells expressing E-cadherin repressors reveals a distinct role for snail, Slug, and E47 Factors in epithelial- mesenchymal transition. *Cancer Research* 66(19), pp. 9543–9556. doi: 10.1158/0008-5472.CAN-06-0479.

Motohara, T. et al. 2019. An evolving story of the metastatic voyage of ovarian cancer cells : cellular and molecular orchestration of the adipose-rich metastatic microenvironment. *Oncogene* , pp. 2885–2898. Available at: http://dx.doi.org/10.1038/s41388-018-0637-x.

Mucinous, H. and Tumors, O. 1994. Advances in Brief Mutation of K-ras Protooncogene Is Associated with Histological Subtypes in., pp. 33–35.

Mulcahy, L.A. 2016. *The effect of stressed cell-derived exosomes on metastatic activity of ovarian and breast cancer cell lines in vitro*. doi: https://doi.org/10.24384/0d6c-td74.

Müller, U.C. and Zheng, H. 2012. Physiological functions of APP family proteins. *Cold Spring Harbor Perspectives in Medicine* 2(2), pp. 1–17. doi: 10.1101/cshperspect.a006288.

Mullock, B.M. et al. 1998. Fusion of Lysosomes with Late Endosomes Produces a Hybrid Organelle of Intermediate Density and Is NSF Dependent. *Journal of cell Biology* 140(3), pp. 591–601.

Muralidharan-chari, V. et al. 2010. Microvesicles : mediators of extracellular communication during cancer progression. *Journal of Cell Science* 123, pp. 1603–1611. doi: 10.1242/jcs.064386.

Murayama, T. et al. 1990. Histamine-stimulated and GTP-binding Phospholipase A2 Activation in Rabbit Platelets *. *The Journal of Biological Chemistry* 265(8), pp. 4290–4295.

Nagasawa, S. et al. 2019. Systematic identification of characteristic genes of ovarian clear cell carcinoma compared with high-grade serous carcinoma based on RNA-sequencing. *International Journal of Molecular Sciences* 20(18), pp. 1–16. doi: 10.3390/ijms20184330.

Nakamura, K. et al. 2017. Exosomes Promote Ovarian Cancer Cell Invasion through Transfer of CD44 to Peritoneal Mesothelial Cells. *Molecular Cancer Research* 15(1), pp. 78–93. doi: 10.1158/1541-7786.MCR-16-0191.

Nakamura, T. et al. 2000. Molecular Cloning and Characterization of a New Human Histamine Receptor , HH4R. *Biochemical and Biophysical Research Communications* 279(2), pp. 615–620. doi: 10.1006/bbrc.2000.4008.

Nakao, M. et al. 2009. Endobronchial metastasis from primary papillary serous carcinoma of the peritoneum. *Internal Medicine* 48(13), pp. 1165–1168. doi: 10.2169/internalmedicine.48.2140.

Nathan, R.A. et al. 1981. A comparision of the actions of H1 and H2 antihistamines on histamine-induced bronchoconstriction and cutaneous wheal response in asthmatic patients. *J Allergy Clin Immunol* 67(3), pp. 171–177.

Natoni, A. et al. 2016. Targeting selectins and their ligands in cancer. *Frontiers in Oncology* 6(APR), pp. 1–12. doi: 10.3389/fonc.2016.00093.

Nazarenko, I. et al. 2010. Cell surface tetraspanin Tspan8 contributes to molecular pathways of exosome-induced endothelial cell activation. *Cancer Research* 70(4), pp. 1668–1678. doi: 10.1158/0008-5472.CAN-09-2470.

Neeft, M. et al. 2005. Munc13-4 is an effector of Rab27a and controls secretion of lysosomes in hematopoietic cells. *Molecular Biology of the Cell* 16(2), pp. 731–741. doi: 10.1091/mbc.E04-10-0923.

Ni, S. et al. 2015a. Expression and clinical role of NF45 as a novel cell cycle protein in esophageal squamous cell carcinoma (ESCC). *Tumor Biology* 36(2), pp. 747–756. doi: 10.1007/s13277-014-2683-5.

Ni, T. et al. 2015b. Upregulated expression of ILF2 in non-small cell lung cancer is associated with tumor cell proliferation and poor prognosis. *Journal of Molecular Histology* 46(4–5), pp. 325–335. doi: 10.1007/s10735-015-9624-5.

Nieto-alamilla, G. and Márquez-gómez, R. 2016. The Histamine H 3 Receptor : Structure , Pharmacology , and Function. *Molecular Pharmacology* (90), pp. 649–673.

Nishida, N. et al. 2006. Angiogenesis in cancer. *Vascular Health and Risk Management* 2(3), pp. 213–219. doi: 10.2147/vhrm.2006.2.3.213.

O'Brien, K. et al. 2013. Exosomes from triple-negative breast cancer cells can transfer phenotypic traits representing their cells of origin to secondary cells. *European Journal of Cancer* 49(8), pp. 1845–1859. Available at: http://dx.doi.org/10.1016/j.ejca.2013.01.017.

Oda, T. et al. 2000. Molecular Cloning and Characterization of a Novel Type of Histamine Receptor Preferentially Expressed in Leukocytes *. *The Journal of Biological Chemistry* 275(47), pp. 36781–36786. doi: 10.1074/jbc.M006480200.

Oikonomopoulou, K. et al. 2008. Prediction of ovarian cancer prognosis and response to chemotherapy by a serum-based multiparametric biomarker panel. *British Journal of Cancer* 99(7), pp. 1103–1113. doi: 10.1038/sj.bjc.6604630.

Olsen, C.M. et al. 2013. Obesity and risk of ovarian cancer subtypes: Evidence from the Ovarian Cancer Association Consortium. *Endocrine-Related Cancer* 20(2), pp. 251–262. doi: 10.1530/ERC-12-0395.

Orci, L. et al. 1993. Budding from Golgi membranes requires the coatomer complex of non-clathrin coat proteins. *Nature* 362(6421), pp. 648–652. doi: 10.1038/362648a0.

Order, S.E. et al. 1972. The Role of Lymphatic Obstruction in the Formation of Ascites in a Murine Ovarian Carcinoma. *Cancer Research* 32(8), pp. 1663–1666.

Ortega, C.E. et al. 2014. Mining CK2 in cancer. *PLoS ONE* 9(12), pp. 1–25. doi: 10.1371/journal.pone.0115609.

Ostenfeld, M.S. et al. 2014. Cellular disposal of miR23b by RAB27-dependent exosome release is linked to acquisition of metastatic properties. *Cancer Research* 74(20), pp. 5758–5771. doi: 10.1158/0008-5472.CAN-13-3512.

Ostrowski, M. et al. 2010. Rab27a and Rab27b control different steps of the exosome secretion

pathway. *Nature Cell Biology* 12(1), pp. 19–30. Available at: http://dx.doi.org/10.1038/ncb2000.

Ozols, R.F. 1991. Ovarian cancer: new clinical approaches. *Cancer Treatment Reviews* 18(SUPPL. A), pp. 77–83. doi: 10.1016/0305-7372(91)90027-W.

Paget, S. 1889. Distribution of secondary growths in cancer of the breast. *The Lance* , pp. 571–573. doi: 10.1007/s12307-014-0163-5.

Pan, B.T. and Johnstone, R.M. 1983. Fate of the transferrin receptor during maturation of sheep reticulocytes in vitro: Selective externalization of the receptor. *Cell* 33(3), pp. 967–978. doi: 10.1016/0092-8674(83)90040-5.

Pantazi, P. et al. 2020. A practical toolkit to study aspects of the metastatic cascade in vitro. *Acta Histochemica* 122(8), p. 151654. Available at: https://doi.org/10.1016/j.acthis.2020.151654.

Park, G.T. and Choi, K.C. 2016. Advanced new strategies for metastatic cancer treatment by therapeutic stem cells and oncolytic virotherapy. *Oncotarget* 7(36), pp. 58684–58695. doi: 10.18632/oncotarget.11017.

Parkinson, C.A. et al. 2011. Management of Malignant Ovarian Germ Cell Tumors. *Obstetrics and gynecology* 66(8)

Pasquier, J. et al. 2014. Microparticles mediated cross-talk between tumoral and endothelial cells promote the constitution of a pro-metastatic vascular niche through Arf6 up regulation. *Cancer Microenvironment* 7(1–2), pp. 41–59. doi: 10.1007/s12307-013-0142-2.

Patel, A. et al. 2016. Histamine induces the production of matrix metalloproteinase-9 in human astrocytic cultures via H1-receptor subtype. *Brain Structure and Function* 221(4), pp. 1845–1860. doi: 10.1007/s00429-015-1007-x.

Patel, R.H. and Mohiuddin, S.S. 2020. Biochemistry, Histamine. *StatPearls Treasure Island*

Paul, C.D. et al. 2017. Cancer cell motility : lessons from migration in confined spaces. *Nature Reviews Cancer* 17(2), pp. 131–140. doi: 10.1038/nrc.2016.123.Cancer.

Peinado, H. et al. 2007. Snail, ZEB and bHLH factors in tumour progression: An alliance against the epithelial phenotype? *Nature Reviews Cancer* 7(6), pp. 415–428. doi: 10.1038/nrc2131.

Peinado, H. et al. 2013. Melanoma exosomes educate bone marrow progenitor cells toward a pro-metastatic phenotype through MET. *Nature Medicine* 18(6), pp. 883–891. doi: 10.1038/nm.2753.Melanoma.

Peinado, H. et al. 2017. Pre-metastatic niches: Organ-specific homes for metastases. *Nature Reviews Cancer* 17(5), pp. 302–317. Available at: http://dx.doi.org/10.1038/nrc.2017.6.

Peng, D.-J. et al. 2010. Role of the Akt/mTOR survival pathway in cisplatin resistance in ovarian cancer cells. *Boiochemical and biophysical research communication* 394(3), pp. 600–605. Available at: https://www.ncbi.nlm.nih.gov/pmc/articles/PMC3624763/pdf/nihms412728.pdf.

Pereira, E.R. et al. 2018. Lymph node metastases can invade local blood vessels, exit the node and colonize distant organs in mice. *Science* 359(6382), pp. 1403–1407. doi: 10.1126/science.aal3622.Lymph.

Perez-Hernandez, D. et al. 2013. The intracellular interactome of tetraspanin-enriched microdomains reveals their function as sorting machineries toward exosomes. *Journal of Biological Chemistry* 288(17), pp. 11649–11661. doi: 10.1074/jbc.M112.445304.

Pérez-Moreno, M.A. et al. 2001. A New Role for E12/E47 in the Repression of E-cadherin Expression and Epithelial-Mesenchymal Transitions. *Journal of Biological Chemistry* 276(29), pp. 27424–27431. doi: 10.1074/jbc.M100827200.

Phuyal, S. et al. 2014. Regulation of exosome release by glycosphingolipids and flotillins. *FEBS Journal* 281(9), pp. 2214–2227. doi: 10.1111/febs.12775.

Piek, J.M.J. et al. 2001. Dysplastic changes in prophylactically removed Fallopian tubes of women predisposed to developing ovarian cancer. *Journal of Phatology* 195, pp. 451–456.

Pillai-Kastoori, L. et al. 2020. Antibody validation for Western blot: By the user, for the user. *Journal of Biological Chemistry* 295(4), pp. 926–939. doi: 10.1074/jbc.RA119.010472.

Pillot, C. et al. 2002. A detailed mapping of the histamine H3 receptor and its gene transcripts in rat brain. *Neuroscience* 114(1), pp. 173–193.

van der Pol, E. et al. 2012. Classification, functions, and clinical relevance of extracellular vesicles. *Pharmacological Reviews* 64(3), pp. 676–705. doi: 10.1124/pr.112.005983.

Popper, L.D. and Batra, S. 1994. Muscarinic acetylcholine and histamine receptor mediated calcium mobilization and cell growth in human ovarian cancer cells. *International Journal of Oncology* 4, pp. 453–459.

Porretti, J.C. et al. 2014. Fibroblasts induce epithelial to mesenchymal transition in breast tumor cells which is prevented by fibroblasts treatment with histamine in high concentration. *International Journal of Biochemistry and Cell Biology* 51(1), pp. 29–38. Available at: http://dx.doi.org/10.1016/j.biocel.2014.03.016.

Pradeed, S. et al. 2014. Hematogenous metastasis of ovarian cancer: Rethinking mode of spread. *Cancer Cell* 26(1), pp. 77–91. doi: 10.1016/j.ccr.2014.05.002.Hematogenous.

Prat, J. 2012. Ovarian carcinomas: Five distinct diseases with different origins, genetic alterations, and clinicopathological features. *Virchows Archiv* 460(3), pp. 237–249. doi: 10.1007/s00428-012-1203-5.

Predescu, D.V. et al. 2019. G protein-coupled receptors (Gpcrs)-mediated calcium signaling in ovarian cancer: Focus on gpcrs activated by neurotransmitters and inflammation-associated molecules. *International Journal of Molecular Sciences* 20(22). doi: 10.3390/ijms20225568.

Pu, X. et al. 2018. COPB2 promotes cell proliferation and tumorigenesis through up-regulating YAP1 expression in lung adenocarcinoma cells. *Biomedicine and Pharmacotherapy* 103(April), pp. 373–380. Available at: https://doi.org/10.1016/j.biopha.2018.04.006.

Purushothaman, A. et al. 2016. Fibronectin on the surface of myeloma cell-derived exosomes mediates exosome-cell interactions. *Journal of Biological Chemistry* 291(4), pp. 1652–1663. doi: 10.1074/jbc.M115.686295.

Pype, J.L. et al. 1998. Desensitization of the histamine H1-receptor and transcriptional down-regulation of histamine H1-receptor gene expression in bovine tracheal smooth muscle. *British Journal of Pharmacology* 125(7), pp. 1477–1484. doi: 10.1038/sj.bjp.0702222.

Qi, Q. et al. 2018. Blockade of Asparagine Endopeptidase Inhibits Cancer Metastasis. *J Med Chem* 60(17), pp. 7244–7255. doi: 10.1021/acs.jmedchem.

Raimondo, S. et al. 2015. Chronic myeloid leukemia-derived exosomes promote tumor growth through an autocrine mechanism. *Cell Communication and Signaling* 13(1), pp. 1–12. doi: 10.1186/s12964-015-0086-x.

Ramovs, V. et al. 2017. The opposing roles of laminin-binding integrins in cancer. *Matrix Biology* 57–58, pp. 213–243. Available at: http://dx.doi.org/10.1016/j.matbio.2016.08.007.

Ramus, S.J. et al. 2015. Germline mutations in the BRIP1, BARD1, PALB2, and NBN genes in women with ovarian cancer. *Journal of the National Cancer Institute* 107(11), pp. 1–8. doi: 10.1093/jnci/djv214.

Ratajczak, J. et al. 2006. Embryonic stem cell-derived microvesicles reprogram hematopoietic progenitors: Evidence for horizontal transfer of mRNA and protein delivery. *Leukemia* 20(5), pp. 847–856. doi: 10.1038/sj.leu.2404132.

Record, M. 2013. Exosomal Lipids in Cell–Cell Communication. *Emerging Concepts of Tumor Exosome-Mediated Cell-Cell Communication* , pp. 1–220. doi: 10.1007/978-1-4614-3697-3.

Record, M. et al. 2014. Exosomes as new vesicular lipid transporters involved in cell-cell communication and various pathophysiologies. *Biochimica et Biophysica Acta - Molecular and Cell Biology of Lipids* 1841(1), pp. 108–120. Available at: http://dx.doi.org/10.1016/j.bbalip.2013.10.004.

Reichman, T.W. et al. 2002. The RNA Binding Protein Nuclear Factor 90 Functions as Both a Positive and Negative Regulator of Gene Expression in Mammalian Cells. *Molecular and Cellular Biology* 22(1), pp. 343–356. doi: 10.1128/mcb.22.1.343-356.2002.

Reid, B.M. et al. 2017. Epidemiology of ovarian cancer: a review. *Cancer Biology and Medicine* 14(1), pp. 9–32. doi: 10.20892/j.issn.2095-3941.2016.0084.

Reinhold, W.C. et al. 2012. CellMiner: A web-based suite of genomic and pharmacologic tools to explore transcript and drug patterns in the NCI-60 cell line set. *Cancer Research* 72(14), pp. 3499–3511. doi: 10.1158/0008-5472.CAN-12-1370.

Reymond, N. et al. 2013. Crossing the endothelial barrier during metastasis. *Nature Reviews Cancer* 13(12), pp. 858–870. Available at: http://dx.doi.org/10.1038/nrc3628.

Ribatti, D. et al. 2020. Epithelial-Mesenchymal Transition in Cancer: A Historical Overview. *Translational Oncology* 13(6), p. 100773. Available at: https://doi.org/10.1016/j.tranon.2020.100773.

Rich, J.T. et al. 2010. A practical guide to understanding Kaplan-Meier curves. *Otolaryngology - Head and Neck Surgery* 143(3), pp. 331–336. doi: 10.1016/j.otohns.2010.05.007.

Risha, Y. et al. 2021. Breast cancer-derived microvesicles are the source of functional metabolic enzymes as potential targets for cancer therapy. *Biomedicines* 9(2), pp. 1–15. doi: 10.3390/biomedicines9020107.

Rivera, E.S. et al. 2000. Histamine as an autocrine growth factor: An unusual role for a widespread mediator. *Seminars in Cancer Biology* 10(1), pp. 15–23. doi: 10.1006/scbi.2000.0303.

Robinson, A.J. and Dickenson, J.M. 2001. Activation of the p38 and p42 / p44 mitogen-activated protein kinase families by the histamine H 1 receptor in DDT 1 MF-2 cells. *British Journal of Pharmacology* 133, pp. 1378–1386.

Rodriguez, A. et al. 2018. HRH1: A Novel GPCR Drug Target in Pancreatic Cancer. *The FASEB Journal* 32(S1), pp. 695.1-695.1.

Rudolph, M.I. et al. 2008. The influence of mast cell mediators on migration of SW756 cervical carcinoma cells. *Journal of Pharmacological Sciences* 106(2), pp. 208–218. Available at: https://doi.org/10.1254/jphs.FP0070736.

Rump, A. et al. 2004. Binding of Ovarian Cancer Antigen CA125 / MUC16 to Mesothelin Mediates Cell Adhesion. *The Jorunal of Biological Chemistry* 279(10), pp. 9190–9198. doi: 10.1074/jbc.M312372200.

Runz, S. et al. 2007. Malignant ascites-derived exosomes of ovarian carcinoma patients contain CD24 and EpCAM. *Gynecologic Oncology* 107(3), pp. 563–571. doi: 10.1016/j.ygyno.2007.08.064.

Ryan, M.C. et al. 2010. Targeting pancreatic and ovarian carcinomas using the auristatin-based anti-CD70 antibody-drug conjugate SGN-75. *British Journal of Cancer* 103(5), pp. 676–684. doi: 10.1038/sj.bjc.6605816.

Sahai, E. 2005. Mechanisms of cancer cell invasion. *Current Opinion in Genetics and Development* 15(1), pp. 87–96. doi: 10.1016/j.gde.2004.12.002.

Sakhalkar, S.P. et al. 2005. Involvement of histamine H1 and H2 receptors in the regulation of STAT-1 phosphorylation : Inverse agonism exhibited by the receptor antagonists. *International Immunopharmacology* 5, pp. 1299–1309. doi: 10.1016/j.intimp.2005.03.019.

Salmeron, C. et al. 2020. HRH1 in Human and Mouse Pancreatic Cancer. *The FASEB Journal* . doi: https://doi.org/10.1096/fasebj.2020.34.s1.06334.

Salmerón, C. et al. 2020. A GPCR candidate in pancreatic ductal adenocarcinoma: A potential repurposing opportunity. *Cancer Research*

Sato, N. et al. 2000. Loss of heterozygosity on 10q23.3 and mutation of the tumor suppressor gene PTEN in benign endometrial cyst of the ovary: Possible sequence progression from benign endometrial cyst to endometrioid carcinoma and clear cell carcinoma of the ovary. *Cancer Research* 60(24), pp. 7052–7056.

Sayasneh, A. et al. 2011. Endometriosis and Ovarian Cancer: A Systematic Review. *ISRN Obstetrics and Gynecology* 2011, pp. 1–6. doi: 10.5402/2011/140310.

Schaner, M.E. et al. 2003. Gene Expression Patterns in Ovarian Carcinomas. *Molecular Biology of the Cell* 14(December), pp. 5069–5081. doi: 10.1091/mbc.E03.

Schayer, R.W. 1952. Biogenesis of histamine. *J Biol Chem* 199(1), pp. 245–50.

Schillaci, O. et al. 2017. Exosomes from metastatic cancer cells transfer amoeboid phenotype to non-metastatic cells and increase endothelial permeability: Their emerging role in tumor heterogeneity. *Scientific Reports* 7(1), pp. 1–15. doi: 10.1038/s41598-017-05002-y.

Schindelin, J. et al. 2012. Fiji: An open-source platform for biological-image analysis. *Nature Methods* 9(7), pp. 676–682. doi: 10.1038/nmeth.2019.

Senturk, E. et al. 2010. A critical re-appraisal of BRCA1 methylation studies in ovarian cancer. *Gynecologic Oncology* 119(2), pp. 376–383. Available at: http://dx.doi.org/10.1016/j.ygyno.2010.07.026.

Shaaban, A.M. et al. 2014. Ovarian malignant germ cell tumors: Cellular classification and clinical and imaging features. *Radiographics* 34(3), pp. 777–801. doi: 10.1148/rg.343130067.

Shahid, M. et al. 2010. *Biological and Pharmacological Aspects of Histamine Receptors and Their Ligands*. doi: 10.1007/978-90-481-9349-3.

Shamseddine, A.A. et al. 2015. Roles and regulation of neutral sphingomyelinase-2 in cellular and pathological processes. *Advances in Biological Regulation* 57(631), pp. 24–41. doi: 10.1016/j.jbior.2014.10.002.

Shan, Y. et al. 2018. Hypoxia-Induced Matrix Metalloproteinase-13 Expression in Exosomes from Nasopharyngeal Carcinoma Enhances Metastases. *Cell Death and Disease* 9(3). Available at: http://dx.doi.org/10.1038/s41419-018-0425-0.

Shih, I.M. and Kurman, R.J. 2004. Ovarian Tumorigenesis: A Proposed Model Based on Morphological and Molecular Genetic Analysis. *American Journal of Pathology* 164(5), pp. 1511–1518. doi: 10.1016/S0002-9440(10)63708-X.

Shim, S.H. et al. 2013. Laparoscopic management of early-stage malignant nonepithelial ovarian tumors surgical and survival outcomes. *International Journal of Gynecological Cancer* 23(2), pp. 249–255. doi: 10.1097/IGC.0b013e318272e754.

Shimamura, K. et al. 2004. Expression of adhesion molecules by sphingosine 1-phosphate and histamine in endothelial cells. *European Journal of Pharmacology* 486(2), pp. 141–150. doi: 10.1016/j.ejphar.2003.12.022.

Shimoda, M. et al. 2014. Loss of the Timp gene family is sufficient for the acquisition of the CAF-like cell state. *Nature Cell Biology* 16(9), pp. 889–901. doi: 10.1038/ncb3021.

Shirakawa, R. et al. 2004. Munc13-4 Is a GTP-Rab27-binding Protein Regulating Dense Core Granule Secretion in Platelets. *Journal of Biological Chemistry* 279(11), pp. 10730–10737. Available at: http://dx.doi.org/10.1074/jbc.M309426200.

Sieja, K. et al. 2005. Concentration of histamine in serum and tissues of the primary ductal breast cancers in women. *Breast* 14(3), pp. 236–241. doi: 10.1016/j.breast.2004.06.012.

Singer, G. et al. 2002. Diverse Tumorigenic Pathways in Ovarian Serous Carcinoma. *The American Journal of Pathology* 160(4), pp. 1223–1228. Available at: http://dx.doi.org/10.1016/S0002-9440(10)62549-7.

Singer, G. et al. 2003. Mutations in BRAF and KRAS Characterize the Development of Low-Grade Ovarian Serous Carcinoma. *Journal of National Cancer Institute* 95(6), pp. 6–8.

Sinha, A. et al. 2014. In-depth proteomic analyses of ovarian cancer cell line exosomes reveals differential enrichment of functional categories compared to the NCI 60 proteome. *Biochemical and Biophysical Research Communications* 445(4), pp. 694–701. Available at: http://dx.doi.org/10.1016/j.bbrc.2013.12.070.

Skog, J. et al. 2008. Glioblastoma microvesicles transport RNA and protein that promote tumor growth and provide diagnostic biomarkers. *Nat Cell Biol* 10(12), pp. 1470–1476. doi: doi:10.1038/ncb1800.

Smith, C.W. 2000. Possible Steps Involved in the Transition to Stationary Adhesion of Rolling Neutrophils: A Brief Review. *Microcirculation* 7(6), pp. 385–394. doi: 10.1111/j.1549-8719.2000.tb00136.x.

Snoek-van Beurden, P. a M. et al. 2005. Zymographic techniques for the analysis of matrix metalloproteinases and their inhibitors. *BioTechniques* 38(1), pp. 73–83. Available at: http://www.ncbi.nlm.nih.gov/pubmed/15679089.

Song, H. et al. 2015. Contribution of germline mutations in the RAD51B, RAD51C, and RAD51D genes to ovarian cancer in the population. *Journal of Clinical Oncology* 33(26), pp. 2901–2907. doi: 10.1200/JCO.2015.61.2408.

Soule, B.P. et al. 2010. Loratadine dysregulates cell cycle progression and enhances the effect of radiation in human tumor cell lines. *Radiation Oncology* 5(1), pp. 1–12. doi: 10.1186/1748-717X-5-8.

Steinberg, F. et al. 1990. The vascular architecture of human xenotransplanted tumors: histological, morphometrical, and ultrastructural studies. *Journal of Cancer Research and Clinical Oncology* 116(5), pp. 517–524. doi: 10.1007/BF01613005.

Stoyanov, E. et al. 2012. Mast cells and histamine enhance the proliferation of non-small cell lung cancer cells. *Lung Cancer* 75(1), pp. 38–44. Available at: http://dx.doi.org/10.1016/j.lungcan.2011.05.029.

Strobel, T. et al. 1997. In Vivo Inhibition of CD44 Limits Intra-Abdominal Peritoneal Implantation1 Spread of a Human Ovarian Cancer Xenograft in Nude Mice : A Novel Role for CD44 in the Process of. *Cancer Research* (57), pp. 1228–1233.

Su, C.Y. et al. 2020. The Biological Functions and Clinical Applications of Integrins in Cancers. *Frontiers in Pharmacology* 11. doi: 10.3389/fphar.2020.579068.

Sung, B.H. et al. 2011. Cortactin controls cell motility and lamellipodial dynamics by regulating ECM Secretion. *Current Biology* 21(17), pp. 1460–1469. Available at: http://dx.doi.org/10.1016/j.cub.2011.06.065.

Sung, B.H. et al. 2015. Directional cell movement through tissues is controlled by exosome secretion. *Nature Communications* 6(May). doi: 10.1038/ncomms8164.

Sung, B.H. et al. 2020. A live cell reporter of exosome secretion and uptake reveals pathfinding behavior of migrating cells. *Nature Communications* 11(1), pp. 1–15. doi: 10.1038/s41467-020-15747-2.

Sung, H. et al. 2021. Global Cancer Statistics 2020: GLOBOCAN Estimates of Incidence and Mortality Worldwide for 36 Cancers in 185 Countries. *CA: A Cancer Journal for Clinicians* 71(3), pp. 209–249. doi: 10.3322/caac.21660.

Tan, G.-J. et al. 2013. Cathepsins mediate tumor metastasis. *World Journal of Biological Chemistry* 4(4), p. 91. doi: 10.4331/wjbc.v4.i4.91.

Tarin, D. et al. 1984. Mechanisms off Human Tumor Metastasis Studied in Patients with Peritoneovenous Shunts. *Cancer Research* 44(8), pp. 3584–3592.

Tauro, B.J. et al. 2013. Oncogenic H-Ras reprograms madin-darby canine kidney (MDCK) cell-derived exosomal proteins following epithelial-mesenchymal transition. *Molecular and Cellular Proteomics* 12(8), pp. 2148–2159. doi: 10.1074/mcp.M112.027086.

Tetlow, L. and Woolley, D.E. 2002. Histamine stimulates matrix metalloproteinase-3 and -13 production by human articular chondrocytes in vitro. *Ann Rheum Dis* 1, pp. 737–740.

Tetlow, L.C. and Woolley, D.E. 2004. Effect of histamine on the production of matrix metalloproteinases-1, -3, -8 and -13, and TNFα and PGE2 by human articular chondrocytes and synovial fibroblasts in vitro: A comparative study. *Virchows Archiv* 445(5), pp. 485–490.

Thakur, B.K. et al. 2014. Double-stranded DNA in exosomes: A novel biomarker in cancer detection. *Cell Research* 24(6), pp. 766–769. doi: 10.1038/cr.2014.44.

The Cancer Genome Atlas Research Network 2011. Integrated genomic analyses of ovariancarcinoma. *Nature* 474, pp. 609–615. Available at: http://www.nature.com/nature/journal/v474/n7353/pdf/nature10166.pdf.

Théry, C. et al. 2001. Proteomic Analysis of Dendritic Cell-Derived Exosomes: A Secreted Subcellular Compartment Distinct from Apoptotic Vesicles. *The Journal of Immunology* 166(12), pp. 7309–7318.

doi: 10.4049/jimmunol.166.12.7309.

Théry, C. et al. 2018. Minimal information for studies of extracellular vesicles 2018 (MISEV2018): a position statement of the International Society for Extracellular Vesicles and update of the MISEV14 guidlines. *Journal of Extracellular Vesicles* 7(1), pp. 1–43.

Thiery, J.P. et al. 2009. Epithelial-Mesenchymal Transitions in Development and Disease. *Cell* 139(5), pp. 871–890. doi: 10.1016/j.cell.2009.11.007.

Thomakos, N. et al. 2019. Rare distant metastatic disease of ovarian and peritoneal carcinomatosis: A review of the literature. *Cancers* 11(8), pp. 1–17. doi: 10.3390/cancers11081044.

Tilghman, S.L. et al. 2013. Proteomic signatures of acquired letrozole resistance in breast cancer: Suppressed estrogen signaling and increased cell motility and invasiveness. *Molecular and Cellular Proteomics* 12(9), pp. 2440–2455. Available at: http://dx.doi.org/10.1074/mcp.M112.023861.

Todorova, D. et al. 2017. Extracellular vesicles in angiogenesis. *Circulation Research* 120(10), pp. 1658–1673. doi: 10.1161/CIRCRESAHA.117.309681.

Tolley, H.D. et al. 2016. *Survival Analysis*. Elsevier Inc. Available at: http://dx.doi.org/10.1016/B978-0-12-404584-2.00010-0.

Tomkinson, B. 2019. Tripeptidyl-peptidase II: Update on an oldie that still counts. *Biochimie* 166, pp. 27–37. Available at: https://doi.org/10.1016/j.biochi.2019.05.012.

Tomsig, J.L. and Creutz, C.E. 2002. Copines: A ubiquitous family of Ca2+-dependent phospholipid-binding proteins. *Cellular and Molecular Life Sciences* 59(9), pp. 1467–1477. doi: 10.1007/s00018-002-8522-7.

Tonzani, S. 2009. TIRF: imaging at the cellular edge. *Nature Cell Biology* 11(S1), pp. S16–S16. doi: 10.1038/ncb1933.

Torre, L.A. et al. 2018. Ovarian cancer statistics, 2018. *CA: A Cancer Journal for Clinicians* 68(4), pp. 284–296. doi: 10.3322/caac.21456.

Traiffort, E. et al. 1992. Expression of a cloned rat histamine H2 receptor mediating inhibition of arachidonate release and activation of cAMP accumulation. *Proc Natl Acad Sci* 89, pp. 2649–2653.

Trajkovic, K. et al. 2008. Ceramide triggers budding of exosome vesicles into multivesicular endosomes. *Science* 319(5867), pp. 1244–1247. doi: 10.1126/science.1153124.

Trajkovic, K. 2008. Ceramide triggers budding of exosome vesicles into multivesicular endosomes (Science (1244)). *Science* 320(5873), p. 179. doi: 10.1126/science.320.5873.179.

Tricarico, C. et al. 2017. Biology and biogenesis of shed microvesicles. *Small GTPases* 8(4), pp. 220–232. Available at: https://doi.org/10.1080/21541248.2016.1215283.

Tsang, J.Y.S. et al. 2018. Proteolytic cleavage of amyloid precursor protein by ADAM10 mediates proliferation and migration in breast cancer. *EBioMedicine* 38, pp. 89–99. Available at: https://doi.org/10.1016/j.ebiom.2018.11.012.

Tung, K.H. et al. 2003. Reproductive factors and epithelial ovarian cancer risk by histologic type: A multiethnic case-control study. *American Journal of Epidemiology* 158(7), pp. 629–638. doi: 10.1093/aje/kwg177.

Tworoger, S.S. and Huang, T. 2016. Obesity and ovarian cancer. *Recent Results in Cancer Research* 208, pp. 155–176. doi: 10.1007/978-3-319-42542-9_9.

Tyanova, S. et al. 2016. The Perseus computational platform for comprehensive analysis of (prote)omics data. *Nature Methods* 13(9), pp. 731–740. doi: 10.1038/nmeth.3901.

Urdiales, J.L. et al. 1992. Chlorpheniramine inhibits the ornithine decarboxylase induction of Ehrlich carcinoma growing in vivo. *FEBS Letters* 305(3), pp. 260–264. doi: 10.1016/0014-5793(92)80682-7.

Usukura, K. et al. 2013. Tripeptidyl peptidase II in human oral squamous cell carcinoma. *Journal of Cancer Research and Clinical Oncology* 139(1), pp. 123–130. doi: 10.1007/s00432-012-1307-y.

Valadi, H. et al. 2007. Exosome-mediated transfer of mRNAs and microRNAs is a novel mechanism of genetic exchange between cells. *Nature Cell Biology* 9(6), pp. 654–659. doi: 10.1038/ncb1596.

Valastyan, S. and Weinberg, R.A. 2011. Tumor metastasis: Molecular insights and evolving paradigms. *Cell* 147(2), pp. 275–292. doi: 10.1016/j.cell.2011.09.024.

Vandewalle, C. et al. 2005. SIP1/ZEB2 induces EMT by repressing genes of different epithelial cell-cell junctions. *Nucleic Acids Research* 33(20), pp. 6566–6578. doi: 10.1093/nar/gki965.

Vandooren, J. et al. 2013. Zymography methods for visualizing hydrolytic enzymes. *Nature Methods* 10(3), pp. 211–220. doi: 10.1038/nmeth.2371.

Varankar, S.S. and Bapat, S.A. 2018. Migratory metrics of wound healing: A Quantification Approach for in vitro Scratch Assays. *Frontiers in Oncology* 8(DEC), pp. 1–13. doi: 10.3389/fonc.2018.00633.

Varol, M. 2020. Cell-extracellular matrix adhesion assay. *Methods in Molecular Biology* 2109, pp. 209–217. doi: 10.1007/7651_2019_246.

Veatch, A.L. et al. 1994. Differential expression of the cell-cell adhesion molecule E-cadherin in ascites and solid human ovarian tumor cells. *International Journal of Cancer* 58(3), pp. 393–399. doi: 10.1002/ijc.2910580315.

Veras, E. et al. 2009. Cystic and adenofibromatous clear cell carcinomas of the ovary: Distinctive tumors that differ in their pathogenesis and behavior: A clinicopathologic analysis of 122 cases. *American Journal of Surgical Pathology* 33(6), pp. 844–853. doi: 10.1097/PAS.0b013e31819c4271.

Verdoodt, F. et al. 2019. Antihistamine use and risk of ovarian cancer: A population-based case-control study. *Maturitas* 120, pp. 47–52. Available at: https://doi.org/10.1016/j.maturitas.2018.11.014.

Verdoodt, F. et al. 2020. Antihistamines and ovarian cancer survival: nationwide cohort study and in vitro cell viability assay Freija Verdoodt. *JNCI J Natl Cancer Inst* 112(9), pp. 964–967. doi: 10.1093/jnci/djz217.

Vermeulen, P.B. et al. 1995. Microvessel quantification in primary colorectal carcinoma: An immunohistochemical study. *British Journal of Cancer* 71(2), pp. 340–343. doi: 10.1038/bjc.1995.68.

Verweij, F.J. et al. 2018. Quantifying exosome secretion from single cells reveals a modulatory role for GPCR signaling Frederik. 217(3), pp. 1129–1142. Available at: https://doi.org/10.1083/jcb.201703206.

Vila-Leahey, A. et al. 2016. Ranitidine modifies myeloid cell populations and inhibits breast tumor development and spread in mice. *OncoImmunology* 5(7). doi: 10.1080/2162402X.2016.1151591.

Villarroya-Beltri, C. et al. 2015. Europe PMC Funders Group Europe PMC Funders Author Manuscripts SORTING IT OUT : REGULATION OF EXOSOME LOADING. *Semin Cancer Biol* 2(28), pp. 3–13. doi: 10.1016/j.semcancer.2014.04.009.SORTING.

Vousden, K.H. and Lane, D.P. 2007. P53 in Health and Disease. *Nature Reviews Molecular Cell Biology* 8(4), pp. 275–283. doi: 10.1038/nrm2147.

Wagner, B.J. et al. 2011. Simvastatin reduces tumor cell adhesion to human peritoneal mesothelial cells by decreased expression of VCAM-1 and β 1 integrin. *International Journal of Oncology* 39, pp. 1593–1600. doi: 10.3892/ijo.2011.1167.

Waldenström, A. et al. 2012. Cardiomyocyte microvesicles contain DNA/RNA and convey biological messages to target cells. *PLoS ONE* 7(4), pp. 1–7. doi: 10.1371/journal.pone.0034653.

Walsh, T. et al. 2011. Mutations in 12 genes for inherited ovarian, fallopian tube, and peritoneal carcinoma identified by massively parallel sequencing. *Proceedings of the National Academy of Sciences of the United States of America* 108(44), pp. 18032–18037. doi: 10.1073/pnas.1115052108.

Wan, C. et al. 2015. NF45 overexpression is associated with poor prognosis and enhanced cell proliferation of pancreatic ductal adenocarcinoma. *Molecular and Cellular Biochemistry* 410(1–2), pp. 25–35. doi: 10.1007/s11010-015-2535-7.

Wandinger-Ness, A. and Zerial, M. 2014. Rab Proteins and the Compartmentalization of the Endosomal System. *Perspectives in Biology*

Wang, J.S. et al. 2008. Enhanced expression of Rab27A gene by breast cancer cells promoting invasiveness and the metastasis potential by secretion of insulin-like growth factor-II. *Molecular Cancer Research* 6(3), pp. 372–382. doi: 10.1158/1541-7786.MCR-07-0162.

Wang, M. et al. 2014. Integrative genomic analyses of the histamine H1 receptor and its role in cancer prediction. *International Journal of Molecular Medicine* 33(4), pp. 1019–1026. doi: 10.3892/ijmm.2014.1649.

Wang, Y. et al. 2020. COPB2 gene silencing inhibits colorectal cancer cell proliferation and induces apoptosis via the JNK/c-Jun signaling pathway. *PLoS ONE* 15(11 November), pp. 1–15. Available at: http://dx.doi.org/10.1371/journal.pone.0240106.

Waters, G.M. et al. 1991. 'Coatomer': a cytosolic protein complex containing subunits of non-clathrin-coated Golgi transport veiscles. *Nature* 354, pp. 56–58.

Webb, P.M. and Jordan, S.J. 2016. Epidemiology of epithelial ovarian cancer. *Best Practice & Research Clinical Obstetrics & Gynaecology* , pp. 1–12. Available at: http://dx.doi.org/10.1016/j.bpobgyn.2016.08.006.

Webber, J. et al. 2015. Differentiation of tumour-promoting stromal myofibroblasts by cancer exosomes. *Oncogene* 34(3), pp. 319–333. doi: 10.1038/onc.2013.560.

Wei, M. et al. 2017. Malignant ascites-derived exosomes promote proliferation and induce carcinoma-associated fibroblasts transition in peritoneal mesothelial cells. *Oncotarget* 8(26), pp. 42262–42271. doi: 10.18632/oncotarget.15040.

Weidle, U.H. et al. 2016. Mechanisms and targets involved in dissemination of ovarian cancer. *Cancer Genomics and Proteomics* 13(6), pp. 407–424. doi: 10.21873/cgp.20004.

Whiteside, T.L. 2016. Exosomes and tumor-mediated immune suppression Find the latest version : Exosomes and tumor-mediated immune suppression. *The Journal of Clinical Investigation* 126(4), pp. 1216–1223. doi: 10.1172/JCI81136.vesicular.

Wilhelmsen, K. et al. 2013. Quantitative In vitro Assay to Measure Neutrophil Adhesion to Activated Primary Human Microvascular Endothelial Cells under Static Conditions. *Journal of Visualized Experiments* (78), pp. 1–8. doi: 10.3791/50677.

Willner, J. et al. 2007. Alternate molecular genetic pathways in ovarian carcinomas of common

histological types. *Human Pathology* 38(4), pp. 607–613. doi: 10.1016/j.humpath.2006.10.007.

Wiltshaw, E. et al. 1979. Cancer of the ovary: a summary of experience with cis-dichlorodiammineplatinum(II) at the Royal Marsden Hospital. *Cancer Treat Rep* 63(9–10), pp. 1545–1548.

Wintzell, M. et al. 2012. Protein markers of cancer-associated fibroblasts and tumor-initiating cells reveal subpopulations in freshly isolated ovarian cancer ascites. *BMC Cancer* 12. doi: 10.1186/1471-2407-12-359.

Witwer, K.W. et al. 2013. Standardization of sample collection, isolation and analysis methods in extracellular vesicle research. *Journal of Extracellular Vesicles* 2(1), pp. 1–25. doi: 10.3402/jev.v2i0.20360.

Witz, I.P. 2008. The selectin-selectin ligand axis in tumor progression. *Cancer and Metastasis Reviews* 27(1), pp. 19–30. doi: 10.1007/s10555-007-9101-z.

Wollert, T. et al. 2009. Membrane scission by the ESCRT-III complex. *Nature* 458(7235), pp. 172–177. Available at: http://dx.doi.org/10.1038/nature07836.

Wortzel, I. et al. 2019. Exosome-Mediated Metastasis: Communication from a Distance. *Developmental Cell* 49(3), pp. 347–360. Available at: https://doi.org/10.1016/j.devcel.2019.04.011.

Wu, R. et al. 2007. Mouse Model of Human Ovarian Endometrioid Adenocarcinoma Based on Somatic Defects in the Wnt/β-Catenin and PI3K/Pten Signaling Pathways. *Cancer Cell* 11(4), pp. 321–333. doi: 10.1016/j.ccr.2007.02.016.

Xavier, C.P.R. et al. 2020. The Role of Extracellular Vesicles in the Hallmarks of Cancer and Drug Resistance. *Cells* 9(5), pp. 1–34. doi: 10.3390/cells9051141.

Xu, R. et al. 2018. Extracellular vesicles in cancer — implications for future improvements in cancer care. *Nature Reviews Clinical Oncology* 15(10), pp. 617–638. Available at: http://dx.doi.org/10.1038/s41571-018-0036-9.

Yamaguchi, H. et al. 2009. Lipid rafts and caveolin-1 are required for invadopodia formation and extracellular matrix degradation by human breast cancer cells. *Cancer Research* 69(22), pp. 8594–8602. doi: 10.1158/0008-5472.CAN-09-2305.

Yáñez-Mó, M. et al. 2015. Biological properties of extracellular vesicles and their physiological functions. *Journal of Extracellular Vesicles* 4(2015), pp. 1–60. doi: 10.3402/jev.v4.27066.

Yang, J. et al. 2004. Twist, a master regulator of morphogenesis, plays an essential role in tumor metastasis. *Cell* 117(7), pp. 927–939. doi: 10.1016/j.cell.2004.06.006.

Yang, J. et al. 2020. Guidelines and definitions for research on epithelial–mesenchymal transition. *Nature Reviews Molecular Cell Biology* 21(6), pp. 341–352. Available at: http://dx.doi.org/10.1038/s41580-020-0237-9.

Yao, D. et al. 2011. Mechanism of the mesenchymal-epithelial transition and its relationship with metastatic tumor formation. *Molecular Cancer Research* 9(12), pp. 1608–1620. doi: 10.1158/1541-7786.MCR-10-0568.

Yeung, T.L. et al. 2015. Cellular and molecular processes in ovarian cancer metastasis. A review in the theme: Cell and molecular processes in cancer metastasis. *American Journal of Physiology - Cell Physiology* 309(7), pp. C444–C456. doi: 10.1152/ajpcell.00188.2015.

Yokoi, A. et al. 2017. Malignant extracellular vesicles carrying MMP1 mRNA facilitate peritoneal dissemination in ovarian cancer. *Nature Communications* 8. doi: 10.1038/ncomms14470.

Yoneda, A. et al. 2012. Breast and Ovarian Cancers : A Survey and Possible Roles for the Cell Surface Heparan Sulfate Proteoglycans. *J Histochem Cytochem* 60(1), pp. 9–21. doi: 10.1369/0022155411428469.

Yoshioka, Y. et al. 2013. Comparative marker analysis of extracellular vesicles in different human cancer types. *Journal of Extracellular Vesicles* 2(1), pp. 1–9. doi: 10.3402/jev.v2i0.20424.

You, Q. et al. 2015a. Distinct prognostic values and potential drug targets of AL DH1 isoenzymes in non-small-cell lung cancer. *Drug Design, Development and Therapy* 9, pp. 5087–5097. doi: 10.2147/DDDT.S87197.

You, Y. et al. 2015b. Matrix metalloproteinase 13-containing exosomes promote nasopharyngeal carcinoma metastasis. *Cancer Science* 106(12), pp. 1669–1677. doi: 10.1111/cas.12818.

Zalel, Y. et al. 1996. Diagnosis and management of malignant germ cell ovarian tumors in young females. *International Journal of Gynecology and Obstetrics* 55(1), pp. 1–10. doi: 10.1016/0020-7292(96)02719-1.

Zerial, M. and Mcbride, H. 2001. Rab proteins as membrane organizers. *Nature Reviews Molecular Cell Biology* 2(February), pp. 107–117.

Zhang, R. and Xie, X. 2012. Tools for GPCR drug discovery. *Acta Pharmacologica Sinica* 33(3), pp. 372–384. Available at: http://dx.doi.org/10.1038/aps.2011.173.

Zhao, J. et al. 2020. Upregulation of histamine receptor H1 promotes tumor progression and contributes to poor prognosis in hepatocellular carcinoma. *Oncogene* 39(8), pp. 1724–1738. Available at: http://dx.doi.org/10.1038/s41388-019-1093-y.

Zhou, W. et al. 2014. Cancer-Secreted miR-105 destroys vascular endothelial barriers to promote metastasis. *Cancer Cell* 25(4), pp. 501–515. Available at: http://dx.doi.org/10.1016/j.ccr.2014.03.007.

Zhu, Y. et al. 2001. Cloning , Expression , and Pharmacological Characterization of a Novel Human Histamine Receptor. *Molecular Pharmacology* 59(3), pp. 434–441.

Zomer, A. et al. 2015. In vivo imaging reveals extracellular vesicle-mediated phenocopying of metastatic behavior. *Cell* 161(5), pp. 1046–1057. doi: 10.1016/j.cell.2015.04.042.